

Structure and Function of Glutamate Receptor-Like Channels (GLRs)

Marriah N. Green

Submitted in partial fulfillment of the  
requirements for the degree of  
Doctor of Philosophy  
under the Executive Committee  
of the Graduate School of Arts and Sciences

COLUMBIA UNIVERSITY

2023

# **Abstract**

## **Structure and Function of Glutamate Receptor-Like Channels (GLRs)**

Marriah N. Green

Glutamate is essential for proper brain function as it is our nervous systems principal excitatory neurotransmitter, a signal that stimulates nerve cells to send messages to other cells. Glutamate activates ionotropic glutamate receptors (iGluRs), which are linked to several neurological diseases in cases when they are improperly regulated. iGluRs are transmembrane channels that allow calcium, as well as other cations, into the post synaptic neuron upon binding of glutamate or other agonists.

Interestingly, iGluR homologs in plants also mediate calcium signaling upon glutamate activation and were accordingly named glutamate receptor-like channels (GLRs). Cell signaling is critical for plant survival to mediate rapid response to growth, defense, and other environmental cues. GLRs are found in all plants and vital for their health, hardiness, and adaptation for growth and survival in unfavorable conditions, such as drought, nutrient poor soil, temperature extremes, pathogens, and predators. Plant research is important with vast applications. Firstly, crops are our primary source of nutrition. In addition, plants are used as sources of drugs that we employ for treating diseases. Some examples of plant-derived neuroactive compounds include caffeine in coffee beans, nicotine in tobacco, and opium from poppy plants. In short, optimizing plant growth is beneficial to maintaining our own survival and potentially achievable by understanding GLRs role in plant health and hardiness. Despite their importance for cell signaling and implication in



plant defense and regeneration, the structural basis underlying the function of these channels remains ambiguous, representing a critical barrier to our understanding of GLR function.

To address this problem, I dedicated my thesis work to study the structure of GLRs and gain insight into their function. There are 20 GLRs in the model plant organism, *Arabidopsis thaliana*, classified into 3 different clades (*AtGLR1-3*). To narrow down which *AtGLRs* to focus our structural studies on, we investigated clade 3 representatives, as many of these GLR3s have been extensively studied in different plant species, especially crops. For example, studying *AtGLR3.4* could provide useful information to how the homolog in rice, *OsGLR3.4*, contributes to growth and production in rice. Studying *AtGLR3.4*'s structure may elucidate how agonistic or antagonistic targets bind and gate the channel, potentially revealing “druggable” targets to alter plant response for defense and regeneration.

Without any structural information available for GLRs, I started my studies by first focusing on their mammalian homologs, iGluRs. I first designed multiple constructs for heterologous expression and purification from cell culture (for example HEK293S GnTI<sup>-</sup> cells). Then, I optimized protein extraction and purification to obtain pure protein samples. Purified proteins were then subjected to cryo-electron microscopy (cryo-EM) which eventually allowed us to solve the structure of *AtGLR3.4*, the first full-length GLR structure.

*AtGLR3.4*'s structure revealed similarities to structures of its mammalian homologs, iGluRs. In comparison to iGluRs, our GLR structure also showed tetrameric subunit assembly, with a three-layer architecture that includes the ligand-binding domain (LBD) in the middle, sandwiched between the extracellular amino terminal domain (ATD) at the top and the transmembrane domain (TMD) at the bottom. In contrast to the majority of iGluR structures, however, *AtGLR3.4* displayed unique symmetry and domain arrangement with the non-swapped

extracellular ATD and LBD domains. We also provided further evidence supporting ligand binding promiscuity that was previously revealed in isolated LBD crystal structures from other *AtGLR3s*. Surprisingly, we found endogenous glutathione bound to the ATDs and demonstrated its contribution to channel activity.

It is important to fill the gaps in knowledge about GLR structure to understand how these channels are activated and gated. In doing so, we will learn more about iGluRs as well as better understand plant defense and growth, which has the potential to enhance crop production for food security and our overall survival.

# Table of Contents

List of Figures .....	iii
Dedication .....	iv
Acknowledgments .....	v
Chapter 1. Background and Introduction .....	1
1.1 Nutrition .....	1
1.2 Plants .....	1
1.3 Introduction to GLRs .....	2
1.3.1 GLRs Discovery .....	2
1.3.1.1 GLRs in Different Plants .....	3
1.3.1.2 Diversity of GLR Genes .....	3
1.3.1.3 Sequence Comparison Amongst GLRs .....	3
1.3.2 Diversity of Plant Functions Related to GLRs .....	4
1.3.3 Physiological Properties of GLRs .....	5
1.3.3.1 <i>AtGLR3.4</i> Role in Plant Reproduction .....	6
1.3.3.2 Roles of <i>AtGLR3.4</i> and <i>AtGLR3.2</i> in Root Growth .....	6
1.3.3.3 GLRs' Signaling in Plant Defense and Immune Response .....	7
1.3.3.4 GLRs in Other Signaling Pathways .....	9
1.3.4 Evolutionary Link GLRs to iGluRs .....	10
1.3.4.1 Homology Between iGluRs and GLRs .....	12
1.4 Introduction to iGluRs .....	12
1.4.1 iGluR Structural Architecture, Domain Layers and Symmetry .....	15

1.4.1.1 iGluR Domain Organization and Subunit Arrangement .....	17
1.4.2 Amino Terminal Domain (ATD) .....	18
1.4.3 Ligand-Binding Domain (LBD) .....	19
1.4.4 Trans Membrane Domain (TMD) .....	22
1.5 Questions Addressed in Thesis .....	25
Chapter 2. Purification and Cryo-EM Structure Determination of <i>Arabidopsis Thaliana</i> GLR3.4 .....	26
Chapter 3. Structure of the <i>Arabidopsis</i> Glutamate Receptor-Like Channel GLR3.2 Ligand- Binding Domain .....	44
Chapter 4. Structure of the <i>Arabidopsis Thaliana</i> Glutamate Receptor-Like Channel GLR3.4 .....	65
References .....	96

## List of Figures and Tables

Figure 1.1. Phylogenetic tree of <i>At</i> GLRs. ....	11
Figure 1.2. Neuronal Synapse. ....	13
Figure 1.3. iGluR Subunit. ....	15
Figure 1.4. Conformational changes of iGluRs. ....	20
Figure 1.5. iGluR functional recording and gating kinetic model. ....	23

## **Dedication**

I would like to dedicate this thesis to my beloved friends and family.

To those who attempt to make the world a better place; to those who spread joy, supply knowledge, and offer peace; to those who participate in protecting our planet for the future; and especially to farmers or anyone providing nutritious food for this hungry world.

## Acknowledgements

I first and foremost want to acknowledge how truly grateful I am to Dr. Alexander Sobolevsky, or Sasha as we call him. I appreciate your mentorship through this PhD thesis work and all my future endeavors. I am forever grateful for Sasha trusting and believing in me (a total novice) to start and pursue this exciting and competitive research project. You showed me how you overcome the challenges and pitfalls in academic research, and plan for success. I admire you as a scientist and a person and hope to someday be an amazing writer and scientist like you. Thank you so much for all your guidance and support.

Thank you to Dr. Jose' A. Feijo', who planted the seeds of interest in this project and fueled my growing obsession with plant science. Deeply grateful and appreciative to all of his insight and guidance and specifically thankful to him and all those who contributed to the work involved in this thesis, providing the necessary plant application background and contributing functional meaning to the structures, in no particular order: Drs. Maria Teresa Portes and Michael A. Lizzio; and especially to those who I have had the pleasure of meeting and learning from, thank you, Drs. Michael M. Wudick, Alexander A. Simon, Erwan Michard, and Juan Barbosa-Caro.

I very much appreciate my qualifying exam committee members, Drs. William S. Blaner, Lawrence S. Shapiro, and Filippo Mancia. Thank you to you all for the stimulating conversations and feedback throughout the years. I also am so very grateful for all your letters of recommendation for my F31 applications. I would also like to thank Drs. Sabrina Diano and Wayne A. Hendrickson, as well as all my dissertation defense committee members (Drs. Sobolevsky, Blaner, and Shapiro) for all your support, time, effort, insight and guidance.

Thank you to all the organizations that allowed me the opportunity to present my research included in this thesis. I learned so much by attending and participating in the Biophysical Society Conference, the ion-channel conferences iGluR Retreat in Pittsburg and Stony Brook, the Plant Calcium Signaling Conference in Milan thanks to Alex Costa, Women in Science at Columbia University Graduate Research Symposium, and thanks to Sam Sternberg, the Columbia University PhD Program Recruitment Event.

I would also like to thank Columbia University Graduate School of Arts and Sciences and the Nutritional and Metabolic Biology PhD Program for accepting me and granting me a fellowship. Thank you all for supporting me and my research throughout the years, including Drs. Debra J. Wolgemuth, Richard J. Deckelbaum, Lori M. Zeltser, Anthony (Tony) W. Ferrante, as well as Zachary Corter, and Sara C. Sternglass.

I am also grateful to those who provided letters of support for my grant applications, Drs. Edward (Ed) T. Eng (from the National Center for CryoEM Access and Training at Simons Electron Microscopy Center and New York Structural Biology Center), Jaime S. Rubin (from Columbia University Department of Medical Sciences) and Robert (Bob) Grassucci (from the Columbia University Cryo-EM Center). I am thankful for support from NYSBC and Pacific Northwest Center for Cryo-EM (PNCC). I am also grateful to have learned so much from Ed's Cryo-EM class and Jaime's grant writing course. I would also like to thank all past and current staff members of Columbia's Cryo-EM center, especially Bob, Zhening Zhang, Surajit Banerjee, Yen-Hong (Harry) Kao, and Thomas. In addition, I would like to thank all those who contributed to my learning experience, Drs. Israel Sanchez Fernandez and his fab vitrification knowledge, Oliver Clarke with his data processing wizardry, Sam Sternberg for supportive



advice and improving how I communicate science, Rosemary J. Cater, Francesca Vallese, Clara Altomare, Brianna Costabile, Aaron P.Owji, and Kookjoo Kim.

I am very appreciative to all the past and current members of the Sobolevsky Lab. Dr. Maria V. Yelshanskaya, also known as Masha, is an excellent lab manager and scientist. She showed me the ropes when I started in lab and provided me comfort during particularly challenging times. Masha maintains all the cell cultures and laboratory reagents, providing us all with the materials so that we can conduct our experiments. Thank you, Masha for always being a source of endless knowledge for us all in lab.

To Dr. Shanti Pal Gangwar, “my partner in crime”, I would like to acknowledge you for your contributions to this thesis and my PhD experience. When you joined the lab and my project, the full-length cryo-EM structure was only at ~9 Angstrom resolution and I was failing to purify the isolated ligand-binding domain. Thanks to your X-ray crystal structure wizardry you showed me the way and provided so much structural biology knowledge. I am so appreciative for your advice, guidance, teamwork, and friendship.

I acknowledge that all past and present Sobolevsky lab members have contributed to my thesis journey. Thank you, Dr. Oleg Klykov, I admire your success and am so appreciative for your contributions to my research experience and to this project. I want to thank Drs. Luke McGoldrick and Appu Kumar Singh, for helping me learn the protocols at the beginning of this project and navigate the Sobolevsky Lab experience. Also thank you to Drs. Jesse B. Yoder, Kirill Nadezhdin, and Arthur Neuberger for all of you emotional and intellectual support with data processing. Kirill and Arthur, thank you both for being like a big brother to me throughout the years.

In addition, I would like to thank rotation students, Ryan G. Casner and Justin P. Williams, for contributing your time and knowledge. To the newest PhD student in the lab, Laura Yen, I would like to thank you providing all your efforts and past experiences to contribute to all those in the lab. I wish you had joined the lab sooner so that we would have had more time together, and I wish you all the joy and success on your PhD journey and beyond. I also would like to express my gratitude to all of my high school and undergraduate mentees, Minjun An, Jeffrey (Jeff) Khau, and Lena Samer Khosrof, for contributing experimentally and bringing energy to the lab. I truly enjoyed teaching you research experiments and being your mentor.

I would also like to thank all my family and friends for their support, faith, and encouragement. Great thanks to my mom and papa, Stephanie and Daniel, you both raised me to believe that I can accomplish anything that I put my mind to and to view happiness as a measurement of success. Special thanks to my little sissy, Allison, I am so proud of you and appreciate you helping me with checking my grammar and punctuation. Sissy, you mean the world to me and thank you for holding my hand through life. To Alene, we have grown up together, ever since meeting in the third grade you have been the best friend and I am forever grateful for your presence in my life. Gabriel, thank you for everything. Thank you, Caroline and Madeline, for showing up and being there for me, my life is enriched with you both by my side.

Thank you to the Kanesters, to Emma, to the Seemanns, to Grandma Connie for inspiring me to be adventurous, to Grandma Doni for teaching me to not worry about things out of my control, and to Grandpa Tom for lessons on expecting more from myself. I am so grateful for the impact all my family, friends and loved ones have had on my life.

Thank you to my cohort for always being there for me, watching my practice presentations, and providing supportive advice through out the years, not sure where I would be with out you all, thank you to Madeline Edwards, Caroline Connors, Marina Triplett, Leonie Brockmann, Xinran Ma, Jonah Einson, Mariko Kanai, Tina Xiang, Debbie Seo Hong, Daniele Neri, Nati Maria Bobba, Andrew Vandenberg, Crystal Colon Ortiz, Tim Zhong, Nikki Aaron, Grace Sarah Herod, Lukas Vlahos, Daniel Moakley, Miles Richardson, Sho Iketani, Lucas Loffredo, Chrystal Mavros, Sanne Klompe, Pedro del Rivero Morfin, Rosa Louise Vincent, Amanda Decker, Ariana Gavin, Caroline Rauffenbart, Jeffrey Bellah, Alyssa Shearer, and to all the members and participants in Women in Science at Columbia and Graduate Initiative for Diversity. I am very appreciative and grateful for all the help I received from the undergraduate financial aid grants and scholarships, the professors and researchers (including Drs. K. Barry Sharpless, Elad Tako, Donald L. Robertson, and Elizabeth Komives), all those who influenced me and were instrumental in my journey leading up to my thesis work.

Thank you, Sasha – none of this would have been possible without you.

# **Chapter 1.**

## **Background and Introduction**

### **1.1 Nutrition**

In 2021, the World Health Organization (WHO) estimated 828 million people in the world were affected by food insecurity, which has been impacted by climate hardships, such as droughts or floods (WHO, 2022). As food security worsens, it is imperative that agriculture and food productivity are improved to facilitate appropriate strategies for defeating hunger and malnutrition (Wu et al., 2014). Global food security concerns can be alleviated by harnessing the ability to enhance crop yield potential and improve agricultural production as means to combat global malnutrition through climate change. However, there is a missing gap in knowledge in order to do so (Chen & Ham, 2022).

### **1.2 Plants**

Worldwide crop production is currently insufficient in meeting human nutritional requirements due to production loss or agricultural issues that arise from environmental factors, such as disease, temperature extremes, drought, pests, and poor water quality from pesticide contamination (Brodt, 2011; Kc et al., 2018; Shipman et al., 2021). In order to improve agricultural productivity and sustainability for a global food supply, research is needed to investigate the mechanisms that regulate plant growth, development, and acclimation to enhance the stress tolerance and wound response in crop plants (Chen & Heidari, 2020). For these mechanisms, plants use signaling and response systems coordinated across the whole organism, critical for maintaining cellular homeostasis, signaling, response to environmental cues, and

overall survival (Brenner et al., 2006; De Bortoli et al., 2016; Grenzi et al., 2022). As plants represent the primary source of food supply for human survival, it is important to fill these gaps of knowledge in plant cellular signaling. Cell signaling plays a role in various plant physiological functions, such as plant reproduction, development, root growth, and immune response to pathogens, herbivore attacks and mechanical wounding. A potential target to enhance plant hardiness is the glutamate receptor-like channels (GLRs) due to their vital roles in mediating cell signaling for overall plant health.

## **1.3 Introduction to GLRs**

### **1.3.1 GLR Discovery**

In 1998, Lam et al. discovered genes encoding putative ionotropic glutamate receptors (iGluRs) in the model plant organism *Arabidopsis thaliana*, also referred to as *Arabidopsis*, and named them glutamate receptor-like channels (GLRs) (Lam et al., 1998). By screening complementary deoxyribonucleic acid (cDNA) libraries with expressed sequence tag clones, Lam et al. isolated full-length *Arabidopsis* GLR (*AtGLR*) cDNAs and presented preliminary evidence for GLR involvement in light-signal transduction (Lam et al., 1998). In addition, *Arabidopsis* genomic sequence of a bacterial and yeast artificial chromosome clones were also used to derive GLR sequences (Lam et al., 1998). This cloning and screening showed that *AtGLR* cDNAs encoded proteins that display amino acid sequence similarity with mammalian iGluRs, thus identifying animal iGluR homologs in plants (Lam et al., 1998). Based on these findings, the authors proposed that a primitive cell signaling mechanism existed before the divergence of plants and animals, one that evolved to the signaling between cells from excitatory

amino acids, as in animal brains. This may explain why neuroactive compounds sourced from plants work on mammalian receptors (Chiu et al., 1999; Lam et al., 1998).

### **1.3.1.1 GLRs in Different Plants**

GLRs are found all throughout the plant kingdom, in the genomes of gymnosperms and angiosperms and *Chlamydomonas*, chlorophytes, mosses, ferns, and flowering plants (De Bortoli et al., 2016) (Chiu et al., 1999; Wudick, Michard, et al., 2018). Nevertheless, GLRs are thus far not found in yeast, eubacteria, fungi, and archaeobacteria (Chiu et al., 1999; Wudick, Michard, et al., 2018). Interestingly, GLRs have also been identified in the nematode *Caenorhabditis elegans* as well as in marine invertebrates, such as the sea anemone *Nematostella vectensis*, and the ctenophora *Pleurobrachia bachei* (Wudick, Michard, et al., 2018).

### **1.3.1.2 Diversity of GLR Genes**

There is a broad diversity in the GLR superfamily, with the highest sequence variability among the algal sequences, includes diatoms (large contributors to the world's oxygen), brown algae, cryptophytes, and green algae (De Bortoli et al., 2016). GLRs are expressed throughout the entire *Arabidopsis* plant, and have been reported in petiole tissue, leaves, stem, and roots, with subcellular localization in plastids, vacuolar system, endoplasmic reticulum, and like iGluRs, in the plasma membrane (Meyerhoff et al., 2005; Nguyen et al., 2018; Teardo et al., 2015; Teardo et al., 2011; Vincill et al., 2013; Wudick, Portes, et al., 2018).

### **1.3.1.3 Sequence Comparison Amongst GLRs**

The GLR superfamily has been divided into subfamilies based on similarities in amino acid sequences. Based on the prediction of subcellular localization, no strong conserved group-

specific feature was developed during the evolution of GLRs (De Bortoli et al., 2016). The evolutionary origin of plant GLRs have been explored via phylogenetic analysis and showed that the plant GLR family had an original group, *GLR0*, that differentiated into stable and distinguishable subgroups GLR1-4 (Forde & Roberts, 2014). There are 4 different GLR clades, GLR1-4, that have been identified in land plants, with *GLR3* clade being the closest to *GLR0* (Chen et al., 2016; De Bortoli et al., 2016; Forde & Roberts, 2014). None of the *At*GLRs falls into clade 4 based on the classification of amino acid sequence similarities (De Bortoli et al., 2016). Clade 3 appears to be the most ancient group of GLRs containing a particularly consistent set of sequences (De Bortoli et al., 2016). Comparing sequences of different *At*GLRs clades (*At*GLR1-3), the region of highest sequence variability is the C-terminus (Wudick, Michard, et al., 2018).

### **1.3.2 Diversity of Plant Functions Related to GLRs**

*Arabidopsis thaliana* is a model plant organism where 20 GLR isoforms have been identified and grouped into 3 different clades (Wudick, Michard, et al., 2018). GLRs play signaling roles throughout the plant that provides a vast variety of vital physiological functions, such as response to mechanical wounding, reproduction, pollen development, response to herbivore attack, sexual reproduction, response to pathogens, chemotaxis, regulation of stomatal aperture, immunity, and root development (Grenzi et al., 2022). More recently explored roles include long-distance electrical and calcium signaling, linked to GLRs' involvement in regulation of ion fluxes across membranes and in particular calcium fluxes, as calcium represents a key second messenger in plant cell responses to both endogenous and exogenous stimuli (Grenzi et al., 2022).

The plant hormone jasmonic acid (JA) signals mediate growth and defense responses (Li et al., 2022). GLRs are involved in the stimulation of JA production, which can be triggered by biotic stress (Li et al., 2020). Biotic stress is stress from another living organism causing damage, like a pest eating a leaf. According to the Food and Agriculture Organization of the United Nations, each year up to 40 percent of global crop production is lost to pests while the global economy loses over \$220 billion due to plant disease related costs (Relations, 2021). A key component to maintain or improve current and future food security is by protecting plants from pests and diseases through curative and preventive measures (*Scientific review of the impact of climate change on plant pests*, 2021).

When sessile plants are physically attacked with mechanical wounding (such as damage from pests), JA increase happens at the site of damage as well as in distal, unharmed tissue. It has been reported that several GLRs, especially those from clade III, are expressed in vascular tissues and play a role in the generation and transmission of long-distance electrical and  $\text{Ca}^{2+}$  signals acting upstream of JA signaling (Moe-Lange et al., 2021; Nguyen et al., 2018; Toyota et al., 2018). When GLRs are mutated, the plant's response to pests are hindered, illustrating GLRs participation in plant stress response (Toyota et al., 2018).

### **1.3.3 Physiological Properties of GLRs**

Plants live in perpetually changing environments and are relentlessly bombarded with various stressors unfavorable for growth and development (Tian et al., 2020; Zhu, 2016). Plants use calcium as a second messenger in cell signaling to respond to stress signal and to cope with these abiotic and biotic stressors for survival (Tian et al., 2020). Adverse environmental conditions include abiotic and biotic stressors, stress conditions imposed by non-biological and



biological factors respectively. Examples of biotic stress for plants include herbivore attack from animals and insects, invasive plant species, and pathogen infection from bacteria, viruses, and fungi (Tian et al., 2020; Zhu, 2016). The non-biological factors that cause stress in plants include various abiotic stressors from the environment, such as pH imbalance from excess salt or toxic metals like aluminum, arsenate, and cadmium in the soil, water conditions, nutrient deficiency, light intensity, and temperature extremes (Tian et al., 2020; Zhu, 2016). These environmental factors not only affect natural geographical distribution of plants, but also threaten food security by limiting plant productivity in agriculture (Zhu, 2016).

### **1.3.3.1 *AtGLR3.4* Role in Plant Reproduction**

A specialized structure in plants, called the pollen tube, is essential for sexual reproduction. It serves as a vehicle to deliver sperm cells, which are known in plant biology as male gametes, to a female gametophyte during double fertilization to eventually lead to seed formation (Adhikari et al., 2020). Pollen tubes growth and function have been reported to be  $\text{Ca}^{2+}$  influx-dependent (Michard et al., 2017). Since GLRs are known to be involved in  $\text{Ca}^{2+}$  signaling and plant reproduction, studies have looked into investigating *AtGLRs* functional roles in pollen tubes (Wudick, Portes, et al., 2018).

For example, *AtGLR3.4* contributes to plant reproduction by regulating pollen tube calcium fluxes in addition to pollen tube development (Green et al., 2021). Pollen grain delivers sperm cells to the embryo sac via polar tip growth of the pollen tube to participate in embryo and endosperm production (Kim et al., 2021). *AtGLR3.4* localizes to the aperture of the pollen grain and is associated with cell polarity in pollen tubes, which is characterized by an influx of calcium at the tip (Green et al., 2021; Michard et al., 2011; Michard et al., 2017).

### **1.3.3.2 Roles of *AtGLR3.4* and *AtGLR3.2* in Root Growth**

Lateral roots span underground as they are the building blocks of the plant's root system (Torres-Martínez et al., 2019). Lateral root primordium is formed as the early stages of lateral root formation and organization (Torres-Martínez et al., 2019; Wachsman & Benfey, 2020). Root branching relies on the formation of lateral roots, which allows the plant to extract nutrients from the soil (Fernández-Marcos et al., 2017; Pechanova & Pechan, 2017). Phloem is the portion of the plants vascular tissue that conducts the transport of soluble organic compounds, such as sugars, along with some water and minerals to the rest of the plant (Mauseth, 2021). The apoplast is another area of the plant, that makes up the intercellular spaces and cell walls of the plant (Mauseth, 2021).

The number of lateral root primordia was increased in *Arabidopsis* when either *Atglr3.2* or *Atglr3.4* were mutated individually or together (Vincill et al., 2013). This increase is suggested to be an apoplastic (pathway through the cell wall) amino acid-dependent response acting through the formation of *AtGLR3.2/AtGLR3.4* heteromeric channels that affect lateral root development via calcium signaling in the phloem (Grenzi et al., 2022; Vincill et al., 2013).

### **1.3.3.3 GLRs' Signaling in Plant Defense and Immune Response**

Plant pathogens, such as pathogenic fungus *Penicillium expansum*, are a major concern to the food industry on a global scale due to its wide occurrence and ability to produce toxic compounds, mycotoxins. Mycotoxins are produced by molds, fungi, and provide a health risk to humans as some can cause disease and even death. Providing protection against plant pathogens is an important step towards providing food security and combating global hunger and malnutrition. Studying ways in which to improve plants hardiness provides valuable efforts

needed for our future survival. For example, it has been discovered that one way to inhibit plant pathogen growth and minimize mold rot on fruit, such as *Penicillium* growth on pears, is with a topical glutamate treatment (Jin et al., 2019).

Plant pathogens can impair plant growth and reproduction. Thus, understanding their innate immune system used in infection response could bolster crop improvement (Jones & Dangl, 2006). For example, in *O. Sativa* and *Solanum lycopersicum* (rice and tomato, respectively), exogenous L-Glu treatment induced the expression of genes involved in pathogen-associated molecular patterns (PAMPs) stimulated by a bacterial flagellin-derived peptide, flg22, response in *Arabidopsis* and fungal resistance (Bethke et al., 2009; Goto et al., 2020; Kadotani et al., 2016; Yang et al., 2017).

Plants use calcium signaling for defense, regeneration, and systemic immune responses upon wounding (Hernández-Coronado et al., 2022; Shanmukhan et al., 2020). The antioxidant glutathione (GSH) has been shown to induce defense response and increase cytosolic calcium concentration,  $[Ca^{2+}]_{cyt}$  (Li et al., 2013). In *Arabidopsis*, GSH-modulated defense genes in a GLR-dependent manner (specifically *AtGLR3.3*) (Li et al., 2013). An example of one of the many defense genes upregulated is Lipxygenase4 for jasmonic acid biosynthesis (Acosta & Farmer, 2010; Li et al., 2013).

GSH suppressed the spread of pathogen in wild type *Arabidopsis* leaves but not in the *Atglr3.3* mutants (Li et al., 2013). Extracellular GSH concentration,  $[GSH]_{ext}$ , induces  $[Ca^{2+}]_{cyt}$  rise and promotes innate immunity responses in *Arabidopsis* leaves through *AtGLR3.3*-dependent pathways (Li et al., 2013). Similar to GSH, glutamate also evokes a *AtGLR3.3*-dependent rise in  $[Ca^{2+}]_{cyt}$  (Li et al., 2013).

In wild type *Arabidopsis*, GSH was not only shown to increase cytosolic calcium concentration but also to induce an upregulation of defense genes (Li et al., 2013). Induced gene expression was also observed for *AtGLR3.4* when exposed to mechanical stress (touch) and cold temperature (Meyerhoff et al., 2005). In addition to cold and touch, *AtGLR3.4* expression was also induced by glutamate (Glu) (Meyerhoff et al., 2005).

### 1.3.3.4 GLRs in Other Signaling Pathways

GLRs have a diverse range of functions in plants and play important physiological roles. In rice (*Oryza sativa*) for example, the GLR gene *OsGLR3.4*, an ortholog to *AtGLR3.4*, has been reported to be required for plant growth and systemic wound signaling (Yu et al., 2022). Like most GLRs, *OsGLR3.4* has been indicated to be a  $\text{Ca}^{2+}$ -permeable channel. In an agonist profile assay, multiple amino acids have been shown to trigger transient  $\text{Ca}^{2+}$  influx in an *OsGLR3.4*-dependent manner (Yu et al., 2022). Out of 20 amino acids tested, the amino acids that induced a  $\text{Ca}^{2+}$  flux via *OsGLR3.4* were Ala, Arg, Asn, Cys, Glu, Gly, Leu, Lys, Pro, Ser, and Thr (Yu et al., 2022). Yu et al., reported *OsGLR3.4* mediates long-distance wounding response and is required for root-to-shoot systemic wound signaling in rice (Yu et al., 2022). When *OsGLR3.4* was lacking, they observed a missing downstream response to leaves upon root injury, a disruption of actin filament organization and growth defects (Yu et al., 2022).

In plant cells, the salt overly sensitive (SOS) signaling pathway is a key regulator to maintain low cytoplasmic sodium concentration (Cheng et al., 2018; Deinlein et al., 2014; Zhu, 2002). Under salt stress, three SOS genes, *SOS1*, *SOS2*, and *SOS3*, showed reduced expression in *Atglr3.4* mutants treated with NaCl, compared to wild type *Arabidopsis* (Cheng et al., 2018). In comparison to wild type, *Atglr3.4* mutants in the presence of high salt (150 and 200 mM

NaCl) showed lower rates of seed germination and a greater increase in  $\text{Na}^+$  concentration accumulated in seeds (Cheng et al., 2018). An increase in NaCl leads to an increase in  $[\text{Ca}^{2+}]_{\text{cyt}}$ , and *AtGLR3.4* modulates  $[\text{Ca}^{2+}]_{\text{cyt}}$  variation when the plant is exposed to salt stress. Accordingly, *Atglr3.4* mutants showed suppressed  $[\text{Ca}^{2+}]_{\text{cyt}}$  increase in response to salt stress (Cheng et al., 2018).

### 1.3.4 Evolutionary Link GLRs to iGluRs

Phylogenetic trees are diagrams that depict the lines of evolutionary descent of organisms, genes, or different species from a common ancestor, and are used to study various aspects of evolution (Baum, 2008). The phylogenetic tree in Figure 1.1 includes all 20 *AtGLRs* that make up the 3 clades. Upon GLR discovery, examination of amino acid sequence similarity with other genes suggested that plant GLRs are most closely related to animal iGluRs and much more distantly related to other ion channels, such as  $\text{GABA}_A$  and acetylcholine receptors, or potassium channels (Chiu et al., 1999; Price et al., 2012). Phylogenetic analyses suggested that plant and animal iGluRs diverged from a common ancestor instead of being products of convergent evolution of genes with similarities (Chiu et al., 1999; Price et al., 2012).

The percent identity between the full-length amino acid sequences from a GLR of the third clade (*AtGLR3.4*) and representatives of the four subtypes of iGluRs ranges from around 21 to 24% (calculated with protein-protein BLAST) (Altschul et al., 1997; Altschul et al., 2005). iGluR subtype representatives in this case are GluA2 for AMPA ( $\alpha$ -amino-3-hydroxy-5-methyl-4-isoxazolepropionic acid) receptors, GluN2A for NMDA (*N*-methyl-D-aspartate) receptors, GluK2 for kainate receptors, and finally GluD1 and GluD2 for the  $\delta$ -receptors. Specifically, *AtGLR3.4* has the following percent identities to these human iGluR subtypes: 23.84% for

GluD1, 21.14% for GluD2, 22.12% for GluA2, 24.88% for GluN2A, and 23.76% for GluK2 (Altschul et al., 1997; Altschul et al., 2005). The common ancestry for these human iGluRs along with all 20 *At*GLRs are shown in Figure 1.1's phylogenetic tree branches.

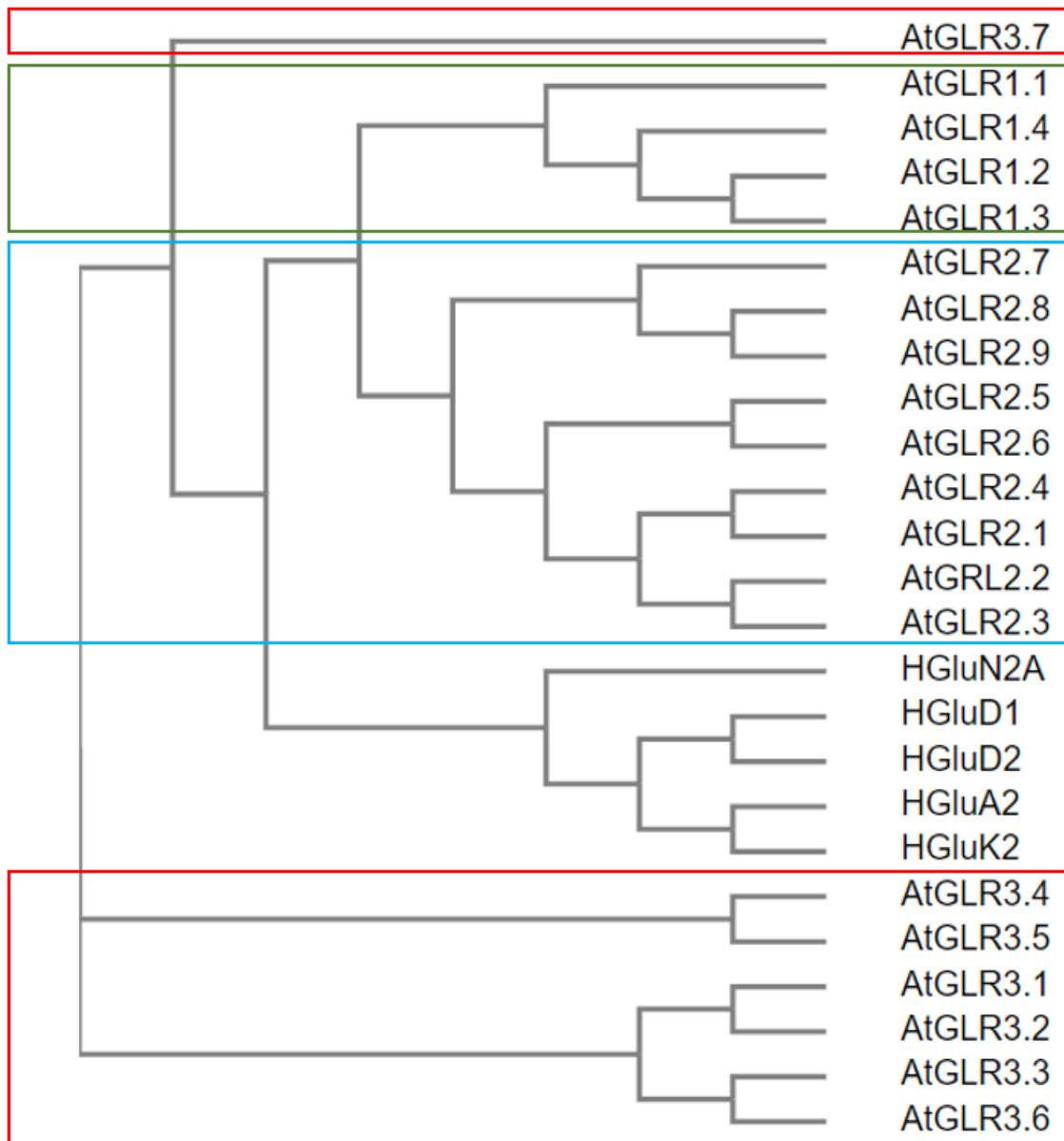


**Figure 1.1. Phylogenetic tree of *At*GLRs.** Phylogenetic tree, including all 20 *At*GLRs that are divided into the 3 clades. Each GLR clade is denoted by a color, clade 1 is boxed in green, clade

2 is boxed in blue, and GLRs of the third clade are boxed in red. The 5 example subtypes of human iGluRs included in the tree are unbox. The phylogenetic tree was created with ClustalOmega viewing cladogram branch length to show common ancestry rather than the amount of evolutionary time separating the GLRs.

### **1.3.4.1 Homology Between iGluRs and GLRs**

Upon GLR discovery, Lam et al. reported that the degree of identity between *At*GLRs and mammalian iGluRs is 16% to 63% within certain regions (the S1, S2, and M1 to M4 domains) that is similar to the degree of identity in the same regions (LBD and TMD) between the kainate and AMPA subtypes of animal iGluRs (Lam et al., 1998). Based on the analysis of sequenced regions and overall sequence homology, plant GLRs were shown to be similar to both NMDA and non-NMDA iGluR subtypes, suggesting that iGluRs and GLRs diverged prior to their clade differentiation (Weiland et al., 2015; Wudick, Michard, et al., 2018).

## **1.4 Introduction to iGluRs**

The most abundant free amino acid in the brain is glutamate (Zhou & Danbolt, 2014). Glutamate is the principle excitatory neurotransmitter in the central nervous system (CNS) and it is crucial for sensory and cognitive functions as it mediates/determines communication between neurons by traveling through their synapses, the electrochemical junctions between neuronal cells (Pankevich, 2011; Traynelis et al., 2010; Volk et al., 2015) (Figure 1.2).

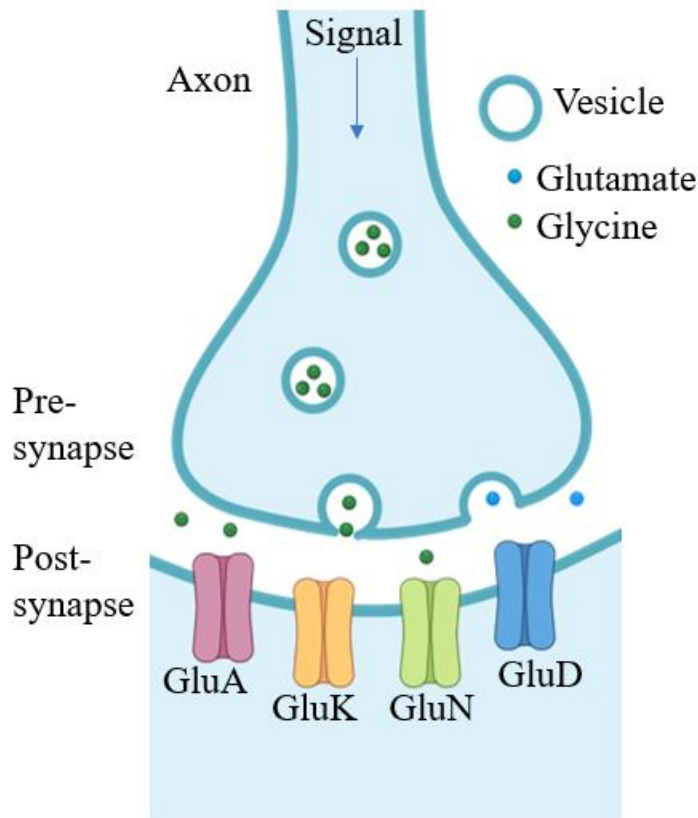


**Figure 1.2. Neuronal Synapse.** Four subtypes of iGluRs are schematically represented in the postsynaptic membrane. The red channel, GluA, represents the AMPA ( $\alpha$ -amino-3-hydroxy-5-methyl-4-isoxazolepropionic acid) receptor, the GluK (kainate receptor) is shown in orange, GluN subtypes of NMDA (*N*-methyl-D-aspartate) receptor is in green and the GluD (delta receptor) is in blue. Created with BioRender.com

Research in the field of glutamate receptors began over 30 years ago. Glutamate, as well as other amino acids, function as ligands that activate glutamate receptors. Ionotropic glutamate receptors (iGluRs) are ligand-gated ion channels. Ligand-gated ion channels allow ions to pass through their pores upon ligand binding and activation. In mammals, iGluRs play an important role in integrative cognitive processes (memory and learning) (Hansen et al., 2021). Abnormal



iGluR function results in a wide range of neurological diseases linking iGluR to the pathology of depression, psychosis, and even neurological diseases, such as Alzheimer's disease (Hansen et al., 2021).

In humans, eighteen iGluR subunits have been identified and divided into four different subtypes, which are distinguished based on their amino acid sequence similarity and were named based on agonist selectivity: AMPA ( $\alpha$ -amino-3-hydroxy-5-methyl-4-isoxazolepropionic acid), NMDA (*N*-methyl-D-aspartate), kainate (KA), and  $\delta$ -receptors (also referred to as delta-receptors or GluD receptors) (Hansen et al., 2021) (Zhou & Danbolt, 2014). There are four subunits of the AMPA (GluA1-4), seven of the NMDA (divided into three clades GluN1-3) and five of the kainate (GluK1-5) subtypes, respectively. The GluD subtype has only two subunits (GluD1-2). Some iGluRs are assembled as homomers, while others are heteromers, formed from subunits of their respective iGluR class. In other words, subunits from two different subtypes would not be able to form a functional receptor. For example, GluN1 and GluA1 are from two different subtypes and would not assemble, but GluN1 and GluN3 form a functional iGluR heteromer.

Glutamate is an agonist that activates three of the four iGluR subtypes, with GluD subtype activated by glycine or D-serine only (Carrillo et al., 2021; Yelshanskaya et al., 2022). Among NMDA receptor (NMDAR) subunits, GluN2 subunits (GluN2A-D) bind glutamate, while GluN1 and GluN3 (GluN3A-B) bind glycine and D-serine (Hansen et al., 2021). The iGluRs that are activated by glutamate show high sequence conservation in the LBD agonist binding pocket, unlike the subunits that bind D-serine or glycine that have more variability in

this region (Hansen et al., 2021). All iGluR subtypes are expressed in the vertebrate central nervous systems (CNS) and mediate the majority of excitatory neurotransmission.

### 1.4.1 iGluR Structural Architecture, Domain Layers and Symmetry

Four individual subunits (monomers denoted A-D) assemble the iGluR tetramer. Starting from the plasma membrane growing out towards the extracellular region, the common architecture of each iGluR subunit consists of a transmembrane domain (TMD), ligand-binding domain (LBD), and an N-terminal domain (NTD), also referred to as the amino-terminal domain (ATD). The ATD, LBD, and TMD are the three domain layers of iGluRs, shown in Figure 1.3.

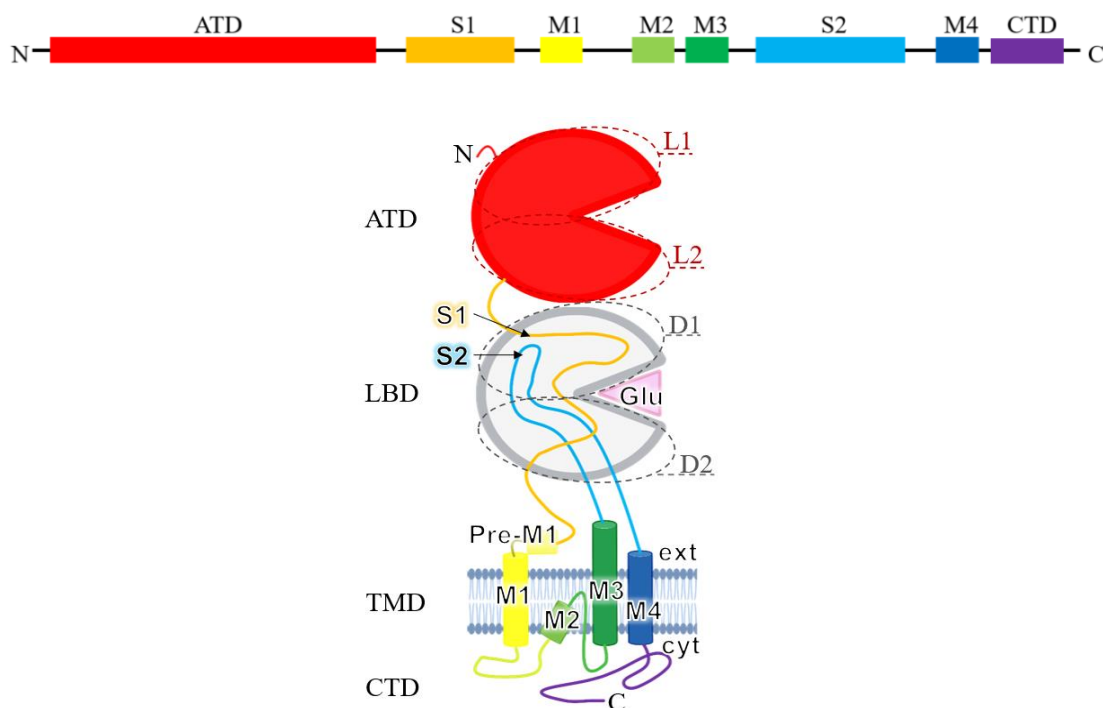


**Figure 1.3. iGluR Subunit.** One iGluR subunit linear representation of the polypeptide chain of above with labeled and color-coded domain that match the below topology of an iGluR subunit.

The extracellular ATD mediates receptor trafficking, assembly, and functional regulation (Ayalon & Stern-Bach, 2001; Hansen et al., 2021; Traynelis et al., 2010; Yelshanskaya & Sobolevsky, 2022). The clamshell shaped ATD is assembled of the upper L1 and lower L2 lobes. While the ATD is formed by single contiguous stretch of the polypeptide, the upper D1 and lower D2 lobes of another iGluR domain, LBD, are assembled from two polypeptide stretches, S1 and S2. The LBD harbors binding sites for agonists, competitive antagonists and positive and negative allosteric modulators (PAMs and NAMs, respectively) (Hansen et al., 2021; Yelshanskaya & Sobolevsky, 2022). PAMs increase the response elicited by agonists; they can either increase the affinity of the agonist to the receptor, for example by slowing down channel deactivation, or inhibit receptor desensitization (Brogi et al., 2019). The TMDs of four subunits include the M1 – M4 segments and together assemble the ion-conducting channel (Wollmuth & Sobolevsky, 2004). M4 is followed by the structurally undetermined intracellular carboxy-terminal domain (CTD), which plays a role in receptor trafficking and synaptic localization (Hansen et al., 2021; Yelshanskaya & Sobolevsky, 2022).

Structural studies of iGluR began at the end of the 20<sup>th</sup> century with a publication on the first crystal structure of the isolated ligand-binding domain of GluA2 in 1998 (Armstrong et al., 1998). This structure confirmed the two-lobe LBD clamshell topology, which was proposed earlier based on homology with bacterial periplasmic amino-acid binding proteins (Stern-Bach et al., 1994). The first full-length iGluR structure was solved eleven years later, in 2009 (Sobolevsky et al., 2009). This 3.6-Å resolution full-length iGluR crystal structure of AMPA-subtype rat GluA2 receptor was determined in complex with a competitive antagonist and for the first time provided a complete view of iGluR structural organization and domain arrangement

(Sobolevsky et al., 2009). Although different iGluR families have varying kinetic and pharmacological properties, their overall structural design remains similar.

### **1.4.1.1 iGluR Domain Organization and Subunit Arrangement**

iGluR structural studies demonstrated the overall two-fold rotational symmetry in extracellular domains where the axis of symmetry runs perpendicular to the cell membrane and the subunits A-D are paired differently into two dimers at the ATD and LBD layers of the structure. The subunits A and B pair forms one dimer (AB) in the ATD layer, while subunit C pairs with subunit D to form the other dimer (CD). Within each ATD dimer, the conformations of subunits are identical, and they are related by a local two-fold rotational symmetry. The distal (A and C) and proximal (B and D) subunits that belong to different ATD dimers also have similar conformations but are related to each other through the axis of the overall two-fold rotational symmetry of the receptor.

In the LBD layer, also known as the agonist binding domain (ABD) layer, the subunits pair differently from the ATD layer creating a so-called domain swapping between these two layers. During this rearrangement, the AB and CD subunit pairs that form the corresponding pair of dimers in the ATD layer swap partners to create a different dimer of dimers in the LBD. In the LBD, subunit A is paired with subunit D, assembling an AD dimer, while subunit B is paired with subunit C, forming a CB dimer.

The overall symmetrical organization and domain arrangement is preserved in AMPA, NMDA, and kainate receptors with the only major iGluR outlier being GluD receptors. As evidenced by the recent structural studies of homotetrameric GluD1 and GluD2, GluD receptors are an exception to the common iGluR domain arrangement because they do not show swapping

of subunit domains between the ATD and LBD layers (Burada et al., 2020a, 2020b). Independent of the presence of domain swapping between the ATD and LBD layers, all iGluRs appear Y-shaped when viewed parallel to the membrane and display an overall two-fold rotational symmetry with the axis of symmetry perpendicular to the membrane. The extracellular domains (ECDs) show similar arrangement of distal and proximal subunit domains in both the LBD and ATD layers. Thus, iGluR subunits A and C are distal, while B and D are proximal in the ATD layer, whereas subunits A and C are proximal while B and D are distal in the LBD layer.

The four iGluR subunits' TMDs come together to assemble a pore in the cellular membrane and form a cation-selective ion channel. The two diagonal subunit pairs that form the 2-fold symmetrical ECD come together to assemble a pseudo-4-fold symmetrical TMD. The TMD of one subunit consists of three transmembrane helices (M1, M3, and M4) and a re-entrant pore loop (M2). Each subunit LBD connects to their TMD by three peptide linkers, S1-M1, M3-S2, and S2-M4. The iGluR pore lining of the permeation pathway is contributed by the extended region of the re-entrant M2 pore loop as well as the M3 transmembrane helices (Hansen et al., 2021; Huettner, 2015; Sobolevsky et al., 2009; Tikhonov & Zhorov, 2020; Traynelis et al., 2010; Wollmuth & Sobolevsky, 2004). iGluRs across all phyla have M1-M3 pore domains present, but the transmembrane helix at the periphery of the pore domain (the M4 segment) is eukaryotic-specific (Stroebe & Paoletti, 2021).

### **1.4.2 Amino Terminal Domain (ATD)**

Initial crystal structures of isolated iGluR ATD (GluA2) demonstrated tightly associated ATD dimers that confirmed the role of this domain in guiding subtype-specific receptor

assembly (Jin et al., 2009). The clamshell shaped ATD of the iGluR subunits are formed from upper and lower lobes (L1 and L2, respectively) and the region with the highest conservation in the ATD is the L1-L1 interface (Herguedas et al., 2013). iGluR ATDs fall into type-1 periplasmic-binding protein (PBP) superfamily due to characterization of two lobes that are separated by a deep cleft (Herguedas et al., 2013; Quirocho & Ledvina, 1996). Indeed, there is a highly conserved sequence Leucine/Isoleucine/Valine binding protein (LIVBP) in the ATD of iGluRs, which is shared with bacterial binding proteins (PBPs), LBDs of metabotropic glutamate receptors (mGluRs) and gamma-aminobutyric acid (GABA) receptors (Kunishima et al., 2000).

### **1.4.3 Ligand-Binding Domain (LBD)**

Based on homology to periplasmic amino acid-binding proteins, iGluR LBD structure was proposed to be formed by two discrete segments separated by channel-forming domains (Stern-Bach et al., 1994). Indeed, the LBD turned out to be composed of the S1 and S2 polypeptides (Arvola & Keinänen, 1996; Kuusinen et al., 1995; Stern-Bach et al., 1994) separated by the M1 transmembrane helix, the M2 pore loop, and another transmembrane helix M3 (Hollmann et al., 1994; Wo & Oswald, 1994). Two polypeptide stretches S1 and S2 of each iGluR subunit form one clamshell-shaped LBD. The binding site for agonists and antagonists is located in the cleft of the clamshell formed by upper (closer to the ATD) and lower (closer to the TMD) lobes of the clamshell, referred to as D1 and D2, respectively. The D1 lobe of LBD of one subunit makes an interface with the D1 LBD lobe of the neighboring subunit, creating an LBD dimer. The ATD-S1 polypeptide linker joins the LBD to the ATD, while the LBD is connected to the TMD via the S1-M1, M3-S2, and S2-M4 linkers.

These LBD-TMD linkers mediate conformational changes that transmit agonist binding to channel gating. The LBD of iGluRs have variations in agonist binding properties, with different iGluR subtypes having different ligand specificity for LBDs. When an agonist binds to the AMPA receptor binding site (also referred to as the binding pocket) in the LBD, the lower D2 lobes moves away from the central axis towards the D1 lobe, resulting in a closed LBD clamshell conformation (Armstrong & Gouaux, 2000; Hansen et al., 2021; Hogner et al., 2002). The movement of the D2 lobe in each AMPA receptor subunit causes a separation of the D2s in the context of the LBD dimer (as the LBD takes a dimer of dimers arrangement via D1 interfaces) and pulls on the LBD-TMD linkers allowing the ion channel to open (Chen et al., 2017; Twomey et al., 2017a; Yelshanskaya & Sobolevsky, 2022). Similar to AMPA receptors (Armstrong & Gouaux, 2000; Sobolevsky et al., 2009; Twomey et al., 2017a; Wollmuth & Sobolevsky, 2004), structural changes in kainate (Bowie, 2010; Nayeem et al., 2011; Perrais et al., 2010) and NMDA (Auerbach & Zhou, 2005; Chang & Kuo, 2008; Kussius et al., 2010) receptors experience LBD clamshell closure upon agonist binding and opening upon competitive antagonist binding (Hansen et al., 2021).

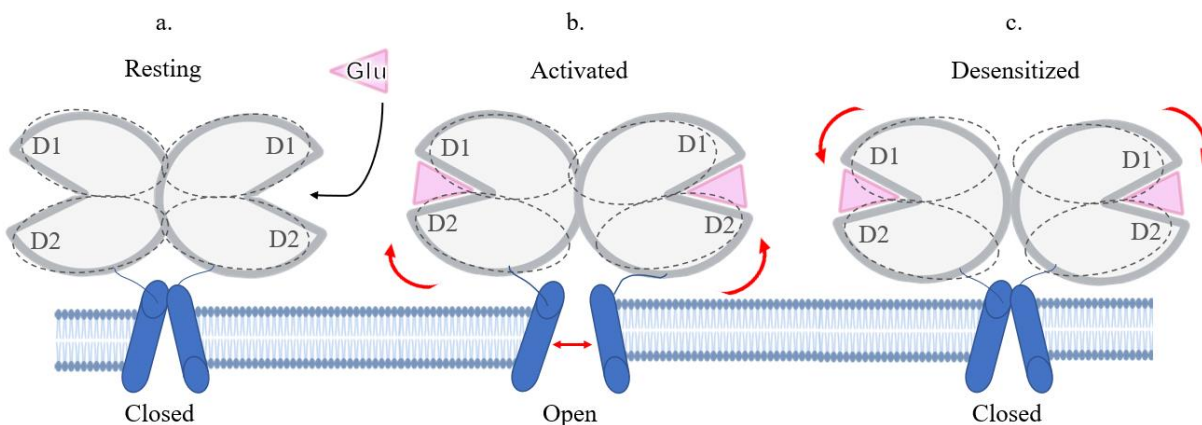


**Figure 1.4. Conformational changes of iGluRs.** Conformational changes from the closed channel resting state (a), to the channel opening in the ligand (Glu) activated state (b), and then closed desensitized state (c). For clarity, the figure shows only two subunits without the ATD. Adapted illustration of the GluA2 AMPA receptor homomer (Armstrong et al., 2006; Hansen et al., 2021).

After agonist binding to the LBDs of the closed-state AMPA receptor, the D2 lobes move towards D1 lobes converting each clamshell to a closed conformation (Figure 1.4a). While the D1-D1 interface remains intact, the resulting D2-D2 separation leads to channel opening (Figure 1.4b). Upon AMPA receptor desensitization, the D1-D1 interface ruptures, separating the D1 lobes and while the clamshells remain agonist-bound and closed, leading to the reduction of distance between D2 lobes (Figure 1.4c). Reduced separation of the D2 lobes releases the strain on linkers and allows the channel to close. Conformational transition of the LBD dimer to the desensitized state can be accompanied by the loss of the local two-fold symmetry of the dimer, like in the GluA2-GSG1L complex for instance, (Twomey et al., 2017b) (Klykov et al., 2021),



while in other cases, such as GluA2-y2 and GluA2-y5 complexes, the dimer remains two-fold symmetrical (Chen et al., 2017; Klykov et al., 2021).

In comparison to AMPA receptors, structural information about desensitization in kainate and NMDA receptors is limited (Hansen et al., 2021). The lack of open- and apo-state structures of kainate receptors prevents detailed comparison of kainate receptor gating to gating in AMPA receptors. However, based on what is known, desensitization in kainate receptors is considered to be accompanied by LBD dimer dissociation, consistent with AMPA receptors (Hansen et al., 2021). Functional characterization has revealed that NMDARs can become desensitized a few different ways, some of which depend on the presence or binding of glutamate, Zinc ( $\text{Zn}^{2+}$ ), glycine, and  $\text{Ca}^{2+}$  (Hansen et al., 2021) (Chen et al., 2004; Sather et al., 1992; Sather et al., 1990) (ADD Hu and Zheng, 2005; Alsaloum et al., 2016) based on functional characterization as the molecular basis underlying desensitization remains essentially unknown.

Currents mediated by iGluRs can be reduced by applying blockers which plug the ion channel pore, competitive antagonist that bind to the same site as agonists, and noncompetitive inhibitors or negative allosteric modulators that bind elsewhere (Yelshanskaya & Sobolevsky, 2022). In the LBD dimers, the interface between monomers serves as a binding site for PAMs and NAMs. When PAMs bind to the LBD interface of AMPA receptors, the LBD dimer interface becomes stabilized, which leads to blocked or reduced desensitization (Partin et al., 1995; Sun et al., 2002; Jin et al., 2005). Accordingly, desensitization in AMPA and kainate receptors becomes reduced when the D1-D1 interface is strengthened by covalent crosslinking or mutations (Stern-Bach et al., 1998; Sun et al., 2002, Weston et al., 2006b; Nayeem et al., 2009).

### 1.4.4 Trans Membrane Domain (TMD)

Plant GLRs are transmembrane proteins that conduct ions in and out of the cell, similar to their mammalian homologs, iGluRs. In the mammalian genome there are hundreds of different ion channels that conduct ions, including  $\text{Na}^+$ ,  $\text{K}^+$ ,  $\text{Ca}^{2+}$ , and  $\text{Cl}^-$ , in and out of cells to maintain homeostasis as well as signal within and between cells (Dolphin et al., 2020). iGluRs TMD forms an ion channel that enables cation current conduction through the [postsynaptic] membrane. Structural studies revealed that this channel opens and closes by the gate composed of the M3 helices bundle crossing at iGluRs extracellular apex (Sobolevsky et al., 2009; Karakas and Furukawa, 2014; Lee et al., 2014; Meyerson et al., 2014). The mechanism of channel opening is considered generally conserved across iGluR subtypes where the M3 segments splay away from the pore's central axis to allow ion flux across the membrane. The gate region of the M3 segment, specifically around the helical bundle crossing, includes the SYTANLAAF motif, the most highly conserved motif of iGluR subunits (Hansen et al., 2021; Wollmuth & Sobolevsky, 2004).

Along with the M3 transmembrane helix, which lines the extracellular portion of the pore, the ion-permeation pathway of an iGluR channel is formed by the M2 loop, with the Q/R/N site at the tip of this loop contributing to pore constriction. The M2 regions that line the intracellular portion of the pore have been characterized as a “selectivity filter” and have a negatively charged surface. The selectivity filter controls channel block, single-channel conductance, ion selectivity, and calcium permeation (Hansen et al., 2021; Traynelis et al., 2010; Wollmuth & Sobolevsky, 2004). Above the narrow constriction (at the tip of the selectivity filter) is the Q/R/N site. The Q/R/N site is a key site for ion permeation that resides above the widened middle portion of the pore, called the central cavity (Hansen et al., 2021).

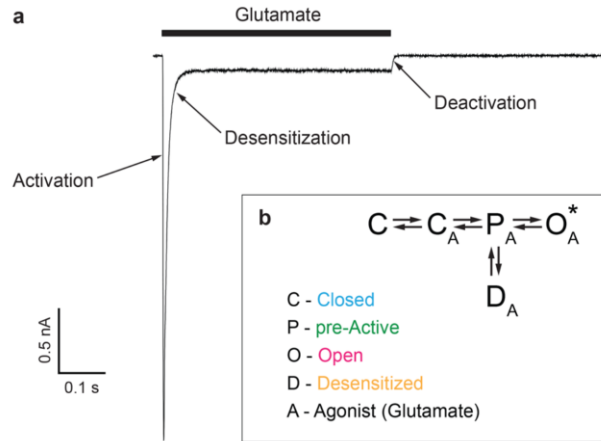


**Figure 1.5. iGluR functional recording and gating kinetic model.** AMPA receptor functional recording of whole-cell patch-clamp (a) and kinetic model of gating (b). (Figure 1.5 from (Twomey & Sobolevsky, 2018)).

There are three major gating processes that determine iGluR function: activation, desensitization, and deactivation (shown in Figure 1.5a functional recording). To describe iGluR gating, one can use a simple kinetic model with four states: closed (C), pre-active (P), open (O), and desensitized (D) (Figure 1.5b). The closed state is a non-conducting state where the iGluRs reside in the absence of agonist (A). In the presence of an agonist, iGluRs undergo a conformational change that brings them to the pre-active state from which it can convert to either the conducting or non-conducting state (the open conducting state and non-conducting desensitized state, respectively) (ref fig (Twomey & Sobolevsky, 2018)). Desensitization is reflected in the decrease of current response to a continuous application of agonist, and recovery from it occurs after agonist withdrawal (Hansen et al., 2021; Katz & Thesleff, 1957).

iGluR open state is generally represented by four subconductance levels (O1-O4) (Cull-Candy & Usowicz, 1987; Jahr & Stevens, 1987; Smith & Howe, 2000; Yelshanskaya et al., 2022). The apo (absence of agonist binding) and competitive antagonist-bound structures of

AMPA receptors have the same closed conformation of the ion channel (Dürr et al., 2014; Hansen et al., 2021; Sobolevsky et al., 2009; Yelshanskaya et al., 2016). Compared to AMPA receptors, kainate receptors undergo greater conformational changes to reach desensitized states. Interestingly, during desensitization the GluK2/GluK5 heteromeric kainate receptor facilitates channel closure by substantial structural rearrangements in the 2 GluK2 subunits but not in the 2 GluK5 subunits (Khanra et al., 2021). Antagonist-bound and desensitized states showed different LBD arrangements but similarly closed ion channels (GluK2/K5) (Khanra et al., 2021).

## **1.5 Questions Addressed in Thesis**

Despite all the iGluR structures available at the beginning of my thesis work, structural information of their plant homolog, GLR, was still missing. After I started my thesis research, the X-ray crystal structure of the isolated LBD of *AtGLR3.3* was revealed (Alfieri et al., 2020). Shortly after this, we contributed the X-ray crystal structure of the isolated *AtGLR3.2* LBD (Gangwar et al., 2021). The LBD structures demonstrated GLRs' promiscuity in ligand binding and activation (Alfieri et al., 2020; Gangwar et al., 2021). This was a big step toward progressing the GLR field of research, however, a full-length GLR structure was still needed. In order to study GLRs structure and gain a mechanistic insight to how the receptor functions as a channel, we set out to determine the first full-length GLR structure via cryogenic electron microscopy (cryo-EM).

## **Chapter 2.**

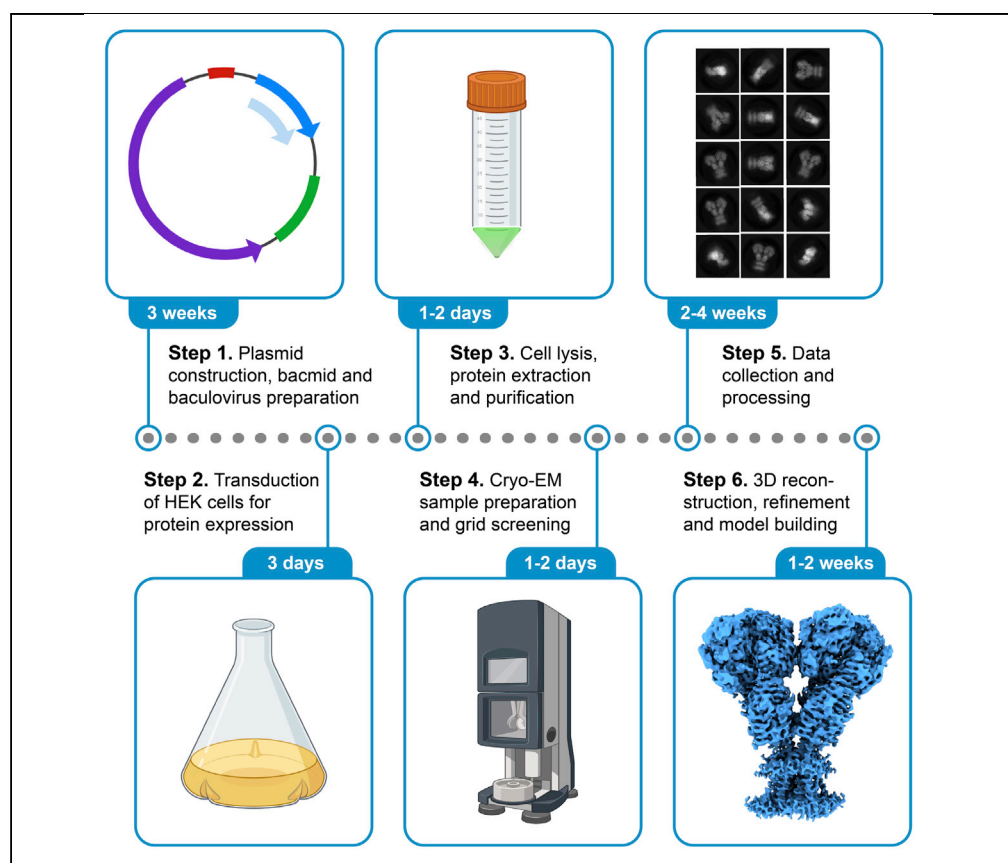
### **Purification and Cryo-EM Structure Determination of**

#### ***Arabidopsis Thaliana* GLR3.4**

This section is a paper originally published in STAR Protocols (Gangwar et al., 2021). The paper reveals protocols in detail on how to obtain a purified *At*GLR3.4 specimen and then proceed to solve the structure via Cryo-EM.

## Protocol

# Purification and cryo-EM structure determination of *Arabidopsis thaliana* GLR3.4



Ionotropic glutamate receptors (iGluRs) are ligand-gated ion channels that play crucial roles in the central nervous system. iGluR homologs, termed glutamate receptor-like channels (GLRs), have been found in plants. Investigating the structural and functional relationship between iGluRs and GLRs was limited by GLR protein expression, purification, and structural characterization. Here, we provide a detailed protocol for *Arabidopsis thaliana* GLR3.4 (AtGLR3.4) expression in a mammalian cell line and purification for structure determination by cryogenic electron microscopy (cryo-EM).

Shanti Pal Gangwar,  
Marriah N. Green,  
Maria V.  
Yelshanskaya,  
Alexander I.  
Sobolevsky

as4005@cumc.columbia.edu

### Highlights

Protocol for expression of plant glutamate receptor-like channel (GLR) in HEK cells

Purification protocol that yields pure monodisperse tetrameric GLR protein

Purified protein subjected to cryo-EM analysis produces high-resolution GLR structure

Gangwar et al., STAR  
Protocols 2, 100855  
December 17, 2021 © 2021  
The Author(s).  
<https://doi.org/10.1016/j.xpro.2021.100855>



## Protocol

Purification and cryo-EM structure determination of *Arabidopsis thaliana* GLR3.4Shanti Pal Gangwar,<sup>1,3</sup> Marriah N. Green,<sup>1,2,3</sup> Maria V. Yelshanskaya,<sup>1</sup> and Alexander I. Sobolevsky<sup>1,4,5,\*</sup><sup>1</sup>Department of Biochemistry and Molecular Biophysics, Columbia University, 650 West 168<sup>th</sup> Street, New York, NY 10032, USA<sup>2</sup>Institute of Human Nutrition, Columbia University, 630 West 168<sup>th</sup> Street, New York, NY 10032, USA<sup>3</sup>These authors contributed equally<sup>4</sup>Technical contact<sup>5</sup>Lead contact\*Correspondence: [as4005@cumc.columbia.edu](mailto:as4005@cumc.columbia.edu)<https://doi.org/10.1016/j.xpro.2021.100855>

## SUMMARY

Ionotropic glutamate receptors (iGluRs) are ligand-gated ion channels that play crucial roles in the central nervous system. iGluR homologs, termed glutamate receptor-like channels (GLRs), have been found in plants. Investigating the structural and functional relationship between iGluRs and GLRs was limited by GLR protein expression, purification, and structural characterization. Here, we provide a detailed protocol for *Arabidopsis thaliana* GLR3.4 (AtGLR3.4) expression in a mammalian cell line and purification for structure determination by cryogenic electron microscopy (cryo-EM).

For the complete details on the use and execution of this protocol, please refer to Green et al. (2021).

## BEFORE YOU BEGIN

This protocol was used in a recent publication (Green et al., 2021) to purify *Arabidopsis thaliana* GLR3.4 (AtGLR3.4) recombinant protein expressed in a mammalian cell line for high-resolution full-length structure determination by single-particle cryo-EM. Before the experiment, prepare all the buffers to be used in subsequent steps one day in advance unless otherwise mentioned.

## Buffer preparation

⌚ Timing: 1 day

Prepare 1L of T buffer, 100 mL of Cell Lysis buffer, 25 mL of Solubilization buffer, 300 mL of Size-Exclusion Chromatography (SEC) buffer and 20 mL of Strep Elution buffer.

## Construct preparation

⌚ Timing: 4 days

1. Subclone DNA for full-length AtGLR3.4 (Met1-Thr959) into a pEG BacMam vector (Goehring et al., 2014) using gene-specific primers. Introduce the thrombin cleavage site (LVPRGS), followed by an eGFP and a streptavidin (strep) affinity tag (WSHPQFEK) at the C-terminus (Figure 1).
2. Design the gene-specific forward primer with the Sall and reverse primer with the NotI site to amplify the AtGLR3.4 DNA flanked by Kozak sequence (KZK) and thrombin site to clone in pEG BacMam. Conduct polymerase chain reaction (PCR) using the information described in the tables below.



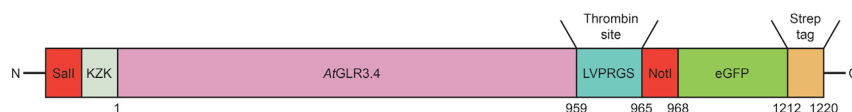


**Figure 1. AtGLR3.4 construct schematic**

**Pause point:** PCR reaction can be stored at 4°C for 24 h or at –20°C for long-term storage.

- Run a 1% agarose gel to verify the size and purity the PCR products.
- Add 1  $\mu$ L of DpnI enzyme and incubate the reaction at 37°C for 1 h.
- Perform DNA cleanup using any commercially available kit. We use Monarch New England Bio Labs' PCR and DNA Cleanup Kit following manufactures protocol.

**Pause point:** DNA can be stored at 4°C for 24 h or at –20°C for long-term storage.

- Digest PCR DNA and pEG BacMam plasmid in two separate 1.5-mL tubes following the instruction in the table below. Incubate the digest reaction at 37°C for 1 h.
- Perform a DNA cleanup using any commercially available kit as mentioned above.
- Ligate both the PCR and linearized plasmid following the instruction in the table below. Incubate the ligation reaction at ~20°C–25°C for 10–15 min. Use the insert and vector DNA at 3:1 molar ratio.
- Transform DH5 $\alpha$  competent cells and select the transformants on LB agar plates containing 100  $\mu$ g/mL ampicillin.
  - Incubate the plates at 37°C for 12–15 h.
  - Inoculate a single colony in LB media supplemented with 100  $\mu$ g/mL ampicillin and perform a miniprep to extract and purify the plasmid DNA.
  - Sequence the DNA to confirm that the construct sequence is correct before proceeding.

**Note:** The circular plasmid that we used was engineered to have a Kozak sequence, thrombin recognition site, eGFP, and Strep-tag as described in [Figure 1](#).

## KEY RESOURCES TABLE

REAGENT or RESOURCE	SOURCE	IDENTIFIER
Chemicals, peptides, and recombinant proteins		
Tris-HCl	Fisher Scientific	Cat# BP152-1
NaCl	Fisher Scientific	Cat# BP358-212
L-Glutamate	Sigma	Cat# 49621
PMSF	Acros Organics	Cat# 215740500
2-Mercaptoethanol ( $\beta$ ME)	Acros Organics	Cat# 125470100
Thrombin	Haematologic Technologies	Cat# HCT-0020
D-Desthiobiotin	Sigma-Aldrich	Cat#D1411
Fetal bovine serum	Gibco	Cat# 16140071
Sf-900 III SFM	Gibco	Cat# 12658027
Freestyle 293 expression medium	Gibco	Cat# 12338018
Sodium butyrate	Acros Organics	Cat# 263191000
Digitonin	Cayman Chemical Company	Cat#14952
Aprotinin	Sigma-Aldrich	Cat#A1153
Leupeptin	Sigma-Aldrich	Cat#L0649
Pepstatin A	Sigma-Aldrich	Cat#P4265
Kanamycin	Fisher Scientific	Cat# BP906-5

(Continued on next page)



### Continued

REAGENT or RESOURCE	SOURCE	IDENTIFIER
Gentamicin sulfate	Sigma-Aldrich	Cat#G1914
Tetracycline	Fisher Scientific	Cat# BP912
Bluo-Gal	Life Technologies	Cat# 15519028
IPTG	Zymo Research	Cat# I1001-5
Sall-HF	New England Biolabs	Cat# R3138S
NotI-HF	New England Biolabs	Cat#3189S
Quick ligase	New England Biolabs	Cat#M2200
Monarch Plasmid Miniprep Kit	New England Biolabs	Cat #T1010L
Monarch DNA and PCR Cleanup Kit	New England Biolabs	Cat #T1030L
Nitrocellulose membrane filter (0.22 µm)	Merck Millipore	Cat#SA1J789H5
Wizard Plus Minipreps DNA Purification System	Promega	Cat#A7510
Phenol:chloroform:isoamylalcohol	Life Technologies	Cat# 15593031
Cellfectin II Reagent	Gibco	Cat#58760
Ethanol 200 Proof	Decon Labs, Inc.	Cat #2701
Centrifugal Filter Unit (Amicon Ultra-15)	Sigma-Aldrich	Cat#UFC910024

### Deposited data

Coordinates of full-length AtGLR3.4	(Green et al., 2021)	PDB: 7LZH
Cryo-EM map of full-length AtGLR3.4	(Green et al., 2021)	EMDB: EMD-23606
Coordinates of AtGLR3.4-S1S2 <sub>Glu</sub>	(Green et al., 2021)	PDB: 7LZO
Crystal structure of GluA2	(Sobolevsky et al., 2009)	PDB: 3KG2

### Experimental models: cell lines

HEK 293S GnTI <sup>−</sup>	ATCC	Cat#CRL-3022
Sf9	Gibco	Cat#12659017
DH10Bac	Life Technologies	Cat#10361012
DH5α	Zymo Research	Cat#T3007

### Oligonucleotides

AtGLR3.4 amplification primer: 5'-gtcgactccgccaccatgggatttttggtgatgataagag -3'	This paper	N/A
AtGLR3.4 amplification primer: 5'-cggcaccagagtaatttcgcatgtgtgattgtga -3'	This paper	N/A

### Software and algorithms

gCTF	(Zhang, 2016)	<a href="http://www.mrc-lmb.cam.ac.uk/kzhang/">http://www.mrc-lmb.cam.ac.uk/kzhang/</a>
Motioncor2	(Zheng et al., 2017)	<a href="https://msg.ucsf.edu/software">https://msg.ucsf.edu/software</a>
RELION 3.0	(Zivanov et al., 2018)	<a href="http://www2.mrc-lmb.cam.ac.uk/relion/">http://www2.mrc-lmb.cam.ac.uk/relion/</a>
UCSF Chimera	(Pettersen et al., 2004)	<a href="https://www.cgl.ucsf.edu/chimera/">https://www.cgl.ucsf.edu/chimera/</a>
cryoSPARC	(Punjani et al., 2017)	<a href="https://cryosparc.com/">https://cryosparc.com/</a>
PHENIX	(Adams et al., 2010)	<a href="https://www.phenix-online.org/">https://www.phenix-online.org/</a>
Coot	(Emsley and Cowtan, 2004)	<a href="http://www2.mrc-lmb.cam.ac.uk/Personal/pemsley/coot">http://www2.mrc-lmb.cam.ac.uk/Personal/pemsley/coot</a>
SWISS-MODEL	(Waterhouse et al., 2018)	<a href="https://swissmodel.expasy.org/">https://swissmodel.expasy.org/</a>

### Other

CF-1.2/1.3-2Au 200 mesh holey carbon grids	Protochips	Cat#CF-1.2/1.3-2Au
Gold wire	Ted Pella, Inc.	Cat#21-10
Superose6 10/300 column	GE Healthcare	Cat# 17-5172-01

## MATERIALS AND EQUIPMENT

### T buffer

Reagent	Final concentration	Amount
Tris-HCl pH 8.0 (1 M)	20 mM	20 mL
NaCl (5 M)	150 mM	30 mL

(Continued on next page)

**Continued**

Reagent	Final concentration	Amount
Milli-Q H <sub>2</sub> O	n/a	950 mL
<b>Total</b>	<b>n/a</b>	<b>1 L</b>

Run T buffer through a 0.22 µm filter and store at 4°C for up to one month.

**Cell Lysis buffer**

Reagent	Final concentration	Amount
T buffer	n/a	100 mL
β-mercaptoethanol (βME) (14.3 M)	1 mM	7.1 µL
Aprotinin (0.8 mM)	0.8 µM	100 µL
Leupeptin (4.3 mM)	4.3 µM	100 µL
Pepstatin A (2 mM)	2 µM	100 µL
Phenylmethylsulphonyl fluoride (1 M)	1 mM	100 µL
<b>Total</b>	<b>n/a</b>	<b>~100 mL</b>

**Note:** Protease inhibitors and βME should be added right before buffer use. Keep at 4°C, if needed can be stored at 4°C for up to 2 hours.

△ **CRITICAL:** Protein degradation during the purification procedure can have detrimental effects on the resulting protein quality. It is, therefore, important that fresh reducing agents and protease inhibitors are added at the steps indicated in the protocol.

**Solubilization buffer**

Reagent	Final concentration	Amount
T buffer	n/a	25 mL
β-mercaptoethanol (βME) (14.3 M)	1 mM	1.78 µL
Aprotinin (0.8 mM)	0.8 µM	25 µL
Leupeptin (4.3 mM)	4.3 µM	25 µL
Pepstatin A (2 mM)	2 µM	25 µL
Phenylmethylsulphonyl fluoride (1 M)	1 mM	25 µL
Digitonin	2%	0.5 g
<b>Total</b>	<b>n/a</b>	<b>~25 mL</b>

**Note:** Digitonin is not readily soluble at room temperature. Therefore, add digitonin to the T buffer, heat the mixture up to 70°C–75°C and stir at medium-low speed until completely dissolved. Keep at 4°C, if needed can be stored at 4°C for up to 2 hours.

△ **CRITICAL:** Protease inhibitors and βME should be added to the chilled digitonin plus T buffer mixture right before membrane solubilization.

**SEC buffer**

Reagent	Final concentration	Amount
T buffer	n/a	300 mL
Digitonin	0.05%	150 mg
<b>Total</b>	<b>n/a</b>	<b>300 mL</b>

**Note:** Digitonin is not readily soluble at room temperature. Therefore, add digitonin to the T buffer, heat the mixture up to 70°C–75°C and stir at medium-low speed until completely dissolved. After digitonin is completely dissolved, cool to ~4°C–20°C. Once

cooled, run SEC buffer through 0.22  $\mu$ M filter. Keep at 4°C, if needed can be stored at 4°C for up to 24 hours.

### Strep Elution buffer

Reagent	Final concentration	Amount
SEC buffer	n/a	20 mL
D-desthiobiotin	2.5 mM	10.8 mg
<b>Total</b>	<b>n/a</b>	<b>20 mL</b>

If needed, adjust the pH of Strep Elution buffer to 8.0, run it through 0.22  $\mu$ M filter and store at 4°C for up to 12 h.

### PCR reaction

Reagents	Final concentration	Volume
Autoclaved Milli-Q H <sub>2</sub> O	n/a	32 $\mu$ L
5 $\times$ Q5 Reaction Buffer	1 $\times$	10 $\mu$ L
Forward Primer (10 $\mu$ M)	0.5 $\mu$ M	2.5 $\mu$ L
Reverse Primer (10 $\mu$ M)	0.5 $\mu$ M	2.5 $\mu$ L
Template DNA	1–10 ng	1 $\mu$ L
dNTPs (10 mM)	200 $\mu$ M	1 $\mu$ L
Q5 High-Fidelity DNA Polymerase	0.04 U/ $\mu$ L	1 $\mu$ L
<b>Total</b>	<b>n/a</b>	<b>50 <math>\mu</math>L</b>

### Thermocycler settings included lid temperature at 105°C and volume of 50 $\mu$ L.

#### PCR cycling conditions

Steps	Temperature	Time	Number of cycles
Initial Denaturation	98°C	3 min	1
Denaturation	98°C	10 s	25–35 cycles
Annealing	55°C	30 s	
Extension	72°C	2 min	
Final extension	72°C	5 min	1
Hold	4°C	Forever	

### Digest reaction

Reagents	Volume
PCR DNA/Plasmid	80 $\mu$ L
CutSmart Buffer 10 $\times$	10 $\mu$ L
Sall-HF	2 $\mu$ L
NotI-HF	2 $\mu$ L
Milli-Q H <sub>2</sub> O	6 $\mu$ L
<b>Total</b>	<b>100 <math>\mu</math>L</b>

### Ligation reaction

Reagents	Volume
PCR DNA	40–50 ng
Plasmid DNA	40–60 ng
Quick ligase buffer (2 $\times$ )	5 $\mu$ L
Quick ligase	0.5 $\mu$ L
Milli-Q H <sub>2</sub> O	—
<b>Total</b>	<b>10 <math>\mu</math>L</b>

## STEP-BY-STEP METHOD DETAILS

Below we provide a detailed step-by-step protocol about the AtGLR3.4 protein purification, sample preparation, and cryo-EM structure determination (Figure 2).

### Bacmid preparation and isolation

⌚ Timing: 4 days

According to the manufacturer protocol, bacmid preparation and isolation were carried out using DH10Bac competent cells (Bac-to-Bac, Invitrogen). The steps are described here.

1. For transposition, prepare LB agar plates containing 50  $\mu\text{g/mL}$  kanamycin, 7  $\mu\text{g/mL}$  gentamicin, 10  $\mu\text{g/mL}$  tetracycline, 200  $\mu\text{g/mL}$  Bluo-gal and 40  $\mu\text{g/mL}$  IPTG.
2. Transformation of bacmid
  - a. Thaw DH10Bac (Life Technologies Cat#10361012) competent cells on ice and dispense 25–30  $\mu\text{L}$  to a prechilled 1.5-mL polypropylene tube.
  - b. Add approximately 1–10 ng (1–2  $\mu\text{L}$ ) of plasmid DNA (pEG BacMam\_AtGLR3.4) and mix gently by flicking/tapping the tube several times.

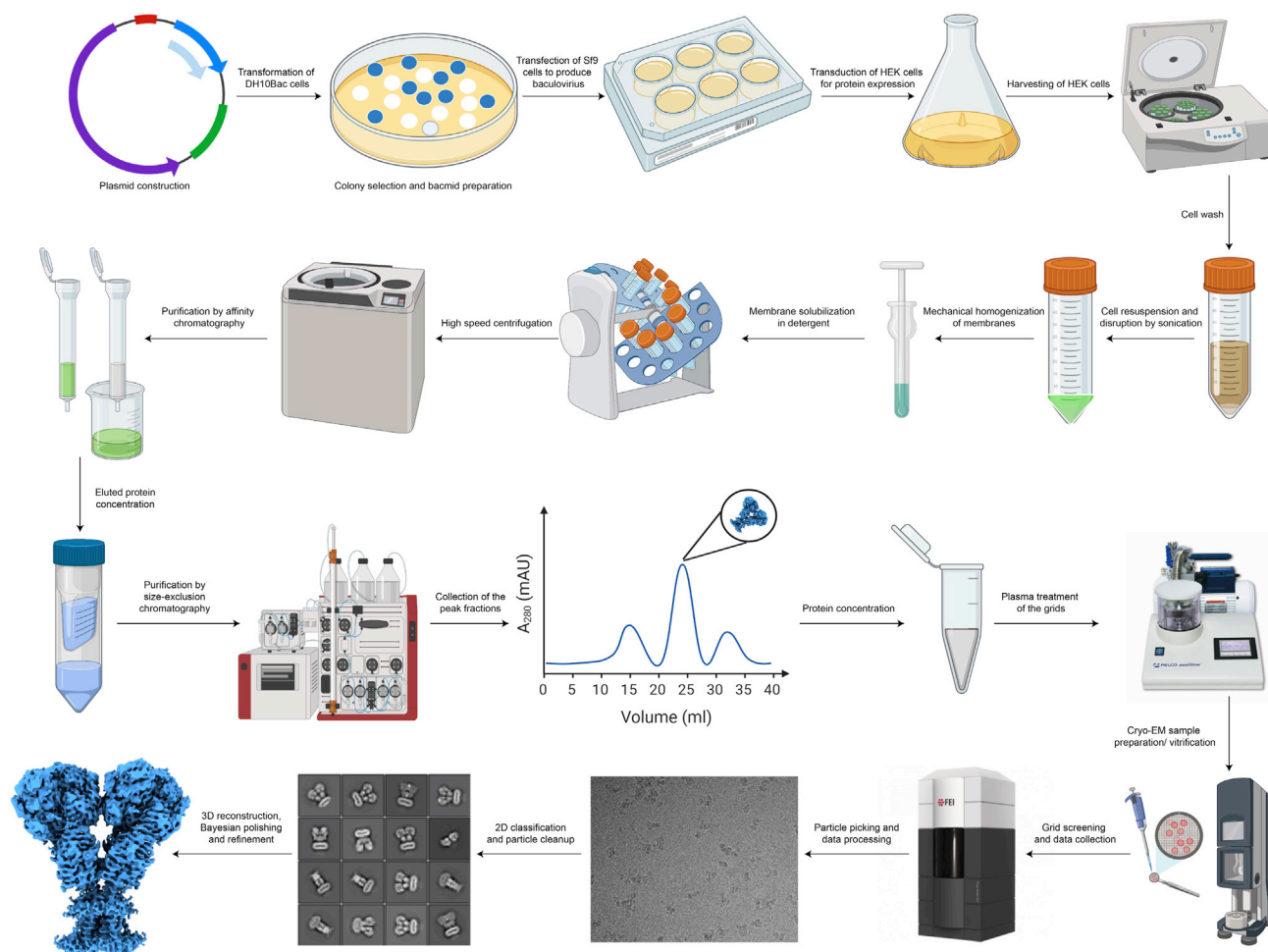


**Figure 2. Overview of the protocol of AtGLR3.4 protein expression, purification, sample preparation, and cryo-EM structure determination**  
The image has been created using BioRender (<https://biorender.com/>).

- c. Incubate on ice for 15–30 min.
- d. Transfer the tube to a water bath at 42°C for 45 s.
- e. After heat shock, immediately transfer the tube back to ice and let it cool on ice for 2–3 min.
- f. Add 200 µL SOC media to the tube and transfer to an incubator shaker set at 220 rpm and incubate for 4 h at 37°C.
- g. Pipette 20–100 µL of transformation reaction on the plates and spread evenly.
3. Grow transformed cells
  - a. Incubate the plates for at least 24 h at 37°C. Blue and white colonies will appear; for better results, incubate the plates for 48 h to distinguish the blue from the white colonies.
  - b. Carefully inoculate a single white colony in 5–6 mL LB broth supplemented with 50 µg/mL kanamycin, 7 µg/mL gentamicin, and 10 µg/mL tetracycline.
  - c. Incubate for 12–15 h at 37°C with continuous rotation at 220–250 rpm.

▮▮ **Pause point:** Overnight (12–16 h)

4. Isolate bacmid DNA
  - a. Centrifuge the culture at ~3,100 g for 10 min. Then, decant to discard the supernatant and save the cell pellet.

**Note:** If needed, the pellet can be stored at –20°C for up to a couple of weeks prior to bacmid DNA isolation. For bacmid isolation, we use reagents from the Promega mini prep kit. Reagents from other mini prep kits can also be used.

- b. Resuspend the cell pellet in 200 µL resuspension buffer until homogeneous, via pipetting up and down and/or by vortexing. Transfer the suspension to a 1.5-mL Eppendorf tube.
- c. Add 200 µL lysis buffer and mix by gently inverting the tube several (~15–20) times. The suspension in the tube turns slightly viscous.
- d. Add 200 µL neutralization buffer and mix by gentle inversion several (~20) times. A white precipitate will be observed.
- e. Centrifuge the tube at ~21,100 g for 10 min at ~20°C–25°C.
- f. Avoiding the pellet, carefully collect and transfer the supernatant to a fresh 1.5-mL Eppendorf tube. In the fume hood, add an equal volume (typically around 500–600 µL) of Tris equilibrated Phenol:Chloroform: Isoamyl-alcohol (25:24:1) and mix by inverting gently several times for 1 min.
- g. Spin at ~21,100 g for 5 min at ~20°C–25°C. In the fume hood, gently collect the top layer supernatant (~500–600 µL) and transfer it to a new 1.5-mL Eppendorf tube. Add 2× volume (~1–1.2 mL) of ice-cold 100% ethanol, mix well by gently inverting for 30 s, and incubate at –20°C for a minimum of 30 min.
- h. Centrifuge at ~21,100 g for 20–30 min at 4°C. A white pellet is observed at the bottom of the tube. Carefully decant to discard the supernatant and add 1 mL ice-cooled 70% ethanol.
- i. Invert the tube gently several times to wash the pellet. Centrifuge for 5 min at ~21,100 g at 4°C.
- j. Discard the supernatant by gentle aspiration (make sure to not discard the pellet as it may dislodge from the bottom).
- k. To avoid traces of remaining ethanol, air dry the pellet for 15–20 min at ~20°C–25°C in a fume hood. Add 40–50 µL of autoclaved milli-Q water and dissolve the pellet by gentle tapping/flicking. Once the pellet is dissolved, place the tube with bacmid DNA on ice. Now the bacmid DNA is ready to be used for baculovirus production and can be stored at –80°C for an extended period.

### Transfection of Sf9 cells with recombinant bacmid DNA

⌚ **Timing:** 4–6 days

Production of the first-generation baculovirus (P1 virus).

**Note:** The following steps should be performed under sterile conditions in a laminar hood.

5. In a 6-well plate, add 2 mL of Sf9 cells per well, with the Sf9 cell density of  $0.5\text{--}0.75 \times 10^6/\text{mL}$  ( $1\text{--}1.5 \times 10^6$  cells per P1 virus). Allow the cells to adhere for 30 min to 1 h in a dark incubator at 27°C.
6. In the meantime, take a 1.5-mL Eppendorf tube and add:
  - a. 180  $\mu\text{L}$  of SF900 media
  - b. 10  $\mu\text{L}$  of Cellfectin II
  - c. 10  $\mu\text{L}$  of thawed bacmid DNA
7. Close and tap the tube to mix. Let mixture sit for 20–30 min in the hood.
8. Add the mixture of SF900 media, bacmid DNA, and Cellfectin II dropwise to the cells in the well.
9. Incubate the plate at 27°C for 4–6 days. Observe the plate under the microscope to monitor cell behavior and fluorescence if the gene of interest is fused with a fluorescent marker gene.

**Note:** It is always better to have a fluorescent marker fused to the protein of interest to monitor baculovirus preparation and protein expression. The AtGLR3.4 P1 virus is typically harvested on the 5<sup>th</sup> day post-transfection because most of the cells already express the protein (monitored by eGFP fluorescence), while very little cell death is observed.

10. To harvest the P1 virus, filter the 2 mL medium using a 0.2  $\mu\text{m}$  sterile syringe filter in a laminar hood and store the filtered virus at 4°C protected from light. The P1 virus can be stored for 4–6 months.

## P2 virus production

⌚ Timing: 5 days

**Note:** The following steps (except for centrifugation and resuspension) should be performed under sterile conditions in a laminar hood.

11. In a laminar hood and sterile conditions, infect 500 mL of Sf9 cells at a cell density of  $1.5 \times 10^6$  cells/mL in a 1-L non-baffled Erlenmeyer flask by adding 500  $\mu\text{L}$  of P1 virus. Incubate the Sf9 cell culture in a shaker at 27°C and 115 rpm for 72–120 h. Keep the cell culture protected from light.
12. Centrifuge the culture at  $\sim 5,000 g$  for 15 min at 4°C in a Sorvall centrifuge. Discard the cell pellet and save the supernatant containing the P2 virus.
13. Ultracentrifuge the supernatant at 4°C for 1 h at  $\sim 61,000 g$  in a preparative ultracentrifuge with a Type 45Ti Beckman Coulter rotor.
14. A small translucent pellet is observed at the bottom of the tube. Discard the supernatant and resuspend the pellet in 50 or 25 mL Gibco FreeStyle 293 expression media supplemented with 2% of  $\gamma$ -irradiated fetal bovine serum (FBS) to get 10 $\times$  or 20 $\times$  concentrated P2 virus, respectively.

**Note:** Always run the FBS through a 0.22  $\mu\text{m}$  filter before adding to the media (perform this procedure under sterile conditions in a laminar hood).

15. Pass the resuspension through a 0.22  $\mu\text{m}$  filter into a sterile 50-mL tube and store at 4°C well protected from light. The P2 virus stock can be stored for 1–2 months at 4°C while protected from light.

**Note:** To fully dissolve the pellet, allow it to stay in the resuspension media in the dark at 4°C for no longer than 24 hours prior to filtration.

## Transduction of HEK 293S GnTI<sup>−</sup> cells with P2 baculovirus

⌚ Timing: 3 days

16. In a laminar hood and sterile conditions, prepare 800 mL of HEK 293S GnT1<sup>−</sup> cell culture at the density of  $2.5\text{--}3.5 \times 10^6$  cells/mL maintained in Freestyle 293 media supplemented with 2% FBS in 2-L baffled Erlenmeyer flask and add 8 mL of 20× concentrated P2 virus stock. Incubate the cell culture at 37°C in an orbital shaker at 110 rpm and 5% CO<sub>2</sub>.
17. To enhance the protein expression, add 10 mM of sodium butyrate to the culture 12–20 h post-transduction and decrease the incubator temperature to 30°C.
18. After 72–74 h post-transduction, harvest the cells by centrifugation at  $\sim 5,000$  g (in a Sorvall RC 5B Plus centrifuge) for 15 min at 4°C. Discard the supernatant, wash the cell pellet by resuspension in phosphate-buffered saline (PBS, pH 8.0), and transfer the suspension to a 50-mL Falcon tube. Centrifuge at  $\sim 3,100$  g for 10 min at 4°C. Discard the supernatant and store the cell pellet at  $-80^\circ\text{C}$  until further use.

### Purification of AtGLR3.4

⌚ Timing: 2 days

**Note:** The buffers should be filtered using 0.22  $\mu\text{m}$  filter (Merck-Millipore) and chilled to 4°C prior to utilization. When required, add  $\beta$ -mercaptoethanol ( $\beta$ ME) and protease inhibitors right before buffer usage. All protein purification steps are to be carried out at 4°C or on ice, unless otherwise noted.

19. Resuspend the cell pellet in ice-cold Cell Lysis buffer. Add a stir bar and  $\sim 40$  mL of the Cell Lysis buffer to the 50-mL falcon tube with the frozen cell pellet till it reaches 45-mL volume and resuspend the pellet by rocking on a platform or by vortexing until the cell pellet becomes detached and dissolved.
20. Disrupt the cells by sonication using Misonix Sonicator with a preset program with six cycles (3 min total process time) at the amplitude of 8, 15 s pulse on time, and 15 s pulse off time. The sonication steps must be carried out on a stir plate (at medium speed stirring) on ice or at 4°C to avoid heating and denaturing of the protein. Repeat this process 2 more times or until optimal cell lysis.

**Note:** For optimal cell lysis, check a small droplet of the lysate under a light microscope to confirm that cells are lysed post-sonication, as the appearance will be distinctly different from cells prior to sonication.

21. Centrifuge the cell lysate suspension at  $\sim 3,100$  g (using an Eppendorf Centrifuge 5810) for 10 min at 4°C to remove cell debris and unbroken cells.
22. Collect the clarified supernatant by decanting the supernatant into a prechilled polycarbonate bottle assembly for ultracentrifugation. Ultracentrifuge in a Type 45Ti Beckman Coulter fixed-angle rotor at  $\sim 186,000$  g for 1 h at 4°C to obtain the membrane fraction.
23. Discard the supernatant and mechanically homogenize the obtained membrane fraction pellet in Cell Lysis buffer ( $\sim 25$  mL) using a homogenizer.

**Note:** We use a prechilled dounce homogenizer and move a plunger forth and back at least 6 times to fully homogenize the pellet in the Cell Lysis buffer.

24. Solubilize the membrane protein from the homogenate by adding an equal volume of solubilization buffer to the homogenate (totaling  $\sim 50$  mL with a final  $\sim 1\%$  concentration of the detergent, digitonin in our case) and stir/rotate (low-medium speed to prevent bubble formation) at 4°C for  $\sim 2$  h (1 h minimum).
25. Ultracentrifuge the solubilize at  $\sim 186,000$  g in a Type 45Ti Beckman Coulter fixed-angle rotor at 4°C for 1 h to remove insoluble material.

26. Collect the supernatant and add 2 mL of strep resin prewashed and equilibrated in T buffer. Rotate the mix for 12–14 h at 4°C.

▮▮ **Pause point:** overnight (12–15 h)

27. Purify the protein using affinity chromatography.
  - a. Equilibrate 30-mL chromatography gravity column by rinsing column with milli-Q water and allowing SEC buffer to flow through.
  - b. Transfer the AtGLR3.4 protein-bound strep resin to the empty pre-equilibrated gravity chromatography column and collect the flow-through.
  - c. Wash the resin by pouring 25 mL of SEC buffer into the column.
  - d. Elute the AtGLR3.4 protein with ~10–15 mL of freshly made Strep Elution buffer. Observe the eGFP-tagged protein eluting from the column by the color of the collected protein appearing green and the resin becoming white. No more Strep Elution buffer is needed once the strep resin is white, stripped of its eGFP green color, indicating that the protein has been eluted from the column.

**Note:** When adding buffer to the column, wait until the buffer from the previous step is almost finished flowing through the column but do not let the column run dry.

28. Measure the concentration of the protein, add 1/300 (w/w) thrombin and incubate at 22°C for 90 min to cleave off eGFP and the strep tag. Protein concentration can be measured using a spectrophotometer set to  $A_{280}$  (absorbance at 280 nm) and blanked with the elution buffer.

**Note:** Successful thrombin cleavage can be monitored by fluorescence-detection size-exclusion chromatography (FSEC) (Kawate and Gouaux, 2006) and SDS-PAGE (Figure 3).

29. Concentrate the thrombin digest reaction to ~500  $\mu$ L using 100-kDa NMWL centrifugal filter.
30. Transfer the concentrated protein to a new 1.5-mL tube and centrifuge the concentrated protein at ~86,500 g for 30 min at 4°C using a Sorvall MTX150 Micro-Ultracentrifuge (Thermo Fisher Scientific) and a S100AT4 rotor.
31. Avoiding the pellet, inject the supernatant into a 500- $\mu$ L loop connected to a Superose™ 6 10/300 GL SEC column attached to an AKTA FPLC (GE Healthcare) and pre-equilibrated in SEC Buffer.
32. At the end of the SEC column run at 0.5 mL/min, pool the peak fractions corresponding to AtGLR3.4 tetramer (Figure 4) and concentrate to 3–4 mg/mL using 100-kDa NMWL centrifugal filter. Typically, ~800 mL of HEK 293S GnTI<sup>−</sup> cell culture yields ~1 mg of purified protein. The concentrated, purified protein can be stored at 4°C, structurally stable, and functionally active for one week.
33. Inspect the purity of the protein by sodium dodecyl sulfate polyacrylamide gel electrophoresis (SDS-PAGE).

**Optional:** Protein purity can also be assessed by FSEC.

### Grid sample preparation

⌚ **Timing:** 2–3 h

34. For cryo-EM grid sample preparation, use UltrAuFoil CF-1.2/1.3-2Au 200 mesh holey carbon grids covered with a thin layer of gold according to the published method (Russo and Passmore, 2014).

**Optional:** The user can optimize various grid types and vitrification parameters however they see fit.



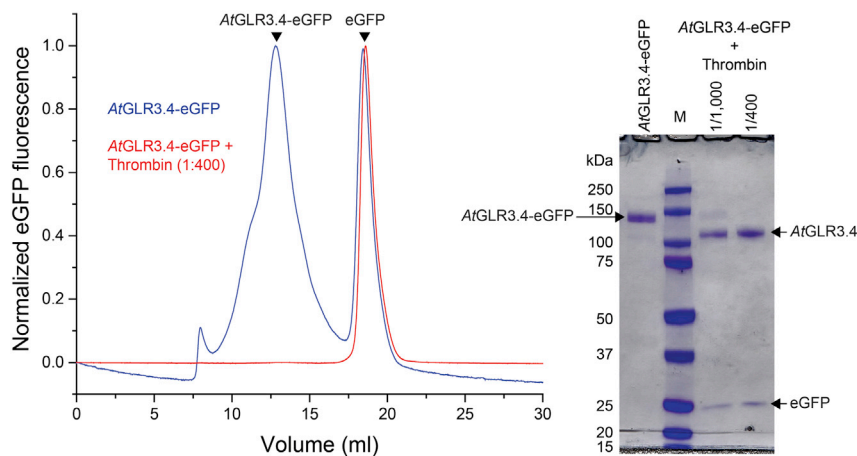


**Figure 3. On the left, FSEC traces for AtGLR3.4 before (blue) and after (red) thrombin cleavage**

The chromatograms were recorded using Superose 6 column at the flow rate of 0.5 mL/min using eGFP fluorescence (excitation, 488 nm; emission, 507 nm). On the right, SDS-PAGE demonstrating AtGLR3.4 bands before and after thrombin digest at two (1/1,000 and 1/300) thrombin/AtGLR3.4-eGFP ratios.

- Deposit ~50 nm of gold onto the grids using gold wire and the Edwards Auto 306 evaporator.

**Note:** This grid gold-coating step is only necessary for carbon-coated grids.

- Then remove the carbon with the Gatan Solarus (model 950) Advanced Plasma Cleaning System Ar/O<sub>2</sub> treatment (4 min, 50 watts, 35.0 sccm Ar, 11.5 sccm O<sub>2</sub>).

**Note:** This carbon removal step is only necessary after the previous grid gold-coating step.

- Before applying the purified protein sample to the gold-coated side of the grid, subject the grids to a H<sub>2</sub>/O<sub>2</sub> plasma treatment using the Gatan Solarus (model 950) Advanced Plasma Cleaning System (20 s, 10 watts, 6.4 sccm H<sub>2</sub>, 27.5 sccm O<sub>2</sub>) with the gold-coated side facing up.

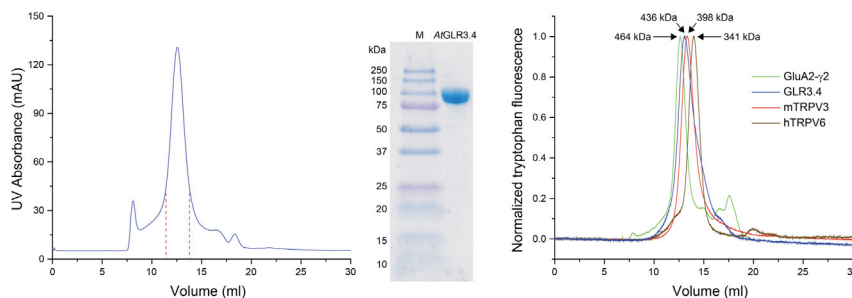


**Figure 4. On the left, SEC profile for purified AtGLR3.4**

The chromatogram was recorded using Superose 6 column at the flow rate of 0.5 mL/min using A<sub>280</sub> absorbance. In the middle, SDS-PAGE for the protein peak fractions outlined by the red dashed lines on the SEC plot. On the right, normalized FSEC traces for purified AtGLR3.4, rat GluA2-γ2 fusion (Twomey et al., 2016, 2017), mouse TRPV3 (Nadezhdin et al., 2021; Singh et al., 2018) and human TRPV6 (Bhardwaj et al., 2020; McGoldrick et al., 2018). The latter three membrane proteins represent molecular weight markers and confirm the tetrameric assembly of AtGLR3.4. The chromatograms were recorded using Superose 6 column at the flow rate of 0.5 mL/min using tryptophan fluorescence (excitation, 280 nm; emission, 334 nm).

**Note:** Glow discharging step could be used as an alternative to plasma cleaning.

35. Prior to applying the purified protein to the grid, ultracentrifuge the protein at  $\sim 86,500$  g for 30 min at  $4^{\circ}\text{C}$  using a SorvallMTX150 Micro-Ultracentrifuge (Thermo Fisher Scientific) and a S100AT4 rotor. Transfer the supernatant to a prechilled tube, avoiding any possible protein precipitation.
36. For vitrification, set the vitrobot to  $4^{\circ}\text{C}$  with 100% humidity, a 15 s wait time, and a 4–5 s blot time with a 4–5 blot force. Apply 3  $\mu\text{L}$  of purified AtGLR3.4 protein at 3–3.5 mg/mL to the gold-coated side of the grid and plunge freeze the grid into liquid ethane cooled to  $\sim -190^{\circ}\text{C}$  in liquid nitrogen using a Mark IV vitrobot (Thermo fisher scientific).

**Note:** After grids are plunge frozen, they must remain at cryogenic temperatures and avoid contamination as well as exposure to humidity or condensation.

▮▮ **Pause point:** The prepared grids can stay in liquid nitrogen for long-term storage.

### Grid screening, cryo-EM data collection, and processing

⌚ **Timing:** 2–4 weeks

37. Test the grids on screening transmission electron microscopes (TEMs), such as Glacios or F20 (FEI Thermo Scientific), and assess particle distribution, orientation, and ice quality.

**Note:** The grids can be loaded onto the F20 microscope straight from the grid storage box. However, the grids need to be clipped before being screened on the Glacios microscope.

38. Collect cryo-EM data from the prescreened grids on a FEI Titan Krios TEM (Thermo Fisher Scientific) operating at 300 kV and equipped with a direct electron detection (DED) camera in counting mode with  $\sim 50$  frames per movie and a total dose of  $\sim 58$  electrons per  $\text{\AA}^2$ , a physical pixel size of  $\sim 0.83$   $\text{\AA}$ , and a defocus value between  $-0.5$  to  $-2.5$   $\mu\text{m}$ . We used Krios with a post-column GIF Quantum energy filter and a Gatan K3 Summit DED camera, Gatan, Pleasanton, CA, USA.
39. Process the data in RELION 3.1 (Zivanov et al., 2018) or CryoSparc (Punjani et al., 2017). Perform beam-induced motion correction using MotionCor2 (Dose per frame of 1.16, EER fractionation -32, B Factor -150, number of patches  $5 \times 5$ ) (Zheng et al., 2017) and contrast transfer function (CTF) estimation using CTFFIND4.1 (Zhang, 2016) in RELION 3.1.

**Note:** All the processing steps can also be performed in cryoSPARC.

40. Manually pick  $\sim 3,000$  particles by selecting any particle shape that commonly appears in the micrographs, recognizing reoccurring shapes as well as any shape that potentially resembles an iGluR.

**Note:** We used the particle/mask diameter of 230  $\text{\AA}$ .

41. 2D-classify these manually selected particles to generate templates for further template-based auto picking in RELION 3.1.
42.  $4 \times 4$  bin the picked particle images to a pixel size of  $\sim 3.32$   $\text{\AA}/\text{pixel}$  and subject them to 3D classification into 10 classes (C1 symmetry). Select the best classes, which corresponded to the Y shape of iGluR (Figure 5).

**Note:** A model-generated iGluR map (for example, using the GluA2 model, PDB: 3KG2 (Sobolevsky et al., 2009)), low-pass filtered to 40  $\text{\AA}$ , can be used as an initial reference.

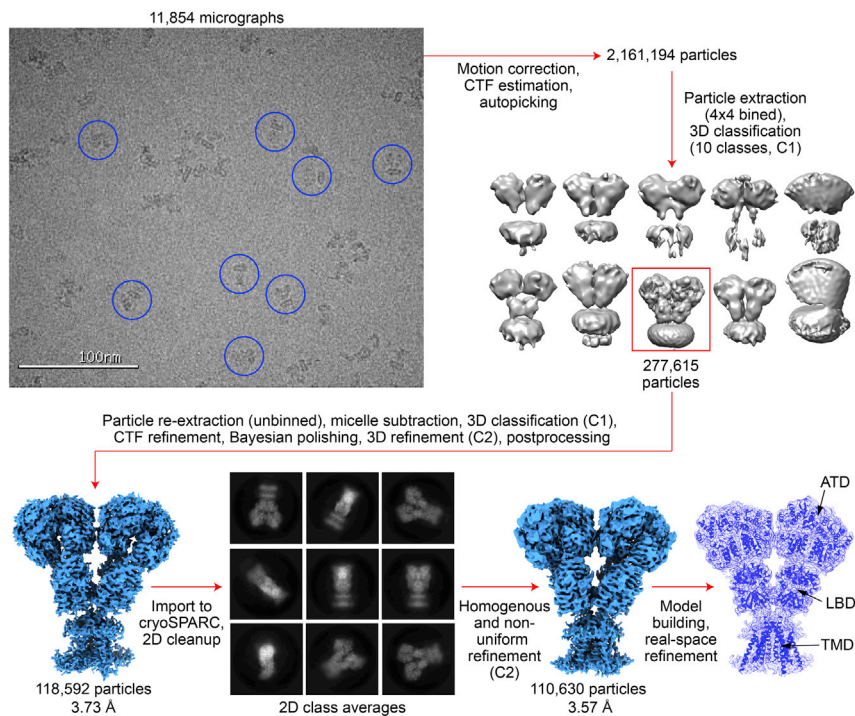


**Figure 5. Cryo-EM processing workflow**

43. Extract particles for the best 3D classes without binning to an original pixel size ( $\sim 0.83$  Å/pixel).

Perform 3D refinement using C2 symmetry in RELION 3.1. At this step, the postprocessed map from RELION had the resolution of  $\sim 3.98$  Å (FSC = 0.143) from 277,615 particles (Figure 5).

44. Carry out micelle subtraction. For micelle subtraction, first create a mask using 3D refined map as input from the last 3D refinement step in Relion. Then run Particle subtraction using optimizer.star file from the last 3D refinement step and the mask as an input. Carry out multiple rounds of 3D classification (C1 symmetry) without angular sampling to reduce particle heterogeneity followed by 3D refinement. Also, perform Bayesian polishing and CTF refinement.

**Note:** Vary the regularization parameter (T) and iterations for 3D classification. We used T= 4 and iterations = 40 in 3D classification without angular sampling. Multiple rounds of 3D classification into 8 classes followed by 3D refinement on the particles from the best class using C2 symmetry and postprocessing yielded a map with resolution of 3.73Å from 118,592 particles (FSC=0.143) in RELION. Every time we used the 3D refined map from the previous job as an input reference in the subsequent 3D classification job.

45. To improve the map quality, import the particles from the last 3D refinement job from RELION to cryoSPARC and clean them up by 2D classification.

46. Select the best 2D classes and subject the corresponding particles to homogeneous and non-uniform refinement in cryoSPARC applying C2 symmetry. The map after non-uniform refinement in cryoSPARC had a resolution of 3.57 Å (FSC = 0.143) (Chen et al., 2013) from 110,630 particles.

47. Estimate the local resolution using the unfiltered half-maps and Resmap (Kucukelbir et al., 2014) (Figure 5).

**Note:** Local resolution can also be estimated in cryoSPARC.

48. Use UCSF Chimera ([Pettersen et al., 2004](#)) to visualize the EM density maps.

### Model building and refinement

⌚ Timing: 1–2 weeks

Once the high-resolution cryo-EM map is obtained, build atomic models of AtGLR3.4.

49. As guides, use the crystal structure of AtGLR3.4-S1S2 (PDB: 7LZ0) ([Green et al., 2021](#)) to build the ligand-binding domain and homology modeling in SWISS-MODEL ([Waterhouse et al., 2018](#)) using the GluA2 crystal structure as a guide (PDB: 3KG2, ([Sobolevsky et al., 2009](#))) to build the amino terminal and transmembrane domains. Finalize the model building manually using COOT ([Emsley and Cowtan, 2004](#)).

**Note:** Since AtGLR3.4 is a tetramer, it is advisable to first build two subunits, A and B, and then duplicate the AB dimer following the C2 symmetry of the map to make the CD dimer and assemble the ABCD tetramer.

50. Refine the obtained atomic model of AtGLR3.4 in real-space using PHENIX ([Adams et al., 2010](#)).

51. Validate the model quality. For this purpose, we used the validation programs MolProbity (score = 1.69, clash score = 4.49, poor rotamers = 0.44%) ([Williams et al., 2018](#)) and EMRinger (EMRinger score = 2.41, optimal Threshold = 0.67, Rotamer-ratio = 0.77) ([Barad et al., 2015](#)) in Phenix.

### EXPECTED OUTCOMES

Approximately ~ 1 mg of purified AtGLR3.4 can be obtained from 800 mL HEK cells.

### LIMITATIONS

The multidomain architecture and flexibility of AtGLR3.4 could limit the resolution.

### TROUBLESHOOTING

#### Problem 1

No PCR fragment amplified or incorrect size of the PCR product (step 3 of the Construct preparation).

#### Potential solution

Optimize the primer annealing temperature by running a gradient PCR and optimize the primer extension time.

#### Problem 2

Few or no transformants (step 9 of the Construct preparation and step 3 of the main protocol).

#### Potential solution

Check the efficiency of the competent cells by transforming a control circular plasmid. Also check the temperature of the water bath for heat shock.

#### Problem 3

For different membrane proteins, one may need to use different detergents for solubilization (step 24 of the main protocol).

#### Potential solution

Check which detergent best extracts the protein of interest by running a detergent screen via FSEC on crude cell samples solubilized in different detergents.

#### Problem 4

Inefficient thrombin cleavage and eGFP removal (step 28 of the main protocol).

#### Potential solution

Optimize the concentration of the protein and thrombin amount in the reaction mixture. Sometimes, extremely high concentration of the protein results in incomplete thrombin digestion.

#### Problem 5

Too high or too low particle density on the grid (step 37 of the main protocol).

#### Potential solution

Adjust the protein concentration accordingly or vary the blot time and blot force when using the Vitrobot.

### RESOURCE AVAILABILITY

#### Lead contact

Further information and requests for resources and reagents should be directed to and will be fulfilled by the lead contact, Dr. Alexander I. Sobolevsky ([as4005@cumc.columbia.edu](mailto:as4005@cumc.columbia.edu)).

#### Materials availability

This study did not generate any new unique reagents. Further information requests about materials and reagents should be directed to the lead contact, Dr. Alexander I. Sobolevsky ([as4005@cumc.columbia.edu](mailto:as4005@cumc.columbia.edu)).

#### Data and code availability

No new code has been generated during this study. The EMDB and PDB codes generated by this data have already been deposited and reported in our previous paper ([Green et al., 2021](#)).

### ACKNOWLEDGMENTS

We are thankful to Kirill Nadezhdin and Arthur Neuberger for providing MW membrane protein standards. A.I.S. was supported by the National Institutes of Health (CA206573, NS083660, and NS107253) and the National Science Foundation (1818086).

### AUTHOR CONTRIBUTIONS

S.P.G., M.N.G., and M.V.Y. performed the experiments. M.N.G., S.P.G., and A.I.S. wrote the manuscript.

### DECLARATION OF INTERESTS

The authors declare no competing interests.

### REFERENCES

- Adams, P.D., Afonine, P.V., Bunkoczi, G., Chen, V.B., Davis, I.W., Echols, N., Headd, J.J., Hung, L.W., Kapral, G.J., Grosse-Kunstleve, R.W., et al. (2010). PHENIX: a comprehensive Python-based system for macromolecular structure solution. *Acta Crystallogr. D Biol. Crystallogr.* **66**, 213–221.
- Barad, B.A., Echols, N., Wang, R.Y., Cheng, Y., DiMaio, F., Adams, P.D., and Fraser, J.S. (2015). EMRinger: side chain-directed model and map validation for 3D cryo-electron microscopy. *Nat. Methods* **12**, 943–946.
- Bhardwaj, R., Lindinger, S., Neuberger, A., Nadezhdin, K.D., Singh, A.K., Cunha, M.R., Derler, I., Gyimesi, G., Reymond, J.L., Hediger, M.A., et al. (2020). Inactivation-mimicking block of the epithelial calcium channel TRPV6. *Sci. Adv.* **6**, eabe1508.
- Chen, S., McMullan, G., Faruqi, A.R., Murshudov, G.N., Short, J.M., Scheres, S.H., and Henderson, R. (2013). High-resolution noise substitution to measure overfitting and validate resolution in 3D structure determination by single particle electron cryomicroscopy. *Ultramicroscopy* **135**, 24–35.
- Emmsley, P., and Cowtan, K. (2004). Coot: model-building tools for molecular graphics. *Acta Crystallogr. D Biol. Crystallogr.* **60**, 2126–2132.
- Goehring, A., Lee, C.H., Wang, K.H., Michel, J.C., Claxton, D.P., Bacongus, I., Althoff, T., Fischer, S., Garcia, K.C., and Gouaux, E. (2014). Screening and large-scale expression of membrane proteins in mammalian cells for structural studies. *Nat. Protoc.* **9**, 2574–2585.
- Green, M.N., Gangwar, S.P., Michard, E., Simon, A.A., Portes, M.T., Barbosa-Caro, J., Wudick, M.M., Lizzio, M.A., Klykov, O., Yelshanskaya, M.V., et al. (2021). Structure of the *Arabidopsis thaliana* glutamate receptor-like channel GLR3.4. *Mol. Cell* **81**, 3216–3226.
- Kawate, T., and Gouaux, E. (2006). Fluorescence-detection size-exclusion chromatography for precrystallization screening of integral membrane proteins. *Structure* **14**, 673–681.

- Kucukelbir, A., Sigworth, F.J., and Tagare, H.D. (2014). Quantifying the local resolution of cryo-EM density maps. *Nat. Methods* 11, 63–65.
- McGoldrick, L.L., Singh, A.K., Saotome, K., Yelshanskaya, M.V., Twomey, E.C., Grassucci, R.A., and Sobolevsky, A.I. (2018). Opening of the human epithelial calcium channel TRPV6. *Nature* 553, 233–237.
- Nadezhdin, K.D., Neuberger, A., Trofimov, Y.A., Krylov, N.A., Sinica, V., Kupko, N., Vlachova, V., Zakharian, E., Efremov, R.G., and Sobolevsky, A.I. (2021). Structural mechanism of heat-induced opening of a temperature-sensitive TRP channel. *Nat. Struct. Mol. Biol.* 28, 564–572.
- Pettersen, E.F., Goddard, T.D., Huang, C.C., Couch, G.S., Greenblatt, D.M., Meng, E.C., and Ferrin, T.E. (2004). UCSF Chimera—a visualization system for exploratory research and analysis. *J. Comput. Chem.* 25, 1605–1612.
- Punjani, A., Rubinstein, J.L., Fleet, D.J., and Brubaker, M.A. (2017). cryoSPARC: algorithms for rapid unsupervised cryo-EM structure determination. *Nat. Methods* 14, 290–296.
- Russo, C.J., and Passmore, L.A. (2014). Electron microscopy: Ultrastable gold substrates for electron cryomicroscopy. *Science* 346, 1377–1380.
- Singh, A.K., McGoldrick, L.L., and Sobolevsky, A.I. (2018). Structure and gating mechanism of the transient receptor potential channel TRPV3. *Nat. Struct. Mol. Biol.* 25, 805–813.
- Sobolevsky, A.I., Rosconi, M.P., and Gouaux, E. (2009). X-ray structure, symmetry and mechanism of an AMPA-subtype glutamate receptor. *Nature* 462, 745–756.
- Twomey, E.C., Yelshanskaya, M.V., Grassucci, R.A., Frank, J., and Sobolevsky, A.I. (2016). Elucidation of AMPA receptor-stargazin complexes by cryo-electron microscopy. *Science* 353, 83–86.
- Twomey, E.C., Yelshanskaya, M.V., Grassucci, R.A., Frank, J., and Sobolevsky, A.I. (2017). Channel opening and gating mechanism in AMPA-subtype glutamate receptors. *Nature* 549, 60–65.
- Waterhouse, A., Bertoni, M., Bienert, S., Studer, G., Tauriello, G., Gumienny, R., Heer, F.T., de Beer, T.A.P., Rempfer, C., Bordoli, L., et al. (2018). SWISS-MODEL: homology modelling of protein structures and complexes. *Nucleic Acids Res.* 46, W296–W303.
- Williams, C.J., Headd, J.J., Moriarty, N.W., Prisant, M.G., Videau, L.L., Deis, L.N., Verma, V., Keedy, D.A., Hintze, B.J., Chen, V.B., et al. (2018). MolProbity: more and better reference data for improved all-atom structure validation. *Protein Sci.* 27, 293–315.
- Zhang, K. (2016). Gctf: real-time CTF determination and correction. *J. Struct. Biol.* 193, 1–12.
- Zheng, S.Q., Palovcak, E., Armache, J.P., Verba, K.A., Cheng, Y., and Agard, D.A. (2017). MotionCor2: anisotropic correction of beam-induced motion for improved cryo-electron microscopy. *Nat. Methods* 14, 331–332.
- Zivanov, J., Nakane, T., Forsberg, B.O., Kimanius, D., Hagen, W.J., Lindahl, E., and Scheres, S.H. (2018). New tools for automated high-resolution cryo-EM structure determination in RELION-3. *Elife* 7, e42166.

## **Chapter 3.**

### **Structure of the *Arabidopsis* Glutamate Receptor-Like Channel**

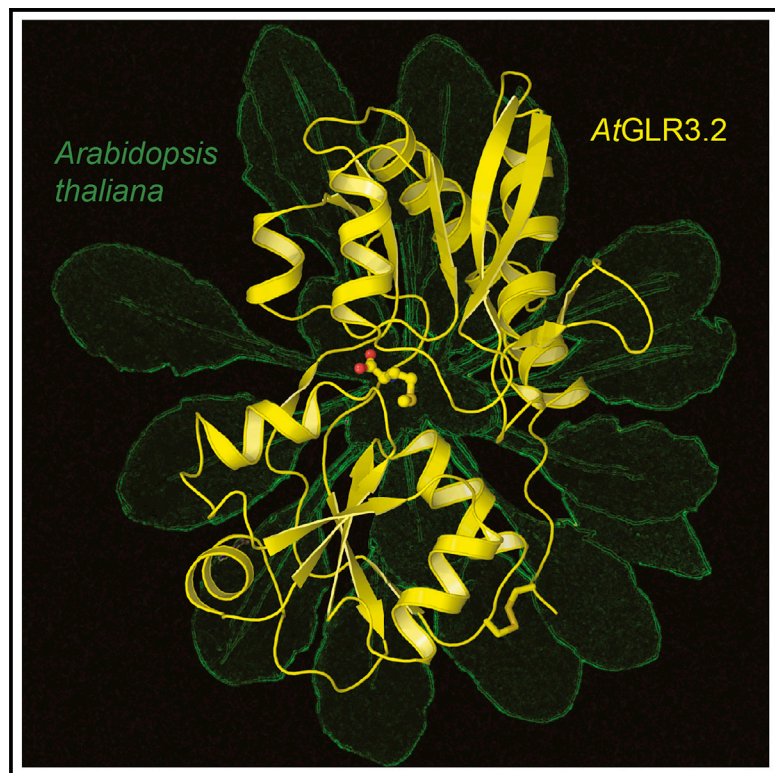
#### **GLR3.2 Ligand-Binding Domain**

This chapter is a paper originally published in *Structure* (Gangwar et al., 2021). The paper reveals the structural basis of an *Arabidopsis thaliana* GLR 3.2 (*AtGLR3.2*) ligand binding activation and ligand binding promiscuity. The structures of the ligand-binding domain (LBD), solved via X-ray crystallography, show *AtGLR3.2* isolated LBD in complex with agonists glycine and methionine.



### Structure of the *Arabidopsis* Glutamate Receptor-like Channel GLR3.2 Ligand-Binding Domain

#### Graphical Abstract



#### Authors

Shanti Pal Gangwar, Marriah N. Green, Erwan Michard, Alexander A. Simon, José A. Feijó, Alexander I. Sobolevsky

#### Correspondence

jfeijo@umd.edu (J.A.F.),  
as4005@cumc.columbia.edu (A.I.S.)

#### In Brief

Glutamate receptor-like channels (GLRs) play important roles in plant physiology but their structural features have just begun to unravel. Gangwar et al. report structures of *Arabidopsis thaliana* GLR3.2 ligand-binding domain in complex with agonists glycine and methionine and discuss structural and functional relationships between GLRs and ionotropic glutamate receptors (iGluRs).

#### Highlights

- AtGLR3.2 LBD structures were solved in complex with agonists glycine and methionine
- AtGLR3.2 LBD structures show clamshell architecture typical for vertebrate iGluRs
- Mutation of R133 that is critical for agonist binding increases channel's activity
- Structural conservation between GLRs and iGluRs predicts common gating principles





## Short Article

# Structure of the *Arabidopsis* Glutamate Receptor-like Channel GLR3.2 Ligand-Binding Domain

Shanti Pal Gangwar,<sup>1,4</sup> Marriah N. Green,<sup>1,2,4</sup> Erwan Michard,<sup>3,4</sup> Alexander A. Simon,<sup>3</sup> José A. Feijó,<sup>3,\*</sup> and Alexander I. Sobolevsky<sup>1,5,\*</sup>

<sup>1</sup>Department of Biochemistry and Molecular Biophysics, Columbia University, 650 West 168<sup>th</sup> Street, New York, NY 10032, USA

<sup>2</sup>Training Program in Nutritional and Metabolic Biology, Institute of Human Nutrition, Columbia University Irving Medical Center, 630 West 168<sup>th</sup> Street, New York, NY 10032, USA

<sup>3</sup>Department of Cell Biology and Molecular Genetics, University of Maryland, 0118 BioScience Research Bldg, College Park, MD 20742-5815, USA

<sup>4</sup>These authors contributed equally

<sup>5</sup>Lead Contact

\*Correspondence: [jfeijo@umd.edu](mailto:jfeijo@umd.edu) (J.A.F.), [as4005@cumc.columbia.edu](mailto:as4005@cumc.columbia.edu) (A.I.S.)

<https://doi.org/10.1016/j.str.2020.09.006>

## SUMMARY

Glutamate receptor-like channels (GLRs) play important roles in numerous plant physiological processes. GLRs are homologous to ionotropic glutamate receptors (iGluRs) that mediate neurotransmission in vertebrates. Here we determine crystal structures of *Arabidopsis thaliana* GLR3.2 ligand-binding domain (LBD) in complex with glycine and methionine to 1.58- and 1.75-Å resolution, respectively. Our structures show a fold similar to that of iGluRs, but with several secondary structure elements either missing or different. The closed clamshell conformation of GLR3.2 LBD suggests that both glycine and methionine act as agonists. The mutation R133A strongly increases the constitutive activity of the channel, suggesting that the LBD mutated at the residue critical for agonist binding produces a more stable closed clamshell conformation. Furthermore, our structures explain the promiscuity of GLR activation by different amino acids, confirm evolutionary conservation of structure between GLRs and iGluRs, and predict common molecular principles of their gating mechanisms driven by bilobed clamshell-like LBDs.

## INTRODUCTION

Ionotropic glutamate receptors (iGluRs) are ligand-gated ion channels that mediate excitatory neurotransmission throughout the vertebrate central nervous system (Kumar and Mayer, 2013; Traynelis et al., 2010). iGluRs are assemblies of four subunits, each containing four main domains: the amino-terminal domain (ATD) implicated in receptor assembly, trafficking, and regulation; the ligand-binding domain (LBD or S1S2) that harbors binding sites for agonists, antagonists, and allosteric modulators; the transmembrane domain forming an ion channel; and the cytosolic carboxy-terminal domain, which is involved in receptor localization and regulation (Sobolevsky, 2015; Twomey and Sobolevsky, 2018). Glutamate and other amino acids that function as neurotransmitters activate iGluRs by binding to the LBD and inducing conformational changes that lead to the opening of the ion channel (Armstrong and Gouaux, 2000; Twomey and Sobolevsky, 2018). Homologs of mammalian iGluRs have been identified in both vascular and non-vascular plants, known as glutamate receptor-like channels or GLRs, and are predicted to share the structural domain organization (Lam et al., 1998; Wudick et al., 2018a).

Recent studies revealed vital roles of GLRs in various physiological processes in plants, including wound response, stomatal

aperture, seed germination, root development, innate immunity, and pollen tube growth (Kong et al., 2015, 2016; Li et al., 2013; Michard et al., 2011; Mousavi et al., 2013; Singh et al., 2016). GLRs are conserved along the plant lineage (2 in mosses, 4 in the lycophyte *Sellaginella*, 9 in *Ginkgo*) but went through an enormous expansion in the higher plants (40 in *Pinus*) and dramatic diversification into different clades in some angiosperms (Aouini et al., 2012; De Bortoli et al., 2016; Ortiz-Ramirez et al., 2017; Price et al., 2012; Wudick et al., 2018b). *Arabidopsis thaliana* has 20 AtGLRs phylogenetically divided into three clades (Chiu et al., 2002; Lacombe et al., 2001; Wudick et al., 2018a). AtGLR3.2, a representative of the third clade, is widely expressed in the plant and displays highest expression in root cells where it localizes in the plasma membrane (Vincill et al., 2013). Overexpression of AtGLR3.2 in transgenic plants resulted in Ca<sup>2+</sup> deprivation that was rescued by exogenous Ca<sup>2+</sup> application, demonstrating ion channel functionality (Kim et al., 2001). While the structure of the LBD of AtGLR3.3 has been recently solved and predicted to accommodate various amino acids (Alfieri et al., 2020), there is no experimental confirmation that the predicted ligand promiscuity bears any functional consequence, namely in terms of activity elicitation, or other physiological consequences. Intriguingly, the sequence divergence of the “gate”



domain (the equivalent of the SYTANLAAF motif in iGluRs) (Wollmuth and Sobolevsky, 2004) has led to the hypothesis that some GLRs might function without ligand-induced activation (Wudick et al., 2018a). This prediction is partially supported by patch-clamp recordings from plant protoplasts where constitutive currents are abolished in *glr* knockout (KO) lines (Mou et al., 2020). When expressed in the mammalian system, three channels (*PpGLR1*, *AtGLR3.2*, and *AtGLR3.3*) display constitutive currents in the absence of canonical ligands but are strongly activated by CORNICHON-homolog proteins (CNIHs) (Ortiz-Ramirez et al., 2017; Wudick et al., 2018b). Despite the constitutive activity reported for some GLRs, they remain to be gated by ligands, and screens designed to measure the effects of all proteinogenic amino acids showed an almost continuous gradient of *AtGLR1.4* activation/inhibition (Tapken et al., 2013). A subsequent screen, using a different assay, showed a similar pattern for *PpGLR1*, but with the strongest activity inducer being the important plant hormone-like non-proteinogenic 1-aminocyclopropane-1-carboxylic acid (Mou et al., 2020). The apparent unique gating properties of GLRs, characterized by background ion channel activity and amino acid stimulation, require structural and functional data to enlighten their possible physiological meaning.

While GLRs, including *AtGLR3.2*, govern a broad range of physiological and pathophysiological processes in plants, fundamental molecular mechanisms underlying their function remain elusive. To gain insight into how *AtGLR3.2* binds to its activating ligands, we embarked on structural studies of its LBD. We found that the LBD of *AtGLR3.2* binds to methionine (Met) and glycine (Gly), but the binding pocket is predicted to accommodate other amino acids as well. The LBD clamshell is closed in both structures, suggesting that they represent an active state of *AtGLR3.2* that favors channel opening. Furthermore, we show that a point mutation of a residue critical for ligand binding increases the channel's constitutive activity in the absence of either ligands or CNIHs.

## RESULTS AND DISCUSSION

### Structure Determination

To determine the LBD structure, we used *A. thaliana* GLR3.2 (*AtGLR3.2*) DNA to make a crystallizing construct, GLR3.2-S1S2. The boundaries of the two segments, S1 and S2 that assemble into the LBD, were determined based on the amino acid sequence alignment of *AtGLR3.2* with mammalian iGluRs (Figure S1). At the beginning of S1 in the GLR3.2-S1S2 construct, there are 46 N-terminal residues that have not been resolved in our crystal structures and presumably remain disordered. We expressed the GLR3.2-S1S2 construct in bacteria and purified the protein using affinity and ion-exchange chromatography (see STAR Methods). Crystals of GLR3.2-S1S2 grew in the presence of Met and Gly in sitting and hanging drops of vapor diffusion crystallization trays and were cryoprotected using glycerol for diffraction data collection at the synchrotron. Crystals of GLR3.2-S1S2 grown in the presence of Gly and Met belonged to the  $P2_12_12_1$  space group, contained one S1S2 protomer in the asymmetric unit, and diffracted to 1.58- and 1.75-Å resolution, respectively (Table 1). We solved the GLR3.2-S1S2<sub>Gly</sub> and GLR3.2-S1S2<sub>Met</sub> structures by molecular replacement, initially

**Table 1. Crystallographic Statistics**

	GLR3.2-S1S2 <sub>Gly</sub>	GLR3.2-S1S2 <sub>Met</sub>
Beamline	NE-CAT 24-ID-C	NE-CAT 24-ID-C
Wavelength (Å)	0.97910	0.97910
Space group	$P2_12_12_1$	$P2_12_12_1$
Cell parameters ( <i>a</i> , <i>b</i> , <i>c</i> , Å)	47.39, 64.37, 75.93	47.65, 65.47, 72.19
Cell parameters ( $\alpha$ , $\beta$ , $\gamma$ , °)	90, 90, 90	90, 90, 90
Resolution (Å)	47.39–1.58 (1.61–1.58)	72.19–1.75 (1.78–1.75)
No. of monomers in AU	1	1
Total observations	146,995 (5,783)	124,336 (3,896)
Unique observations	32,133 (1,553)	23,419 (1,258)
$R_{\text{merge}}$	0.06 (0.61)	0.078 (0.67)
$R_{\text{meas}}$	0.06 (0.67)	0.87 (0.80)
$R_{\text{pim}}$	0.03 (0.35)	0.03 (0.43)
Mean $I/\sigma(I)$	14.9 (2.1)	13.3 (1.8)
Completeness (%)	99.2 (98.7)	99.8 (99.1)
Multiplicity	4.6 (3.7)	5.3 (3.1)
$CC_{1/2}$	0.99 (0.69)	0.99 (0.65)
Wilson <i>B</i> factor (Å <sup>2</sup> )	17.33	19.7
Refinement		
Resolution	48.23–1.58	48.50–1.75
Reflections used in refinement	32,086 (3,190)	23,364 (2,295)
$R_{\text{work}}$	0.157	0.165
$R_{\text{free}}$	0.183	0.199
No. of non-hydrogen atoms	2,052	1,962
Macromolecules	1,852	1,839
Ligands	9	11
Average <i>B</i> factor	21.13	23.87
Macromolecules	20.13	23.40
Protein residues	240	238
No. of water molecules	202	112
RMSD bond lengths (Å)	0.01	0.01
RMSD angles (°)	1.89	1.90
Ramachandran plot		
Preferred regions (%)	97.90	99.15
Allowed regions (%)	2.10	0.85
Outliers (%)	0	0
PDB entry	6VEA	6VE8

Values in parentheses are for the highest-resolution shell.

using a homology modeled search probe (see STAR Methods). The clarity of the resulting electron density maps was sufficient (Figure 1) for the *de novo* building of the structural models that included residues G47 to N286, with a 108-residue-long S1 GT linked to a 130-residue-long S2.

The structures of approximately  $57 \times 37 \times 35 \text{ Å}^3$  in dimension have a bilobed clamshell architecture (Figures 2A and 2B), with the ligand-binding site between the upper D1 lobe and the lower D2 lobe, similar to iGluR LBDs (Gouaux, 2004; Mollerud et al., 2017; Pohlsgaard et al., 2011). The GLR3.2-S1S2<sub>Gly</sub> and

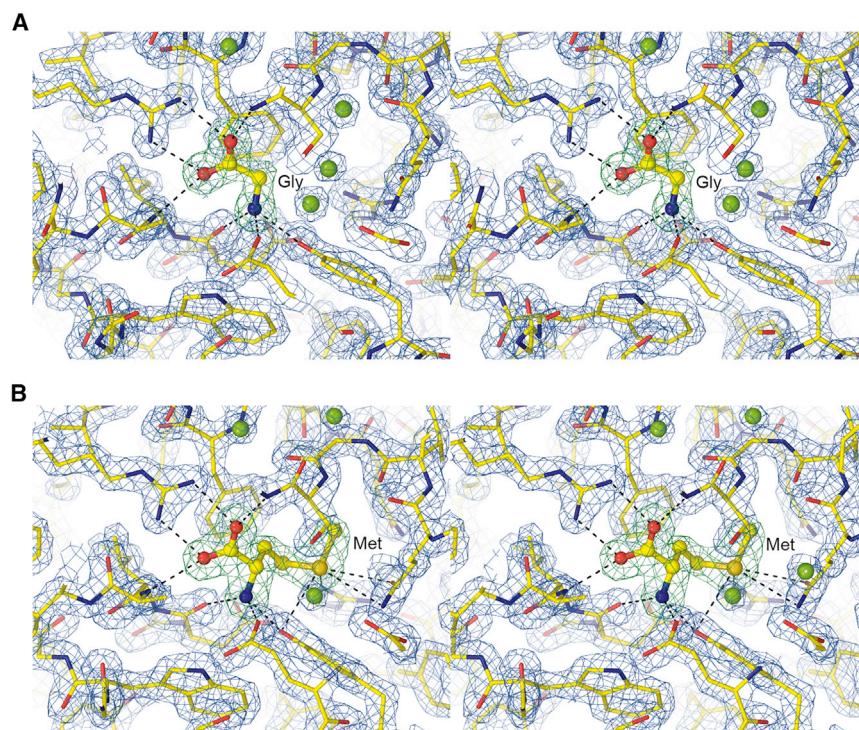


**Figure 1. AtGLR3.2-LBD Electron Density**

Close-up stereo views of AtGLR3.2 LBD (S1S2) in complex with glycine (A) and methionine (B). Mesh shows a  $2F_o - F_c$  electron density map contoured at  $2\sigma$  (blue) and  $F_o - F_c$  map contoured at  $4\sigma$  (green) when ligands were not present in the model. See also Figure S2.

GLR3.2-S1S2<sub>Met</sub> structures superpose very well with the root-mean-square deviation (RMSD) of 0.275 Å for C $\alpha$  atoms. For the ligand-binding pocket, even side-chain orientations are very similar between GLR3.2-S1S2<sub>Gly</sub> and GLR3.2-S1S2<sub>Met</sub>.

### Ligand Binding

The ligand-binding pocket of GLR3.2-S1S2 resembles the ligand-binding pocket of iGluR LBDs (Figures 2C and 2D), with the key interactions and binding residues conserved (Figure S1). The ligand Gly forms hydrogen bonds with Asp126, Ala128, Arg133, and Tyr178 and non-bonded contacts with Phe108, Asp126, Ile127, Ala128, Arg133, Ser177, Tyr178, Glu218, and Tyr221 (Figure S2A). Similarly, the ligand Met establishes hydrogen bonds with Asp126, Ala128, Arg133, and Tyr221 and forms non-bonded contacts with Arg57, Phe108, Asp126, Ile127, Ala128, Arg133, Gln174, Val175, Gly176, Ser177, Tyr178, Glu218, and Tyr221 (Figure S2B).

For both Gly and Met, the guanidinium group of Arg133 and the backbone amines of Ala128 and Tyr178 are hydrogen bonded to the carboxyl group of the ligand, while the backbone carbonyl oxygen of Asp126, the carboxyl group of Glu218, and the hydroxyl group of Tyr221 coordinate the amino group of the ligand. The thioether group of Met is additionally coordinated by the hydroxyl group of Tyr221, guanidinium group of Arg57, and the amide group of Gln174. These interactions are specific to Met and are missing in the case of Gly, which lacks the bulky side chain. Instead, two water molecules occupy the space that in the case of Met is occupied by the thioether group. These two water molecules are stabilized by hydrogen bonds with Ser177 and Arg57.

Overall, the ligand-binding pocket of GLR3.2-S1S2 is shaped to bind differently sized amino acids (for example, Gly versus

Met) by exploiting the same interactions for binding the conserved amino acid core and adjusting the fit of the side chains into the corresponding binding pocket cavity with water. This explains a diverse range of ligand specificity previously observed for GLRs, with at least 12 of the 20 proteinogenic amino acids and D-serine serving as agonists for the most studied AtGLR1.2, AtGLR1.4, AtGLR3.3, AtGLR3.4, and AtGLR3.5 (Forde and Roberts, 2014; Kong et al., 2016; Michard et al., 2011; Tapken et al., 2013; Vincill et al., 2012, 2013; Wudick et al., 2018a). In agreement with our results, the recently determined structures of the AtGLR3.3-S1S2 (Alfieri et al., 2020) revealed similar ligand-binding promiscuity. The binding pocket and the mode of ligand binding, however, might be somewhat different among GLRs. For example, Trp, Phe, and Tyr can serve as agonists of AtGLR1.4 but not AtGLR3.3 or AtGLR3.4 (Tapken et al., 2013; Vincill et al., 2012, 2013), suggesting that the ligand-binding pocket in AtGLR1.4 is likely larger to accommodate bulkier hydrophobic side chains. In part, differences in ligand binding among GLRs can originate from residues directly interacting with the ligand. For example, among eight GLR3.2 residues interacting with the ligand, six are conserved between clade 3 GLRs (Arg57, Asp126, Arg133, Tyr178, Glu218, and Tyr221) but two are not (Figure S1). Ala128 is Thr in GLR3.6, GLR3.4, and GLR3.7, while Gln174 is Pro in GLR3.6. Ligand binding can also be allosterically influenced by ATDs, which are much more variable in sequence compared with LBDs. In addition, GLR ligands may bind sites distinct from the site inside the LBD clamshell. For example, a bulky tripeptide glutathione that activates some GLRs is unlikely to fit the pocket accommodating Gly and Met (Figure 2) in the GLR3.2 LBD but it might bind somewhere else on the full-length protein.

### Effect of a Point Mutation on Gating

Given the structural determinants of ligand binding, we investigated the effects of possible disruption of ligand binding by mutating critical amino acids. We focused on the highly conserved Arg133, since the guanidinium group of this arginine coordinates the carboxyl group of both bound ligands and is critical for their binding. The possible effects of this point mutation were assayed by the transfection of mammalian COS-7 cells expressing the Ca<sup>2+</sup> indicator Yellow CaMeleon 3.6 (YC3.6). To assay Ca<sup>2+</sup> influx, we first placed COS-7 cells in a Ca<sup>2+</sup>-free solution containing EGTA and subsequently subjected them to



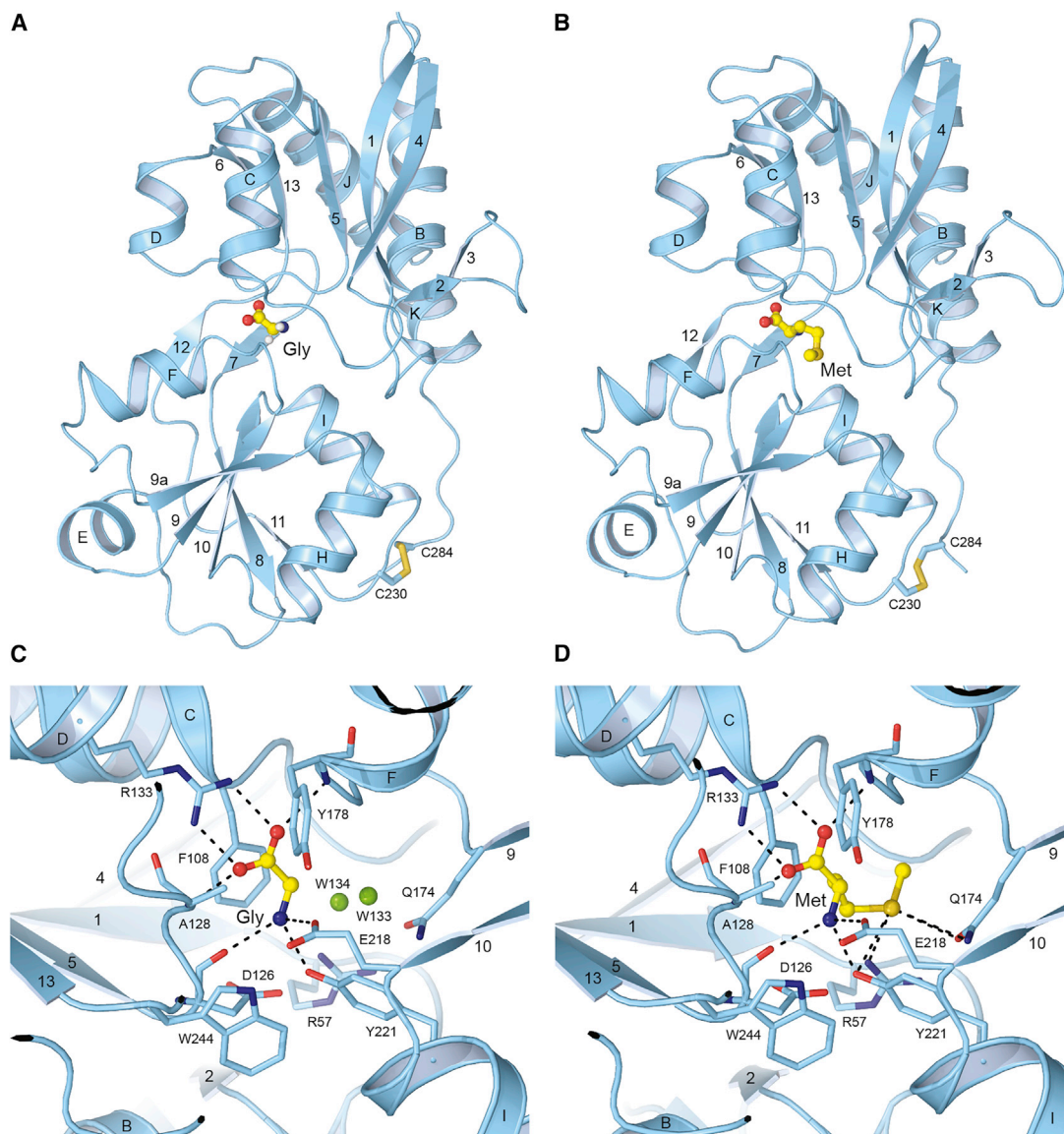


**Figure 2. AtGLR3.2 Ligand-Binding Domain Structure**

(A and B) Structures of isolated AtGLR3.2 LBD (S1S2) in complex with glycine (A) and methionine (B). The ligands are in ball-and-stick representation. Highly conserved cysteines, C230 and C284, are connected by disulfide bonds and shown as sticks.

(C and D) Close-up views of the ligand-binding pocket with bound glycine (C) and methionine (D). Residues involved in ligand binding are shown as sticks. Interactions between the ligands and the binding pocket residues are indicated by dashed lines.

See also [Figures S1](#) and [S2](#).

14.5 mM  $\text{Ca}^{2+}$  (see the top bar in [Figure 3A](#)). In the absence of ligand ([Figure 3A](#), black dots), cytosolic  $\text{Ca}^{2+}$  showed a slight increase, revealing some basal conductance. When the experiment was repeated in the presence of 0.5 mM Gly, this elevation peaked at the same  $[\text{Ca}^{2+}]_{\text{cyt}}$  level and timing. Yet, while  $[\text{Ca}^{2+}]_{\text{cyt}}$  dropped immediately after peaking without the ligand, in the presence of 0.5 mM Gly,  $[\text{Ca}^{2+}]_{\text{cyt}}$  levels were sustained for longer, producing a statistically detectable difference between assays ( $p < 0.01$ ). However, in the presence of 1 mM Gly, the elevation of cytosolic  $\text{Ca}^{2+}$  was more pronounced and statistically significant when compared with the other two experiments ( $p < 10^{-6}$  compared with control and  $p = 0.01$  with 0.5 mM Gly).

These elevations suggest that the wild-type AtGLR3.2 alone is moderately gated by 1 mM Gly. We then tested the effect of CNIHs that were previously shown to strongly promote ligand-independent activation of AtGLR3.2 currents ([Wudick et al., 2018b](#)). Expression of AtCNIH4 alone in COS-7 cells induces an increased  $\text{Ca}^{2+}$  influx ([Figure S3](#)). Given the conservation of CNIHs in plants and their capacity to complement other CNIH homologs, namely in yeast ([Wudick et al., 2018b](#)), we interpret this increase as a reflection of non-specific activation of COS-7 endogenous transport proteins. The effect of AtCNIH4 was insensitive to ligand addition ([Figure S3](#)). Yet, simultaneous expression of AtGLR3.2 and AtCNIH4 ([Figure 3B](#)) rendered

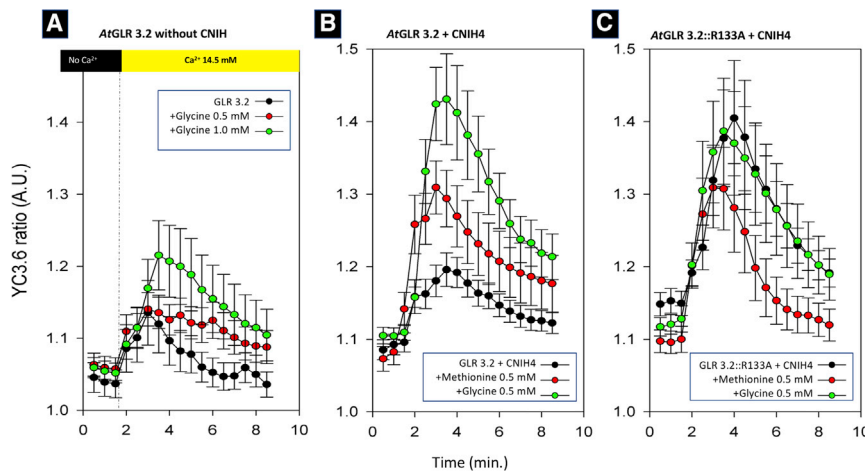


**Figure 3. Effect of Point Mutations in Ligand Gating**

The effect of a point mutation in the LBD on AtGLR3.2 channel gating was assayed by the transfection of mammalian COS-7 cells expressing a  $\text{Ca}^{2+}$  indicator (YC3.6).

(A) Expression of wild-type channel alone shows its  $\text{Ca}^{2+}$  conductance to be gated by glycine at 1.0 mM. The experimental sequence is shown on the top black/yellow bar. Cells are  $\text{Ca}^{2+}$ -starved with EGTA and then perfused with 14.5 mM  $\text{Ca}^{2+}$ . In the absence of ligand (black dots), a slight increase occurs in cytosolic  $\text{Ca}^{2+}$ . When the experiment is done in the presence 0.5 mM glycine, this elevation is slightly, but significantly, prolonged ( $p < 0.01$ ), but in the presence of 1.0 mM glycine there is a visible and statistically significant elevation of cytosolic  $\text{Ca}^{2+}$  ( $p < 10^{-6}$  compared with control and  $p = 0.01$  compared with 0.5 mM Gly). (B and C) Simultaneous expression of AtGLR3.2 and AtCNIH4 (B) renders the channel gated by

both methionine (red) and glycine (green) at 0.5 mM in comparison with the control ( $p < 0.01$  for all comparisons). However, when the critical residue 133 is substituted from arginine to alanine (C), the channel behaves as being constitutively open (black; compare with black control in B). Data are presented as mean  $\pm$  SEM. All statistics obtained by two-way ANOVA with Tukey's HSD.

See also Figures S3 and S4.

much larger and robust  $\text{Ca}^{2+}$  elevations induced by both Met (red) and Gly (green) at 0.5 mM concentrations in comparison with the control ( $p < 0.01$  for both).

Finally, we tested the  $\text{Ca}^{2+}$  uptake by AtGLR3.2 with R133A mutation in the LBD, which was predicted to disrupt ligand binding (Figure 3C). Our  $\text{Ca}^{2+}$  uptake traces suggest that AtGLR3.2-R133A behaved as a constitutively open channel (compare black traces in Figures 3B and 3C), reaching the peak values of  $\text{Ca}^{2+}$  influx similar to or higher than that in the non-mutated channel in the presence of 0.5 mM Gly (green;  $p > 0.1$ ) or 0.5 mM Met (red;  $p < 0.01$ ). This apparent constitutive activation of the channel is independent of the presence of AtCNIH4 (Figure S4), which reached a similar level of  $\text{Ca}^{2+}$  flux in the presence or absence of AtCNIH4. Remarkably, the presence of AtCNIH4 affects the ligand-binding properties, unveiling an apparent inhibitory effect of Gly (see Figures 3A and 3C). R133A mutation likely produces an alteration in the clamshell structure similar to ligand binding, i.e., clamshell closure, resulting in a similar effect on the pore. This result is difficult to reconcile with no full-length GLR structure available, but highlights the importance of the LBD for GLR gating. Mutations in the iGluR LBD have been shown to make  $\alpha$ -amino-3-hydroxy-5-methylisoxazole-4-propionic acid (AMPA) receptors more responsive to kainate and less responsive to AMPA (Armstrong et al., 2003), to increase the efficacy of kainate receptor agonists (Meyerson et al., 2014), and to render *N*-methyl-D-aspartic acid (NMDA) receptors constitutively active (Blanke and VanDongen, 2008).

The strong increase in ligand-induced AtGLR3.2 activation caused by the presence of CNIH4 is consistent with the open-state-stabilizing effects of HsCNIH2 and HsCNIH3 on AMPA receptors, where CNIHs slow down the deactivation and desensitization kinetics (Gill et al., 2011; Kato et al., 2010; Schwenk et al., 2009; Shi et al., 2010) and increase single-channel conductance (Coombs et al., 2012). While AMPA receptors are activated by ligands in the absence of CNIHs, the AtCNIH4 presence appears to always result in significant additional activation of

AtGLR3.2. In the presence of AtCNIH4, Gly and Met appear to act as an agonist and partial agonist on wild-type AtGLR3.2 (Figure 3B). Met, however, acts like an inverse agonist on the R133A mutant. Indeed, strong activation of AtGLR3.2 by R133A in the presence of AtCNIH4 is not altered by Gly but suppressed to the level of partial activation in the presence of Met (Figure 3C). Why these ligands, which cause the same clamshell closure in wild-type LBD (Figure 2), behave so differently is currently unclear and may require full-length AtGLR3.2 structures to be understood.

### Comparison of GLR and iGluR LBD Structures

The LBD, which binds agonists, competitive antagonists, and positive allosteric modulators, adopts a similar bilobed D1-D2 clamshell architecture in vertebrate, invertebrate, and plant glutamate receptors (Figures 4A–4F). We compared the AtGLR3.2 LBD with the LBDs of three different mammalian iGluRs (AMPA, kainate, and NMDA subtypes), rotifer *Adianta vaga* subunit 1 (AvGluR1), and *A. thaliana* GLR3.3. These species are separated by millions of years of evolution and their LBD sequences share poor sequence identity. In Figure 4, we superimposed the GLR3.2-S1S2 with the previously solved agonist-bound S1S2 structures of GluA2 (PDB: 1FTJ) (Armstrong and Gouaux, 2000), GluK2 (PDB: 1S50) (Mayer, 2005), GluN1 (PDB: 1PB7) (Furukawa and Gouaux, 2003), GluN2A (PDB: 2A5S) (Furukawa et al., 2005), AvGluR1 (PDB: 4IO2) (Lomash et al., 2013), and AtGLR3.3 (PDB: 6R88) (Alfieri et al., 2020). The RMSD values calculated for all C $\alpha$  atoms in each superposition with GLR3.2-S1S2 are 1.9 Å for GluA2, 1.5 Å for GluK2, 1.8 Å for GluN1, 4.5 Å for GluN2, 3 Å for AvGluR1, and 0.77 Å for AtGLR3.3. Structures of AtGLR3.3 and AtGLR3.2 LBDs are very similar, consistent with their sequence similarity. The amino acid sequences of AtGLR3.2 and AtGLR3.3 LBDs share 61.6% identity, and all eight residues that interact with the agonist are 100% conserved, including Arg in the  $\beta$ 1- $\beta$ 2 loop, Asp and Ala in the  $\beta$ 5- $\alpha$ D loop, Arg in  $\alpha$ D, Gln in  $\beta$ 9, Tyr in  $\alpha$ F, Glu in  $\beta$ 10, and Tyr in  $\alpha$ I (Figures

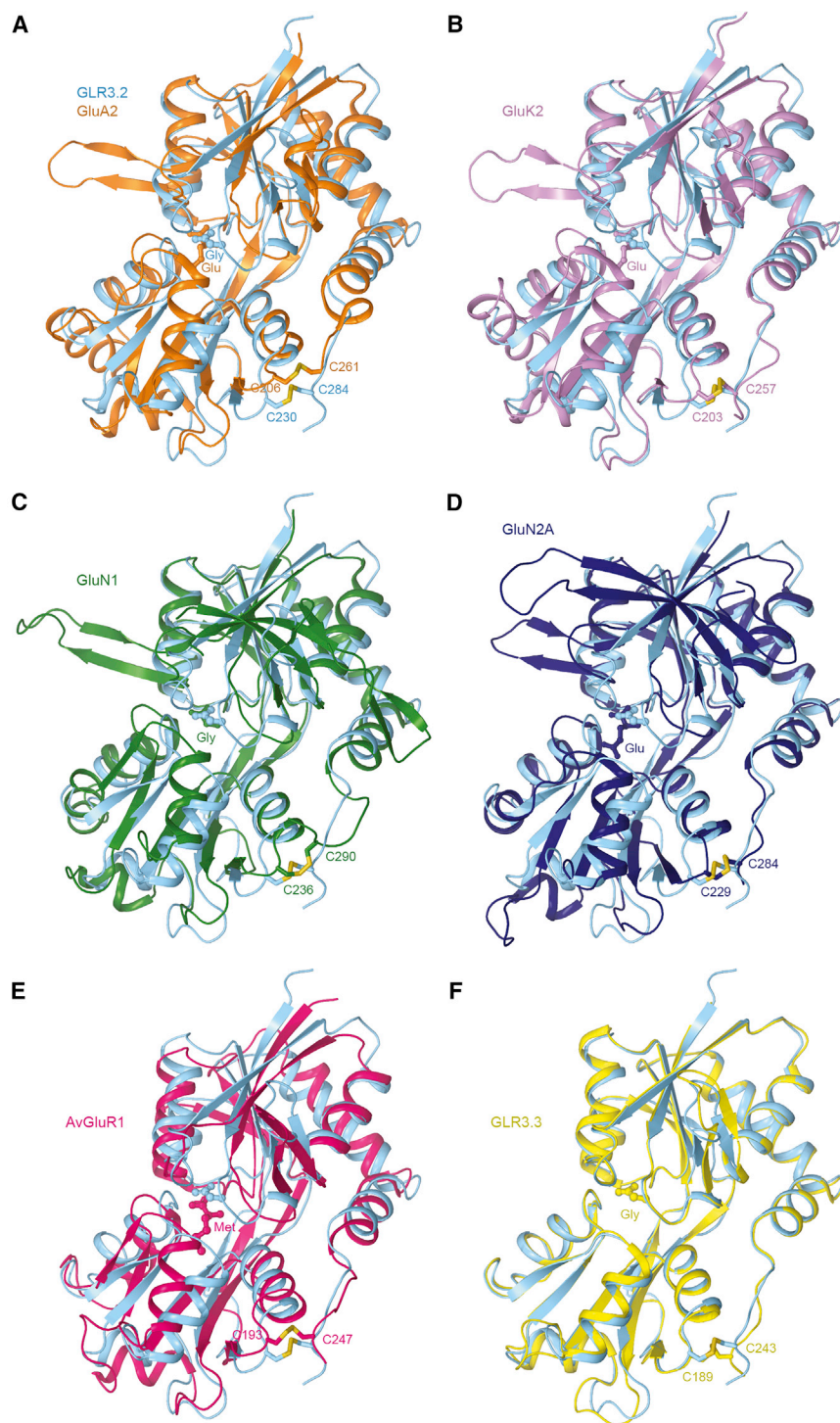


**Figure 4. Comparison of AtGLR3.2 and iGluR LBDs**

Structural superpositions of isolated LBDs from AtGLR3.2 (cyan) in complex with glycine and (A) rat GluA2 (PDB: 1FTJ, orange) in complex with glutamate, (B) rat GluK2 (PDB: 1S50, purple) in complex with glutamate, (C) rat GluN1 (PDB: 1PB7, green) in complex with glycine, (D) rat GluN2A (PDB: 2A5S, blue) in complex with glutamate, (E) rotifer AvGluR1 (PDB: 4IO2, magenta) in complex with methionine, and (F) *Arabidopsis* GLR3.3 (PDB: 6R88, yellow) in complex with glycine. The ligands are in ball-and-stick representation. Highly conserved cysteines connected by disulfide bonds are shown as sticks.

present in iGluRs but absent in GLRs. Instead of the helix G, GLRs have a short  $\beta$  strand that we named 9a. In addition, NMDA receptor LBDs have a large hairpin loop between  $\beta$ 1 and  $\alpha$ B, which is missing in GLRs, AMPA, and kainate receptors. Apart from these regions, the secondary structure organization of LBD is conserved between mammalian, rotifer, and plant receptors. The arginine in the  $\alpha$ D helix (R133 in GLR3.2-S1S2 and R551 in the full-length GLR3.2), which forms bidentate hydrogen bonds with the ligand's carboxyl group, is highly conserved across all species (Lomash et al., 2013; Mayer, 2020). Other conserved residues include cysteines that form a disulfide bond between the C-terminal ends of the helices I and K (Cys230 and Cys284 in GLR3.2-S1S2), which are only missing in prokaryotic receptors (Lee et al., 2008; Mayer et al., 2001).

Compared with iGluRs that are selectively activated by certain amino acids, AtGLRs and AvGluR1 can be activated by different amino acids. Such promiscuity in amino acid ligand binding is supported by structures of S1S2 that were solved for AvGluR1 in complex with Glu, Asp, Ser, Ala, Met, and Phe (Lomash et al., 2013), AtGLR3.3 in complex with Met, Glu, Ala, and Gly (Alfieri et al., 2020), and AtGLR3.2 in complex with Met and Gly (this study). This promiscuity

S1 and S2). The extent of clamshell closure in AtGLR3.3 and AtGLR3.2 is also nearly identical and greatly resembles the one in AvGluR1 of the rotifer *A. vaga* (Lomash et al., 2013). More significant differences were observed in superpositions of GLR3.2-S1S2 with S1S2 of AMPA, kainate, and NMDA receptors. The main regions of distinction are the  $\beta$ 1- $\alpha$ B loop that is extended in GLRs compared with iGluRs, as well as the protruding  $\beta$ -hairpin loop  $\beta$ 2- $\alpha$ C and the helices  $\alpha$ A and  $\alpha$ G, which are

is likely due to unique features of the LBDs in these receptors compared with mammalian iGluRs. The AvGluR1 requires a  $\text{Cl}^-$  ion in the binding pocket for Ala, Ser, and Met complex. AtGLR3.3 did not require ions to interact with their ligand, and not a trace of ion density was found in its binding pocket (Alfieri et al., 2020; Lomash et al., 2013). Moreover, only GLR3.2-S1S2<sub>Gly</sub> has two water molecules in the ligand-binding pocket but GLR3.2-S1S2<sub>Met</sub> complex does not have any, unlike



AvGluR1 and iGluRs. Interestingly, the AvGluR1 and AtGLR LBDs bound to different amino acid ligands have the same extent of clamshell closure, which is also similar to agonist-bound iGluR LBDs. Since these AvGluR1 and AtGLRs ligands have different affinities and full versus partial agonistic character (Alfieri et al., 2020; Lomash et al., 2013), the extent of the LBD clamshell closure seems to be independent of these two characteristics. In some iGluR studies, the extent of the LBD clamshell closure was postulated as a measure of the ligand partial agonistic character (Jin et al., 2003), while other studies argued that it is rather the fraction of time that the clamshell spends in the fully closed conformation that matters (Ramaswamy et al., 2012; Salazar et al., 2017; Twomey and Sobolevsky, 2018). For example, based on the higher  $\text{Ca}^{2+}$  signal observed for Gly versus Met, we hypothesize that Met is rather a partial agonist compared with Gly. This difference in agonistic character is consistent with the previous reports on AtGLR3.1/3.5, where Met-activated  $\text{Ca}^{2+}$  currents were shown to be responsible for maintaining cytosolic  $\text{Ca}^{2+}$  (Kong et al., 2016). However, the structural basis for such differences will remain unclear until the structures of full-length GLRs are available as well as more detailed analysis of their kinetics and energetics.

In summary, the overall architecture of our GLR3.2-S1S2<sub>Gly</sub> and GLR3.2-S1S2<sub>Met</sub> structures as well as the type of ligand binding suggest that similar to iGluRs, the clamshell-like closure of LBDs in GLRs might provide a driving force to gate the GLR-associated ion channel (Armstrong and Gouaux, 2000; Twomey and Sobolevsky, 2018). To test this hypothesis, one would need to capture the full-length structure of a GLR. The observed similarity in the LBD clamshell architecture, ligand binding, and predicted gating mechanism also suggests that plant GLRs and iGluRs originate from a common ancestor to function in different kingdoms of life yet utilize similar molecular mechanisms. Our structures of AtGLR3.2 LBD in complex with two different amino acid ligands along with the role of CNH in  $\text{Ca}^{2+}$  uptake indicate that both ligand and auxiliary protein binding are necessary for AtGLR3.2 function.

## STAR★METHODS

Detailed methods are provided in the online version of this paper and include the following:

- KEY RESOURCES TABLE
- RESOURCE AVAILABILITY
  - Lead Contact
  - Materials Availability
  - Data and Code Availability
- EXPERIMENTAL MODEL AND SUBJECT DETAILS
- METHOD DETAILS
  - Cloning and Mutagenesis
  - Protein Expression and Purification
  - Crystallization and Structure Determination
  - COS-7 Cells Transfection and Calcium Imaging
- QUANTIFICATION AND STATISTICAL ANALYSIS

## SUPPLEMENTAL INFORMATION

Supplemental Information can be found online at <https://doi.org/10.1016/j.str.2020.09.006>.

## ACKNOWLEDGMENTS

We thank Dr. Surajit Banerjee for assistance with the data collection, Dr. Jesse Yoder for help with the molecular replacement, Dr. Appu K. Singh for advice in the crystallographic data processing, and Drs. Maria Yelshanskaya and Kirill Nadezhdin for comments on the manuscript and for helpful discussions. pCI-YC3.6 construct was kindly supplied by Dr. Jörg Kudla (Univ. Muenster). We thank Dr. Daniel Damineli (Univ. São Paulo) for help with statistical analysis. A.I.S. is supported by the NIH (R01 CA206573, R01 NS083660, R01 NS107253), NSF (1818086), and the Irma T. Hirsch Career Scientist Award. Data were collected at the beamline 24-ID-C of the Advanced Photon Source. 24-ID-C is one of the Northeastern Collaborative Access Team beamlines, which are funded by the National Institute of General Medical Sciences from the National Institutes of Health (P30 GM124165). The Pilatus 6M detector on the 24-ID-C beamline is funded by an NIH-ORIP HEI grant (S10 RR029205). M.N.G. received support from the Institute of Human Nutrition training grant, Graduate Training in Nutrition (5T32DK007647-30). J.A.F. was supported by the NIH (R01 GM131043) and the NSF (MCB1616437, MCB1714993, and MCB1930165).

## AUTHOR CONTRIBUTIONS

A.I.S. and J.A.F. supervised the project. S.P.G. and M.N.G. made constructs and prepared protein samples. S.P.G. and A.I.S. carried out crystallographic data collection and processing, and built molecular models. E.M. and A.A.S. generated the constructs for mammalian expression and carried out point mutagenesis, calcium imaging, and data processing. S.P.G., M.N.G., E.M., A.A.S., J.A.F., and A.I.S. wrote the manuscript.

## DECLARATION OF INTERESTS

The authors declare no competing interests.

Received: June 11, 2020

Revised: August 21, 2020

Accepted: September 15, 2020

Published: October 6, 2020

## REFERENCES

- Adams, P.D., Afonine, P.V., Bunkoczi, G., Chen, V.B., Davis, I.W., Echols, N., Headd, J.J., Hung, L.W., Kapral, G.J., Grosse-Kunstleve, R.W., et al. (2010). PHENIX: a comprehensive Python-based system for macromolecular structure solution. *Acta Crystallogr. D Biol. Crystallogr.* 66, 213–221.
- Alfieri, A., Doccula, F.G., Pederzoli, R., Grenzi, M., Bonza, M.C., Luoni, L., Candeo, A., Romano Armada, N., Barbiroli, A., Valentini, G., et al. (2020). The structural bases for agonist diversity in an *Arabidopsis thaliana* glutamate receptor-like channel. *Proc. Natl. Acad. Sci. U S A* 117, 752–760.
- Aouini, A., Matsukura, C., Ezura, H., and Asamizu, E. (2012). Characterisation of 13 glutamate receptor-like genes encoded in the tomato genome by structure, phylogeny and expression profiles. *Gene* 493, 36–43.
- Armstrong, N., and Gouaux, E. (2000). Mechanisms for activation and antagonism of an AMPA-sensitive glutamate receptor: crystal structures of the GluR2 ligand binding core. *Neuron* 28, 165–181.
- Armstrong, N., Mayer, M., and Gouaux, E. (2003). Tuning activation of the AMPA-sensitive GluR2 ion channel by genetic adjustment of agonist-induced conformational changes. *Proc. Natl. Acad. Sci. U S A* 100, 5736–5741.
- Armstrong, N., Sun, Y., Chen, G.Q., and Gouaux, E. (1998). Structure of a glutamate-receptor ligand-binding core in complex with kainate. *Nature* 395, 913–917.
- Blanke, M.L., and VanDongen, A.M. (2008). Constitutive activation of the N-methyl-D-aspartate receptor via cleft-spanning disulfide bonds. *J. Biol. Chem.* 283, 21519–21529.
- Chiu, J.C., Brenner, E.D., DeSalle, R., Nitabach, M.N., Holmes, T.C., and Coruzzi, G.M. (2002). Phylogenetic and expression analysis of the glutamate-receptor-like gene family in *Arabidopsis thaliana*. *Mol. Biol. Evol.* 19, 1066–1082.

- Coombs, I.D., Soto, D., Zonouzi, M., Renzi, M., Shelley, C., Farrant, M., and Cull-Candy, S.G. (2012). Cornichons modify channel properties of recombinant and glial AMPA receptors. *J. Neurosci.* 32, 9796–9804.
- De Bortoli, S., Teardo, E., Szabo, I., Morosinotto, T., and Alboresi, A. (2016). Evolutionary insight into the ionotropic glutamate receptor superfamily of photosynthetic organisms. *Biophys. Chem.* 218, 14–26.
- DeLano, W.L. (2002). The PyMOL Molecular Graphics System (DeLano Scientific).
- Emsley, P., and Cowtan, K. (2004). Coot: model-building tools for molecular graphics. *Acta Crystallogr. D Biol. Crystallogr.* 60, 2126–2132.
- Forde, B.G., and Roberts, M.R. (2014). Glutamate receptor-like channels in plants: a role as amino acid sensors in plant defence? *F1000prime Rep.* 6, 37.
- Furukawa, H., and Gouaux, E. (2003). Mechanisms of activation, inhibition and specificity: crystal structures of the NMDA receptor NR1 ligand-binding core. *EMBO J.* 22, 2873–2885.
- Furukawa, H., Singh, S.K., Mancusso, R., and Gouaux, E. (2005). Subunit arrangement and function in NMDA receptors. *Nature* 438, 185–192.
- Gibson, D.G., Young, L., Chuang, R.Y., Venter, J.C., Hutchison, C.A., 3rd, and Smith, H.O. (2009). Enzymatic assembly of DNA molecules up to several hundred kilobases. *Nat. Methods* 6, 343–345.
- Gill, M.B., Kato, A.S., Roberts, M.F., Yu, H., Wang, H., Tomita, S., and Brecht, D.S. (2011). Cornichon-2 modulates AMPA receptor-transmembrane AMPA receptor regulatory protein assembly to dictate gating and pharmacology. *J. Neurosci.* 31, 6928–6938.
- Gouaux, E. (2004). Structure and function of AMPA receptors. *J. Physiol.* 554, 249–253.
- Jalali-Yazdi, F., Chowdhury, S., Yoshioka, C., and Gouaux, E. (2018). Mechanisms for zinc and proton inhibition of the GluN1/GluN2A NMDA receptor. *Cell* 175, 1520–1532 e1515.
- Jin, R., Banke, T.G., Mayer, M.L., Traynelis, S.F., and Gouaux, E. (2003). Structural basis for partial agonist action at ionotropic glutamate receptors. *Nat. Neurosci.* 6, 803–810.
- Kabsch, W. (2010). XDS. *Acta Crystallogr. D Biol. Crystallogr.* 66, 125–132.
- Kato, A.S., Gill, M.B., Ho, M.T., Yu, H., Tu, Y., Siuda, E.R., Wang, H., Qian, Y.W., Nisenbaum, E.S., Tomita, S., et al. (2010). Hippocampal AMPA receptor gating controlled by both TARP and cornichon proteins. *Neuron* 68, 1082–1096.
- Kim, S.A., Kwak, J.M., Jae, S.K., Wang, M.H., and Nam, H.G. (2001). Overexpression of the AtGluR2 gene encoding an *Arabidopsis* homolog of mammalian glutamate receptors impairs calcium utilization and sensitivity to ionic stress in transgenic plants. *Plant Cell Physiol.* 42, 74–84.
- Kong, D., Hu, H.C., Okuma, E., Lee, Y., Lee, H.S., Munemasa, S., Cho, D., Ju, C., Pedoeim, L., Rodriguez, B., et al. (2016). L-met activates *Arabidopsis* GLR Ca(2+) channels upstream of ROS production and regulates stomatal movement. *Cell Rep.* 17, 2553–2561.
- Kong, D., Ju, C., Parihar, A., Kim, S., Cho, D., and Kwak, J.M. (2015). *Arabidopsis* glutamate receptor homolog3.5 modulates cytosolic Ca<sup>2+</sup> level to counteract effect of abscisic acid in seed germination. *Plant Physiol.* 167, 1630–1642.
- Kumar, J., and Mayer, M.L. (2013). Functional insights from glutamate receptor ion channel structures. *Annu. Rev. Physiol.* 75, 313–337.
- Lacombe, B., Becker, D., Hedrich, R., DeSalle, R., Hollmann, M., Kwak, J.M., Schroeder, J.I., Le Novère, N., Nam, H.G., Spalding, E.P., et al. (2001). The identity of plant glutamate receptors. *Science* 292, 1486–1487.
- Lam, H.M., Chiu, J., Hsieh, M.H., Meisel, L., Oliveira, I.C., Shin, M., and Coruzzi, G. (1998). Glutamate-receptor genes in plants. *Nature* 396, 125–126.
- Laskowski, R.A., Jabłońska, J., Pravda, L., Vařeková, R.S., and Thornton, J.M. (2018). PDBsum: structural summaries of PDB entries. *Prot. Sci.* 27, 129–134.
- Lee, J.H., Kang, G.B., Lim, H.H., Jin, K.S., Kim, S.H., Ree, M., Park, C.S., Kim, S.J., and Eom, S.H. (2008). Crystal structure of the GluR0 ligand-binding core from *Nostoc punctiforme* in complex with L-glutamate: structural dissection of the ligand interaction and subunit interface. *J. Mol. Biol.* 376, 308–316.
- Li, F., Wang, J., Ma, C., Zhao, Y., Wang, Y., Hasi, A., and Qi, Z. (2013). Glutamate receptor-like channel3.3 is involved in mediating glutathione-triggered cytosolic calcium transients, transcriptional changes, and innate immunity responses in *Arabidopsis*. *Plant Physiol.* 162, 1497–1509.
- Lomash, S., Chittori, S., Brown, P., and Mayer, M.L. (2013). Anions mediate ligand binding in *Adineta vaga* glutamate receptor ion channels. *Structure* 21, 414–425.
- Mayer, M.L. (2005). Crystal structures of the GluR5 and GluR6 ligand binding cores: molecular mechanisms underlying kainate receptor selectivity. *Neuron* 45, 539–552.
- Mayer, M.L. (2020). Glutamate receptors from diverse animal species exhibit unexpected structural and functional diversity. *J. Physiol.* <https://doi.org/10.1113/JP279026>.
- Mayer, M.L., Olson, R., and Gouaux, E. (2001). Mechanisms for ligand binding to GluR0 ion channels: crystal structures of the glutamate and serine complexes and a closed apo state. *J. Mol. Biol.* 311, 815–836.
- McCoy, A.J. (2007). Solving structures of protein complexes by molecular replacement with Phaser. *Acta Crystallogr. D* 63, 32–41.
- Meyerson, J.R., Kumar, J., Chittori, S., Rao, P., Pierson, J., Bartsaghi, A., Mayer, M.L., and Subramaniam, S. (2014). Structural mechanism of glutamate receptor activation and desensitization. *Nature* 514, 328–334.
- Michard, E., Lima, P.T., Borges, F., Silva, A.C., Portes, M.T., Carvalho, J.E., Gilliam, M., Liu, L.H., Obermeyer, G., and Feijo, J.A. (2011). Glutamate receptor-like genes form Ca<sup>2+</sup> channels in pollen tubes and are regulated by pistil D-serine. *Science* 332, 434–437.
- Mou, W., Michard, E., Sittman, J., Simon, A., Dong-Dong, A., Feijo, J.A., and Chang, C. (2020). Ethylene-independent signalling by the ethylene precursor ACC in *Arabidopsis* ovular pollen tube attraction. *Nat. Commun.* 11, 4082.
- Møllerud, S., Frydenvang, K., Pickering, D.S., and Kastrup, J.S. (2017). Lessons from crystal structures of kainate receptors. *Neuropharmacology* 112, 16–28.
- Mousavi, S.A., Chauvin, A., Pascaud, F., Kellenberger, S., and Farmer, E.E. (2013). GLUTAMATE RECEPTOR-LIKE genes mediate leaf-to-leaf wound signalling. *Nature* 500, 422–426.
- Ortiz-Ramirez, C., Michard, E., Simon, A.A., Damineli, D.S.C., Hernandez-Coronado, M., Becker, J.D., and Feijo, J.A. (2017). GLUTAMATE RECEPTOR-LIKE channels are essential for chemotaxis and reproduction in mosses. *Nature* 549, 91–95.
- Pohlsgaard, J., Frydenvang, K., Madsen, U., and Kastrup, J.S. (2011). Lessons from more than 80 structures of the GluA2 ligand-binding domain in complex with agonists, antagonists and allosteric modulators. *Neuropharmacology* 60, 135–150.
- Price, M.B., Jelesko, J., and Okumoto, S. (2012). Glutamate receptor homologs in plants: functions and evolutionary origins. *Front. Plant Sci.* 3, 235.
- Ramaswamy, S., Cooper, D., Poddar, N., MacLean, D.M., Rambhadrar, A., Taylor, J.N., Uhm, H., Landes, C.F., and Jayaraman, V. (2012). Role of conformational dynamics in alpha-amino-3-hydroxy-5-methylisoxazole-4-propionic acid (AMPA) receptor partial agonism. *J. Biol. Chem.* 287, 43557–43564.
- Salazar, H., Eibl, C., Chebli, M., and Plested, A. (2017). Mechanism of partial agonism in AMPA-type glutamate receptors. *Nat. Commun.* 8, 14327.
- Schwenk, J., Harmel, N., Zolles, G., Bildl, W., Kulik, A., Heimrich, B., Chisaka, O., Jonas, P., Schulte, U., Fakler, B., et al. (2009). Functional proteomics identify cornichon proteins as auxiliary subunits of AMPA receptors. *Science* 323, 1313–1319.
- Shi, Y., Suh, Y.H., Milstein, A.D., Isozaki, K., Schmid, S.M., Roche, K.W., and Nicoll, R.A. (2010). Functional comparison of the effects of TARPs and cornichons on AMPA receptor trafficking and gating. *Proc. Natl. Acad. Sci. U S A* 107, 16315–16319.
- Singh, S.K., Chien, C.T., and Chang, I.F. (2016). The *Arabidopsis* glutamate receptor-like gene GLR3.6 controls root development by repressing the Kip-related protein gene KRP4. *J. Exp. Bot.* 67, 1853–1869.
- Sobolevsky, A.I. (2015). Structure and gating of tetrameric glutamate receptors. *J. Physiol.* 593, 29–38.



Sobolevsky, A.I., Rosconi, M.P., and Gouaux, E. (2009). X-ray structure, symmetry and mechanism of an AMPA-subtype glutamate receptor. *Nature* **462**, 745–756.

Tapken, D., Anschutz, U., Liu, L.H., Huelsken, T., Seebohm, G., Becker, D., and Hollmann, M. (2013). A plant homolog of animal glutamate receptors is an ion channel gated by multiple hydrophobic amino acids. *Sci. Signal.* **6**, ra47.

Traynelis, S.F., Wollmuth, L.P., McBain, C.J., Menniti, F.S., Vance, K.M., Ogden, K.K., Hansen, K.B., Yuan, H., Myers, S.J., and Dingledine, R. (2010). Glutamate receptor ion channels: structure, regulation, and function. *Pharmacol. Rev.* **62**, 405–496.

Twomey, E.C., and Sobolevsky, A.I. (2018). Structural mechanisms of gating in ionotropic glutamate receptors. *Biochemistry* **57**, 267–276.

Vincill, E.D., Bieck, A.M., and Spalding, E.P. (2012). Ca<sup>2+</sup> conduction by an amino acid-gated ion channel related to glutamate receptors. *Plant Physiol.* **159**, 40–46.

Vincill, E.D., Clarin, A.E., Molenda, J.N., and Spalding, E.P. (2013). Interacting glutamate receptor-like proteins in Phloem regulate lateral root initiation in *Arabidopsis*. *Plant Cell* **25**, 1304–1313.

Wallace, A.C., Laskowski, R.A., and Thornton, J.M. (1995). LIGPLOT: a program to generate schematic diagrams of protein-ligand interactions. *Protein Eng. Des. Select.* **8**, 127–134.

Waterhouse, A., Bertoni, M., Bienert, S., Studer, G., Tauriello, G., Gumienny, R., Heer, F.T., de Beer, T.A.P., Rempfer, C., Bordoli, L., et al. (2018). SWISS-MODEL: homology modelling of protein structures and complexes. *Nucleic Acids Res.* **46**, W296–W303.

Winn, M.D., Ballard, C.C., Cowtan, K.D., Dodson, E.J., Emsley, P., Evans, P.R., Keegan, R.M., Krissinel, E.B., Leslie, A.G., McCoy, A., et al. (2011). Overview of the CCP4 suite and current developments. *Acta Crystallogr. D Biol. Crystallogr.* **67**, 235–242.

Wollmuth, L.P., and Sobolevsky, A.I. (2004). Structure and gating of the glutamate receptor ion channel. *Trends Neurosci.* **27**, 321–328.

Wudick, M.M., Michard, E., Oliveira Nunes, C., and Feijo, J.A. (2018a). Comparing plant and animal glutamate receptors: common traits but different fates? *J. Exp. Bot.* **10**, <https://doi.org/10.1093/jxb/ery153>.

Wudick, M.M., Portes, M.T., Michard, E., Rosas-Santiago, P., Lizzio, M.A., Nunes, C.O., Campos, C., Santa Cruz Damineli, D., Carvalho, J.C., Lima, P.T., et al. (2018b). CORNICHON sorting and regulation of GLR channels underlie pollen tube Ca<sup>2+</sup> homeostasis. *Science* **360**, 533–536.

## STAR★METHODS

## KEY RESOURCES TABLE

REAGENT or RESOURCE	SOURCE	IDENTIFIER
Chemicals, Peptides, and Recombinant Proteins		
Ampicillin	Sigma	Cat# A8351
Kanamycin	Fisher scientific	Cat# BP906-5
Tetracycline	Fisher scientific	Cat# BP912
IPTG	Zymo Research	Cat# I1001-5
Tris	Fisher scientific	Cat# BP152-1
NaCl	Fisher scientific	Cat# BP358-212
L-Glutamate	Sigma	Cat# 49621
L-Methionine	Sigma	Cat# M9625
MgSO <sub>4</sub>	Fluka	Cat# 13143
DNAse	Sigma	Cat# DN25-1
PMSF	Acros Organics	Cat# 215740500
2-Mercaptoethanol (βME)	Acros Organics	Cat# 125470100
Ni-Affinity Resin	Takara	Cat# 635660
Imidazole	Acros Organics	Cat# 301870025
Thrombin	Haematologic Technologies	Cat# HCT-0020
Glycerol	Fisher scientific	Cat# BP229-4
MES buffer	Sigma	Cat# M2933
PEG 2000 MME	Fluka	Cat# 81321
Ammonium Sulfate	Fisher scientific	Cat# A702-500
Glycine	Jena Biosciences	Cat# CS-507L
Ammonium acetate	Fisher scientific	Cat# BP326-500
Sodium Acetate	Fisher scientific	Cat# S209-500
Dulbecco's Modified Eagle's Medium	Gibco	Cat# 10566024
Fetal bovine serum	Gibco	Cat# 16140071
Penicillin Streptomycin Fungizone	Cytiva HyClone	Cat# SV3007901
FugeneHD	Promega	Cat# E2311
EGTA	Sigma	Cat# E4378
Bis-Tris Propane	RPI	Cat# B78000100.0
HEPES	Sigma	Cat# H3375-250G
D-mannitol	Fisher scientific	Cat# M120-500
Ca-Gluconate	Sigma	Cat# C8231-100G
Deposited Data		
Coordinates of GLR3.2-S1S2-Glycine	This paper	PDB: 6VEA
Coordinates of GLR3.2-S1S2-Methionine	This paper	PDB: 6VE8
S1S2 of GluA2	(Armstrong and Gouaux, 2000)	PDB: 1FTJ
S1S2 of GluK2	(Mayer, 2005)	PDB: 1S50
S1S2 of GluN1	(Furukawa and Gouaux, 2003)	PDB: 1PB7
S1S2 of GluN2A	(Furukawa et al., 2005)	PDB: 2A5S
S1S2 of AvGluR1	(Lomash et al., 2013)	PDB: 4IO2
S1S2 of AtGLR3.3	(Alfieri et al., 2020)	PDB: 6R88
Ligand-binding domain of NMDA receptor	(Jalali-Yazdi et al., 2018)	PDB: 6MMS
Experimental Models: Cell Lines		
COS-7	ATTC	CRL-1651
<i>E. coli</i> Origami B (DE3)	Novagen	Cat# 70837

(Continued on next page)

**Continued**

REAGENT or RESOURCE	SOURCE	IDENTIFIER
Recombinant DNA		
pEF1-YC3.6	Dr. Jörg Kudla lab, Univ. Muenster, Germany	N/A
Oligonucleotides		
AtGLR3.2 amplification primer: 5'-gtaacggccgcccagtgctggaattcA TGT TTTGGGTTTGGTTCTGT-3'	This paper	N/A
AtGLR3.2 amplification primer: 5'-ataggccctctagatgcatgctcg aGTCATATTGGTCTAGAAGGT-3'	This paper	N/A
pcDNA3	Invitrogen	N/A
pCI-AtCNIH4	Wudick et al., 2018b	Genebank: NC_003070.9; At1g12390; Salk_145991
pcDNA3-AtGLR3.2	This paper	GeneBank: NC_003075; Araprot: At4G35290
pET22b-GLR3.2-S1S2	This paper	GeneBank: NC_003075; Araprot: At4G35290
Software and Algorithms		
Pymol (Schrödinger)	DeLano, 2002	<a href="http://www.pymol.org">http://www.pymol.org</a>
PHENIX	Adams et al., 2010	<a href="https://www.phenix-online.org/">https://www.phenix-online.org/</a>
CCP4	Winn et al., 2011	<a href="http://www.ccp4.ac.uk/">http://www.ccp4.ac.uk/</a>
COOT	Emsley et al., 2004	<a href="http://www2.mrc-lmb.cam.ac.uk/Personal/pemsley/coot">http://www2.mrc-lmb.cam.ac.uk/Personal/pemsley/coot</a>
XDS	Kabsch, 2010	<a href="http://xds.mpimf-heidelberg.mpg.de/">http://xds.mpimf-heidelberg.mpg.de/</a>
Swiss-Model	Waterhouse et al., 2018	<a href="https://swissmodel.expasy.org/">https://swissmodel.expasy.org/</a>
PDBsum	Laskowski et al., 2018	<a href="https://www.ebi.ac.uk/thornton-srv/databases/cgi-bin/pdbsum/GetPage.pl?pdbcode=index.html">https://www.ebi.ac.uk/thornton-srv/databases/cgi-bin/pdbsum/GetPage.pl?pdbcode=index.html</a>
SigmaPlot 11.0	Systat Software Inc.	<a href="http://Systatsoftware.com">Systatsoftware.com</a>
Other		
DeltaVision Elite Deconvolution/TIRF microscope system	GE Healthcare	Part # 53-851206-001
Ion Exchange Hi-Trap Q HP column	GE Healthcare	Cat# 17-1154-01
Size Exclusion Superose 10/300 column	GE Healthcare	Cat# 17-5172-01

## RESOURCE AVAILABILITY

### Lead Contact

Further information and requests for resources and reagents should be directed to and will be fulfilled by the Lead Contact, Alexander Sobolevsky ([as4005@cumc.columbia.edu](mailto:as4005@cumc.columbia.edu)).

### Materials Availability

This study did not generate new unique reagents.

### Data and Code Availability

Coordinates and structure factors for the GLR3.2-S1S2<sub>Gly</sub> and GLR3.2-S1S2<sub>Met</sub> structures have been deposited to the PDB with the accession codes 6VEA and 6VE8, respectively. This study did not generate new code.

## EXPERIMENTAL MODEL AND SUBJECT DETAILS

Protein expression was performed in *Escherichia coli* Origami B (DE3) cells. Cells were cultured in LB media at 37°C until OD<sub>600</sub> reached the value of 1.0-1.2, then cooled down to 20°C, induced with 250 μM IPTG and incubated for another 20 hours at 20°C.

COS-7 cells for calcium imaging experiments were maintained at 37°C and 5% CO<sub>2</sub> in Dulbecco's Modified Eagle's Medium, supplemented with 5 % fetal bovine serum and 1 % penicillin/streptomycin.

## METHOD DETAILS

### Cloning and Mutagenesis

RNA was isolated from col-0 leaf tissue using Bioline ISOLATE II RNA Plant Kit. The Bioline SensiFAST cDNA Synthesis kit was used to generate cDNA from the col-0 RNA. The CDS for AtGLR3.2 was amplified from cDNA using the primers: 5'-gtaacggccgcc agtgtgctggaattcA TGTTTTGGGTTTTGGTTCTGT-3', 5'- atagggccctctagatgcatgctcgaGTCATATTGGTCTAGAAGGT-3'. The glr3.2 CDS PCR fragment was cloned into EcoRI/XhoI digested pCDNA3 via Gibson Isothermal Assembly to yield pCDNA3-AtGLR3.2(cDNA). The final construct was verified by Sanger Sequencing. The point mutant was amplified from pCDNA3-AtGLR3.2(cDNA) by two PCRs using overlapping mutagenic oligonucleotide primers. Primers were as follows, PCR one: 5'- TGAT ACTGTCTGGATCATTGC TCGAGCTGTTAAGAGACTTCTAG -3'; 5'-GAAATCCACAA TCCTTGTTGC TTTCGTAACAATAGCTA TGTCTCC-3'. PCR two: 5'-GAGACATAGCTATT GTTACGAAAGC AACAAAGGATTGTGGATTTCATCAGC-3'; 5'-atagggccctctaga tgcgtgctcgaG TCA TATTGGTCTAGAAGGCT-3'. Inserts were ligated with a backbone of pCDNA3-AtGLR3.2 linearized at XhoI restriction sites to construct the final mutant vector by Gibson Assembly (Gibson et al., 2009).

### Protein Expression and Purification

The boundaries of the GLR3.2 ligand-binding domain (S1S2) were determined based on the sequence alignment with GluA2 (Armstrong et al., 1998; Sobolevsky et al., 2009). The DNA encoding AtGLR3.2 residues, S420-V572 (S1) and P682-N811 (S2), were amplified using gene-specific primers and subcloned into the pET22b vector (Novagen) between NcoI and XhoI sites with a GT linker between S1 and S2 (Armstrong and Gouaux, 2000). For purification purposes, an 8xHis affinity tag followed by a thrombin cleavage site (LVPRG) was introduced at N-terminal.

The construct pET22b carrying GLR3.2-S1S2 was transformed into *Escherichia coli* Origami B (DE3) cells and grown in LB media supplemented with 100 µg/ml ampicillin, 15 µg/ml kanamycin and 12.5 µg/ml tetracycline. The freshly inoculated culture was grown at 37°C until OD<sub>600</sub> reached the value of 1.0-1.2. Then cells were cooled down to 20°C, induced with 250 µM IPTG, and incubated in the orbital shaker for another 20 hours at 20°C. Cells were harvested by centrifugation at 5488 g for 15 min at 4°C and the cell pellet was washed with the buffer containing 20 mM Tris pH 8.0 and 150 mM NaCl. For protein extraction, cells were resuspended in lysis buffer consisting of 20 mM Tris pH 8.0, 200 mM NaCl, 1 mM glutamate, 5 mM methionine, 1 mM βME, 1 mM PMSF, 100 µg/ml lysozyme, 5 mM MgSO<sub>4</sub> and DNase. All purification steps were carried out in buffers supplemented with 1 mM glutamate and 5 mM methionine. The cells were disrupted by sonication and centrifuged at 18600 g in the Ti45 rotor for 1 hour at 4°C. The supernatant was mixed with His60 Ni superflow resin (Takara) and rotated for 2 hours at 4°C. The protein-bound resin was washed with the buffer containing 15 mM imidazole and the protein was eluted in 20 mM Tris pH 8.0, 150 mM NaCl, 1 mM glutamate, 5 mM methionine, 1 mM βME, and 200 mM imidazole. The protein was dialyzed overnight in the buffer containing 20 mM Tris pH 8.0, 75 mM NaCl, 1 mM glutamate, 5 mM methionine, 1 mM βME, and 4% (v/v) glycerol. After thrombin digest (1:500 w/w) at 22°C for 1-hour, the protein was further purified using ion-exchange Hi-Trap Q HP- (GE Healthcare). The protein quality was assessed by SDS-PAGE and analytical size-exclusion chromatography using the Superpose 10/300 column (GE Healthcare).

### Crystallization and Structure Determination

Crystallization screening was performed with GLR3.2-S1S2 protein at a concentration of ~7 mg/ml using Mosquito robot (TTP Labtech) and sitting drop vapor diffusion in 96-well crystallization plates. Small needle-shaped crystals, which appeared after two weeks of incubating crystallization trays at 4°C and 20°C, were further optimized using the hanging drop method and 24-well crystallization plates. The best-diffracting long needle-shaped crystals of methionine-bound GLR3.2-S1S2 grew at 20°C in 0.1 M MES pH 6.5, 18% PEG MME 2K and 0.1 M ammonium sulfate. Crystals of glycine-bound GLR3.2-S1S2 grew in a similar condition but in the presence of 0.3 µl of 1M glycine that supplemented the 4 µl crystallization drop as an additive. The best-diffracting needle-shaped crystals of glycine-bound GLR3.2-S1S2 grew at 4°C in 22 % PEG 4K, 0.1 M ammonium acetate, and 0.1 M sodium acetate pH 4.6. All crystals were cryoprotected using 25% glycerol and flash-frozen in liquid nitrogen for data collection. Crystal diffraction data were collected at the beamline 24-ID-C of the Advanced Photon Source and processed using XDS (Kabsch, 2010) and Aimless as a part of the CCP4 suite (Winn et al., 2011).

The structure of methionine-bound GLR3.2-S1S2 was solved by molecular replacement using Phaser (McCoy, 2007) and a search probe generated by SWISS-MODEL homology modeling (Waterhouse et al., 2018) from the ligand-binding domain of NMDA receptor (PDB ID: 6MMS) (Jalali-Yazdi et al., 2018). The initial partial solution was used again as a search probe for subsequent rounds of molecular replacement, which ultimately resulted in a complete GLR3.2-S1S2 model. The model was refined by alternating cycles of building in COOT (Emsley and Cowtan, 2004) and automatic refinement in Phenix (Adams et al., 2010). The structure of glycine-bound GLR3.2-S1S2 was solved by molecular replacement using the methionine-bound GLR3.2-S1S2 structure as a search probe. Water molecules were added in Coot and Phenix refine. All structural figures were prepared in PyMol (DeLano, 2002). The protein-ligand interaction plot was created using the Ligplot server (Wallace et al., 1995; Laskowski et al., 2018).

### COS-7 Cells Transfection and Calcium Imaging

Protocols for COS-7 cells transfection and  $\text{Ca}^{2+}$  imaging were adapted from [Ortiz-Ramirez et al. \(2017\)](#). COS-7 cells (ATTC) were maintained at 37°C and 5%  $\text{CO}_2$  in Dulbecco's Modified Eagle's Medium, supplemented with 5 % fetal bovine serum and 1 % penicillin/streptomycin (Cytiva HyClone), and transfected at low passage ( $P < 7$ ). Cells were plated at a density at 50% confluence in 35-mm diameter dishes and transfected using EugeneHD (Promega) as specified by the supplier. Cells were co-transfected with three plasmids: pCI-AtCNIH4 or empty pCI (0.3  $\mu\text{g}$ ) plus pcDNA3-AtGLR3.2 or empty pcDNA3 (0.9  $\mu\text{g}$ ) were co-transfected with pEF1-YC3.6 (0.5  $\mu\text{g}$ ). The co-transfection with pCI-AtCNIH4 was an experimental stratagem used to enhance functional expression of GLRs on the plasma membrane ([Wudick et al., 2018b](#)). Cells were used for imaging 38 to 41 hours after transfection. They were washed in a  $\text{Ca}^{2+}$ -free solution (1 mM EGTA, 10 mM Bis-Tris propane buffered to pH 7.3 with HEPES and set to 350 mosmol.kg<sup>-1</sup> with D-mannitol). Cells were imaged in the  $\text{Ca}^{2+}$ -free solution for 1.5 min before the addition of  $\text{Ca}^{2+}$  to a final concentration of 14.5 mM (using Ca-Gluconate). The ligands (Met or Gly, 0.5 or 1.0 mM) are added at the beginning (even before calcium is added). Time-lapse acquisition was performed with a sampling interval of 30 secs. 8 to 12 cells were imaged in each dish using the stage position recording tool of the microscope system. Imaging was performed at room temperature using a DeltaVision Elite Deconvolution/TIRF microscope system (Olympus inverted IX-71) under a 60X lens (1.2NA UPLSAPO water /WD 0.28 mm). A xenon lamp from the DeltaVision system was used with a CFP excitation filter (438-424 nm). Two simultaneous emission records were captured: YFP emission (548-522 nm) and CFP emission (475-424 nm). To minimize bleaching, the laser was set to 2%. YFP and CFP imaging were recorded with 0.6 sec exposure time. Images were processed using ImageJ. Ratios were obtained after background subtraction and signal clipping using the "Ratio-plus" plug-in for ImageJ. The signal of each channel was averaged in a circle in the middle of the cell (with 100-200 pixel diameter, depending on the size of the cell). The YFP/CFP ratio was obtained by dividing the emission recorded for YFP (548-522 nm) by the one recorded for CFP (475-424 nm). No significant bleaching or ratio drift was observed in our experimental conditions.

### QUANTIFICATION AND STATISTICAL ANALYSIS

The X-ray structures of GLR3.2-S1S2 were determined using software listed in the Key Resources Table. Statistics generated from the data processing, refinement and validation are displayed in [Table 1](#).

Statistical significance in calcium imaging experiments was calculated by two-way ANOVA with TukeyHSD using an R custom script or SigmaPlot 11.0 (Systat Software Inc).


**Structure, Volume 29**


## **Supplemental Information**


### **Structure of the *Arabidopsis* Glutamate**


### **Receptor-like Channel GLR3.2 Ligand-Binding Domain**


**Shanti Pal Gangwar, Marriah N. Green, Erwan Michard, Alexander A. Simon, José A. Feijó, and Alexander I. Sobolevsky**



  
 GLR3.2 (47)-----GRRLRIGVFDRA<sup>\*</sup>SFKEFVSRLDGS----- (70)
   
 GLR3.1-----GRRLRIGVFDRA<sup>\*</sup>SKDFVSRVNGSS-----
   
 GLR3.3-----GKELKIGVPLRVSYKEFVSQIRGTE-----
   
 GLR3.6-----GRHLRIGVFNRYRFEVVS<sup>\*</sup>VKSNG-----
   
 GLR3.4-----GKPLRIGVFNRVSYTDYVSKDKNP-----
   
 GLR3.7-----ADPLKIVVRRVSFVEFVTEEKNS-----
   
 AvGluR1-----ARLKGITLRIGVIESVPFTIVANVIDTSGRNT-----
   
 GluA2--NKTVVVTTILESPYVMMKN-----HEMLEGN-----
   
 GluK2GSNRS<sup>\*</sup>LIVTTILEEPVVLFKKS-----DKPLYGN-----
   
 GluN1-MSTRLKIVTIHQEPFVYVKPTMSDGTCKEEFTVNGDPVKKVICTGPN<sup>\*</sup>DTSFGSPRH<sup>\*</sup>TVP
   
 GluN2PDDN<sup>\*</sup>HSIVTLEEAPFVIVEDIDPLTETCVRNTVPCRKFVKIN-NSTNEGMN-----VK


  
 GLR3.2 (71)NKVQGYAIDVFEAAVKLISYPVPHEFVLPDGLKNPNFNEFVNNVTIGV-----FDA (122)
   
 GLR3.1NKVQGYCIDVFEAAVKLLSYVPHEFIFPGDGLTNPNYNELVNKVTIGVD-----FDA
   
 GLR3.3NMFKGFCIDVFEAAVNLLPYAVPVKFI<sup>\*</sup>YPYNGKENPSYTHMVEMIT<sup>\*</sup>TGN-----FDG
   
 GLR3.6-MITGFCVDFEIAAINLLPYAVPFELVAFNGHNDNPSNELVRLITTGV-----YDA
   
 GLR3.4PGVRCYCIDVFEAAIELLPYPVPRTYILYDGKRNPSYDNLVNEVVADN-----FDV
   
 GLR3.7HRIQCFCIDVEIEALKFVPYSVYIFEPFGNGHSEPNYNHLIQMVTDSV-----YDA
   
 AvGluR1TKLTGYVLDLIEYLRDKMGFVADVLAP-----PNTSYTGLVLLALANGD-----YDI
   
 GluA2ERYEGYCVDLAAEIAKHCGFKYKLTIVGDG-----KYGARDADTKIWNMGVGLVYGKADI
   
 GluK2DRFEGYCIDLLRELSTILGF<sup>\*</sup>TYEIRLVEDG-----KYGAQDDVNGQWNGMVRELIDHKADL
   
 GluN1QCCYGFCDLLIKLARTMNFTYEVHLVADGKFGTQERVNNSNKKEWNGMMGELL<sup>\*</sup>SGQADM
   
 GluN2KCCKGFCDILK<sup>\*</sup>KLRSRTVKFTYDLYLTNG-----KHGKKVNNVWNGMIGEVVYQRAVM


  
 GLR3.2 (123)VVGDIATVTKRTRIVDETQPFYIESGLVVVAPV---GT---PIRGVDTL<sup>\*</sup>ISS-----SG (169)
   
 GLR3.1VVGDIATVTKRTRIVDETQPFYIESGLVVVAPV---GGT---PIKGVDTL<sup>\*</sup>ISS-----TG
   
 GLR3.3VVGDAIVTNRKIVDETQPYAASGLVVVAPF-----PIKGIESLRER-----DD
   
 GLR3.6GVGDITITITEKMADETQPYVESGLVVVAPV-----PIKGIE<sup>\*</sup>TLQTN-----HD
   
 GLR3.4AVGDITIVTNTRYVDETQPFYIESGLVVVAPV-----RIEGIDSLVTS-----NE
   
 GLR3.7AVGDIAIVPSKSLVD<sup>\*</sup>SQHYASTGLVVVIPA-----AITGIDSLRAS-----EV
   
 AvGluR1AIGDITVTSAREIVAFSNSISDN<sup>\*</sup>SMRILMRK---GT---LIDGMDDLKNGK---IPYN
   
 GluA2AIAPLTTILVREEVIDESKF<sup>\*</sup>FMSLGISIMIKK---GT---PIESAEDLSKOT---EI
   
 GluK2AVAPLAI<sup>\*</sup>TYVEKVIDSKPFMTLGISILYRK---GT---PIDSADDLAKQT---KI
   
 GluN1IVAPLITNNEAQYIE<sup>\*</sup>SKPFKYQGLTILVKK---GT---RITGTINDPRLRN---PSDK
   
 GluN2AVGSLTINEE<sup>\*</sup>SEVVDESVEFVETGISVMVSR---GT---QVTGLSDKKFQRPHDYSPPF


  
 GLR3.2 (170)RVGFQVGSYAENYMI<sup>\*</sup>DELNIARSRLVPLGSPKEYAAALQNGT-----VAAIVDE (218)
   
 GLR3.1RIGFQVGSFAENYMTDELNIASSRLVPLASPEEYANALQNGT-----VAAIVDE
   
 GLR3.3PIGYQVGSFAESYLRLNELNISESRLVPLGTPEAYAKALKDGP-----KGGVAAIVDE
   
 GLR3.6PIGYQGSFVRDYLIELN<sup>\*</sup>IHVSRVLPLRSP<sup>\*</sup>EEDKALRDGP-----KGGVAAIVDE
   
 GLR3.4PIGVQDGTFARNYLINELN<sup>\*</sup>ILPSRIVPLKDEEQYLSALQRGPN-----AGGVAAIVDE
   
 GLR3.7PIGYQAGTFTLEYLTYSLGMARSRVLPLDSTEEYEKALKLGPT-----NWGGVAAIVDE
   
 AvGluR1RIGIRIGTAGEDY<sup>\*</sup>YLRISGGSRNFYPLKSRQEMYDSL<sup>\*</sup>LAGI-----IDVSEMD
   
 GluA2AYGTLDSGSTKEFFRRRSKIAVFDKMWTYMRSA<sup>\*</sup>PSVFVRTTAEGVARVRKSKGKYAYLLE
   
 GluK2EYGAVEDGATMTFFKSKISTYDKMWAFFSSRRQSVLVKSNEEG---IQRVLTS<sup>\*</sup>DYAFIME
   
 GluN1FIYATVKQSSVDIYFR<sup>\*</sup>RQVELSTMYRMEKHNYESA<sup>\*</sup>AAEAIQAV-----RDNKLHAFIWD
   
 GluN2RFGTVPNGSTERNIRNNYPYMHQYMT<sup>\*</sup>RFNQRGVEDALVSLKTG-----KLDAFIYD


  
 GLR3.2 (219)RPYVDLFLS--EFGFAIR<sup>\*</sup>Q--EFT<sup>\*</sup>RS<sup>\*</sup>GWGFAPPRDSPLAIDMSTAI<sup>\*</sup>GLSETGOLQKI (274)
   
 GLR3.1RPYIDLFLS--DYCKFAIR<sup>\*</sup>Q--EFT<sup>\*</sup>RCGWGFAPPRDSPLAVDMSTAI<sup>\*</sup>GLSETGELQKI
   
 GLR3.3RPYVELFLS--SNCA<sup>\*</sup>YRIV<sup>\*</sup>Q--EFTKSGWGFAPPRDSPLAIDLSTAI<sup>\*</sup>LELAENGDLQRI
   
 GLR3.6RAYIELFLS--NRCEFGIV<sup>\*</sup>Q--EFTKNGWGFAPPRNSPLAVDVSAAI<sup>\*</sup>QLSENGDMQRI
   
 GLR3.4LPYIEVLLTN-SNCKFRTV<sup>\*</sup>Q--EFTRTGWGFAPPRDSPLAVDMSTAI<sup>\*</sup>QLSEEGELEKI
   
 GLR3.7LPYIELFLA--ERTGFKIV<sup>\*</sup>Q--PFMHRGWGFAPKRDSP<sup>\*</sup>LAI<sup>\*</sup>DMSTAI<sup>\*</sup>KLSETRKLQEI
   
 AvGluR1IGTAEYVTNN-IYCNLT<sup>\*</sup>LVGE--DFDKSTFGIVTPKEWLYAKDL<sup>\*</sup>VDNI<sup>\*</sup>SLRETGILDNL
   
 GluA2STMNEYIEQR-KPCDTMKV<sup>\*</sup>CG--NLDSKGYGIA<sup>\*</sup>TPKGS<sup>\*</sup>SLGTPVNLAV<sup>\*</sup>KLSEQGVLDKL
   
 GluK2STTIEFVTQ--RNCNL<sup>\*</sup>TQIG--LIDSKGYGVGT<sup>\*</sup>PMGSFYRDKITIAI<sup>\*</sup>QLQEEGKLHMM
   
 GluN1SAVLEFEAS--QKCDLV<sup>\*</sup>TTGE--LFFRS<sup>\*</sup>GF<sup>\*</sup>GIMRK<sup>\*</sup>DSPWKQNVSLSI<sup>\*</sup>LKSHENGFMEDL
   
 GluN2AAVLNYKAGRDEGCKLV<sup>\*</sup>TI<sup>\*</sup>SGYIFATTG<sup>\*</sup>YGLALQKGS<sup>\*</sup>PWKQRIDLAI<sup>\*</sup>QFVGDGEMEEL


  
 GLR3.2 (275)HDKWLSRSN--SN (286)
   
 GLR3.1HDRWLSKSN--SS
   
 GLR3.3HDKWLMKNA--TL
   
 GLR3.6RDKWLLRKA--SL
   
 GLR3.4HRKWLN<sup>\*</sup>YKHESS--
   
 GLR3.7RKKWLCKTN--AG
   
 AvGluR1KKKWFQTKA--CPQ
   
 GluA2KNKWYDKGE--CG
   
 GluK2KEKWWRGNG--CPE
   
 GluN1DKTAVRYQE--CDS
   
 GluN2ETLWLTGI--CHN

**Figure S1 (related to Figure 2 and STAR Methods): Amino acid sequence alignment.**

Shown are amino acid sequences for the GLR3.2-S1S2 construct and ligand-binding domains of *AtGLR3.2* (NP\_567981.1), *AtGLR3.1* (NP\_028351.2), *AtGLR3.3* (NP\_174978.1), *AtGLR3.6* (NP\_190716.3), *AtGLR3.4* (NP\_001030971.1), *AtGLR3.7* (NP\_565744.1), *AvGluR1* (ADW94593.1), AMPA subtype rat GluA2 (NP\_058957), kainate subtype rat GluK2 (P42260.2), and NMDA subtype rat GluN1 (EDL93606.1) and GluN2A (NP\_036705.3) subunits. Numbering is for the mature protein. Secondary structure elements for GLR3.2-S1S2 are shown as cylinders ( $\alpha$ -helices), arrows ( $\beta$ -strands), and lines (loops) colored according to domains S1 (orange and purple) and S2 (red and green). The names of  $\alpha$ -helices and  $\beta$ -strands (capital letters and numbers, respectively) are kept the same as in structures of isolated LBD (Armstrong et al., 1998). Identical residues are highlighted in yellow and conserved residues are highlighted in blue. Green circles indicate cysteines connected by disulfide bonds. Red stars indicate residues involved in ligand binding.



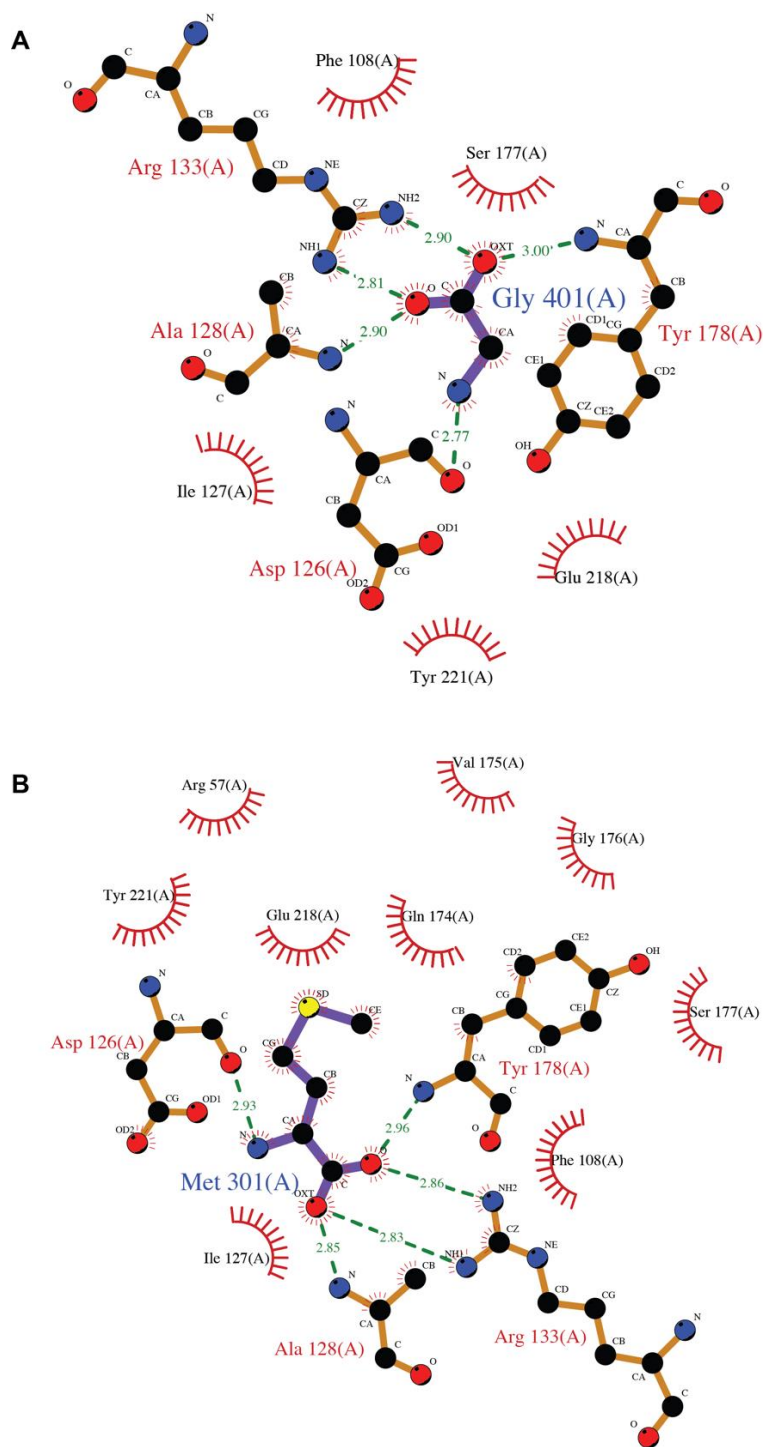


**Figure S2 (related to Figures 1 and 2): Ligplots showing the interactions of protein and ligand for GLR3.2-S1S2<sub>Gly</sub> (A) and GLR3.2-S1S2<sub>Met</sub> (B).** The ligand and residues involved in hydrogen bonding (green dotted lines) with the ligand are shown in ball-and-stick representation. The interatomic distances are indicated in Å. The red arcs show non-bonded contacts.

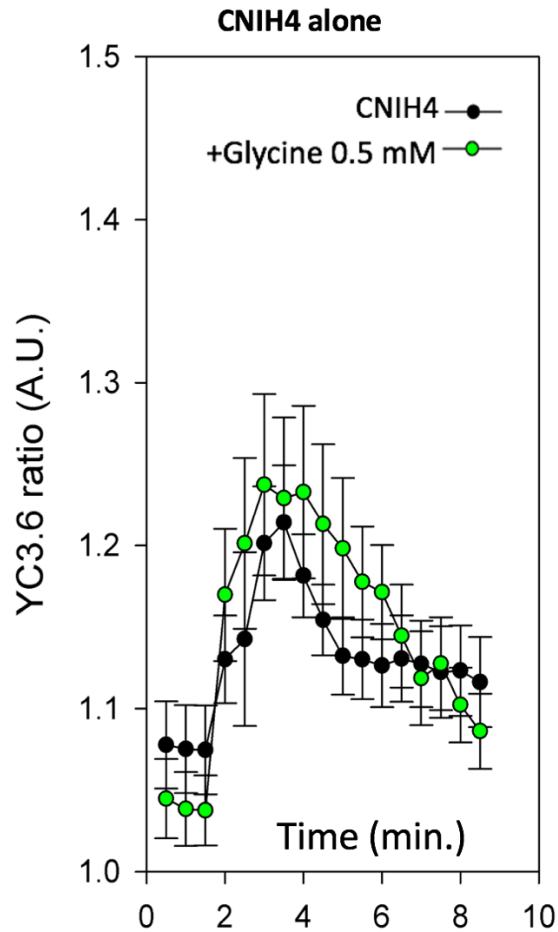


**Figure S3 (related to Figure 3): Effect of *At*CNIH4 alone in the  $\text{Ca}^{2+}$  influx of COS cells.**

The experimental protocol is the same as in Figure 3A. *At*CNIH4 alone induces an increase in the influx of  $\text{Ca}^{2+}$ , but significantly lower than the expression of *At*GLR3.2 alone (Figure 3A). The *Arabidopsis* CNIHs are conserved with mammalian CNIHs, and they complement the yeast homologue mutant (Wudick et al., 2018). Thus, this effect is expected as *At*CNIH4 is likely to affect other endogenous proteins. Data are represented as mean  $\pm$  SEM.

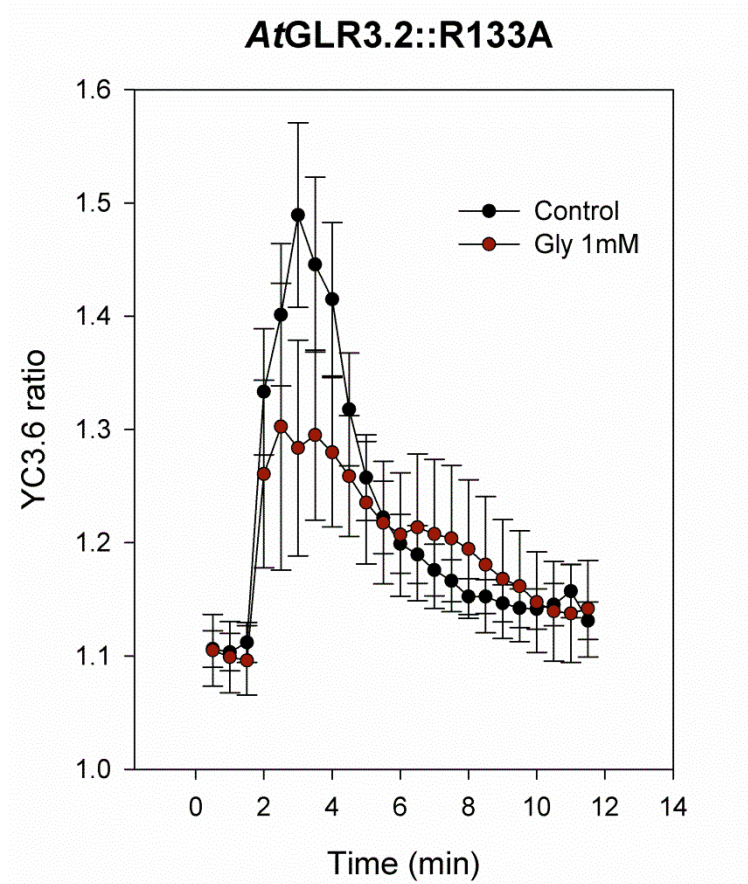


**Figure S4 (related to Figure 3): Control of the effect of the mutation R133A in *AtGLR3.2*, without *AtCNIH4*.** The mutation alone induces a  $\text{Ca}^{2+}$  influx at the same amplitude than when *AtGLR3.2* is co-expressed with *AtCNIH4* and the ligand at the optimized concentration (0.5 mM Gly, Figure 3C). Surprisingly, in the absence of *AtCNIH4*, the presence of 0.5 mM Gly seems to have an inhibitory effect, which is not observed for the wild-type channel (Figures 3A and C). Data are represented as mean  $\pm$  SEM.

## **Chapter 4.**

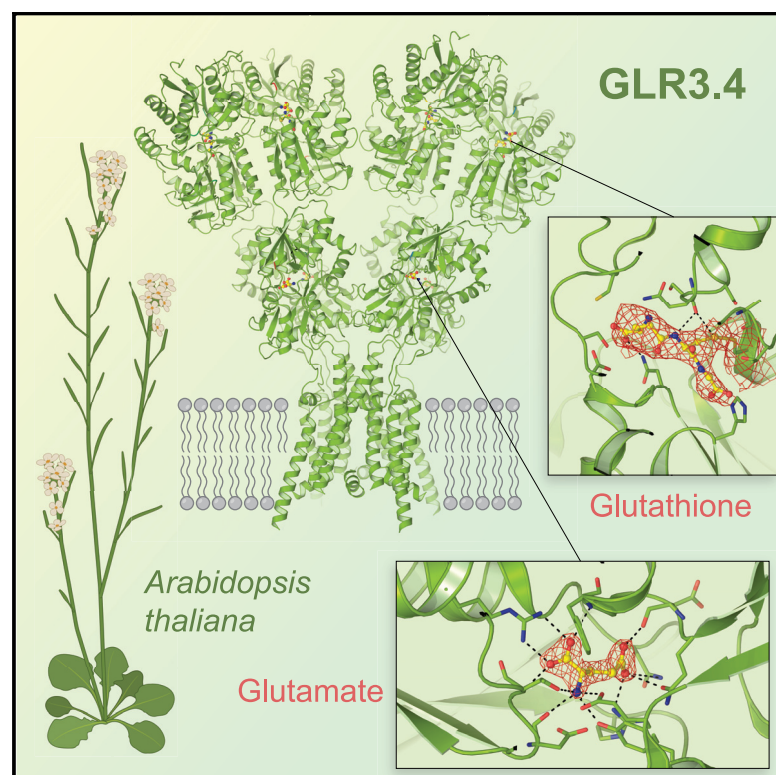
### **Structure of the *Arabidopsis Thaliana* Glutamate Receptor-Like**

#### **Channel GLR3.4**

This chapter is a paper originally published in Molecular Cell (Green et al., 2021). We solved the first full-length GLR structure, specifically *Arabidopsis thaliana* GLR 3.4 (GLR3.4), and the structures of the isolated ligand-binding domain (LBD) in complex with agonists methionine, serine, and glutamate; revealing the structural basis of a GLR activation and gating.

# Structure of the *Arabidopsis thaliana* glutamate receptor-like channel GLR3.4

## Graphical abstract



## Authors

Marriah N. Green, Shanti Pal Gangwar, Erwan Michard, ..., Maria V. Yelshanskaya, José A. Feijó, Alexander I. Sobolevsky

## Correspondence

as4005@cumc.columbia.edu

## In brief

Green et al. solve structures of *Arabidopsis thaliana* glutamate receptor-like channel GLR3.4 that shows tetrameric subunit assembly with three-layer architecture, similar to its mammalian homologs, ionotropic glutamate receptors, but with distinct symmetry, inter-domain interfaces, ligand specificity, and non-swapped domain arrangement between layers of ligand-binding and glutathione-bound amino-terminal domains.

## Highlights

- Cryo-EM structure of *Arabidopsis thaliana* glutamate receptor-like channel GLR3.4
- Glutathione regulates channel activity by binding to C205 in amino-terminal domain
- Crystal structures of GLR3.4 ligand-binding domain illustrate ligand promiscuity
- Amino-terminal and ligand-binding domain layers show non-swapped domain arrangement



## Article

# Structure of the *Arabidopsis thaliana* glutamate receptor-like channel GLR3.4

Marriah N. Green,<sup>1,2,6</sup> Shanti Pal Gangwar,<sup>1,6</sup> Erwan Michard,<sup>3,4,7</sup> Alexander A. Simon,<sup>3,7</sup> Maria Teresa Portes,<sup>3,8</sup> Juan Barbosa-Caro,<sup>3</sup> Michael M. Wudick,<sup>3,5</sup> Michael A. Lizzio,<sup>3</sup> Oleg Klykov,<sup>1</sup> Maria V. Yelshanskaya,<sup>1</sup> José A. Feijó,<sup>3</sup> and Alexander I. Sobolevsky<sup>1,9,\*</sup>

<sup>1</sup>Department of Biochemistry and Molecular Biophysics, Columbia University, 650 West 168th Street, New York, NY 10032, USA

<sup>2</sup>Training Program in Nutritional and Metabolic Biology, Institute of Human Nutrition, Columbia University Irving Medical Center, 630 West 168th Street, New York, NY 10032, USA

<sup>3</sup>University of Maryland, Department of Cell Biology and Molecular Genetics, 0118 BioScience Research Building, College Park, MD 20742-5815, USA

<sup>4</sup>Instituto de Ciencias Biológicas, 2 Norte 685, Universidad de Talca, 3460000 Talca, Chile

<sup>5</sup>Institute for Molecular Physiology, Heinrich Heine Universität, Universitätsstrasse 1, 40225 Düsseldorf, Germany

<sup>6</sup>These authors contributed equally

<sup>7</sup>These authors contributed equally

<sup>8</sup>Current address: Departamento de Botânica, Instituto de Biociências, Universidade de São Paulo, 05508-090, São Paulo, Brazil

<sup>9</sup>Lead contact

\*Correspondence: [as4005@cumc.columbia.edu](mailto:as4005@cumc.columbia.edu)

<https://doi.org/10.1016/j.molcel.2021.05.025>

## SUMMARY

Glutamate receptor-like channels (GLRs) play vital roles in various physiological processes in plants, such as wound response, stomatal aperture control, seed germination, root development, innate immune response, pollen tube growth, and morphogenesis. Despite the importance of GLRs, knowledge about their molecular organization is limited. Here we use X-ray crystallography and single-particle cryo-EM to solve structures of the *Arabidopsis thaliana* GLR3.4. Our structures reveal the tetrameric assembly of GLR3.4 subunits into a three-layer domain architecture, reminiscent of animal ionotropic glutamate receptors (iGluRs). However, the non-swapped arrangement between layers of GLR3.4 domains, binding of glutathione through S-glutathionylation of cysteine C205 inside the amino-terminal domain clamshell, unique symmetry, inter-domain interfaces, and ligand specificity distinguish GLR3.4 from representatives of the iGluR family and suggest distinct features of the GLR gating mechanism. Our work elaborates on the principles of GLR architecture and symmetry and provides a molecular template for deciphering GLR-dependent signaling mechanisms in plants.

## INTRODUCTION

Glutamate receptor-like channels (GLRs) have been identified as homologs of mammalian ionotropic glutamate receptors (iGluRs), which mediate the majority of the excitatory neurotransmission in the central nervous system (Traynelis et al., 2010). GLR homologs have been identified in both vascular and non-vascular plants (Lam et al., 1998; Wudick et al., 2018a) and in genomes across the entire plant evolutionary tree, including *Chlamydomonas*, chlorophytes, mosses, ferns, gymnosperms, and angiosperms (De Bortoli et al., 2016; Wudick et al., 2018a). On the basis of phylogenetic analysis, the 20 GLRs identified in the model flowering plant *Arabidopsis thaliana* have been organized into three different clades: GLR1, GLR2, and GLR3 (Lam et al., 1998). In contrast to iGluRs, which are targeted mainly to the plasma membrane, GLRs have not only been located in the plasma membrane but also located in the plant mitochondria, chloroplast, tonoplast, endoplasmic reticulum, and sperm cell (endo)membranes (Teardo et al.,

2015; Vincill et al., 2013; Wudick et al., 2018a). GLRs play vital roles in various physiological processes in plants, such as cell signaling, metabolism, wound response, stomatal aperture, seed germination, root development, innate immune response, pollen tube growth, and water loss (Wudick et al., 2018a). Given the diverse range of crucial physiological roles, targeting GLRs can have practical applications, especially related to biotic and abiotic environmental stress, which constitute a major problem for sustainability (Jones et al., 2008). Genetic efforts to explore GLR potential have been hindered by the apparent high functional redundancy and a large number of genes coding for GLRs in the majority of angiosperms, including crops. An alternative to traditional strategies for regulating GLR functions in plants could use approaches that target their specific molecular features (De Bortoli et al., 2016; Michard et al., 2017; Wudick et al., 2018a, 2018b).

The molecularly oriented approaches to harness GLR function rely on the detailed knowledge of GLR structural organization. Recent studies of the GLR3.2 and GLR3.3 ligand-binding



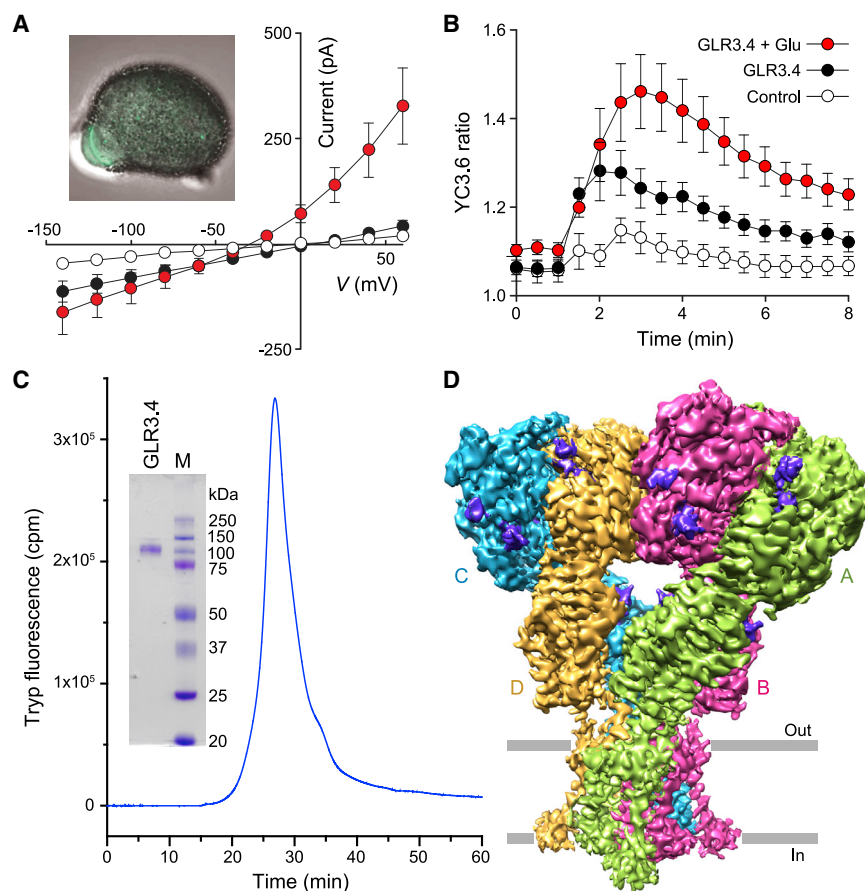


**Figure 1. Functional, biochemical, and structural characterization of GLR3.4**

(A) Voltage dependence of whole-cell patch-clamp currents recorded from COS-7 cells expressing GLR3.4, CNIH1, and CNIH4 before (black circles) and after (red circles) application of 1 mM Glu (n = 3, mean ± SEM). The control (white circles) is endogenous currents recorded from COS-7 cells transfected with the empty vector (n = 5, mean ± SEM). Inset shows specific GFP labeling of GLR3.4 at the plasma membrane of the pollen grain aperture, an outgrowth spot where the pollen tube will emerge.

(B) Changes in cytosolic Ca<sup>2+</sup> measured in COS-7 cells expressing the Ca<sup>2+</sup> sensor Yellow CaMeleon 3.6 (YC3.6) and expressing either CNIH1+4 alone (control, white circles) or GLR3.4 and CNIH1+4, in response to application of 14.5 mM Ca<sup>2+</sup> in the absence (black circles; n = 27, mean ± SEM) or presence (red circles; n = 33, mean ± SEM) of 1 mM Glu.

(C) FSEC trace and SDS-PAGE gel for purified GLR3.4.

(D) Cryo-EM density for 3.57 Å 3D reconstruction of GLR3.4, with four subunits colored in green, pink, blue, and orange, and non-protein densities representing carbohydrates and ligands colored in purple.

See also Figures S1–S3 and Table S1.

domains (LBDs), from the model organism *Arabidopsis thaliana*, provided the first glimpse of the fragment of GLR structure responsible for ligand binding (Alfieri et al., 2020; Gangwar et al., 2021). GLR3.2 and GLR3.3 LBD structures identified similar overall folds to iGluRs' LBD structures, with the distinct features in the ligand-binding pocket that are responsible for the promiscuous GLR activation by various amino acids. Despite the important insights from the recent structural studies of GLR LBDs, structures of other GLR domains, principles of their assembly into the full-length receptor, its architecture, and the structural basis of gating have remained an enigma. To fill this gap in knowledge, we embarked on the endeavor to determine the structure of a full-length GLR.

## RESULTS

### Functional characterization and structure determination

We screened several full-length GLRs from the three different clades using fluorescence-detection size-exclusion chromatography (FSEC) (Kawate and Gouaux, 2006) and identified GLR3.4 from *Arabidopsis thaliana* as a promising candidate for structural studies. GLR3.4 expresses at the plasma membrane of root phloem cells, vascular bundles, mesophyll cells, and guard cells (Meyerhoff et al., 2005; Vincill et al., 2013). We show that GLR3.4

localizes specifically to the aperture of the pollen grain (Figure 1A) and appears to be associated with cell polarity, from the formation of the early bulge, which will develop into the pollen tube, to the retention in the apical tips after the formation of the callose plugs, or in root phloem cells (Vincill et al., 2013; Figures S1A–S1C). Cell polarity in *Arabidopsis* pollen tubes has also been characterized by the tip-focused influx of calcium (Ca<sup>2+</sup>) (Michard et al., 2011, 2017). Supporting the role of GLR3.4 in this cell polarity process, two mutant alleles of *glr3.4* showed reduced pollen tube Ca<sup>2+</sup> fluxes compared with wild-type (Figure S1D).

GLR3.4 was reported to mediate currents activated by a broad range of amino acids (Meyerhoff et al., 2005; Stephens et al., 2008; Vincill et al., 2012). GLR3.4 expressing COS-7 cells showed robust ionic currents in response to application of Glu or Asn only when co-expressed with CORNICHON HOMOLOG (CNIH) proteins CNIH1 and/or CNIH4 (Figure 1A; Figures S2A–S2D), consistent with the recently discovered role of CNIHs in GLR sorting and activation (Wudick et al., 2018b). GLR3.4 activation in the presence of Glu or Asn resulted in an increase in cytosolic calcium (Figure 1B; Figures S2E and S2F), which may work as a signaling mechanism in plants (Michard et al., 2011; Mousavi et al., 2013; Ortiz-Ramírez et al., 2017).

We expressed full-length GLR3.4 in HEK293 cells, purified the protein to sufficient purity and homogeneity (Figure 1C), and subjected it to single-particle cryoelectron microscopy (cryo-EM). We reconstructed a three-dimensional (3D) map to an overall 3.57 Å resolution (Figure 1D), with the core of the molecule resolved at ~3 Å resolution (Figure S3; Table S1; Video S1).

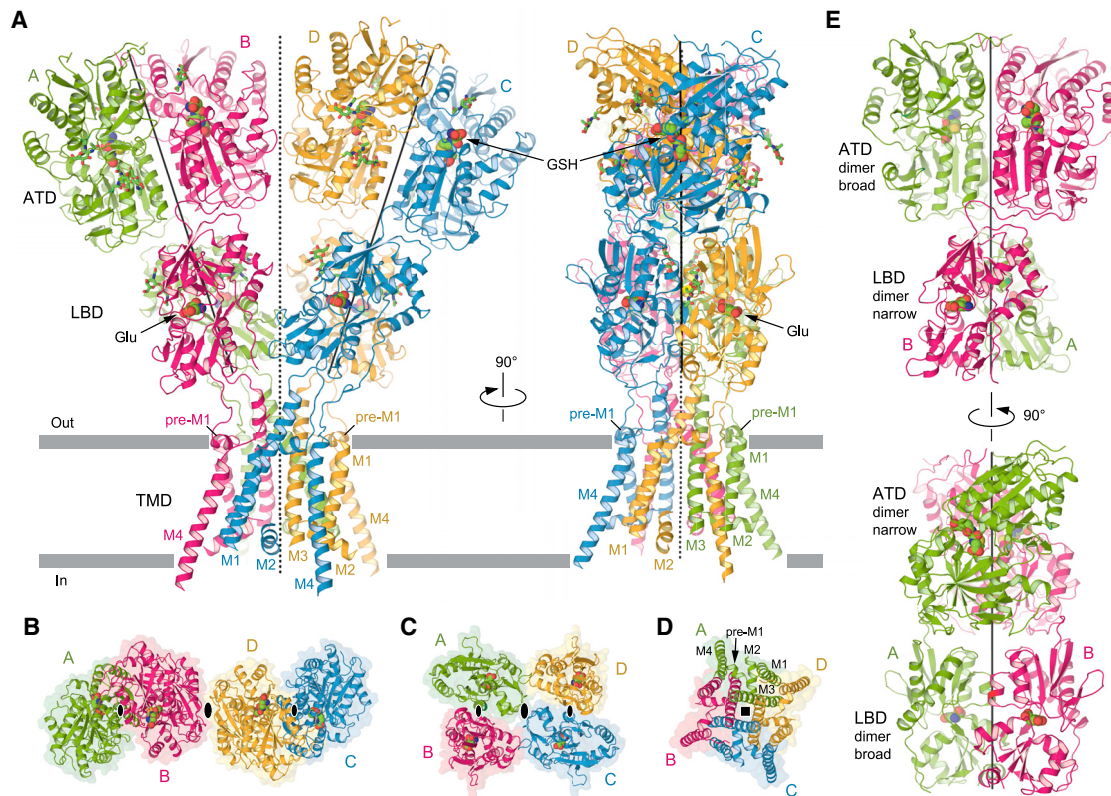


**Figure 2. Overall architecture and symmetry**

(A) GLR3.4 structure viewed parallel to the membrane (gray bars), with four subunits colored differently, molecules of GSH and Glu shown as space-filling models and carbohydrates as sticks. The axes of the overall and local two-fold symmetries are shown as dotted and solid lines, respectively.

(B–D) ATD (B), LBD (C) and TMD (D) layers viewed extracellularly, with the overall (large ovals) and local (small ovals) two-fold and four-fold (square) symmetries indicated.

(E) ATD and LBD dimers formed by subunits A and B, viewed perpendicular to the axis of the local two-fold symmetry and showing their broad and narrow faces. See also [Figures S4](#) and [S5](#).

The map quality was adequate for building each subunit of the GLR3.4 tetramer, excluding the S2-M4 linkers and loops connecting M1 to M2 and M2 to M3, which were not represented clearly by resolved density.

### Architecture and symmetry

The Y shape of the 175-Å-tall GLR3.4 structure resembles the shape of non-NMDA subtype iGluR structures ([Burada et al., 2020b](#); [Meyerson et al., 2016](#); [Sobolevsky et al., 2009](#); [Figure 2A](#)). Similar to all iGluRs, the structure of GLR3.4 has a three-layer architecture, which includes the amino-terminal domain (ATD) layer at the top, the LBD layer in the middle, and the transmembrane domain (TMD) layer at the base of the “Y.” The ATDs and LBDs of subunits A/B and C/D form dimers with monomers related by two-fold rotational symmetry. The GLR3.4 tetramer has an overall two-fold rotational symmetry that relates one ATD dimer to another, one LBD dimer to the second, and half of the TMD to another half. The axes of local two-fold rotational symmetry for the LBD and ATD dimers coincide and make a 20° angle with the axis of the overall two-fold rotational symmetry of the tetramer. This is very different from the domain organization of AMPA, kainate, and NMDA subtypes of iGluRs, where the ATD

and LBD dimers have distinct axes of local two-fold rotational symmetry. An even more striking feature of GLR3.4 architecture is the lack of domain swapping between the ATD and LBD dimers, which is an inherent property of all major iGluR subtypes. The only exception among iGluRs are orphan delta receptors, which have been recently proposed to follow non-swapped domain architecture similar to GLR3.4 on the basis of low-resolution cryo-EM reconstructions ([Burada et al., 2020a, 2020b](#)).

We confirmed the unorthodox subunit and domain arrangement of GLR3.4 by introducing cysteine substitutions at intersubunit interfaces and observing redox-dependent dimer formation as a result of spontaneous subunit crosslinking ([Figure S4](#)). There are five intersubunit interfaces that keep the four GLR3.4 subunits together by means of hydrogen bonds and hydrophobic and ionic interactions ([Figure S4](#)). In the ATD layer, the intradimer interfaces between subunits A and B as well as C and D are large (3,180 Å<sup>2</sup>) and involve both the upper (L1) and lower (L2) lobes. In contrast, the interdimer interface between subunits B and D, which is mediated primarily by ionic interactions between R436 and E431, is small (209 Å<sup>2</sup>) but keeps the A/B and C/D dimers from falling apart. Similarly, in the LBD layer, the intradimer interfaces between subunits A and B as well as C and D are large (800 Å<sup>2</sup>), while



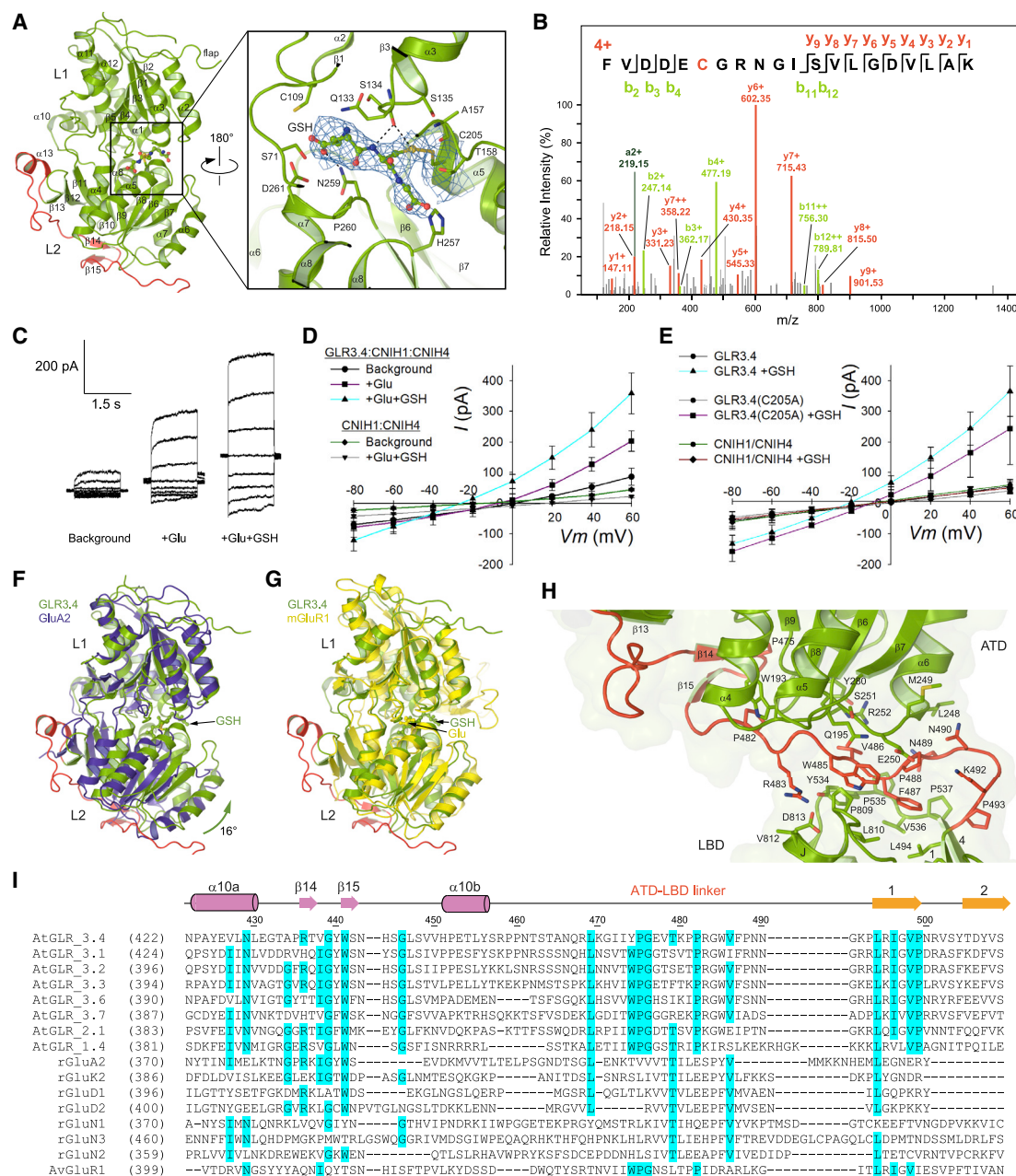


**Figure 3. Amino-terminal domain**

(A) Structure of the GLR3.4 ATD with secondary structure elements labeled. The ATD-LBD linker domain is colored red. The inset shows a close-up view of the GSH binding pocket. GSH is covalently bound to C205 and shown in ball-and-stick representation. Binding pocket residues are shown as sticks, and their interactions with GSH are indicated by dashed lines. Density for GSH is shown as a blue mesh.

(B) Spectrum annotation of the peptide containing C205 modified by GSH.

(C) Representative whole-cell patch-clamp recordings from COS-7 cells expressing GLR3.4:CNII1:CNII4 prior to treatment (background; without exogenous GSH or Glu), after application of 1 mM Glu (+Glu) or after application of 1 mM Glu and 1 mM GSH together (+Glu+GSH).

(D) Voltage dependencies of currents recorded from COS-7 cells expressing GLR3.4:CNII1:CNII4 (like those shown in C) in comparison with the ones recorded from COS-7 cells expressing CNII1 and CNII4 only, before and after application of 1 mM Glu and 1 mM GSH (n = 8 for GLR3.4 background condition, n = 5 for GLR3.4 +Glu, n = 5 for GLR3.4+Glu+GSH, n = 5 for CNII1:CNII4 background, and n = 5 for CNII1:CNII4+Glu+GSH).

(E) Voltage dependencies of currents recorded from COS-7 cells expressing wild-type GLR3.4 (n = 6), GLR3.4(C205A) (n = 4), and CNII1:CNII4 (n = 5) before and after application of 1 mM GSH. Both wild-type and mutant GLR constructs were co-transfected with CNII1 and CNII4. All data shown in (D) and (E) are mean ± SEM.

(legend continued on next page)

the interdimer interface between subunits A and C is small (218 Å<sup>2</sup>) and mediated by hydrogen bonds between T717 and N719. The four GLR3.4 subunits interact most extensively at the TMD, where each of the four pairs of the neighboring subunits (A/B, B/C, C/D, and D/A) contribute a large (1,547 Å<sup>2</sup>) intersubunit interface. Apart from numerous hydrophobic interactions, which are typical for transmembrane regions, these interfaces are also stabilized by hydrogen bonds between residues T613, E615, L686, N689, S690, T693, T697, S698, L700, K856, and S857 that belong to the adjacent subunits.

The symmetrical dimer-of-dimers organization of GLR3.4 is maintained over the ATD and LBD layers (Figures 2B and 2C) but changes to pseudo-four-fold symmetrical organization in the TMD layer (Figure 2D). Correspondingly, interfaces among four GLR3.4 subunits are equivalent at the level of TMD but distinct between the ATDs and LBDs, with only the proximal pairs contributing to the interdimer interfaces. Interestingly, the pairs of proximal and distal subunits in GLR3.4 are exactly the same as in iGluRs' swapped topology, despite the lack of domain swapping between the ATD and LBD layers. Indeed, the A/C pair is distal in the ATD layer and proximal in the LBD layer, while the B/D pair is proximal in the ATD layer and distal in the LBD layer (Figures 2B and 2C). Switching of the proximal and distal subunit pairs becomes possible because of the perpendicular orientation of the ATD and LBD dimers with respect to each other (Figure 2E).

The overall two-fold rotational symmetry of the GLR3.4 tetramer with pseudo-four-fold symmetrical TMD (Figure 2D) is a result of two diagonal pairs, A/C and B/D, of chemically identical subunits adapting two different conformations (Figure S5A). Although their extracellular domains related by the local two-fold rotational symmetry have the same conformations, their TMDs are displaced in a 93° rotation (Figure S5B). As a result of such dramatic conformational changes, the A/C and B/D subunit pairs play different structural roles in the extracellular portion of GLR3.4, while contributing equally to the ion channel. As a reflection of the different structural roles of the A/C and B/D subunit pairs, the subunits B and D ATDs are in direct contact, while the subunits A and C ATDs are separated by more than 70 Å (Figures S5C and S5D).

### ATDs

The ATDs of GLR3.4 adapt a clamshell architecture that was previously observed in the ATDs of iGluRs (Hansen et al., 2010), bacterial periplasmic amino acid binding proteins (Trakhanov et al., 2005), the extracellular domain of the natriuretic peptide receptor (He et al., 2001), and the LBDs of family C G protein-coupled receptors, including metabotropic glutamate (Koehl

et al., 2019) and GABA<sub>B</sub> receptors (Papaserghi-Scott et al., 2020; Park et al., 2020; Shaye et al., 2020). The dimer-of-dimers assembly of ATDs in iGluRs is important for their tetrameric stability, but functionally these domains are orphan in AMPA and kainate subtypes because of their open clamshells that have not been reported to bind to any ligand and pronounced interfaces between the upper L1 and lower L2 lobes that restrain clamshell opening/closing transformations (Jin et al., 2009). NMDA receptors, which bind the inhibitor zinc ion inside the GluN2B subunit ATD clamshell and conduct the conformational changes in the ATDs to the LBDs and the ion channel (Jalali-Yazdi et al., 2018; Karakas et al., 2009), are an exception. As the overall domain organization and shape of GLR3.4 resembles more AMPA and kainate than NMDA receptors, we expected the ATD clamshells to be similar to non-NMDA receptors. Against these expectations, we found that the GLR3.4 ATDs are all bound to glutathione (GSH) through S-glutathionylation of cysteine C205 (Figure 3A).

The binding of GSH in the middle of the ATD clamshell explains why GSH has been previously described as an activator of GLRs (Qi et al., 2006). The reversible covalent linking to cysteine C205 endows GSH with the potential to act as a biological switch and be integral in several critical oxidative signaling events (Xiong et al., 2011), including stress response in plants (Dixon et al., 2005). Apart from its disulfide bond to C205, GSH is held in its binding pocket by hydrogen bonds to the backbone carbonyl of Q133 and the amide nitrogen of N259 as well as several non-bonded contacts. As a result of all these interactions, GSH binding is strong, signified by the clearly resolved density that unambiguously identifies the position and pose of this molecule in its binding pocket (Figure 3A, inset). Covalent modification of C205 by GSH was also confirmed by the standard bottom-up proteomics approach (Figure 3B). Wild-type GLR3.4 and C205A mutant protein samples digested in reducing and non-reducing conditions were subjected to mass spectrometry analysis. Samples digested in reducing conditions showed no GSH modification. However, when the digest was carried out in non-reducing conditions, GSH was detected at the residue 205 in the wild-type protein but not in the C205A mutant.

We tested a potential role of GSH in GLR3.4 function by heterologously expressing the channel in COS-7 cells. When GLR3.4 was co-expressed with CNIH1 and CNIH4, Glu with GSH elicited larger currents than Glu alone (Figures 3C and 3D). This activating effect of GSH was impaired by C205A mutation (Figure 3E), suggesting that cysteine C205 and the GSH binding pocket identified in the ATD play an important role in GLR3.4 function. On the other hand, significant GSH-induced potentiation of GLR3.4(C205A) currents indicates that there is a

(F and G) Superposition of the GLR3.4 ATD with GluA2 ATD (blue; PDB: 3H5V) (F) and mGluR1 ligand-binding domain (yellow; PDB: 1EWK) (G). Closure by 16° of the GLR3.4 ATD clamshell compared with the GluA2 ATD clamshell is indicated by the green arrow.

(H) Close-up view of the GLR3.4 interface between ATD and LBD, with the contributing residues shown as sticks.

(I) Amino acid sequence alignment for the ATD-LBD linker region of AtGLR3.4 (NP\_001030971.1), AtGLR3.1 (NP\_028351.2), AtGLR3.2 (NP\_567981.1), AtGLR3.3 (NP\_174978.1), AtGLR3.6 (NP\_190716.3), AtGLR3.7 (NP\_565744.1), AtGLR2.1 (NP\_198062.2), AtGLR1.4 (NP\_187408.2), AMPA subtype rat GluA2 (NP\_058957), kainate subtype rat GluK2 (P42260.2), delta subtype rat GluD1 (NP\_077354.1) and GluD2 (NP\_077355.1), NMDA subtype rat GluN1 (EDL93606.1), GluN3A (NP\_612555.1), and GluN2A (NP\_036705.3), and AvGluR1 (ADW94593.1). Numbering is for the mature protein. Secondary structure elements are shown as cylinders (α helices), arrows (β strands), and lines (loops) and colored according to domains, ATD (purple) and LBD (orange). Conserved residues are highlighted in blue.

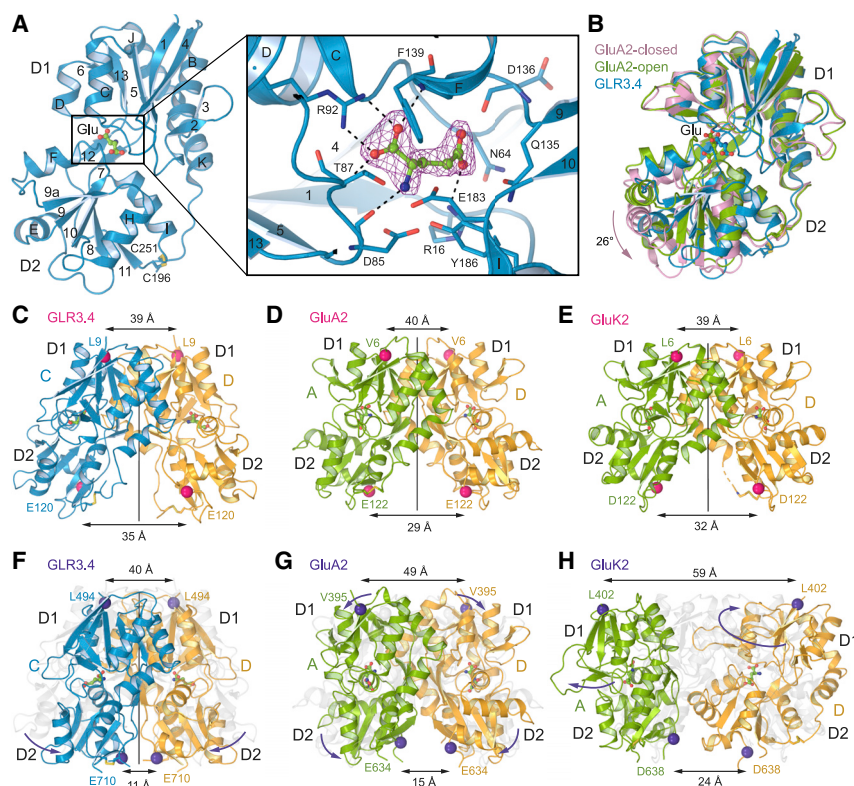


**Figure 4. Ligand-binding domain**

(A) Structure of the Glu-bound isolated GLR3.4 LBD with secondary structure elements labeled. The inset shows a close-up view of the Glu binding pocket, with Glu shown in ball-and-stick representation and the omit map density for Glu at 5 $\sigma$  shown as purple mesh. Binding pocket residues are shown as sticks, and their interactions with Glu are indicated by dashed lines.

(B) Superposition of the Glu-bound isolated GLR3.4 LBD (blue) with Glu-bound isolated GluA2 LBD (green; PDB: 1FTJ) and isolated apo-state GluA2 LBD (pink; PDB: 1FTO). Opening of the apo-state GluA2 LBD clamshell by 26° compared with the Glu-bound LBD clamshells is indicated by the pink arrow.

(C–E) Glu-bound dimers of isolated GLR3.4 LBD (C), GluA2 LBD (PDB: 1FTJ) (D), and GluK2 LBD (PDB: 3G3F) (E), with the distances between upper and lower lobes indicated. The two-fold symmetry axes are shown as vertical black lines.

(F–H) LBD dimers from the full-length structures of GLR3.4 (F), GluA2 in complex with GSG1L (PDB: 5VHZ) (G), and GluK2 (PDB: 5KUF) (H), in complex with Glu, L-quisqualate, and 2S,4R-4-methylglutamate, respectively, and superposed with the corresponding isolated LBD dimers (C–E) shown in gray. Rearrangements of LBDs in the full-length structures compared with isolated LBDs are indicated by purple arrows.

See also Figure S6 and Table S2.

C205A-independent component of activation by GSH. For example, this component can be mediated by GSH binding to the same site in the ATD but without covalent attachment to C205.

To infer whether GSH binding has the potential to produce conformational changes in the GLR3.4 protein, we compared its ATD to the ATD of the AMPA subtype iGluR GluA2, which has the same overall fold but does not bind to any ligands. Strikingly, GSH-bound clamshell of the GLR3.4 ATD is 16° more closed than the ATD clamshell of GluA2 (Figure 3F). This conformation is reminiscent of the conformation of mGluR LBD after it closes in response to the binding of agonist glutamate (Figure 3G). Thus, a comparison of the GLR3.4 ATD with the domains of a similar fold suggests that GSH binding can cause conformational changes in the GLR protein, which might contribute to gating of its ion channel.

For conformational changes in the ATD to be effectively transmitted to the LBD and TMD, the ATD must have a strong structural connection to the LBD, such as the one observed in NMDA receptors (Karakas and Furukawa, 2014; Lee et al., 2014) and which is largely missing in AMPA, kainate, or delta receptors (Burada et al., 2020b; Meyerson et al., 2016; Sobolevsky et al., 2009). In GLR3.4, a unique ATD-LBD linker plays the role of an inter-domain connector, creating a strong interface between the ATD and LBD through a network of hydrophobic (residues W485, F487, L494, Y534, P535, V536, P809, and L810) and electrostatic (residues L248, R483, N489, N490, Y534, P535, P809, and D813) interactions (Figure 3H). Such a strong connection be-

tween the ATD and LBD ensures that conformational changes in the ATD are allosterically transmitted to the LBD. This interaction appears highly specific to GLRs, as the ATD-LBD linker amino acid sequence alignment shows low similarity between GLRs and iGluRs (Figure 3I). On the other hand, the majority of residues in the ATD-LBD linker are conserved among GLRs and highly conserved among clade 3 GLRs (Figure 3I).

## LBDs

LBDs are typically the drivers of conformational changes in iGluRs that start with agonist binding to the LBD and end up with the opening of the ion channel for current conductance. To get a high-resolution view of GLR3.4 LBD and ligand binding, we purified this domain separately and solved crystal structures of the isolated LBD in complex with agonists glutamate, serine, and methionine (Table S2). The structure of GLR3.4 LBD has a clamshell architecture (Figure 4A; Figures S6A–S6C) that is typical for iGluRs and similar to the recently published structures of isolated GLR3.2 and GLR3.3 LBDs (Figure S6D). The agonist binds in the middle of the LBD clamshell, to the binding site between its upper D1 and lower D2 lobes, resulting in a closed clamshell conformation (Figure 4B), and agonist binding can be monitored using microscale thermophoresis (Figure S6E). The serine-bound LBD structure was solved without adding the ligand to the protein, indicating serine's endogenous origin (see STAR Methods). Accordingly, in thermophoresis experiments, serine binding was not detected, likely because it was already bound to the LBD (Figure S6E). As a consequence, the



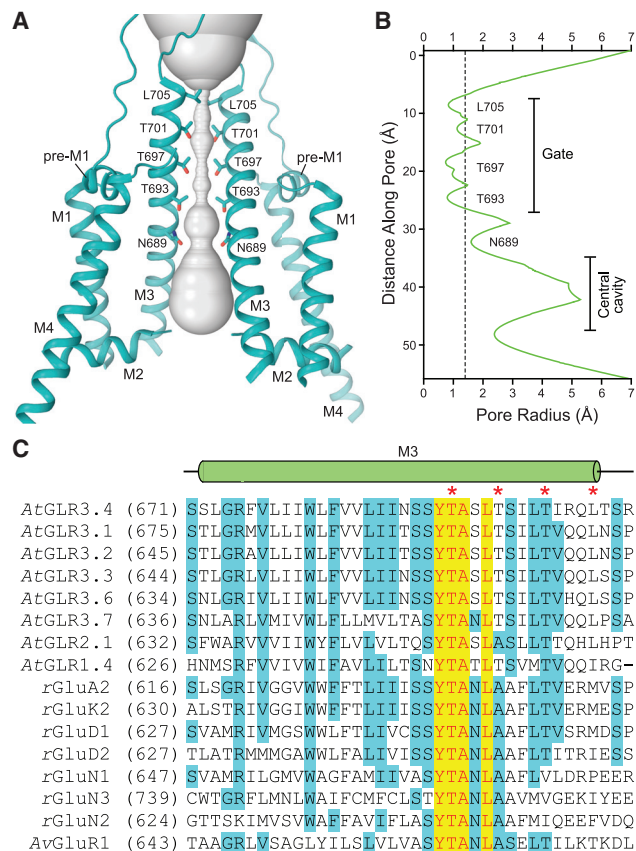


**Figure 5. Ion channel**

(A) Ion conduction pathway (gray) in GLR3.4, with residues lining the pore shown as sticks. Only two of four GLR3.4 subunits are shown, with the front and back subunits removed for clarity.

(B) Pore radius calculated using HOLE. The dashed line corresponds to 1.4 Å (radius of a water molecule).

(C) Amino acid sequence alignment for the M3 region of GLRs and iGluRs. The gate-forming residues are indicated by asterisks.

apparent dissociation constants for glutamate and methionine unlikely report their true affinities but rather effective concentrations to outcompete endogenous serine.

The key interactions with agonists and binding residues are conserved among iGluRs and GLRs (Alfieri et al., 2020; Gangwar et al., 2021). For all three agonists, the guanidinium group of R92 (R577 in the full-length GLR3.4) and the backbone amines of T87 and F139 are hydrogen bonded to the carboxyl group of the ligand, while the backbone carbonyl oxygen of D85, the hydroxyl groups of T87 and Y186, and the carboxyl group of E183 coordinate the amino group of the ligand. The ligand side chains are stabilized differently. The side-chain carboxyl group of glutamate and the thioether group of methionine are additionally coordinated by the guanidinium group of R16, amide groups of N64 and Q135, the phenol group of Y67, and the backbone carbonyl oxygen of D136 (Figure 4A, inset; Figure S6C). These interactions are missing in the case of serine, which lacks the bulky side chain. Instead, a water molecule occupies the void, where it is stabilized by hydrogen bonds with the hydroxymethyl side chain

of serine, the guanidinium group of R16, the amide group of Q135, and the backbone carbonyl oxygen of D136 (Figure S6B). Water molecules played a similar role in the binding of glycine to the LBDs of GLR3.2 and GLR3.3 (Alfieri et al., 2020; Gangwar et al., 2021). Altogether, these data illustrate how the ligand-binding pocket of GLRs evolved to bind differently sized amino acids by exploiting the same interactions for binding the conserved amino acid core and adjusting the fit of the side chains with water. This explains the ligand-binding promiscuity of GLRs, which are activated by at least 12 of the 20 proteinogenic amino acids and the non-proteinogenic amino acid ACC (1-aminocyclopropane-1-carboxylic acid) (Forde and Roberts, 2014; Kong et al., 2016; Michard et al., 2011; Mou et al., 2020; Tapken et al., 2013; Vincill et al., 2012; Vincill et al., 2013; Wudick et al., 2018a, 2018b), in contrast to vertebrate iGluRs, which are activated only by specific amino acids (Traynelis et al., 2010). Interestingly, ACC was shown to be a partial agonist for the NMDA receptor GluN1 subunit (Inanobe et al., 2005), while invertebrate iGluRs can also be activated by different amino acids (Lomash et al., 2013).

In our crystal structures, the isolated LBDs form dimers that show back-to-back arrangement of monomers (Figure 4C), typical for the open-state LBD dimers in iGluRs. Indeed, the dimers are held together through D1-D1 interfaces, reminiscent of GluA2 (Figure 4D), and GluK2 (Figure 4E) LBD dimers. Interestingly, the LBD dimers in the context of full-length GLR3.4 show a very different assembly of monomers, with about the same distance between the upper lobes as in the isolated LBD structures but a much shorter distance between their bottom lobes (Figure 4F). The reduced separation of the D2 lobes in dimers of agonist-bound LBDs is the characteristic feature of the iGluR desensitized state (Figures 4G and 4H). In contrast to the open state, which also has LBD clamshells closed with agonists, the desensitized state is characterized by a non-conducting ion channel.

### Ion channel

Similar to iGluRs, the ion channel of GLR3.4 is assembled of the TMDs of four subunits in a four-fold symmetrical manner, each TMD contributing the transmembrane helices M1, M3, and M4 and a re-entrant intracellular loop M2 (Figures 2D and 5A). The extracellular part of the channel's ion conduction pathway is lined by the M3 helices that form the gate. Its intracellular part, which is typically responsible for ion selectivity, is lined by the non-helical portions of M2, apparently disordered in our cryo-EM maps. M1 and M4 are on the periphery of the ion channel and contact the surrounding TMD membrane lipid. M1 helices are preceded by the short pre-M1 helices that form an extracellular collar around the ion permeation pathway, which in AMPA receptors harbors binding sites for non-competitive inhibitors, including the antiepileptic drug perampanel (Yelshanskaya et al., 2016).

Measurements of the pore radius (Figures 5A and 5B) suggest that the ion channel is in the closed non-conducting conformation. The pore's narrow constriction is formed by the extracellular portions of the M3 helices, specifically by four rings of residues, including T693, T697, T701, and L705. The homologous residues in iGluRs that also form the pore's narrow constriction are either

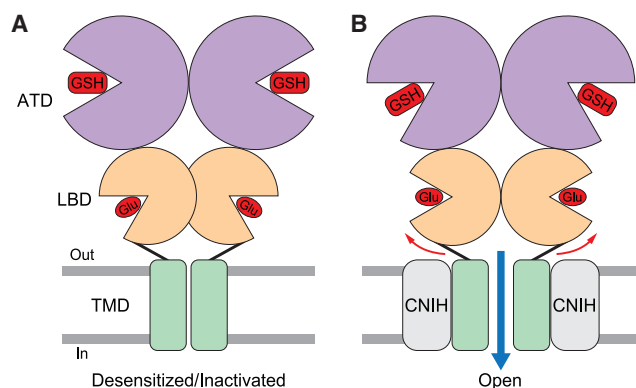


**Figure 6. GLR3.4 gating**

(A) In the absence of CNIHs (HEK and COS-7 cells), GLR3.4 adapts desensitized or inactivated conformation, where GSH is bound to ATD (purple), Glu is bound to LBD (orange), and the channel (green) is in closed, non-conducting conformation.

(B) In the presence of CNIHs (gray, COS-7 cells), ligand-induced conformational changes in the extracellular domain (red arrows) can lead to opening of the ion channel and ion conductance (blue arrow).

part of the highly conserved SYTANLAAF motif or just C-terminal to it (Figure 5C). The distinct character of gate-forming residues in GLR3.4 compared with iGluRs suggest that gating and permeation properties of GLRs might differ from iGluRs.

## DISCUSSION

In the GLR3.4 structure, the ATDs (Figure 3) and LBDs (Figure 4) are bound to agonist molecules. The ATDs are bound to GSH and adapt closed clamshell conformations. The LBDs also adapt closed clamshell conformations and are modeled bound to Glu, which we added to the protein before subjecting it to cryo-EM. There is a possibility, however, that the LBDs in the full-length GLR3.4 structure are bound to Ser, similar to the isolated LBD, which was found bound to Ser of endogenous origin (Figure S6; STAR Methods). In fact, it is practically impossible to distinguish Glu from Ser in cryo-EM maps at 3.57 Å resolution (Figures 1 and S3; Video S1). Independent of whether the LBDs are bound to Glu or Ser, their closed clamshell conformations are identical (Figure S6A).

Closed clamshell conformations observed for the ATDs and LBDs are active conformations of the clamshell domains, which can drive the opening of the GLR3.4 ion channel. However, the ion channel in the GLR3.4 structure is in a closed non-conducting state (Figure 5), suggesting that the structure represents a desensitized or inactivated state. This conclusion is supported by the arrangement of monomers in the GLR3.4 LBD dimers, where the lower lobes D2 are separated by a much smaller distance (Figure 4F) than expected from dimers representing the active state (Figures 4C–4E), recently confirmed by the open-state structures of the intact AMPA receptor (Chen et al., 2017; Twomey et al., 2017). Consistently, the smaller separation of the D2 lobes was also observed in the desensitized states of AMPA (Figure 4G) and kainate (Figure 4H) receptors. The conformational state of the GLR3.4 structure, therefore, suggests com-

mon features of the gating mechanisms of GLRs and iGluRs. At the level of LBD, gating is triggered by the binding of agonist that presumably leads to individual clamshell closures and separation of the D2 lobes (Figure 6). Applied to the LBD-TMD linkers, the separation of the D2 lobes would cause ion channel opening. During desensitization, the monomers of the LBD dimers could rearrange to decrease the distance between the D2 lobes, relieve the strain on the LBD-TMD linkers and convert the channel to the closed non-conducting state.

Despite the apparent similarities in the general principles of gating between GLRs and iGluRs, there are substantial differences. First, in COS-7 cells, GLR3.4 requires CNIHs to conduct currents (Figure 1; Figure S2). The majority of iGluRs conduct currents in the absence of CNIHs, although surface expression and gating of AMPA-subtype iGluRs are strongly regulated by CNIHs (Nakagawa, 2019; Schwenk et al., 2009). The only iGluR exception is GluD-subtype channels, which alone conduct currents only if they acquire mutations in the pore region (Kohda et al., 2000; Yadav et al., 2011). Interestingly, these silent iGluRs are the only iGluRs that share GLR3.4's non-swapped arrangement of ATD and LBD domains (Burada et al., 2020a, 2020b). Whether GluDs can mediate currents by binding to CNIHs or other auxiliary subunits remains undiscovered. Similarly, the possible roles of CNIHs in GLR trafficking to the cell surface and acting as chaperones to alter subunit conformations and assembly will require further investigation.

Second, agonist molecules can bind not only to the LBD but also to the ATD (Figure 3), suggesting that GLR3.4's channel opening can be triggered from both extracellular domain layers (Figure 6). The unique architecture of GLR3.4 with non-swapped pairs of the ATD and LBD dimers and tight ATD-LBD linkage through the connecting domain is likely important for transmitting conformational changes in the ATD and LBD layers to the ion channel. Similarly, the unique GLR3.4 architecture allows the arrangement of monomers within the LBD dimers, which is clearly different from AMPA and kainate receptors (Figures 4F–4H). Accordingly, the distinct conformational ensemble may be an indication that GLRs and iGluRs have principally different desensitization mechanisms. Additional structural and functional studies are necessary to decipher the GLR gating mechanisms, its regulation by CNIHs, and the way it shapes GLRs' functions in plants.

## Limitations of the study

According to our experiments, function of GLR3.4 requires CNIH auxiliary subunits. In contrast, our full-length structure of GLR3.4 is determined in the absence of CNIH subunits. Solving structures of GLR3.4-CNIH complexes will be necessary to confirm the physiological relevance of the GLR3.4 structure and to better understand the molecular bases of GLR3.4 function. Our full-length structure of GLR3.4 reports only a single conformation, which we interpret as a desensitized state. We propose that GLR3.4 can undergo conformational changes and open its ion channel to carry out GLR3.4 physiological functions. To verify this hypothesis and to characterize gating and conformational ensemble of GLR3.4 more completely, it will be necessary to solve structures of GLR3.4 and GLR3.4-CNIH complexes in the closed and open states. The unique modulation of GLR3.4

function by GSH binding to the ATD is particularly interesting, as it has not been observed in iGluRs. To understand the molecular mechanism of this modulation, it will be necessary to solve structures of GLR3.4 and GLR3.4-CNIH complexes in the absence of bound GSH.

## STAR★METHODS

Detailed methods are provided in the online version of this paper and include the following:

- **KEY RESOURCES TABLE**
- **RESOURCE AVAILABILITY**
  - Lead contact
  - Materials availability
  - Data and code availability
- **EXPERIMENTAL MODEL AND SUBJECT DETAILS**
- **METHOD DETAILS**
  - Constructs
  - Plant transformation
  - GLR3.4-S1S2 expression and purification
  - GLR3.4-S1S2 crystallization and structure determination
  - Measurements of ligand binding to GLR3.4-S1S2 using microscale thermophoresis
  - Full-length GLR3.4 expression and purification
  - Cryo-EM sample preparation and data collection
  - Image processing
  - Model building
  - Cysteine crosslinking
  - COS-7 cells transfection and Ca<sup>2+</sup> imaging
  - Patch-clamp recordings
  - Extracellular calcium influx measurements
  - Confocal microscopy of *Arabidopsis* pollen
  - Liquid chromatography and mass spectrometry
- **QUANTIFICATION AND STATISTICAL ANALYSIS**

## SUPPLEMENTAL INFORMATION

Supplemental information can be found online at <https://doi.org/10.1016/j.molcel.2021.05.025>.

## ACKNOWLEDGMENTS

We thank R. Grassucci, Z. Zhang, Y.-C. Chi, and L. Zheng (Columbia University Cryo-Electron Microscopy Center) for help with microscope operation and cryo-EM data collection; Surajit Banerjee (beamline 24-ID-C of the Advanced Photon Source) for assistance with crystallographic data collection; Rajesh Kumar Soni (Proteomics and Macromolecular Crystallography Shared Resource, Herbert Irving Comprehensive Cancer Center, Columbia University) for mass spectrometry data acquisition; and Renato Bruni (New York Structural Biology Center) for help with microscale thermophoresis (MST). The crystallographic data were collected at beamline 24-ID-C of the Advanced Photon Source, one of the Northeastern Collaborative Access Team beamlines, which are funded by the National Institute of General Medical Sciences of the National Institutes of Health (P30 GM124165). The Pilatus 6M detector on the 24-ID-C beamline is funded by an NIH Office of Research Infrastructure Programs (ORIP) High-End Instrumentation (HEI) grant (S10 RR029205). A.I.S. was supported by the NIH (R01 CA206573, R01 NS083660, and R01 NS107253) and the National Science Foundation (NSF) (1818086). J.A.F. was supported by the NIH (R01 GM131043) and the NSF (MCB1714993 and

MCB1930165). M.M.W. was supported by Deutsche Forschungsgemeinschaft (DFG; 267205415- SFB 1208). The graphical abstract was made with the *Arabidopsis thaliana* image adapted from BioRender.com.

## AUTHOR CONTRIBUTIONS

M.N.G. and S.P.G. made constructs and prepared protein samples for crystallography and cryo-EM and carried out cryo-EM data collection and processing. S.P.G. carried out crystallographic data collection and processing. S.P.G. and A.I.S. built molecular models. M.N.G. made constructs for cross-linking experiments. M.N.G., O.K., and M.V.Y. prepared protein samples. M.N.G. carried out the crosslinking experiments. O.K. performed mass spectrometry experiments and data analysis. J.A.F., A.A.S., and E.M. conceived physiological experiments. E.M., J.B.-C., M.A.L., and A.A.S. carried out patch-clamp recordings and calcium imaging. M.M.W. and M.A.L. performed GFP imaging, genotyping, and phenotyping characterization of wild-type and mutant *Atglr3.4* in plants and pollen. M.T.P. carried out vibrating-probe calcium flux measurements in pollen tubes. M.N.G., S.P.G., E.M., A.A.S., O.K., M.V.Y., J.A.F., and A.I.S. wrote the manuscript.

## DECLARATION OF INTERESTS

The authors declare no competing interests.

Received: April 2, 2021

Revised: April 23, 2021

Accepted: May 19, 2021

Published: June 22, 2021

## REFERENCES

- Adams, P.D., Afonine, P.V., Bunkóczi, G., Chen, V.B., Davis, I.W., Echols, N., Headd, J.J., Hung, L.W., Kapral, G.J., Grosse-Kunstleve, R.W., et al. (2010). PHENIX: a comprehensive Python-based system for macromolecular structure solution. *Acta Crystallogr. D Biol. Crystallogr.* 66, 213–221.
- Afonine, P.V., Grosse-Kunstleve, R.W., Echols, N., Headd, J.J., Moriarty, N.W., Mustyakimov, M., Terwilliger, T.C., Urzhumtsev, A., Zwart, P.H., and Adams, P.D. (2012). Towards automated crystallographic structure refinement with phenix.refine. *Acta Crystallogr. D Biol. Crystallogr.* 68, 352–367.
- Alfieri, A., Doccia, F.G., Pederzoli, R., Grenzi, M., Bonza, M.C., Luoni, L., Candeo, A., Romano Armada, N., Barbiroli, A., Valentini, G., et al. (2020). The structural bases for agonist diversity in an *Arabidopsis thaliana* glutamate receptor-like channel. *Proc. Natl. Acad. Sci. U S A* 117, 752–760.
- Armstrong, N., and Gouaux, E. (2000). Mechanisms for activation and antagonism of an AMPA-sensitive glutamate receptor: crystal structures of the GluR2 ligand binding core. *Neuron* 28, 165–181.
- Armstrong, N., Sun, Y., Chen, G.Q., and Gouaux, E. (1998). Structure of a glutamate-receptor ligand-binding core in complex with kainate. *Nature* 395, 913–917.
- Burada, A.P., Vinnakota, R., and Kumar, J. (2020a). The architecture of GluD2 ionotropic delta glutamate receptor elucidated by cryo-EM. *J. Struct. Biol.* 211, 107546.
- Burada, A.P., Vinnakota, R., and Kumar, J. (2020b). Cryo-EM structures of the ionotropic glutamate receptor GluD1 reveal a non-swapped architecture. *Nat. Struct. Mol. Biol.* 27, 84–91.
- Chen, S., McMullan, G., Faruqi, A.R., Murshudov, G.N., Short, J.M., Scheres, S.H., and Henderson, R. (2013). High-resolution noise substitution to measure overfitting and validate resolution in 3D structure determination by single particle electron cryomicroscopy. *Ultramicroscopy* 135, 24–35.
- Chen, S., Zhao, Y., Wang, Y., Shekhar, M., Tajkhorshid, E., and Gouaux, E. (2017). Activation and desensitization mechanism of AMPA receptor-TARP complex by cryo-EM. *Cell* 170, 1234–1246.e14.
- Chi, H., Liu, C., Yang, H., Zeng, W.F., Wu, L., Zhou, W.J., Wang, R.M., Niu, X.N., Ding, Y.H., Zhang, Y., et al. (2018). Comprehensive identification of

- pptides in tandem mass spectra using an efficient open search engine.
- Nat. Biotechnol.*
- 36, 1059–1061.
- De Bortoli, S., Teardo, E., Szabò, I., Morosinotto, T., and Alboresi, A. (2016). Evolutionary insight into the ionotropic glutamate receptor superfamily of photosynthetic organisms. *Biophys. Chem.* 218, 14–26.
- DeLano, W.L. (2002). The PyMOL Molecular Graphics System (San Carlos, CA: DeLano Scientific).
- Dixon, D.P., Skipsey, M., Grundy, N.M., and Edwards, R. (2005). Stress-induced protein S-glutathionylation in Arabidopsis. *Plant Physiol.* 138, 2233–2244.
- Emsley, P., and Cowtan, K. (2004). Coot: model-building tools for molecular graphics. *Acta Crystallogr. D Biol. Crystallogr.* 60, 2126–2132.
- Forde, B.G., and Roberts, M.R. (2014). Glutamate receptor-like channels in plants: a role as amino acid sensors in plant defence? *F1000Prime Rep.* 6, 37.
- Gangwar, S.P., Green, M.N., Michard, E., Simon, A.A., Feijó, J.A., and Sobolevsky, A.I. (2021). Structure of the Arabidopsis glutamate receptor-like channel GLR3.2 ligand-binding domain. *Structure* 29, 161–169.e4.
- Goehring, A., Lee, C.H., Wang, K.H., Michel, J.C., Claxton, D.P., Bacongus, I., Althoff, T., Fischer, S., Garcia, K.C., and Gouaux, E. (2014). Screening and large-scale expression of membrane proteins in mammalian cells for structural studies. *Nat. Protoc.* 9, 2574–2585.
- Hansen, K.B., Furukawa, H., and Traynelis, S.F. (2010). Control of assembly and function of glutamate receptors by the amino-terminal domain. *Mol. Pharmacol.* 78, 535–549.
- He, X., Chow, D., Martick, M.M., and Garcia, K.C. (2001). Allosteric activation of a spring-loaded natriuretic peptide receptor dimer by hormone. *Science* 293, 1657–1662.
- Inanobe, A., Furukawa, H., and Gouaux, E. (2005). Mechanism of partial agonist action at the NR1 subunit of NMDA receptors. *Neuron* 47, 71–84.
- Jalali-Yazdi, F., Chowdhury, S., Yoshioka, C., and Gouaux, E. (2018). Mechanisms for zinc and proton inhibition of the GluN1/GluN2A NMDA receptor. *Cell* 175, 1520–1532.e15.
- Jin, R., Singh, S.K., Gu, S., Furukawa, H., Sobolevsky, A.I., Zhou, J., Jin, Y., and Gouaux, E. (2009). Crystal structure and association behaviour of the GluR2 amino-terminal domain. *EMBO J.* 28, 1812–1823.
- Jones, A.M., Chory, J., Dangl, J.L., Estelle, M., Jacobsen, S.E., Meyerowitz, E.M., Nordborg, M., and Weigel, D. (2008). The impact of Arabidopsis on human health: diversifying our portfolio. *Cell* 133, 939–943.
- Kabsch, W. (2010). XDS. *Acta Crystallogr. D Biol. Crystallogr.* 66, 125–132.
- Karakas, E., and Furukawa, H. (2014). Crystal structure of a heterotetrameric NMDA receptor ion channel. *Science* 344, 992–997.
- Karakas, E., Simorowski, N., and Furukawa, H. (2009). Structure of the zinc-bound amino-terminal domain of the NMDA receptor NR2B subunit. *EMBO J.* 28, 3910–3920.
- Kawate, T., and Gouaux, E. (2006). Fluorescence-detection size-exclusion chromatography for precrystallization screening of integral membrane proteins. *Structure* 14, 673–681.
- Kimanius, D., Forsberg, B.O., Scheres, S.H., and Lindahl, E. (2016). Accelerated cryo-EM structure determination with parallelisation using GPUs in RELION-2. *eLife* 5, e18722.
- Koehl, A., Hu, H., Feng, D., Sun, B., Zhang, Y., Robertson, M.J., Chu, M., Kobilka, T.S., Laeremans, T., Steyaert, J., et al. (2019). Structural insights into the activation of metabotropic glutamate receptors. *Nature* 566, 79–84.
- Kohda, K., Wang, Y., and Yuzaki, M. (2000). Mutation of a glutamate receptor motif reveals its role in gating and delta2 receptor channel properties. *Nat. Neurosci.* 3, 315–322.
- Kong, D., Hu, H.C., Okuma, E., Lee, Y., Lee, H.S., Munemasa, S., Cho, D., Ju, C., Pedoim, L., Rodríguez, B., et al. (2016). L-Met activates arabidopsis GLR Ca<sup>2+</sup> channels upstream of ROS production and regulates stomatal movement. *Cell Rep.* 17, 2553–2561.
- Krissinel, E., and Henrick, K. (2007). Inference of macromolecular assemblies from crystalline state. *J. Mol. Biol.* 372, 774–797.
- Kucukelbir, A., Sigworth, F.J., and Tagare, H.D. (2014). Quantifying the local resolution of cryo-EM density maps. *Nat. Methods* 11, 63–65.
- Lam, H.M., Chiu, J., Hsieh, M.H., Meisel, L., Oliveira, I.C., Shin, M., and Coruzzi, G. (1998). Glutamate-receptor genes in plants. *Nature* 396, 125–126.
- Laskowski, R.A., Jabłońska, J., Pravda, L., Vařeková, R.S., and Thornton, J.M. (2018). PDBsum: Structural summaries of PDB entries. *Protein Sci.* 27, 129–134.
- Lee, C.H., Lü, W., Michel, J.C., Goehring, A., Du, J., Song, X., and Gouaux, E. (2014). NMDA receptor structures reveal subunit arrangement and pore architecture. *Nature* 511, 191–197.
- Lomash, S., Chittori, S., Brown, P., and Mayer, M.L. (2013). Anions mediate ligand binding in Adineta vaga glutamate receptor ion channels. *Structure* 21, 414–425.
- McCoy, A.J. (2007). Solving structures of protein complexes by molecular replacement with Phaser. *Acta Crystallogr. D Biol. Crystallogr.* 63, 32–41.
- Meyerhoff, O., Müller, K., Roelfsema, M.R., Latz, A., Lacombe, B., Hedrich, R., Dietrich, P., and Becker, D. (2005). AtGLR3.4, a glutamate receptor channel-like gene is sensitive to touch and cold. *Planta* 222, 418–427.
- Meyerson, J.R., Chittori, S., Merk, A., Rao, P., Han, T.H., Serpe, M., Mayer, M.L., and Subramaniam, S. (2016). Structural basis of kainate subtype glutamate receptor desensitization. *Nature* 537, 567–571.
- Michard, E., Lima, P.T., Borges, F., Silva, A.C., Portes, M.T., Carvalho, J.E., Gilliam, M., Liu, L.H., Obermeyer, G., and Feijó, J.A. (2011). Glutamate receptor-like genes form Ca<sup>2+</sup> channels in pollen tubes and are regulated by pistil D-serine. *Science* 332, 434–437.
- Michard, E., Simon, A.A., Tavares, B., Wudick, M.M., and Feijó, J.A. (2017). Signaling with ions: the keystone for apical cell growth and morphogenesis in pollen tubes. *Plant Physiol.* 173, 91–111.
- Mou, W., Kao, Y.T., Michard, E., Simon, A.A., Li, D., Wudick, M.M., Lizzio, M.A., Feijó, J.A., and Chang, C. (2020). Ethylene-independent signaling by the ethylene precursor ACC in Arabidopsis ovular pollen tube attraction. *Nat. Commun.* 11, 4082.
- Mousavi, S.A., Chauvin, A., Pascaud, F., Kellenberger, S., and Farmer, E.E. (2013). Glutamate receptor-like genes mediate leaf-to-leaf wound signalling. *Nature* 500, 422–426.
- Nakagawa, T. (2019). Structures of the AMPA receptor in complex with its auxiliary subunit cornichon. *Science* 366, 1259–1263.
- Ortiz-Ramírez, C., Michard, E., Simon, A.A., Damineli, D.S.C., Hernández-Coronado, M., Becker, J.D., and Feijó, J.A. (2017). Glutamate receptor-like channels are essential for chemotaxis and reproduction in mosses. *Nature* 549, 91–95.
- Papaserghi-Scott, M.M., Robertson, M.J., Seven, A.B., Panova, O., Mathiesen, J.M., and Skiniotis, G. (2020). Structures of metabotropic GABA<sub>B</sub> receptor. *Nature* 584, 310–314.
- Park, J., Fu, Z., Frangaj, A., Liu, J., Mosyak, L., Shen, T., Slavkovich, V.N., Ray, K.M., Taura, J., Cao, B., et al. (2020). Structure of human GABA<sub>B</sub> receptor in an inactive state. *Nature* 584, 304–309.
- Petersen, E.F., Goddard, T.D., Huang, C.C., Couch, G.S., Greenblatt, D.M., Meng, E.C., and Ferrin, T.E. (2004). UCSF Chimera—a visualization system for exploratory research and analysis. *J. Comput. Chem.* 25, 1605–1612.
- Punjani, A., Rubinstein, J.L., Fleet, D.J., and Brubaker, M.A. (2017). cryoSPARC: algorithms for rapid unsupervised cryo-EM structure determination. *Nat. Methods* 14, 290–296.
- Qi, Z., Stephens, N.R., and Spalding, E.P. (2006). Calcium entry mediated by GLR3.3, an Arabidopsis glutamate receptor with a broad agonist profile. *Plant Physiol.* 142, 963–971.
- Rappsilber, J., Mann, M., and Ishihama, Y. (2007). Protocol for micro-purification, enrichment, pre-fractionation and storage of peptides for proteomics using StageTips. *Nat. Protoc.* 2, 1896–1906.
- Russo, C.J., and Passmore, L.A. (2014). Electron microscopy: ultrastable gold substrates for electron cryomicroscopy. *Science* 346, 1377–1380.



- Scheres, S.H. (2012). RELION: implementation of a Bayesian approach to cryo-EM structure determination. *J. Struct. Biol.* **180**, 519–530.
- Schwenk, J., Harmel, N., Zolles, G., Bildl, W., Kulik, A., Heimrich, B., Chisaka, O., Jonas, P., Schulte, U., Fakler, B., and Klöcker, N. (2009). Functional proteomics identify cornichon proteins as auxiliary subunits of AMPA receptors. *Science* **323**, 1313–1319.
- Shaye, H., Ishchenko, A., Lam, J.H., Han, G.W., Xue, L., Rondard, P., Pin, J.P., Katritch, V., Gati, C., and Cherezov, V. (2020). Structural basis of the activation of a metabotropic GABA receptor. *Nature* **584**, 298–303.
- Sobolevsky, A.I., Rosconi, M.P., and Gouaux, E. (2009). X-ray structure, symmetry and mechanism of an AMPA-subtype glutamate receptor. *Nature* **462**, 745–756.
- Stephens, N.R., Qi, Z., and Spalding, E.P. (2008). Glutamate receptor subtypes evidenced by differences in desensitization and dependence on the GLR3.3 and GLR3.4 genes. *Plant Physiol.* **146**, 529–538.
- Suloway, C., Pulokas, J., Fellmann, D., Cheng, A., Guerra, F., Quispe, J., Stagg, S., Potter, C.S., and Carragher, B. (2005). Automated molecular microscopy: the new Legimon system. *J. Struct. Biol.* **151**, 41–60.
- Tapken, D., Anshütz, U., Liu, L.H., Huelsken, T., Seeböhm, G., Becker, D., and Hollmann, M. (2013). A plant homolog of animal glutamate receptors is an ion channel gated by multiple hydrophobic amino acids. *Sci. Signal.* **6**, ra47.
- Teardo, E., Carraretto, L., De Bortoli, S., Costa, A., Behera, S., Wagner, R., Lo Schiavo, F., Formentin, E., and Szabo, I. (2015). Alternative splicing-mediated targeting of the Arabidopsis glutamate receptor3.5 to mitochondria affects organelle morphology. *Plant Physiol.* **167**, 216–227.
- Trakhanov, S., Vyas, N.K., Luecke, H., Kristensen, D.M., Ma, J., and Quijcho, F.A. (2005). Ligand-free and -bound structures of the binding protein (LivJ) of the *Escherichia coli* ABC leucine/isoleucine/valine transport system: trajectory and dynamics of the interdomain rotation and ligand specificity. *Biochemistry* **44**, 6597–6608.
- Traynelis, S.F., Wollmuth, L.P., McBain, C.J., Menniti, F.S., Vance, K.M., Ogden, K.K., Hansen, K.B., Yuan, H., Myers, S.J., and Dingledine, R. (2010). Glutamate receptor ion channels: structure, regulation, and function. *Pharmacol. Rev.* **62**, 405–496.
- Twomey, E.C., Yelshanskaya, M.V., Grassucci, R.A., Frank, J., and Sobolevsky, A.I. (2017). Channel opening and gating mechanism in AMPA-subtype glutamate receptors. *Nature* **549**, 60–65.
- Vincill, E.D., Bieck, A.M., and Spalding, E.P. (2012). Ca<sup>2+</sup> conduction by an amino acid-gated ion channel related to glutamate receptors. *Plant Physiol.* **159**, 40–46.
- Vincill, E.D., Clarin, A.E., Molenda, J.N., and Spalding, E.P. (2013). Interacting glutamate receptor-like proteins in phloem regulate lateral root initiation in Arabidopsis. *Plant Cell* **25**, 1304–1313.
- Waterhouse, A., Bertoni, M., Bienert, S., Studer, G., Tauriello, G., Gumienny, R., Heer, F.T., de Beer, T.A.P., Rempfer, C., Bordoli, L., et al. (2018). SWISS-MODEL: homology modelling of protein structures and complexes. *Nucleic Acids Res.* **46** (W1), W296–W303.
- Winn, M.D., Ballard, C.C., Cowtan, K.D., Dodson, E.J., Emsley, P., Evans, P.R., Keegan, R.M., Krissinel, E.B., Leslie, A.G., McCoy, A., et al. (2011). Overview of the CCP4 suite and current developments. *Acta Crystallogr. D Biol. Crystallogr.* **67**, 235–242.
- Wudick, M.M., Michard, E., Oliveira Nunes, C., and Feijó, J.A. (2018a). Comparing plant and animal glutamate receptors: common traits but different fates? *J. Exp. Bot.* **69**, 4151–4163.
- Wudick, M.M., Portes, M.T., Michard, E., Rosas-Santiago, P., Lizzio, M.A., Nunes, C.O., Campos, C., Santa Cruz Daminelli, D., Carvalho, J.C., Lima, P.T., et al. (2018b). CORNICHON sorting and regulation of GLR channels underlie pollen tube Ca. *Science* **360**, 533–536.
- Xiong, Y., Uys, J.D., Tew, K.D., and Townsend, D.M. (2011). S-glutathionylation: from molecular mechanisms to health outcomes. *Antioxid. Redox Signal.* **15**, 233–270.
- Yadav, R., Rimerman, R., Scofield, M.A., and Dravid, S.M. (2011). Mutations in the transmembrane domain M3 generate spontaneously open orphan glutamate  $\delta 1$  receptor. *Brain Res.* **1382**, 1–8.
- Yelshanskaya, M.V., Singh, A.K., Sampson, J.M., Narangoda, C., Kurnikova, M., and Sobolevsky, A.I. (2016). Structural bases of noncompetitive inhibition of AMPA subtype ionotropic glutamate receptors by antiepileptic drugs. *Neuron* **91**, 1305–1315.
- Zhang, K. (2016). Gctf: Real-time CTF determination and correction. *J. Struct. Biol.* **193**, 1–12.
- Zheng, H., Cooper, D.R., Porebski, P.J., Shabalin, I.G., Handing, K.B., and Minor, W. (2017a). CheckMyMetal: a macromolecular metal-binding validation tool. *Acta Crystallogr. D Struct. Biol.* **73**, 223–233.
- Zheng, S.Q., Palovcak, E., Armache, J.P., Verba, K.A., Cheng, Y., and Agard, D.A. (2017b). MotionCor2: anisotropic correction of beam-induced motion for improved cryo-electron microscopy. *Nat. Methods* **14**, 331–332.
- Zivanov, J., Nakane, T., Forsberg, B.O., Kimanius, D., Hagen, W.J., Lindahl, E., and Scheres, S.H. (2018). New tools for automated high-resolution cryo-EM structure determination in RELION-3. *eLife* **7**, e42166.



# STAR★METHODS

## KEY RESOURCES TABLE

REAGENT or RESOURCE	SOURCE	IDENTIFIER
Chemicals, peptides, and recombinant proteins		
Ampicillin	Sigma	Cat# A8351
Kanamycin	Fisher scientific	Cat# BP906-5
Tetracycline	Fisher scientific	Cat# BP912
IPTG	Zymo Research	Cat# I1001-5
Tris	Fisher scientific	Cat# BP152-1
NaCl	Fisher scientific	Cat# BP358-212
L-Glutamate	Sigma	Cat# 49621
L-Methionine	Sigma	Cat# M9625
MgSO <sub>4</sub>	Fluka	Cat# 13143
DNase	Sigma	Cat# DN25-1
PMSF	Acros Organics	Cat# 215740500
2-Mercaptoethanol (BME)	Acros Organics	Cat# 125470100
Ni-Affinity Resin	Takara	Cat# 635660
Imidazole	Acros Organics	Cat# 301870025
Thrombin	Haematologic Technologies	Cat# HCT-0020
Glycerol	Fisher scientific	Cat# BP229-4
MES buffer	Sigma	Cat# M2933
PEG 2000 MME	Fluka	Cat# 81321
Ammonium Sulfate	Fisher scientific	Cat# A702-500
Glycine	Jena Biosciences	Cat# CS-507L
Ammonium acetate	Fisher scientific	Cat# BP326-500
Sodium Acetate	Fisher scientific	Cat# S209-500
CAA	Sigma-Aldrich	Cat# C0267
TCEP	Sigma-Aldrich	Cat# C4706
Urea	Fischer Scientific	Cat# BP169-500
LysC	Wako Chemicals	Cat# 129-02541
Trypsin	Promega	Cat# V5280
Formic Acid	Sigma-Aldrich	Cat# F0507
CDS Empore™ SDB-RPS	Fischer Scientific	Cat# 13-110-023
Dulbecco's Modified Eagle's Medium	GIBCO	Cat# 10566024
Fetal bovine serum	GIBCO	Cat# 16140071
Sf-900 III SFM	GIBCO	Cat# 12658027
Freestyle 293 expression medium	GIBCO	Cat# 12338018
DMEM media	Corning	Cat# 10-013-CV
Sodium butyrate	ACROS Organics	Cat# 263191000
Lipofectamine 2000	Invitrogen	Cat#11668027
Penicillin Streptomycin Fungizone	Cytiva HyClone	Cat# SV3007901
FugeneHD	Promega	Cat# E2311
EGTA	Sigma	Cat# E4378
Bis-Tris Propane	RPI	Cat# B78000100.0
HEPES	Sigma	Cat# H3375-250G
D-mannitol	Fisher	Cat# M120-500
Ca-Gluconate	Sigma	Cat# C8231-100G

(Continued on next page)

**Continued**

REAGENT or RESOURCE	SOURCE	IDENTIFIER
<b>Deposited data</b>		
Coordinates of GLR3.4-S1S2-Glu	This paper	PDB: 7LZ0
Coordinates of GLR3.4-S1S2-Ser	This paper	PDB: 7LZ1
Coordinates of GLR3.4-S1S2-Met	This paper	PDB: 7LZ2
Coordinates of full-length GLR3.4	This paper	PDB: 7LZH
Cryo-EM map of full-length GLR3.4	This paper	EMD-23606
Coordinates of ATD and micelle subtracted GLR3.4	This paper	PDB: 7LZI
Cryo-EM map of ATD and micelle subtracted GLR3.4	This paper	EMD-23607
MS raw files and output tables	This paper	PXD024563
S1S2 of AtGLR3.2	<a href="#">Gangwar et al., 2021</a>	PDB: 6VE8
S1S2 of AtGLR3.3	<a href="#">Alfieri et al., 2020</a>	PDB: 6R8A
<b>Experimental models: cell lines</b>		
HEK293S GnT1 <sup>-</sup>	ATCC	Cat#CRL-3022
Sf9	GIBCO	Cat#12659017
COS-7	ATTC	CRL-1651
<i>E. coli</i> Origami B (DE3)	Novagen	Cat# 70837
<b>Experimental models: organisms/strains</b>		
<i>Agrobacterium tumefaciens</i> strain GV3101	GoldBio	CC-207-A
<i>Arabidopsis thaliana</i> Col-0 ecotype	ABRC	CS70000
<i>Arabidopsis thaliana</i> tDNA mutant Atglr3.4-1	ABRC	Salk_201768C
<i>Arabidopsis thaliana</i> tDNA mutant Atglr3.4-2	ABRC	Salk_079842
<b>Recombinant DNA</b>		
pEF1-YC3.6	Dr. Jörg Kudla lab, Univ. Muenster, Germany	N/A
pcDNA3	Invitrogen	N/A
pcDNA3-AtGLR3.4	This paper	N/A
pcDNA3-AtGLR3.4(C205A)	This paper	N/A
pCI	Promega	N/A
pCI-AtCNIH1	<a href="#">Wudick et al., 2018b</a>	N/A
pCI-AtCNIH4	<a href="#">Wudick et al., 2018b</a>	N/A
pDONR201	Invitrogen	N/A
pDONR201-AtGLR3.4(gDNA)	This paper	N/A
pDS_EF1-XB-glrl3.4-CFP	Dr. Edgar Spalding, University of Wisconsin, Madison	N/A
pIRES-CD8	Clontech	N/A
pK7FWG2-Lat52	<a href="#">Wudick et al., 2018b</a>	N/A
pSoup	Hellens, R.P.	GenBank: EU048870.1
<b>Oligonucleotides</b>		
AtGLR3.4 amplification primer: 5'- gtcgact ccgccaccatgggatttttggtgatgataagag -3'	This paper	N/A
AtGLR3.4 amplification primer: 5'- cgcca ccagagtaatttcgccatgttgattgtga -3'	This paper	N/A
B193 5' - CACTATAGGGCGAATTGGGTAC CGTCGACATAC TCGACTCAGAAGG - 3'	This paper	N/A

(Continued on next page)

# Continued

REAGENT or RESOURCE	SOURCE	IDENTIFIER
B204 5' – AGGGAACAAAAGCTGGGG AATTCAGGTCACCTG GATTTTGTTT TAGG – 3'	This paper	N/A
B278 5' – CGTAATACGACTCACTATAGGGC GAATTGGGT ACC GTCGACGAGT CAGTAATAAACG – 3'	This paper	N/A
B279 5' – TCGTTCAGCTTTTTTGT ACAAACTTGTGATATCA CTAGTCT GTTAATCAGAAAACTCAG – 3'	This paper	N/A
B394 5' – GGGGACAAGTTTGTACAAAAAAGC AGGCTTCA TGGGATTTTGGTGATGA TAA – 3'	This paper	N/A
B395 5' – GGGGACCACTTTGTACAAG AAAGCTGGGTCAG TAATTCGCCATGT TGTGAT – 3'	This paper	N/A
B579 5' – TGCAGATATCCATCACACT GGCGGCCGCATGG GATTTTGGT GATGATAAGAG – 3'	This paper	N/A
B580 5' – ATAGGGCCCTCTAGATGC ATGCTCGAGTTAAGT AATTCGCC ATGTTGTGATTGT – 3'	This paper	N/A
C328 5' – CCCGTTCTGCCAGCCT CATCATCAACGAATA – 3'	This paper	N/A
C329 5' – CGTTGATGATGAGGCTGGCAG GAACGGGAT ATC – 3'	This paper	N/A

# Software and algorithms

Leginon	Suloway et al., 2005	<a href="https://emg.nysbc.org/redmine/projects/legion/wiki/Leginon_Homepage">https://emg.nysbc.org/redmine/projects/legion/wiki/Leginon_Homepage</a>
gCTF	Zhang, 2016	<a href="https://www.mrc-lmb.cam.ac.uk/kzhang/Gctf/">https://www.mrc-lmb.cam.ac.uk/kzhang/Gctf/</a>
Motioncor2	Zheng et al., 2017b	<a href="https://msg.ucsf.edu/em/software/motioncor2.html">https://msg.ucsf.edu/em/software/motioncor2.html</a>
RELION 2.0	Kimanius et al., 2016	<a href="https://www2.mrc-lmb.cam.ac.uk/relion/">https://www2.mrc-lmb.cam.ac.uk/relion/</a>
UCSF Chimera	Pettersen et al., 2004	<a href="https://www.cgl.ucsf.edu/chimera/">https://www.cgl.ucsf.edu/chimera/</a>
Pymol (Schrödinger)	DeLano, 2002	<a href="https://www.pymol.org/2/">https://www.pymol.org/2/</a>
PHENIX	Adams et al., 2010	<a href="https://phenix-online.org/">https://phenix-online.org/</a>
CCP4	Winn et al., 2011	<a href="https://www.ccp4.ac.uk/">https://www.ccp4.ac.uk/</a>
COOT	Emsley and Cowtan, 2004	<a href="https://www2.mrc-lmb.cam.ac.uk/Personal/pemsley/coot">https://www2.mrc-lmb.cam.ac.uk/Personal/pemsley/coot</a>
XDS	Kabsch, 2010	<a href="https://xds.mr.mpg.de/">https://xds.mr.mpg.de/</a>
Swiss-Model	Waterhouse et al., 2018	<a href="https://swissmodel.expasy.org/">https://swissmodel.expasy.org/</a>
PDBsum	Laskowski et al., 2018	<a href="https://www.ebi.ac.uk/thornton-srv/databases/cgi-bin/pdbsum/GetPage.pl?pdbcode=index.html">https://www.ebi.ac.uk/thornton-srv/databases/cgi-bin/pdbsum/GetPage.pl?pdbcode=index.html</a>
SigmaPlot 11.0	Systat Software Inc.	Systatsoftware.com
Origin 2015 Sr2	OriginLab Corporation	<a href="https://www.originlab.com/doc/">https://www.originlab.com/doc/</a>
pFind	Chi et al., 2018	<a href="http://pfind.ict.ac.cn/">http://pfind.ict.ac.cn/</a>
PDBePISA	Krissinel and Henrick, 2007	<a href="https://www.ebi.ac.uk/pdbe/prot_int/pistart.html">https://www.ebi.ac.uk/pdbe/prot_int/pistart.html</a>
CheckMyMetal	Zheng et al., 2017a	<a href="https://cmm.minorlab.org/">https://cmm.minorlab.org/</a>

(Continued on next page)

**Continued**

REAGENT or RESOURCE	SOURCE	IDENTIFIER
Other		
DeltaVision Elite Deconvolution/TIRF microscope system	GE Healthcare	Part # 53-851206-001
CF-1.2/1.3-2Au 200 mesh holey carbon grids	Protochips	Cat#CF-1.2/1.3-2Au
Gold wire	Ted Pella, Inc.	Cat#21-10
Ion Exchange Hi-Trap Q HP column	GE Healthcare	Cat# 17-1154-01
Size Exclusion Superose 10/300 column	GE Healthcare	Cat# 17-5172-01

**RESOURCE AVAILABILITY****Lead contact**

Further information and requests for the resources and reagents should be directed to and will be fulfilled by the lead contact, Alexander Sobolevsky ([as4005@cumc.columbia.edu](mailto:as4005@cumc.columbia.edu)).

**Materials availability**

New materials listed in key resources are available upon request.

**Data and code availability**

Cryo-EM map for full-length GLR3.4 and after ATD and micelle subtraction have been deposited to the EMDB with the accession codes EMD-23606 and EMD-23607, respectively. Coordinates for full-length GLR3.4 and after ATD and micelle subtraction have been deposited to the PDB with the accession codes 7LZH and 7LZI, respectively. Coordinates and structure factors for GLR3.4-S1S2<sub>Glu</sub>, GLR3.4-S1S2<sub>Ser</sub> and GLR3.4-S1S2<sub>Met</sub> structures have been deposited to the PDB with the accession codes 7LZ0, 7LZ1 and 7LZ2, respectively. Raw files and full output tables for mass spectrometry results are available through PRIDE repository with identifier PXD024563 (reviewer access username: [reviewer\\_pxd024563@ebi.ac.uk](mailto:reviewer_pxd024563@ebi.ac.uk), password: UDehuNMe). This study did not generate new code.

**EXPERIMENTAL MODEL AND SUBJECT DETAILS**

Expression of the full-length GLR3.4 protein was performed in HEK293S GnT1<sup>-</sup> cells (ATCC) that were cultured in the Freestyle 293 expression medium (GIBCO) at 37°C and 5% CO<sub>2</sub>. Baculovirus for infecting HEK293S GnT1<sup>-</sup> cells was produced in Sf9 cells (GIBCO) that were cultured in the Sf-900 III SFM media (GIBCO) at 27°C. S1S2 protein expression was performed in *Escherichia coli* Origami B (DE3) cells (Novagen). Cells were cultured in LB media at 37°C until OD<sub>600</sub> reached the value of 1.0-1.2, then cooled down to 20°C, induced with 250 μM IPTG and incubated for another 20 hours at 20°C. COS-7 cells for calcium imaging experiments were maintained at 37°C and 5% CO<sub>2</sub> in Dulbecco's Modified Eagle's Medium, supplemented with 5% fetal bovine serum and 1% penicillin/streptomycin.

**METHOD DETAILS****Constructs**

The full-length *Arabidopsis thaliana* GLR3.4 (residues 1-959; Uniprot Q8GXJ4, NCBI NP\_001030971.1) was introduced into a pEG BacMam vector for baculovirus-based protein expression in mammalian cells (Goehring et al., 2014), with the C-terminal thrombin cleavage site (LVPRGS), followed by eGFP and streptavidin affinity tag (WSHPQFEK). The GLR3.4-S1S2 construct for expression of the isolated LBD was made by introducing S1 (residues 492-601) and S2 (residues 709-842) fragments of GLR3.4 connected by the glycine-threonine (GT) linker into a pET22b vector (Novagen), with the N-terminal 8xHis affinity tag followed by the thrombin cleavage site. The boundaries of S1 and S2 were determined based on sequence alignment of GLR3.4 with GluA2 and GLR3.2 LBDs (Armstrong and Gouaux, 2000; Armstrong et al., 1998; Sobolevsky et al., 2009).

For expression in COS-7 cells, full-length GLR3.4 cDNA was amplified by PCR from vector pDS\_EF1-XB-glr3.4-CFP (from Spalding's lab) with the primer pair B579/B580. The resulting PCR product was cloned into NotI/XhoI digested pcDNA3 via GIA (Gibson Isothermal Assembly) to yield pcDNA3-atglr3.4. In order to generate the mutant pcDNA3-atglr3.4(C205A), two PCRs were performed using pcDNA3-atglr3.4 as template with the primer pairs B579/C328 and C329/B580. The resulting PCR products were cloned into NotI/XhoI digested pcDNA3 via GIA.

For expression in *Arabidopsis* pollen, a custom gateway destination vector, pGreenII-OLE1p::OLE1::eGFP atUBQ10p::Gateway::eGFP, was generated. The pLat52 Gateway cassette with C-terminal eGFP was PCR amplified with the primer pair B193/B204

using pK7FWG2-Lat52 (Wudick et al., 2018b) as a template and the resulting product was digested with SpeI and purified. PCR using *Arabidopsis* Col-0 gDNA was performed with the primer pair B278/B279 to amplify the atUBQ10 (At4g05320) promoter. Both PCR products were then cloned into KpnI/EcoRI digested pGreenII-OLE1p::OLE1::eGFP Lat52p::Gateway (Wudick et al., 2018b) via GIA. The genomic coding sequence of atglr3.4 was amplified with primer pair B394/B395 via PCR using *Arabidopsis* Col-0 gDNA as a template. The resulting PCR product was then used in a Gateway BP reaction with pDONR201 to create the donor clone, pDONR201-atglr3.4. A Gateway LR reaction was performed with donor clone pDONR201-atglr3.4(gDNA) and destination clone pGreenII-OLE1p::OLE1::eGFP atUBQ10p::Gateway::eGFP to generate the expression clone pGreenII-OLE1p::OLE1::eGFP atUBQ10p::atglr3.4(gDNA)::eGFP.

### Plant transformation

Expression construct pGreenII-OLE1p::OLE1::eGFP atUBQ10p::atglr3.4(gDNA)::eGFP was transformed into *Agrobacterium* strain GV3101 harboring the pSoup helper plasmid via electroporation. *Arabidopsis thaliana* Col-0 plants were then transformed via the floral dip method according to standard protocols (Wudick et al., 2018b).

### GLR3.4-S1S2 expression and purification

GLR3.4-S1S2 was transformed into *Escherichia coli* Origami B (DE3) cells and grown in LB media supplemented with 100  $\mu$ g/ml ampicillin, 15  $\mu$ g/ml kanamycin and 12.5  $\mu$ g/ml tetracycline. The freshly inoculated culture was grown at 37°C until OD<sub>600</sub> reached the value of 0.8–1.2. Then cells were cooled down to 20°C, induced with 250  $\mu$ M isopropyl  $\beta$ -D-1-thiogalactopyranoside (IPTG) and incubated in the orbital shaker for 20 hours at 20°C. The cells were harvested by centrifugation at 5,000 rpm for 15 min at 4°C and washed with the buffer containing 150 mM NaCl and 20 mM Tris pH 8.0.

For GLR3.4-S1S2<sub>Glu</sub>, all buffers in the following purification steps were supplemented with 1 mM L-glutamate. First, the cells were resuspended in the lysis buffer containing 200 mM NaCl, 20 mM Tris pH 7.5, 1 mM  $\beta$ -mercaptoethanol ( $\beta$ ME), 1 mM phenylmethylsulfonyl fluoride (PMSF), 200  $\mu$ g/ml lysozyme, 5% glycerol and DNase and disrupted by sonication. After the lysate was centrifuged at 40,000 rpm using the Ti45 rotor for 1 hour at 4°C, the supernatant was mixed with His60 Ni superflow resin (Takara) and rotated for 2 hours at 4°C. The protein-bound resin was washed with the buffer containing 200 mM NaCl, 20 mM Tris pH 7.5, 1 mM  $\beta$ ME and 20 mM imidazole and the protein was eluted using the same buffer but containing 200 mM instead of 20 mM imidazole. The protein was 3x diluted in the buffer containing 150 mM NaCl, 20 mM Tris pH 7.5, 1 mM  $\beta$ ME and 5% glycerol and subjected to thrombin digestion (1:500 w/w) for 1.5 hour at 22°C. The protein was further purified using ion-exchange Hi-Trap Sepharose-SP (GE Healthcare).

For GLR3.4-S1S2<sub>Met</sub> and GLR3.4-S1S2<sub>Ser</sub>, protein purification was similar, except 1 mM L-glutamate was omitted from all purification buffers. In addition, instead of ion exchange chromatography, we used size-exclusion chromatography with the Superdex 16/60 column (GE Healthcare) and the buffer containing 150 mM NaCl, 20 mM Tris pH 7.5, 1 mM  $\beta$ ME, and 5% glycerol. The purified protein was evaluated using SDS-PAGE and FSEC (Superose 10/30 column, GE Healthcare) and supplemented with the corresponding ligand (Met) before subjecting it to crystallization.

### GLR3.4-S1S2 crystallization and structure determination

Purified GLR3.4-S1S2<sub>Glu</sub> protein concentrated to  $\sim$ 8–10 mg/ml was first subjected to crystallization screening using Mosquito robot (TTP Labtech) in sitting drop vapor diffusion 96-well crystallization plates at 4°C. After two weeks, small octagonal crystals appeared in the condition consisting of 2 M ammonium sulfate and 0.1 M Sodium Acetate pH 4.6. For GLR3.4-S1S2<sub>Met</sub>, 1 mM methionine was added to the purified protein and the ligand-protein mixture was incubated for 30–40 min on ice before crystallization screening with Mosquito. By not adding any ligands to the protein we intended to solve the S1S2 structure in the apo state, but instead ended up solving the GLR3.4-S1S2<sub>Ser</sub> structure with serine of an apparent endogenous origin. Small octagon-shaped crystals of GLR3.4-S1S2<sub>Met</sub> and GLR3.4-S1S2<sub>Ser</sub> grew in 2 M ammonium sulfate at 4°C. All crystals were cryoprotected using crystal growth buffers supplemented with 25% glycerol and flash-frozen in liquid nitrogen. Crystal diffraction data were collected at the beamline 24-ID-C of the Advanced Photon Source (APS) and processed using XDS (Kabsch, 2010) and Aimless as a part of the CCP4 suite (Winn et al., 2011).

The structure of GLR3.4-S1S2<sub>Glu</sub> was solved by molecular replacement using Phaser (McCoy, 2007) and GLR3.2-S1S2<sub>Gly</sub> (PDB 6VEA) as a search probe. The model was refined by alternating cycles of building in COOT (Emsley and Cowtan, 2004) and automatic refinement in Phenix or Refmac (Adams et al., 2010). The structures of GLR3.4-S1S2<sub>Met</sub> and GLR3.4-S1S2<sub>Ser</sub> were solved by molecular replacement using the GLR3.4-S1S2<sub>Glu</sub> structure as a search probe. Water molecules were added manually in Coot. Analysis of possible inclusion of metal ions in the S1S2 crystal structures was performed using the CheckMyMetal validation tool (<https://cmm.minorlab.org/>) (Zheng et al., 2017a). All structural figures were prepared in Pymol (DeLano, 2002).

### Measurements of ligand binding to GLR3.4-S1S2 using microscale thermophoresis

GLR3.4-S1S2 was purified as described above, except the N-terminal 8xHis tag was not cleaved by thrombin and remained with the protein. The unlabeled GLR3.4-S1S2 protein was subjected to microscale thermophoresis (MST) in the Monolith NT Label free (Nano Temper Technologies), which detected its intrinsic tryptophan fluorescence. The 1.5- $\mu$ M purified protein stock solution was made using the interaction buffer containing 150 mM NaCl and 20 mM Tris pH 7.5. The stock solutions of the ligands L-glutamate,

L-methionine, and L-serine were prepared at the concentration of 16 mM and serially diluted using the same buffer. For interaction measurements, the protein and ligand solutions were mixed at the 1:1 (v/v) ratio, with the protein concentration kept constant and the ligand concentration varied. The interaction mix was incubated at room temperature for 5–10 min and subjected to thermophoresis measurements in 16 capillaries with medium MST and 20% LED power at 24°C. For each ligand, the experiment was repeated 3–4 times and the data was averaged, normalized and fitted with the logistic equation using Origin 2015 software (OriginLab Corporation).

### Full-length GLR3.4 expression and purification

The GLR3.4 bacmid and baculovirus were made by using the standard methods (Goehring et al., 2014). The P2 virus was produced in Sf9 cells (GIBCO, 12659017) and added to HEK293S GnTI<sup>−</sup> cells (ATCC, CRL-3022) incubated at 37°C and 5% CO<sub>2</sub>. Cells were supplemented with 10 mM sodium butyrate 12 hours post infection and the temperature was changed to 30°C. Cells were harvested 72 hours post infection using low-speed centrifugation (5,500 g, 10 min), washed using 1X PBS pH 8.0 and pelleted again (5,500 g, 15 min). The pellet was resuspended in 50 mL per 1 L of the initial cell culture lysis buffer consisting of 150 mM NaCl, 20 mM Tris pH 8.0, 1 mM βME, 0.8 μM aprotinin, 2 μg/ml leupeptin, 2 μM pepstatin A and 1 mM PMSF and lysed by sonication. The lysate was centrifuged (9,900 g, 15 min) to remove cell debris and the supernatant was subjected to ultracentrifugation (186,000 g, 40 min) to pellet cell membranes. The membranes were mechanically homogenized and solubilized for 2 hours in the buffer containing 150 mM NaCl, 20 mM Tris-HCl pH 8.0, 1 mM βME and 1% digitonin (Cayman Chemical Company, 14952). Insoluble material was removed by ultracentrifugation (186,000 g, 40 min), while the supernatant was added to the pre-equilibrated Streptavidin-linked resin (2 mL resin per 1 L of the initial cell culture) and the mixture was rotated for 10–14 hours at 4°C. The protein-bound resin was washed with 25 mL of the buffer containing 150 mM NaCl, 20 mM Tris-HCl pH 8.0 and 0.05% digitonin and the protein was eluted using the same buffer supplemented with 2.5 mM D-desthiobiotin. The eluted protein was subjected to thrombin digestion (1:300 w/w) at 22°C for 1 hour. The digest reaction was injected into Superose 6 10/30 size-exclusion column (GE Healthcare) equilibrated with the buffer containing 150 mM NaCl, 20 mM Tris-HCl pH 8.0, and 0.05% digitonin. The tetrameric GLR3.4 peak fractions were pooled, concentrated to ~2.5 mg/ml and used for cryo-EM sample preparation. All the steps, unless otherwise noted, were performed at 4°C.

### Cryo-EM sample preparation and data collection

Au/Au grids were prepared as described in the literature (Russo and Passmore, 2014). Briefly, grids were prepared by first coating C-flat (Protochips, Inc., Morrisville, NC) CF-1.2/1.3-2Au 200 mesh holey carbon grids with ~50 nm of gold using an Edward Auto 306 evaporator. Subsequently, an Ar/O<sub>2</sub> plasma treatment (6 minutes, 50 W, 35.0 sccm Ar, 11.5 sccm O<sub>2</sub>) was used to remove the carbon with a Gatan Solarus (model 950) Advanced Plasma Cleaning System. The grids were again plasma treated (H<sub>2</sub>/O<sub>2</sub>, 20 s, 10 W, 6.4 sccm H<sub>2</sub>, 27.5 sccm O<sub>2</sub>) prior to sample application in order to make their surfaces hydrophilic. Purified GLR3.4 protein was mixed with 1 mM L-Glutamate and incubated on ice for ~30 min before grid preparation. A Vitrobot Mark IV (FEI) was used to plunge-freeze the grids after the application of 3 μl protein solution with 100% humidity at 4°C, a blot time of 3 s, blot force set to 3, and a wait time of 20 s. The grids were clipped and loaded into a 300 kV Titan Krios microscope equipped with Gatan K3 direct electron detection camera. 11,854 micrographs were collected in counting mode with a pixel size of 0.83 Å (~105,000x magnification) across a defocus range of −1.0 μm to −2 μm. The total dose of 58 e<sup>−</sup> Å<sup>−2</sup> was attained by using a dose rate of ~16.0 e<sup>−</sup> pixel<sup>−1</sup> s<sup>−1</sup> across 50 frames for 2.5 s total exposure time.

### Image processing

The total of 11,854 micrographs were collected as two datasets, dataset 1 (6,119 micrographs) and dataset 2 (5,735 micrographs) and initially processed in Relion 3.1 (Zivanov et al., 2018). Frame alignment was done using MotionCor2 (Zheng et al., 2017b). CTF estimation was performed using Gctf (Zhang, 2016) on non-dose-weighted micrographs while subsequent data processing was done on dose-weighted micrographs. For each dataset, ~3,000 particles were manually selected to generate 2D classes that were used as templates to autopick 1,044,465 particles from dataset 1 and 1,116,729 particles from dataset 2. The particle images were 4x4 binned to a pixel size of 3.32 Å/pixel and subjected to 3D classification, each dataset into ten classes. A density map was generated in Chimera from the crystal structure of GluA2 (PDB ID: 3KG2), low-pass filtered to 40 Å, and used as an initial reference. The best 3D classes contained 190,076 particles for dataset 1 and 145,948 particles for dataset 2, which were further unbinned to a pixel size of 0.83 Å/pixel and re-extracted. These particles were cleaned up by 3D classification and subsequently subjected to Bayesian polishing and CTF refinement. After refinement and postprocessing, the resulting 109,759 particles for dataset 1 and 117,856 particles for dataset 2 produced 3D maps at the resolution of 5.0 and 4.2 Å, respectively. Then the particles for datasets 1 and 2 were joined and subjected to micelle subtraction and multiple rounds of 3D classification to reduce particle heterogeneity. After additional beam tilt CTF refinement, followed by regular refinement and postprocessing, the remaining 118,592 cleaned up particles produced a map at the resolution of 3.73 Å. These particles were imported into cryoSPARC (Punjani et al., 2017) and subjected to several rounds of 2D clean up, homogeneous and non-uniform refinement with C2 symmetry, resulting in a final map at 3.57 Å resolution (110,630 particles). Focused classification and focused refinement were performed to improve density in the TMD region (Figure S3D). The total of 227,615 combined particles from the two datasets were particle subtracted in Relion 3.1 by providing a soft mask around the LBD-TMD region. The subtracted particles were refined, cleaned by several rounds of 2D classification in Relion 3.1 and refined again with a soft mask to yield a final map at 4.39 Å resolution (174,044 particles). The overall resolution was estimated using the Fourier shell correlation (FSC = 0.143) criterion on masking-effect-corrected FSC curves calculated between two independent half-maps.



(Chen et al., 2013; Scheres, 2012). The local resolutions were estimated with unfiltered half-maps using ResMap (Kucukelbir et al., 2014) and EM density maps were visualized using UCSF Chimera (Pettersen et al., 2004).

### Model building

For model building of the LBD, the GLR3.4-S1S2<sub>Glu</sub> crystal structure was used as a guide. To guide model building of the ATD and TMD, homology models of these domains were created using Swiss-Model (Waterhouse et al., 2018) and the GluA2 structure (PDB ID: 3KG2) as a template. The remaining parts of GLR3.4 were built *de novo* using cryo-EM density as a guide. The resulting model was real space refined in Phenix (Afonine et al., 2012) and visualized using Chimera (Pettersen et al., 2004) or Pymol (DeLano, 2002). The analysis of intersubunit interfaces as well as surface area calculations were performed using the PDBEPIA web service ([https://www.ebi.ac.uk/pdbe/prot\\_int/pistart.html](https://www.ebi.ac.uk/pdbe/prot_int/pistart.html)) (Krissinel and Henrick, 2007).

### Cysteine crosslinking

Cysteine substitutions were introduced using conventional PCR-based methods. Constructs were verified by sequencing over the entire length of the GLR3.4 coding region. Wild-type and cysteine-substituted GLR3.4 proteins were expressed and purified as described above, except 1% lauryl maltose neopentyl glycol (LMNG) detergent (Anatrace) was used instead of digitonin for protein extraction. Binding of protein to streptavidin-linked resin lasted for 1 hour. Instead of 0.05% of digitonin, 0.1 mM LMNG was in the buffers that were used to wash the protein-bound resin, elute the protein, and for size-exclusion chromatography. For crosslinking, ~2.5 μg of protein was subjected to denaturing conditions by addition of SDS sample buffer in the absence (non-reducing condition) or presence (reducing condition) of 600 mM dithiothreitol (DTT). The protein samples were then run on a 4%–15% gradient SDS-PAGE gel and protein bands were visualized by AquaStain Protein Gel Stain (Bulldog Bio). The oligomeric state of wild-type and cysteine-substituted GLR3.4 was assessed by subjecting ~2 μg of protein to FSEC.

### COS-7 cells transfection and Ca<sup>2+</sup> imaging

Protocols for COS-7 cells transfection and Ca<sup>2+</sup> imaging were adapted from the previous studies (Ortiz-Ramírez et al., 2017). COS-7 cells (Sigma-Aldrich) were maintained at 37°C and 5% CO<sub>2</sub> in Dulbecco's Modified Eagle's Medium, supplemented with 5% fetal bovine serum and 1% penicillin/streptomycin (GIBCO), and transfected at low passage (p < 7). Cells were plated at a density at 50% confluence in 35-mm diameter dishes and transfected using EugeneHD (Promega) as specified by the supplier. Cells were co-transfected with pCI-AtCNIH4 (0.2 μg), pCI-AtCNIH1 (0.2 μg), pcDNA3-AtGLR3.4 (0.8 μg) and pEF1-YC3.6 (0.5 μg). The co-transfection with pCI-AtCNIH4 and pCI-AtCNIH1 was previously shown to enhance functional expression and activity of GLRs (Wudick et al., 2018b). In experiments illustrated in Figure S2E, pCI-AtCNIH4 was increased to 0.4 μg (red circles) and replaced by empty pCI plasmid in cells expressing AtGLR3.4 alone (black circles). Cells were used for imaging 38 to 41 hours after transfection. They were washed in a Ca<sup>2+</sup>-free solution (1 mM EGTA, 10 mM Bis-Tris propane buffered to pH 7.3 with HEPES and set to 350 mOsmol with D-mannitol). Cells were imaged in the Ca<sup>2+</sup>-free solution for 1.5 min before the addition of Ca<sup>2+</sup> to a final concentration of 14.5 mM (using Ca-Gluconate). The ligands (Glu, Asn, or Gly; 0.5 or 1.0 mM) were added at the beginning, before Ca<sup>2+</sup> was introduced. L-glutamate, Glycine and L-Asparagine were prepared as 100 mM stock solutions (Sigma-Aldrich, St. Louis, MO, USA). L-Glu stock solution was adjusted to pH 7.0 with Bis-tris propane. Time-lapse acquisition was performed with a sampling interval of 30 s. 8 to 12 cells were imaged in each dish using the stage position recording tool of the microscope system. Imaging was performed at room temperature using a DeltaVision Elite Deconvolution/TIRF microscope system (Olympus inverted IX-71) under a 60X lens (1.2NA UPLSAPO water /WD 0.28 mm). A xenon lamp from the DeltaVision system was used with a CFP excitation filter (438–424 nm). Two simultaneous emission records were captured: YFP emission (548–522 nm) and CFP emission (475–424 nm). To minimize bleaching, the laser was set to 2%. YFP and CFP imaging were recorded with 0.6 s exposure time. Images were processed using ImageJ. Ratios were obtained after background subtraction and signal clipping using the “Ratio-plus” plug-in for ImageJ. The signal of each channel was averaged in a circle in the middle of the cell (with 100–200 pixel diameter, depending on the size of the cell). The YFP/CFP ratio was obtained by dividing the emission recorded for YFP (548–522 nm) by the one recorded for CFP (475–424 nm). No significant bleaching or ratio drift was observed in our experimental conditions.

### Patch-clamp recordings

For patch-clamp recordings, COS-7 cells were maintained and transfected according to the protocol described in the COS-7 cells transfection and Ca<sup>2+</sup> imaging section. Cells were co-transfected with pCI-AtCNIH4 (0.2 μg), pCI-AtCNIH1 (0.2 μg), pcDNA3-AtGLR3.4 (0.4 μg) and pIRES-CD8 (0.05 μg), the latter to select transfected cells with the help of anti-CD8 antibody-coated beads (Dynabeads, Thermo Fisher Scientific, USA). In experiments described in Figure S2B, the quantity of pcDNA3-AtGLR3.4 was increased to 0.8 μg. Patch-clamp was performed in the whole-cell configuration, 39 to 45 hours after transfection. Pipettes were pulled using a P97 puller (Sutter Instrument, Novato, CA, USA). Their resistance was 3–5 MΩ in the bath solution. Whole-cell currents were recorded at the sampling frequency of 2–4 kHz and filtered at 1–2 kHz using an Axopatch 200A amplifier with an Axon 1200 DigiData analog-to-digital converter and pCLAMP software (Molecular Devices, Sunnyvale, CA, USA). The pipette solution contained 150 mM Na-Gluconate, 3 mM MgCl<sub>2</sub>, 4 mM HCl, 5 mM EGTA, and 10 mM Bis-tris-propane pH 7.2 (adjusted using HEPES). The bath solution contained 20 mM Ca-Gluconate, 10 mM Na-Gluconate and 10 mM Bis-tris propane pH 6.5 (adjusted using MES). Solutions were adjusted to 350 mOsmol with D-mannitol. L-glutamate, Glycine and L-Asparagine were prepared as 100 mM stock solutions (Sigma-Aldrich, St. Louis, MO, USA). L-Glu stock solution was adjusted to pH 7.0 with Bis-tris propane. In experiments illustrated in

**Figure S2C**, washout was performed by gravity perfusion at the rate of 1 mL per minute. For the experiments with GSH, the pipette solution contained: 150 mM NaCl, 3 mM MgCl<sub>2</sub>, 10 mM BTP, 5 mM EGTA, and 100 nM free Ca<sup>2+</sup>. pH was adjusted to 7.3 with HEPES and osmolality to 350 mOsmol with D-mannitol. Bathing solution contained: 15 mM CaCl<sub>2</sub> and 10 mM BTP. pH was adjusted to 7.3 with HEPES and osmolality to 350 mOsmol with D-mannitol. The voltage protocol during current acquisition followed the sequence: (1) cells were clamped at a holding potential of 0 mV, and (2) 1.5-s voltage pulses were applied in the range of –100 to +60 mV with the 20-mV steps. The holding potential was returned to 0 mV for 1.1 s between the pulses.

### Extracellular calcium influx measurements

Extracellular Ca<sup>2+</sup> influx was measured at the tip of the pollen tubes using the ion-selective vibrating probe with simultaneous growth rate monitoring, as described previously (Wudick et al., 2018b). Measurements were performed in two *Arabidopsis thaliana* independent T-DNA insertion lines, *Atglr3.4-1* (SALK\_201768) and *Atglr3.4-2* (SALK\_079842), while *Col-0* was used as wild-type. Plants were grown under short-day conditions (12 hours of light at 22°C and 12 hours of dark at 18°C, with an irradiance of ca. 100 μmol m<sup>-2</sup>sec<sup>-1</sup>). *Arabidopsis* pollen grains were collected from fresh flowers and then germinated in liquid medium containing 500 μM KCl, 500 μM CaCl<sub>2</sub>, 125 μM MgSO<sub>4</sub>, 0.005% H<sub>3</sub>BO<sub>3</sub>, 125 μM HEPES pH 7.5 and 16% sucrose. Pollen grains were incubated at 21.5°C for at least 3 hours. Growing pollen tubes longer than 150 μm were selected for flux and growth rate measurements.

### Confocal microscopy of *Arabidopsis* pollen

Wild-type *Col-0* pollen stably expressing UBQ10:GLR3.4-GFP was mounted in germination medium (500 μM KCl, 500 μM CaCl<sub>2</sub>, 125 μM MgSO<sub>4</sub>, 0.005% H<sub>3</sub>BO<sub>3</sub>, 125 μM HEPES pH 7.5 and 16% sucrose) and visualized using the 63 × /1.4 plan- apochromat objective of a Zeiss LSM700 laser scanning confocal microscope using the 488 nm laser for excitation (emission recorded at 500–530 nm). Image analysis was performed using ImageJ (<https://rsbweb.nih.gov/ij/>).

### Liquid chromatography and mass spectrometry

Purified full-length GLR3.4 was alkylated with 40 mM 2-chloroacetamide (CAA, Sigma-Aldrich) followed by the addition of Urea (Sigma-Aldrich) to a final concentration of 8 M. For reducing conditions, tris(2-carboxyethyl)phosphine hydrochloride (TCEP, Sigma-Aldrich) was added to a final concentration of 10 mM. The resulting solution was heated to 37°C for 1 h. Next, the samples were diluted with 50 mM ammonium bicarbonate (Sigma-Aldrich) and digested by a combination of LysC (Wako) and Trypsin (Promega). The final peptide mixtures were acidified with formic acid (Sigma-Aldrich) to a final concentration of 1% and then desalted with CDS Empore<sup>TM</sup> SDB-RPS (Fischer Scientific) in house-packed stage-tips (Rappsilber et al., 2007).

Desalted peptides were injected into an EASY-Spray PepMap RSLC C18 50 cm x 75 μm column (Thermo Scientific), which was coupled to the Orbitrap Fusion Tribrid mass spectrometer (Thermo Scientific). Peptides were eluted at the flow rate of 250 nL/min with a non-linear 120-min gradient of 5%–30% buffer B consisted of 0.1% (v/v) formic acid and 100% acetonitrile. The column temperature was maintained at 50°C throughout the entire experiment. Thermo Scientific Orbitrap Fusion Tribrid mass spectrometer was used for peptide MS/MS analysis. Survey scans of peptide precursors were performed from 350 to 1500 m/z at 120K FWHM resolution (at 200 m/z) with a 2 × 10<sup>5</sup> ion count target and a maximum injection time of 60 ms. The instrument was set to run in top speed mode with 3 s cycles for the survey and the MS/MS scans. After the survey scan, tandem MS was performed on the most abundant precursors exhibiting a charge state from 2 to 6 of greater than 2 × 10<sup>5</sup> intensity by isolating them in the quadrupole at 1.6 Th. HCD fragmentation was applied with 30% collision energy and the resulting fragments were detected using the auto: m/z Normal in the Orbitrap. The AGC target for MS/MS was set to 5 × 10<sup>4</sup> and the maximum injection time limited to 30 ms. The dynamic exclusion was set to 30 s with a 10 ppm mass tolerance around the precursor and its isotopes. Monoisotopic precursor selection was enabled.

The acquired raw data were analyzed with pFind software platform (Chi et al., 2018) against reduced database based on the reviewed *Arabidopsis thaliana* proteins (16,268 entries, version 2021\_02, downloaded from UniProt) from which 1,000 random entries plus GLR3.4 were retained. Full-specific mode with TrypsinKR\_C and up to two missed cleavages were used. Precursor tolerance and Fragment tolerance were set to 20 ppm. Modification search was performed in an open mode with Carbamidomethyl (C), Glutathione (C), and Oxidation (M) set as dynamic modifications. In case of Glutathione, a neutral loss was defined as 129.1148 Da. The FDR was set as 1% with the peptides mass in the range of 600–10,000 Da and the length between 6 and 100 residues. The raw files and full output tables are available through PRIDE repository with identifier PXD024563 (reviewer access username: [reviewer\\_pxd024563@ebi.ac.uk](mailto:reviewer_pxd024563@ebi.ac.uk), password: UDehuNMe).

### QUANTIFICATION AND STATISTICAL ANALYSIS

Calcium imaging and confocal microscopy data (Figures 1B, S1, S2E, and S2F) were analyzed using ImageJ. Mass spectrometry data (Figure 3B) was analyzed using pFind. Statistical analysis was performed using SigmaPlot 11.0 (Figures 1A, 1B, 3C–3E, S1D, and S2) and Origin 2015 Sr2 (Figure S6E). In all figure legends, n represents the number of independent biological replicates. All quantitative data were presented as mean ± SEM. Statistical analyses were conducted using one-way ANOVA followed by the post hoc Dunnett test (Figures S1D and S2D). Values of p < 0.05 were considered statistically significant.



**Supplemental information**

**Structure of the *Arabidopsis thaliana*  
glutamate receptor-like channel GLR3.4**

**Marriah N. Green, Shanti Pal Gangwar, Erwan Michard, Alexander A. Simon, Maria Teresa Portes, Juan Barbosa-Caro, Michael M. Wudick, Michael A. Lizzio, Oleg Klykov, Maria V. Yelshanskaya, José A. Feijó, and Alexander I. Sobolevsky**

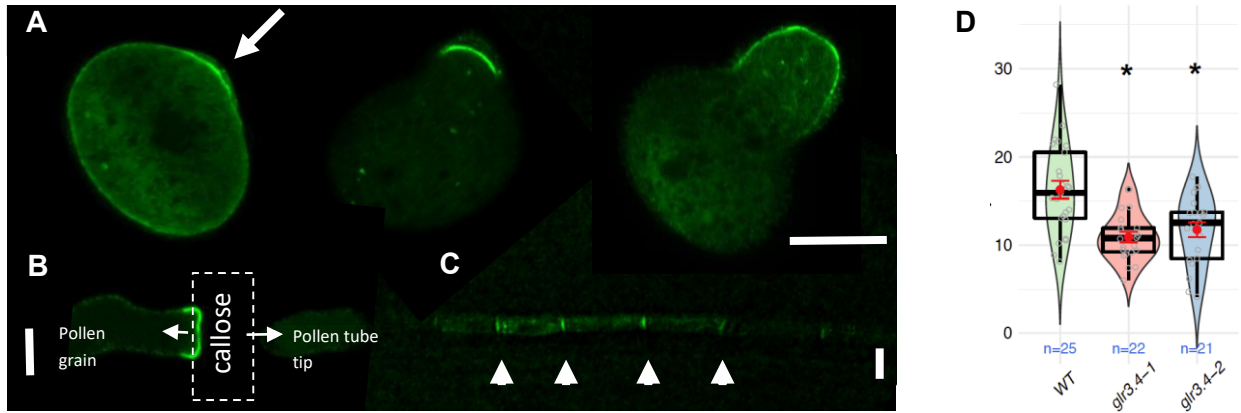


**Figure S1. GLR3.4 is associated with cell polarity and  $\text{Ca}^{2+}$  influx in growing pollen tubes, Related to Figure 1**

**A.** GLR3.4 is an early marker of differentiation of the aperture domain of the plasma membrane that will outgrow into the pollen tube (sequence from left to right). **B.** GLR3.4 remains a marker of the apical end of the pollen after the formation of a callose plug. **C.** GLR3.4 labels the top ends of root phloem cells (arrows). Bars are 10  $\mu\text{m}$ -long. **D.** Extracellular  $\text{Ca}^{2+}$  influx is reduced at the pollen tube tip of two allele mutant lines (*Atglr3.4-1* and *Atglr3.4-2*) when compared to wild-type (*Col-0*). Violin plots show the probability density with color-filled curves obtained from individual replicates (open gray circles), boxplots (thick black lines and outliers as black dots) overlaid with the mean and SEM (red circles and lines). Asterisks indicate the significant difference ( $p < 0.001$ ) compared to wild type (one-way ANOVA followed by the post-hoc Dunnett test).

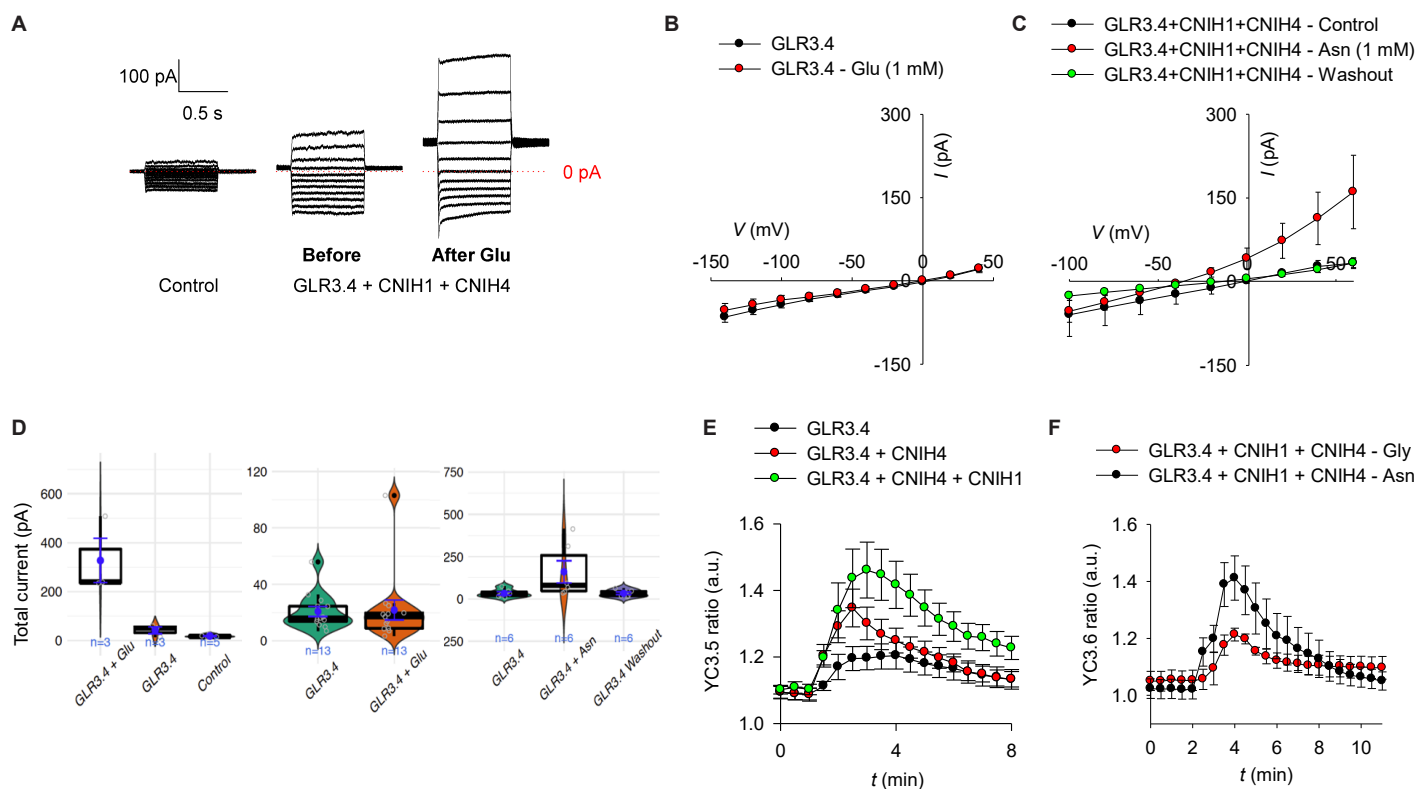


**Figure S2. GLR3.4 are ligand-gated  $\text{Ca}^{2+}$ -permeable channels that need CNIHs for functional expression in COS-7 cells, Related to Figure 1**

**A.** Currents recorded from COS-7 cells expressing GLR3.4 alone (left traces) or co-expressing it with CNIH1+4 in the absence (middle traces) or presence of 1 mM Glu (right traces). The recording conditions are the same as for Figure 1a. **B.** Voltage-dependence of currents recorded from COS-7 cells expressing GLR3.4 alone (without CNIHs) before (black circles) or after (red circles) application of 1 mM Glu ( $n = 13$ , mean  $\pm$  SEM). **C.** Voltage-dependence of currents recorded from COS-7 cells co-expressing GLR3.4, CNIH1 and CNIH4 before (black circles) or after (red circles) application of 1 mM Asn. The current amplitude increases in response to Asn application but returns to the basal level after washout (green circles) ( $n = 6$ , mean  $\pm$  SEM). **D.** Violin plots of data distribution shown in Figure 1A (+60 mV, left plot), as well as this figure panels **B** (+40 mV, middle plot) and **C** (+60 mV, right plot). The values presented are non-normalized total current amplitudes overlaid with the mean and SEM (blue circles and lines). **E.** Changes in cytosolic  $\text{Ca}^{2+}$  measured in COS-7 cells expressing YC3.6 and either GLR3.4 alone (black circles;  $n = 21$ , mean  $\pm$  SEM), GLR3.4 and CNIH4 (red circles;  $n = 13$ , mean  $\pm$  SEM) or GLR3.4 and CNIH1 and CNIH4 (green circles;  $n = 33$ , mean  $\pm$  SEM). Note the additive activating effect of CNIHs on the GLR3.4-mediated  $\text{Ca}^{2+}$  influx. **F.** Changes in cytosolic  $\text{Ca}^{2+}$  measured in COS-7 cells expressing YC3.6 and GLR3.4 and CNIH1 and CNIH4 in response to applications of 0.5 mM Gly (black circles;  $n = 9$ , mean  $\pm$  SEM) or 0.5 mM Asn (red circles;  $n = 3$ , mean  $\pm$  SEM). Asn elicits comparable to Glu  $\text{Ca}^{2+}$  influx, while the response to Gly is much smaller.

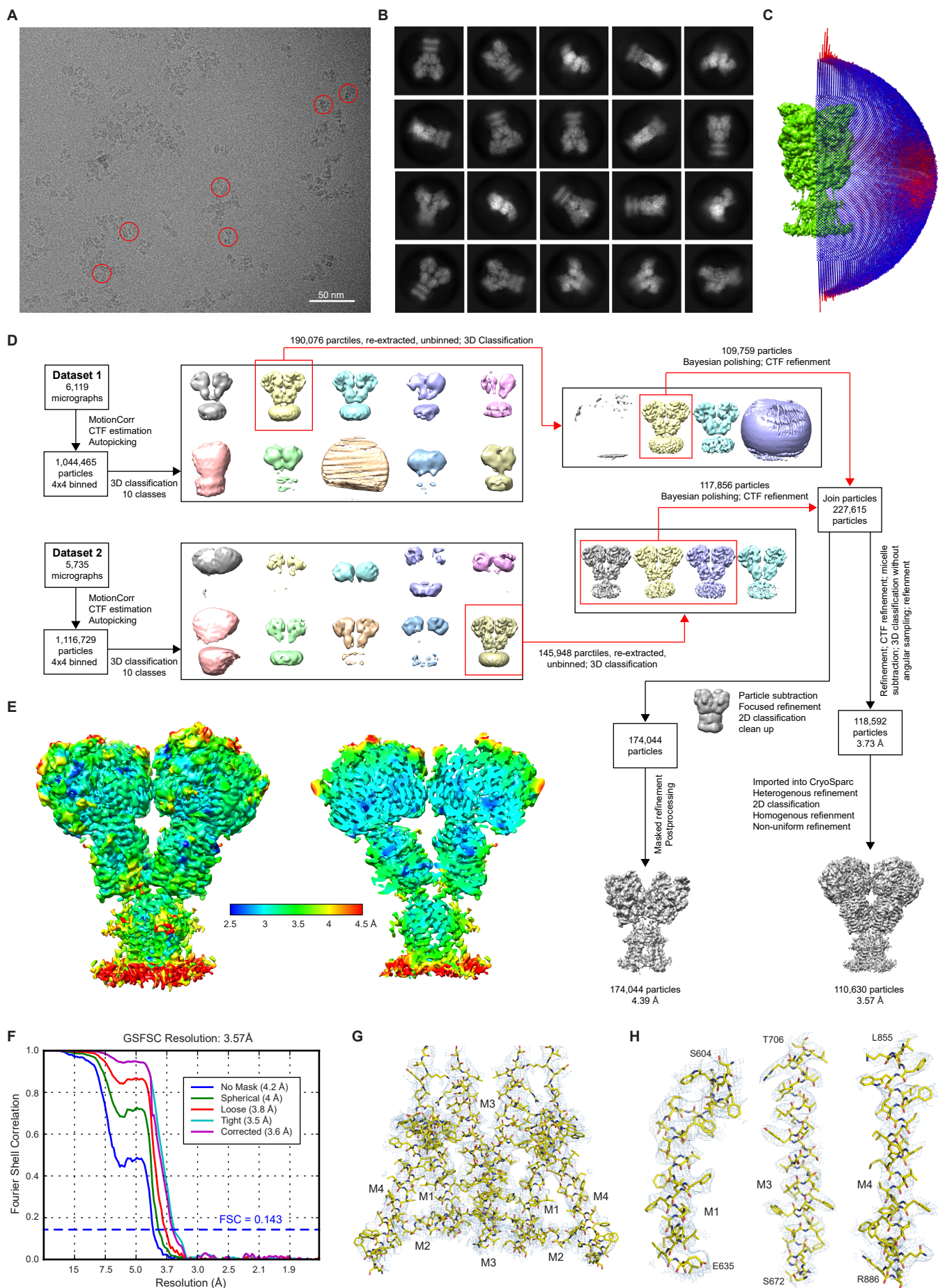


**Figure S3. Overview of single-particle cryo-EM for GLR3.4, Related to Figure 1**

**A.** Example cryo-EM micrograph for GLR3.4 with example particles circled in red. **B.** Reference-free 2D class averages of GLR3.4 illustrating different particle orientations. **C.** Distribution of particle Euler angle orientations contributing to the final reconstruction, with larger red cylinders representing orientations comprising more particles. **D.** 3D reconstruction workflow. **E.** Local resolution mapped on the GLR3.4 density viewed parallel to the membrane either in its entirety (left) or coronally halved (right). **F.** Fourier shell correlation (FSC) curves from refinement. **G.** Density for the transmembrane domain of 4.39-Å reconstruction after ATD and micelle subtraction. Shown are subunits A and C, with subunits B and D omitted for clarity. **H.** Fragments of the 3.57-Å resolution full-length GLR3.4 cryo-EM map for the transmembrane segments M1, M3 and M4 of subunit A.



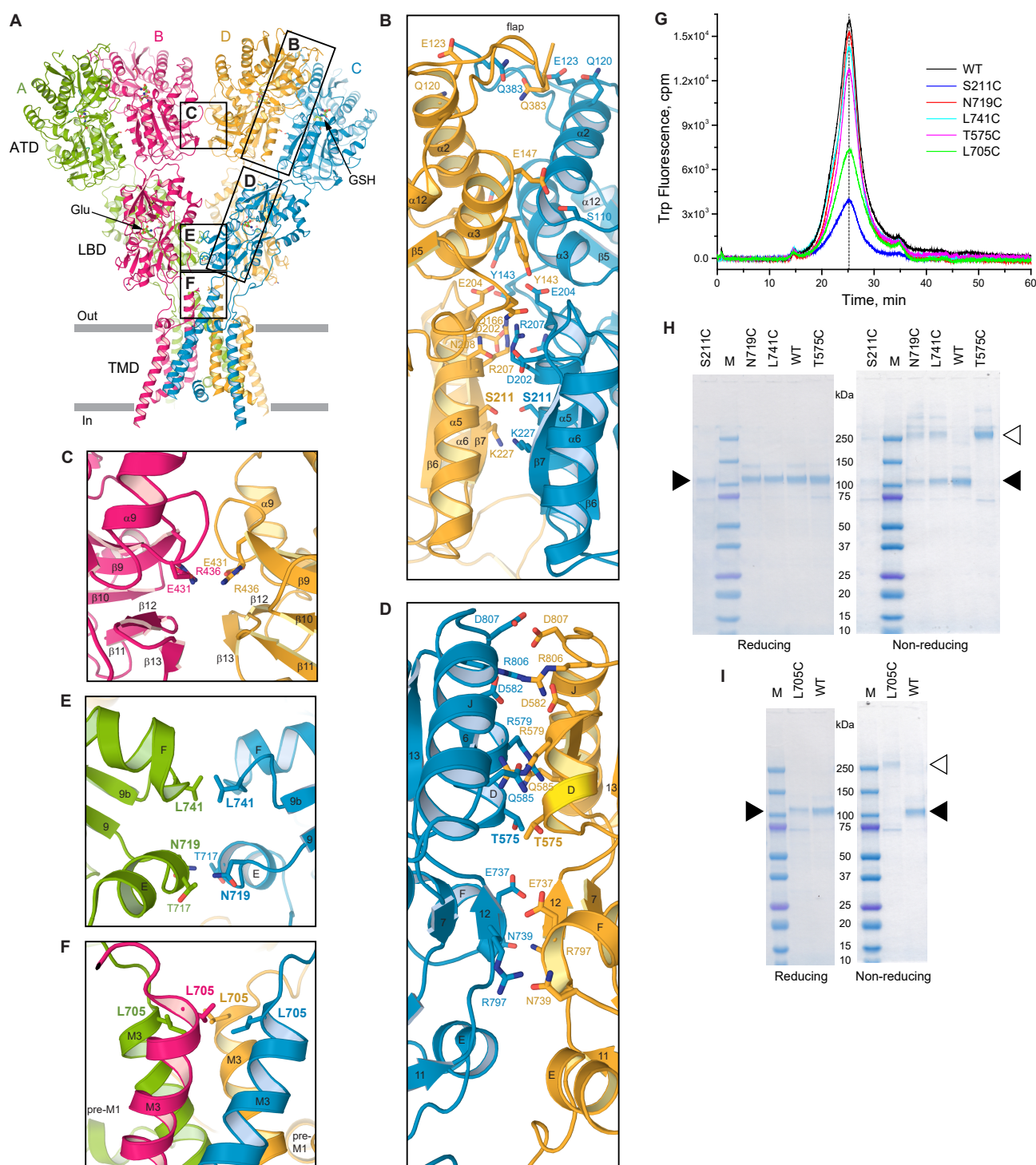


**Figure S4. Probing intersubunit interfaces in GLR3.4, Related to Figure 2**

**A.** GLR3.4 structures with each subunit in a different color. **B-F.** Close-up views of ATD intradimer (**B**), ATD interdimer (**C**), LBD intradimer (**D**), LBD interdimer (**E**) and TMD (**F**) interfaces, with residues contributing to the interfaces shown in sticks and mutated to cysteine labeled in bold font. **G.** FSEC traces for purified wild type GLR3.4 and cysteine-substituted mutants showing a single tetrameric protein peak tracked by intrinsic tryptophan fluorescence. **H-I.** SDS-PAGE analysis of spontaneous crosslinking of cysteines introduced at intersubunit interfaces. Left and right panels illustrate experiments carried out in reducing and non-reducing conditions, respectively. Filled and open triangles indicate positions of monomeric and dimeric bands, respectively.

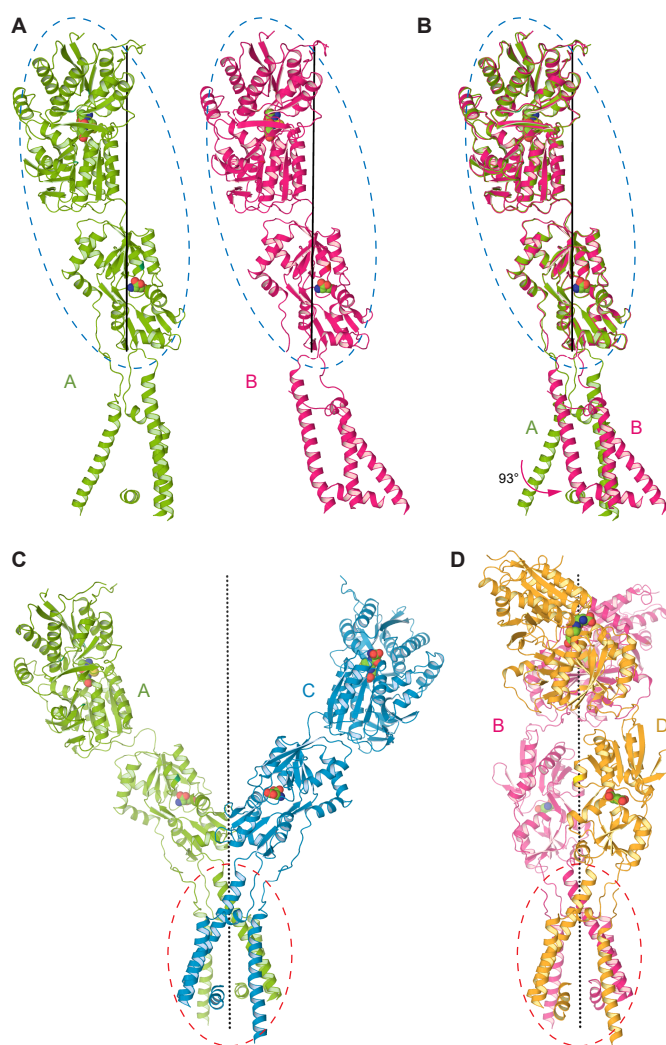


**Figure S5. Non-equivalence of subunits in GLR3.4, Related to Figure 2**

**A.** Subunits A and B with the same orientation of ATDs and LBDs (blue ovals). The axis of the local two-fold symmetry is shown as a vertical solid line. **B.** Superposition of subunits A and B with the difference in TMD conformation illustrated by the pink arrow. **C-D.** Diagonal A/C (**C**) and B/D (**D**) subunit pairs with the same orientation of TMDs (red ovals). The axis of the overall two-fold symmetry is shown as a dotted line.

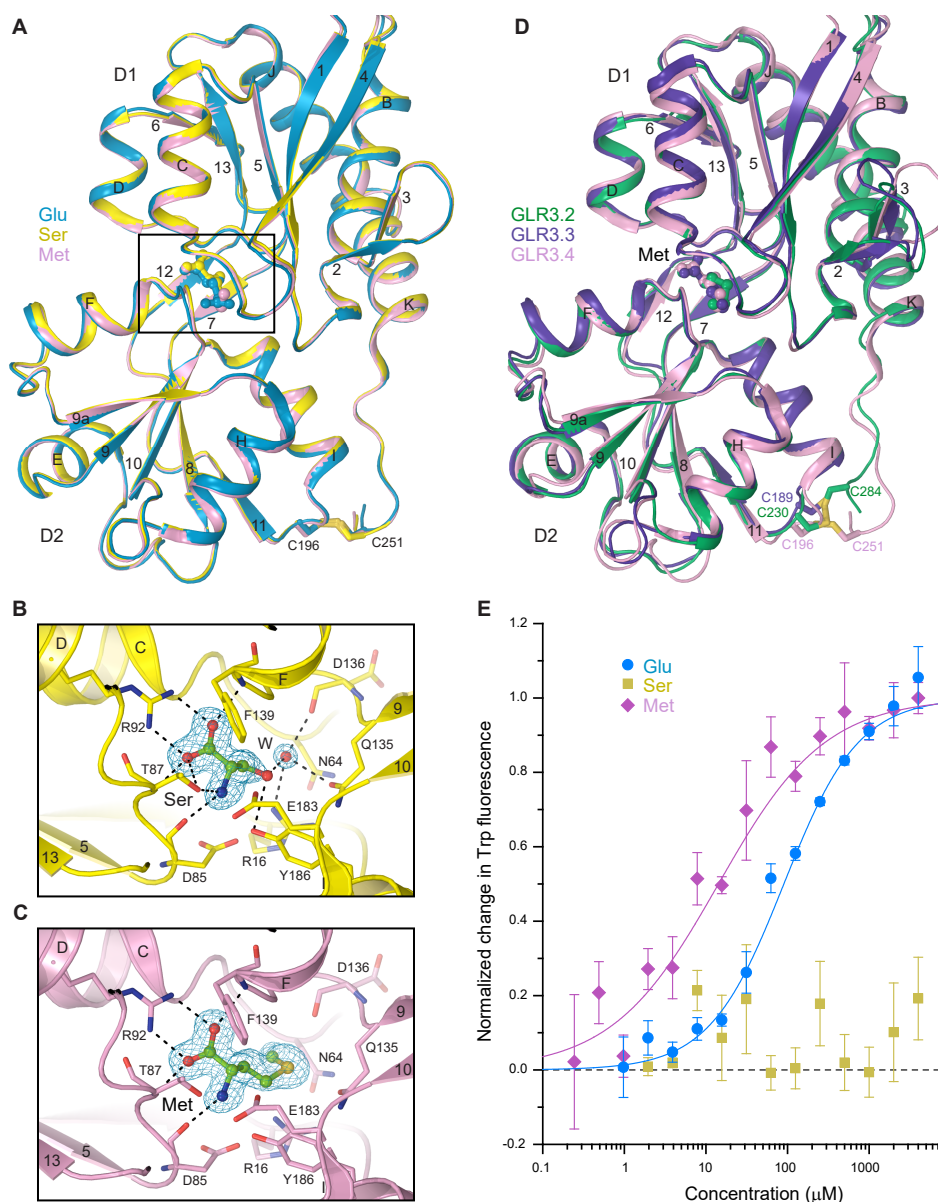


**Figure S6. Structures of isolated LBDs, Related to Figure 4**

**A.** Superposition of GLR3.4-S1S2 structures in complex with Glu (blue), Ser (yellow) and Met (pink). The ligands are shown in ball-and-stick representation. Black rectangle indicates the region expanded in **(B-C)**. Secondary structure elements are labeled. **B-C.** Closeup views of the ligand binding pocket in GLR3.4-S1S2<sub>Ser</sub> (**B**) and GLR3.4-S1S2<sub>Met</sub> (**C**), with the omit map density for Ser and water (**B**) and Met (**C**) at  $2.5\sigma$  shown as a blue mesh. Binding pocket residues are shown in sticks and their interactions with the ligands and water (W) are indicated by dashed lines. **D.** Superposition of the Met-bound isolated LBDs for GLR3.2 (PDB ID: 6VE8; green), GLR3.3 (PDB ID: 6R8A; purple) and GLR3.4 (pink). **E.** Changes in tryptophan fluorescence of GLR3.4-S1S2 detected by microscale thermophoresis at different concentrations of Glu, Ser and Met. The straight lines are logistic equation fits with the apparent dissociation constants for Glu,  $90 \pm 12 \mu\text{M}$  ( $n = 4$ ), and Met,  $14.2 \pm 5.9 \mu\text{M}$  ( $n = 4$ ). Note, Ser, which is already bound to GLR3.4-S1S2, shows no binding ( $n = 3$ ). Data are represented as mean  $\pm$  SEM.



**Table S1. Cryo-EM data collection, refinement, and validation statistics, Related to STAR Methods and Figure 1.**

<b>Data collection and processing</b>	<b>Full-length GLR3.4</b>	<b>GLR3.4 after ATD and micelle subtraction</b>
PBD accession code	7LZH	7LZI
EMDB accession code	EMD-23606	EMD-23607
Magnification	105,000	105,000
Voltage (kV)	300	300
Electron exposure (e-/Å <sup>2</sup> )	58	58
Defocus range (μm)	-1 to -2	-1 to -2
Pixel size (Å)	0.83	0.83
Symmetry imposed	C2	C2
Initial particle images (no.)	2,159,194	227,615
Final particle images (no.)	110,630	174,044
Map resolution (Å)	3.57	4.39
FSC threshold	0.143	0.143
Map resolution range (Å)	2.27 to 8.25	4.2 to 5.0
<b>Refinement</b>		
Model resolution (Å)	3.57	4.39
FSC threshold	0.143	0.143
Model resolution range (Å)	2.27 to 8.25	4.2 to 5.0
Map sharpening B factor (Å <sup>2</sup> )	-118.3	-170.6
<b>Model composition</b>		
Non-hydrogen atoms	25,306	11,782
Ligands-Glu	40	40
Ligands-GSH	80	0
Sugar-NAG	224	112
Number of Protein residues	3,192	1,480
<b>B factors (Å<sup>2</sup>)</b>		
Protein	98.54	184.96
Ligands	77.13	129.34
<b>r.m.s. deviations</b>		
Bond lengths (Å)	0.009	0.005
Bond angles (°)	1.271	1.187
<b>Validation</b>		
MolProbity score	1.69	1.60
Clashscore	4.49	4.41
Poor rotamers (%)	0.44	0.16
<b>Ramachandran plot</b>		
Favored (%)	92.57	94.49
Allowed (%)	7.43	5.51
Outliers (%)	0	0

**Table S2. Crystallographic data collection and refinement statistics, Related to STAR Methods and Figure 4.**

	<b>GLR3.4-S1S2<sub>Glu</sub></b>	<b>GLR3.4-S1S2<sub>Ser</sub></b>	<b>GLR3.4-S1S2<sub>Met</sub></b>
PDB accession code	7LZ0	7LZ1	7LZ2
Beamline	NE-CAT 24-ID-C	NE-CAT 24-ID-C	NE-CAT 24-ID-C
Wavelength (Å)	0.97910	0.97918	0.97918
Space group	P6522	P6522	P6522
Cell parameters (a, b, c, Å)	74.34, 74.34, 513.56	74.51, 74.51, 507.98	74.58, 74.58, 508.89
Cell parameters ( $\alpha$ , $\beta$ , $\gamma$ , °)	90, 90, 120	90, 90, 120	90, 90, 120
Resolution (Å)	64.38-2.29 (2.29-2.23)	64.53-1.51 (1.54-1.51)	84.81 - 1.50 (1.55 - 1.50)
N of monomers per AU	3	3	3
Total observations	366,555 (33,632)	2,020,815 (92,162)	1,796,831 (89,595)
Unique reflections	39,519 (3,657)	133,111 (6,458)	136,052 (6,600)
R <sub>merge</sub> (%)	0.117 (0.769)	0.084 (1.438)	0.060 (1.141)
R <sub>mease</sub> (%)	0.131 (0.858)	0.090 (1.544)	0.065 (1.231)
R <sub>pim</sub> (%)	0.057 (0.376)	0.031 (0.559)	0.024 (0.460)
Mean (I)/sigma (I)	12.9 (2.8)	15.4 (1.5)	19.3 (1.9)
Completeness (%)	99.7 (97.0)	100 (100)	99.9 (100)
Multiplicity	9.3 (9.2)	15.2 (14.3)	13.2 (13.6)
CC (1/2)	0.998 (0.805)	0.999 (0.524)	0.999 (0.654)
Wilson B-factors (Å <sup>2</sup> )	36.3	22.3	21.7
<b>Refinement</b>			
Resolution	64.46-2.29	64.61-1.51	84.96-1.50
Reflections used in refinement	37,406	126,247	129,095
R <sub>work</sub>	21.12	20.42	18.59
R <sub>free</sub>	24.76	23.09	20.88
<b>Number of non-hydrogen atoms</b>			
Macromolecule	5,877	5,867	5,899
Ligands	30	21	27
Average B factor (all atoms)	39.0	28.5	28.0
Average B Factor Macromolecule	39.36	28.36	27.58
Number of Protein Residues	751	749	755
Number of water molecules	98	211	335
RMSD bond lengths (Å)	0.0042	0.0113	0.0135
RMSD angles (°)	1.2528	1.6652	1.8753
<b>Ramachandran plot</b>			
Preferred regions (%)	97.58	97.04	97.45
Allowed regions (%)	2.42	2.69	2.14
Outliers (%)	0	0.27	0.40

## References

- Acosta, I. F., & Farmer, E. E. (2010). Jasmonates. *The Arabidopsis Book / American Society of Plant Biologists*, 8, e0129. <https://doi.org/10.1199/tab.0129>
- Adhikari, P. B., Liu, X., & Kasahara, R. D. (2020). Mechanics of Pollen Tube Elongation: A Perspective. *Frontiers in Plant Science*, 11. <https://www.frontiersin.org/articles/10.3389/fpls.2020.589712>
- Armstrong, N., & Gouaux, E. (2000). Mechanisms for Activation and Antagonism of an AMPA-Sensitive Glutamate Receptor: Crystal Structures of the GluR2 Ligand Binding Core. *Neuron*, 28(1), 165-181. [https://doi.org/10.1016/S0896-6273\(00\)00094-5](https://doi.org/10.1016/S0896-6273(00)00094-5)
- Armstrong, N., Sun, Y., Chen, G.-Q., & Gouaux, E. (1998). Structure of a glutamate-receptor ligand-binding core in complex with kainate. *Nature*, 395(6705), 913-917. <https://doi.org/10.1038/27692>
- Arvola, M., & Keinänen, K. (1996). Characterization of the Ligand-binding Domains of Glutamate Receptor (GluR)-B and GluR-D Subunits Expressed in Escherichia coli as Periplasmic Proteins\*. *Journal of Biological Chemistry*, 271(26), 15527-15532. <https://doi.org/10.1074/jbc.271.26.15527>
- Auerbach, A., & Zhou, Y. (2005). Gating Reaction Mechanisms for NMDA Receptor Channels. *Journal of Neuroscience*, 25(35), 7914-7923. <https://doi.org/10.1523/JNEUROSCI.1471-05.2005>
- Baum, D. (2008). Reading a Phylogenetic Tree: The Meaning of Monophyletic Groups. *1(1):190*. <http://www.nature.com/scitable/topicpage/reading-a-phylogenetic-tree-the-meaning-of-41956>  
<files/932/reading-a-phylogenetic-tree-the-meaning-of-41956.html>

- Bethke, G., Unthan, T., Uhrig, J. F., Pöschl, Y., Gust, A. A., Scheel, D., & Lee, J. (2009). Flg22 regulates the release of an ethylene response factor substrate from MAP kinase 6 in *Arabidopsis thaliana* via ethylene signaling. *Proceedings of the National Academy of Sciences*, 106(19), 8067-8072. <https://doi.org/10.1073/pnas.0810206106>
- Bowie, D. (2010). Ion-dependent gating of kainate receptors. *The Journal of Physiology*, 588(Pt 1), 67-81. <https://doi.org/10.1113/jphysiol.2009.178863>
- Brenner, E. D., Stahlberg, R., Mancuso, S., Vivanco, J., Baluška, F., & Van Volkenburgh, E. (2006). Plant neurobiology: an integrated view of plant signaling. *Trends in Plant Science*, 11(8), 413-419. <https://doi.org/10.1016/j.tplants.2006.06.009>
- Brodt, S., Six, J., Feenstra, G., Ingels, C. & Campbell, D. . (2011). Sustainable Agriculture *Nature Education Knowledge* 3(10):1. <https://www.nature.com/scitable/knowledge/library/sustainable-agriculture-23562787/files/837/sustainable-agriculture-23562787.html>
- Brogi, S., Campiani, G., Brindisi, M., & Butini, S. (2019). Allosteric Modulation of Ionotropic Glutamate Receptors: An Outlook on New Therapeutic Approaches To Treat Central Nervous System Disorders. *ACS Medicinal Chemistry Letters*, 10(3), 228-236. <https://doi.org/10.1021/acsmmedchemlett.8b00450>
- Burada, A. P., Vinnakota, R., & Kumar, J. (2020a). The architecture of GluD2 ionotropic delta glutamate receptor elucidated by cryo-EM. *Journal of Structural Biology*, 211(2), 107546. <https://doi.org/10.1016/j.jsb.2020.107546>
- Burada, A. P., Vinnakota, R., & Kumar, J. (2020b). Cryo-EM structures of the ionotropic glutamate receptor GluD1 reveal a non-swapped architecture. *Nature Structural & Molecular Biology*, 27(1), 84-91. <https://doi.org/10.1038/s41594-019-0359-y>

- Carrillo, E., Gonzalez, C. U., Berka, V., & Jayaraman, V. (2021). Delta glutamate receptors are functional glycine- and D-serine-gated cation channels in situ. *Science Advances*, 7(52), eabk2200. <https://doi.org/10.1126/sciadv.abk2200>
- Chang, H.-R., & Kuo, C.-C. (2008). The Activation Gate and Gating Mechanism of the NMDA Receptor. *Journal of Neuroscience*, 28(7), 1546-1556. <https://doi.org/10.1523/JNEUROSCI.3485-07.2008>
- Chen, J.-T., & Heidari, P. (2020). Cell Signaling in Model Plants. *International Journal of Molecular Sciences*, 21(17), 6062. <https://doi.org/10.3390/ijms21176062>
- Chen, J., & Ham, B.-K. (2022). Systemic Signaling: A Role in Propelling Crop Yield. *Plants*, 11(11), 1400. <https://doi.org/10.3390/plants11111400>
- Chen, J., Jing, Y., Zhang, X., Li, L., Wang, P., Zhang, S., Zhou, H., & Wu, J. (2016). Evolutionary and Expression Analysis Provides Evidence for the Plant Glutamate-like Receptors Family is Involved in Woody Growth-related Function. *Scientific Reports*, 6(1), 32013. <https://doi.org/10.1038/srep32013>
- Chen, N., Li, B., Murphy, T. H., & Raymond, L. A. (2004). Site within N-Methyl-D-aspartate Receptor Pore Modulates Channel Gating. *Molecular Pharmacology*, 65(1), 157-164. <https://doi.org/10.1124/mol.65.1.157>
- Chen, S., Zhao, Y., Wang, Y., Shekhar, M., Tajkhorshid, E., & Gouaux, E. (2017). Activation and Desensitization Mechanism of AMPA Receptor-TARP Complex by Cryo-EM. *Cell*, 170(6), 1234-1246.e1214. <https://doi.org/10.1016/j.cell.2017.07.045>
- Cheng, Y., Zhang, X., Sun, T., Tian, Q., & Zhang, W.-H. (2018). Glutamate Receptor Homolog3.4 is Involved in Regulation of Seed Germination Under Salt Stress in

- Arabidopsis. *Plant and Cell Physiology*, 59(5), 978-988.  
<https://doi.org/10.1093/pcp/pcy034>
- Chiu, J., DeSalle, R., Lam, H. M., Meisel, L., & Coruzzi, G. (1999). Molecular evolution of glutamate receptors: a primitive signaling mechanism that existed before plants and animals diverged. *Molecular Biology and Evolution*, 16(6), 826-838.  
<https://doi.org/10.1093/oxfordjournals.molbev.a026167>
- Cull-Candy, S. G., & Usowicz, M. M. (1987). Multiple-conductance channels activated by excitatory amino acids in cerebellar neurons. *Nature*, 325(6104), 525-528.  
<https://doi.org/10.1038/325525a0>
- De Bortoli, S., Teardo, E., Szabò, I., Morosinotto, T., & Alboresi, A. (2016). Evolutionary insight into the ionotropic glutamate receptor superfamily of photosynthetic organisms. *Biophysical Chemistry*, 218, 14-26. <https://doi.org/10.1016/j.bpc.2016.07.004>
- Deinlein, U., Stephan, A. B., Horie, T., Luo, W., Xu, G., & Schroeder, J. I. (2014). Plant salt-tolerance mechanisms. *Trends in Plant Science*, 19(6), 371-379.  
<https://doi.org/10.1016/j.tplants.2014.02.001>
- Dolphin, A. C., Insel, P. A., Blaschke, T. F., & Meyer, U. A. (2020). Introduction to the Theme “Ion Channels and Neuropharmacology: From the Past to the Future”. *Annual Review of Pharmacology and Toxicology*, 60(1), 1-6. <https://doi.org/10.1146/annurev-pharmtox-082719-110050>
- Dürr, K. L., Chen, L., Stein, R. A., De Zorzi, R., Folea, I. M., Walz, T., McHaourab, H. S., & Gouaux, E. (2014). Structure and Dynamics of AMPA Receptor GluA2 in Resting, Pre-Open, and Desensitized States. *Cell*, 158(4), 778-792.  
<https://doi.org/10.1016/j.cell.2014.07.023>

- Fernández-Marcos, M., Desvoves, B., Manzano, C., Liberman, L. M., Benfey, P. N., del Pozo, J. C., & Gutierrez, C. (2017). Control of Arabidopsis lateral root primordium boundaries by MYB36. *New Phytologist*, 213(1), 105-112. <https://doi.org/10.1111/nph.14304>
- Forde, B. G., & Roberts, M. R. (2014). Glutamate receptor-like channels in plants: a role as amino acid sensors in plant defence? *Frontiers in Plant Science*, 6, 37. <https://doi.org/10.12703/P6-37>
- Goto, Y., Maki, N., Ichihashi, Y., Kitazawa, D., Igarashi, D., Kadota, Y., & Shirasu, K. (2020). Exogenous Treatment with Glutamate Induces Immune Responses in Arabidopsis. *Molecular Plant-Microbe Interactions*®, 33(3), 474-487. <https://doi.org/10.1094/MPMI-09-19-0262-R>
- Green, M. N., Gangwar, S. P., Michard, E., Simon, A. A., Portes, M. T., Barbosa-Caro, J., Wudick, M. M., Lizzio, M. A., Klykov, O., Yelshanskaya, M. V., Feijó, J. A., & Sobolevsky, A. I. (2021). Structure of the Arabidopsis thaliana glutamate receptor-like channel GLR3.4. *Molecular Cell*, 81(15), 3216-3226.e3218. <https://doi.org/10.1016/j.molcel.2021.05.025>
- Grenzi, M., Bonza, M. C., & Costa, A. (2022). Signaling by plant glutamate receptor-like channels: What else! *Current Opinion in Plant Biology*, 68, 102253. <https://doi.org/10.1016/j.pbi.2022.102253>
- Hansen, K. B., Wollmuth, L. P., Bowie, D., Furukawa, H., Menniti, F. S., Sobolevsky, A. I., Swanson, G. T., Swanger, S. A., Greger, I. H., Nakagawa, T., McBain, C. J., Jayaraman, V., Low, C.-M., Dell'Acqua, M. L., Diamond, J. S., Camp, C. R., Perszyk, R. E., Yuan, H., & Traynelis, S. F. (2021). Structure, Function, and Pharmacology of Glutamate

Receptor Ion Channels. *Pharmacological Reviews*, 73(4), 1469-1658.

<https://doi.org/10.1124/pharmrev.120.000131>

Herguedas, B., Krieger, J., & Greger, I. H. (2013). Receptor Heteromeric Assembly—How It Works and Why It Matters. In *Progress in Molecular Biology and Translational Science* (Vol. 117, pp. 361-386). Elsevier.

<https://linkinghub.elsevier.com/retrieve/pii/B9780123869319000131>

Hernández-Coronado, M., Dias Araujo, P. C., Ip, P.-L., Nunes, C. O., Rahni, R., Wudick, M. M., Lizzio, M. A., Feijó, J. A., & Birnbaum, K. D. (2022). Plant glutamate receptors mediate a bet-hedging strategy between regeneration and defense. *Developmental Cell*, 57(4), 451-465.e456. <https://doi.org/10.1016/j.devcel.2022.01.013>

Hollmann, M., Maron, C., & Heinemann, S. (1994). N-glycosylation site tagging suggests a three transmembrane domain topology for the glutamate receptor GluR1. *Neuron*, 13(6), 1331-1343. [https://doi.org/10.1016/0896-6273\(94\)90419-7](https://doi.org/10.1016/0896-6273(94)90419-7)

Huettnner, J. E. (2015). Glutamate receptor pores. *The Journal of Physiology*, 593(1), 49-59. <https://doi.org/10.1113/jphysiol.2014.272724>

Jahr, C. E., & Stevens, C. F. (1987). Glutamate activates multiple single channel conductances in hippocampal neurons. *Nature*, 325(6104), 522-525. <https://doi.org/10.1038/325522a0>

Jin, L., Cai, Y., Sun, C., Huang, Y., & Yu, T. (2019). Exogenous l-glutamate treatment could induce resistance against *Penicillium expansum* in pear fruit by activating defense-related proteins and amino acids metabolism. *Postharvest Biology and Technology*, 150, 148-157. <https://doi.org/10.1016/j.postharvbio.2018.11.009>



- Jin, R., Singh, S. K., Gu, S., Furukawa, H., Sobolevsky, A. I., Zhou, J., Jin, Y., & Gouaux, E. (2009). Crystal structure and association behaviour of the GluR2 amino-terminal domain. *The EMBO Journal*, 28(12), 1812-1823. <https://doi.org/10.1038/emboj.2009.140>
- Jones, J. D. G., & Dangl, J. L. (2006). The plant immune system. *Nature*, 444(7117), 323-329. <https://doi.org/10.1038/nature05286>
- Kadotani, N., Akagi, A., Takatsuji, H., Miwa, T., & Igarashi, D. (2016). Exogenous proteinogenic amino acids induce systemic resistance in rice. *BMC Plant Biology*, 16(1), 60. <https://doi.org/10.1186/s12870-016-0748-x>
- Katz, B., & Thesleff, S. (1957). A study of the ‘desensitization’ produced by acetylcholine at the motor end-plate. *The Journal of Physiology*, 138(1), 63-80. <https://doi.org/10.1113/jphysiol.1957.sp005838>
- Kc, K. B., Dias, G. M., Veeramani, A., Swanton, C. J., Fraser, D., Steinke, D., Lee, E., Wittman, H., Farber, J. M., Dunfield, K., McCann, K., Anand, M., Campbell, M., Rooney, N., Raine, N. E., Acker, R. V., Hanner, R., Pascoal, S., Sharif, S., . . . Fraser, E. D. G. (2018). When too much isn’t enough: Does current food production meet global nutritional needs? *PLOS ONE*, 13(10), e0205683. <https://doi.org/10.1371/journal.pone.0205683>
- Khanra, N., Brown, P. M. G. E., Perozzo, A. M., Bowie, D., & Meyerson, J. R. (2021). Architecture and structural dynamics of the heteromeric GluK2/K5 kainate receptor. *eLife*, 10, e66097. <https://doi.org/10.7554/eLife.66097>
- Kim, M.-J., Jeon, B. W., Oh, E., Seo, P. J., & Kim, J. (2021). Peptide Signaling during Plant Reproduction. *Trends in Plant Science*, 26(8), 822-835. <https://doi.org/10.1016/j.tplants.2021.02.008>

Klykov, O., Gangwar, S. P., Yelshanskaya, M. V., Yen, L., & Sobolevsky, A. I. (2021).

Structure and desensitization of AMPA receptor complexes with type II TARP  $\gamma 5$  and GSG1L. *Molecular Cell*, 81(23), 4771-4783.e4777.

<https://doi.org/10.1016/j.molcel.2021.09.030>

Kunishima, N., Shimada, Y., Tsuji, Y., Sato, T., Yamamoto, M., Kumasaka, T., Nakanishi, S., Jingami, H., & Morikawa, K. (2000). Structural basis of glutamate recognition by a dimeric metabotropic glutamate receptor. *Nature*, 407(6807), 971-977.

<https://doi.org/10.1038/35039564>

Kussius, C. L., Popescu, A. M., & Popescu, G. K. (2010). Agonist-specific Gating of NMDA Receptors. *Channels (Austin, Tex.)*, 4(2), 78-82.

<https://www.ncbi.nlm.nih.gov/pmc/articles/PMC3150751/>

Kuusinen, A., Arvola, M., & Keinänen, K. (1995). Molecular dissection of the agonist binding site of an AMPA receptor. *The EMBO Journal*, 14(24), 6327-6332.

<https://www.ncbi.nlm.nih.gov/pmc/articles/PMC394757/>

Lam, H.-M., Chiu, J., Hsieh, M.-H., Meisel, L., Oliveira, I. C., Shin, M., & Coruzzi, G. (1998). Glutamate-receptor genes in plants. *Nature*, 396(6707), 125-126.

<https://doi.org/10.1038/24066>

Li, F., Wang, J., Ma, C., Zhao, Y., Wang, Y., Hasi, A., & Qi, Z. (2013). Glutamate Receptor-Like Channel3.3 Is Involved in Mediating Glutathione-Triggered Cytosolic Calcium Transients, Transcriptional Changes, and Innate Immunity Responses in Arabidopsis. *Plant Physiology*, 162(3), 1497-1509. <https://doi.org/10.1104/pp.113.217208>

Mauseth, J. D. (2021). *Botany: An Introduction to Plant Biology* (Vol. Vol Seventh edition.). Jones & Bartlett Learning.

<https://web.s.ebscohost.com/ehost/ebookviewer/ebook/bmxlYmtfXzIyNTgzOTZfX0FO0?sid=52a09324-d9b2-464d-8484-96ff9c271b8f@redis&vid=0&format=EK&rid=1>

files/1447/bmxlYmtfXzIyNTgzOTZfX0FO0.html

- Meyerhoff, O., Müller, K., Roelfsema, M. R. G., Latz, A., Lacombe, B., Hedrich, R., Dietrich, P., & Becker, D. (2005). AtGLR3.4, a glutamate receptor channel-like gene is sensitive to touch and cold. *Planta*, 222(3), 418-427. <https://www.jstor.org/stable/23389017>
- Michard, E., Lima, P. T., Borges, F., Silva, A. C., Portes, M. T., Carvalho, J. E., Gilliam, M., Liu, L.-H., Obermeyer, G., & Feijó, J. A. (2011). Glutamate Receptor–Like Genes Form Ca<sup>2+</sup> Channels in Pollen Tubes and Are Regulated by Pistil d-Serine. *Science*, 332(6028), 434-437. <https://doi.org/10.1126/science.1201101>
- Michard, E., Simon, A. A., Tavares, B., Wudick, M. M., & Feijó, J. A. (2017). Signaling with Ions: The Keystone for Apical Cell Growth and Morphogenesis in Pollen Tubes1[OPEN]. *Plant Physiology*, 173(1), 91-111. <https://doi.org/10.1104/pp.16.01561>
- Moe-Lange, J., Gappel, N. M., Machado, M., Wudick, M. M., Sies, C. S. A., Schott-Verdugo, S. N., Bonus, M., Mishra, S., Hartwig, T., Bezruczyk, M., Basu, D., Farmer, E. E., Gohlke, H., Malkovskiy, A., Haswell, E. S., Lercher, M. J., Ehrhardt, D. W., Frommer, W. B., & Kleist, T. J. (2021). Interdependence of a mechanosensitive anion channel and glutamate receptors in distal wound signaling. *Science Advances*, 7(37), eabg4298. <https://doi.org/10.1126/sciadv.abg4298>
- Nayem, N., Mayans, O., & Green, T. (2011). Conformational Flexibility of the Ligand-Binding Domain Dimer in Kainate Receptor Gating and Desensitization. *Journal of Neuroscience*, 31(8), 2916-2924. <https://doi.org/10.1523/JNEUROSCI.4771-10.2011>

- Nguyen, C. T., Kurenda, A., Stolz, S., Chételat, A., & Farmer, E. E. (2018). Identification of cell populations necessary for leaf-to-leaf electrical signaling in a wounded plant. *Proceedings of the National Academy of Sciences*, 115(40), 10178-10183.  
<https://doi.org/10.1073/pnas.1807049115>
- Pankevich, D. E. (2011). Overview of the Glutamatergic System. In a. B. M. A. Miriam Davis (Ed.), *Institute of Medicine (US) Forum on Neuroscience and Nervous System Disorders. Glutamate-Related Biomarkers in Drug Development for Disorders of the Nervous System: Workshop Summary*. Washington (DC): National Academies Press (US).
- Pechanova, O., & Pechan, T. (2017). Chapter 3 - Proteomics as a Tool to Understand Maize Biology and to Improve Maize Crop. In M. L. Colgrave (Ed.), *Proteomics in Food Science* (pp. 35-56). Academic Press.  
<https://www.sciencedirect.com/science/article/pii/B9780128040072000035>  
[files/1443/B9780128040072000035.html](https://www.sciencedirect.com/science/article/pii/B9780128040072000035)
- Perrais, D., Veran, J., & Mulle, C. (2010). Gating and permeation of kainate receptors: differences unveiled. *Trends in Pharmacological Sciences*, 31(11), 516-522.  
<https://doi.org/10.1016/j.tips.2010.08.004>
- Price, M. B., Jelesko, J., & Okumoto, S. (2012). Glutamate Receptor Homologs in Plants: Functions and Evolutionary Origins. *Frontiers in Plant Science*, 3, 235.  
<https://doi.org/10.3389/fpls.2012.00235>
- Quioco, F. A., & Ledvina, P. S. (1996). Atomic structure and specificity of bacterial periplasmic receptors for active transport and chemotaxis: variation of common themes. *Molecular Microbiology*, 20(1), 17-25. <https://doi.org/10.1111/j.1365-2958.1996.tb02484.x>

- Relations, F. M. (2021). FAO - News Article: Climate change fans spread of pests and threatens plants and crops, new FAO study. *FAO Food and Agriculture Organization of the United Nations*. <https://www.fao.org/news/story/en/item/1402920/icode/>
- Sather, W., Dieudonné, S., MacDonald, J. F., & Ascher, P. (1992). Activation and desensitization of N-methyl-D-aspartate receptors in nucleated outside-out patches from mouse neurones. *The Journal of Physiology*, 450, 643-672. <https://www.ncbi.nlm.nih.gov/pmc/articles/PMC1176143/>
- Sather, W., Johnson, J. W., Henderson, G., & Ascher, P. (1990). Glycine-insensitive desensitization of NMDA responses in cultured mouse embryonic neurons. *Neuron*, 4(5), 725-731. [https://doi.org/10.1016/0896-6273\(90\)90198-O](https://doi.org/10.1016/0896-6273(90)90198-O)
- Scientific review of the impact of climate change on plant pests*. (2021). FAO on behalf of the IPCC Secretariat. <http://www.fao.org/documents/card/en/c/cb4769en>
- Shanmukhan, A. P., Mathew, M. M., Radhakrishnan, D., Aiyaz, M., & Prasad, K. (2020). Regrowing the damaged or lost body parts. *Current Opinion in Plant Biology*, 53, 117-127. <https://doi.org/10.1016/j.pbi.2019.12.007> (Growth and development)
- Shipman, E. N., Yu, J., Zhou, J., Albornoz, K., & Beckles, D. M. (2021). Can gene editing reduce postharvest waste and loss of fruit, vegetables, and ornamentals? *Horticulture Research*, 8(1), 1-21. <https://doi.org/10.1038/s41438-020-00428-4>
- Smith, T. C., & Howe, J. R. (2000). Concentration-dependent substate behavior of native AMPA receptors. *Nature Neuroscience*, 3(10), 992-997. <https://doi.org/10.1038/79931>
- Sobolevsky, A. I., Rosconi, M. P., & Gouaux, E. (2009). X-ray structure of AMPA-subtype glutamate receptor: symmetry and mechanism. *Nature*, 462(7274), 745-756. <https://doi.org/10.1038/nature08624>

- Stern-Bach, Y., Bettler, B., Hartley, M., Sheppard, P. O., O'Hara, P. J., & Heinemann, S. F. (1994). Agonist selectivity of glutamate receptors is specified by two domains structurally related to bacterial amino acid-binding proteins. *Neuron*, 13(6), 1345-1357. [https://doi.org/10.1016/0896-6273\(94\)90420-0](https://doi.org/10.1016/0896-6273(94)90420-0)
- Stroebe, D., & Paoletti, P. (2021). Architecture and function of NMDA receptors: an evolutionary perspective. *The Journal of Physiology*, 599(10), 2615-2638. <https://doi.org/10.1113/JP279028>
- Teardo, E., Carraretto, L., De Bortoli, S., Costa, A., Behera, S., Wagner, R., Lo Schiavo, F., Formentin, E., & Szabo, I. (2015). Alternative Splicing-Mediated Targeting of the Arabidopsis GLUTAMATE RECEPTOR3.5 to Mitochondria Affects Organelle Morphology1. *Plant Physiology*, 167(1), 216-227. <https://doi.org/10.1104/pp.114.242602>
- Teardo, E., Formentin, E., Segalla, A., Giacometti, G. M., Marin, O., Zanetti, M., Lo Schiavo, F., Zoratti, M., & Szabò, I. (2011). Dual localization of plant glutamate receptor AtGLR3.4 to plastids and plasmamembrane. *Biochimica et Biophysica Acta (BBA) - Bioenergetics*, 1807(3), 359-367. <https://doi.org/10.1016/j.bbabi.2010.11.008>
- Tian, W., Wang, C., Gao, Q., Li, L., & Luan, S. (2020). Calcium spikes, waves and oscillations in plant development and biotic interactions. *Nature Plants*, 6(7), 750-759. <https://doi.org/10.1038/s41477-020-0667-6>
- Tikhonov, D. B., & Zhorov, B. S. (2020). The pore domain in glutamate-gated ion channels: Structure, drug binding and similarity with potassium channels. *Biochimica et Biophysica Acta (BBA) - Biomembranes*, 1862(10), 183401. <https://doi.org/10.1016/j.bbamem.2020.183401>

- Torres-Martínez, H. H., Rodríguez-Alonso, G., Shishkova, S., & Dubrovsky, J. G. (2019). Lateral Root Primordium Morphogenesis in Angiosperms. *Frontiers in Plant Science*, 10, 206. <https://doi.org/10.3389/fpls.2019.00206>
- Toyota, M., Spencer, D., Sawai-Toyota, S., Jiaqi, W., Zhang, T., Koo, A. J., Howe, G. A., & Gilroy, S. (2018). Glutamate triggers long-distance, calcium-based plant defense signaling. *Science*, 361(6407), 1112-1115. <https://doi.org/10.1126/science.aat7744>
- Traynelis, S. F., Wollmuth, L. P., McBain, C. J., Menniti, F. S., Vance, K. M., Ogden, K. K., Hansen, K. B., Yuan, H., Myers, S. J., & Dingledine, R. (2010). Glutamate Receptor Ion Channels: Structure, Regulation, and Function. *Pharmacological Reviews*, 62(3), 405-496. <https://doi.org/10.1124/pr.109.002451>
- Twomey, E. C., & Sobolevsky, A. I. (2018). Structural Mechanisms of Gating in Ionotropic Glutamate Receptors. *Biochemistry*, 57(3), 267-276. <https://doi.org/10.1021/acs.biochem.7b00891>
- Twomey, E. C., Yelshanskaya, M. V., Grassucci, R. A., Frank, J., & Sobolevsky, A. I. (2017a). Channel opening and gating mechanism in AMPA-subtype glutamate receptors. *Nature*, 549(7670), 60-65. <https://doi.org/10.1038/nature23479>
- Twomey, E. C., Yelshanskaya, M. V., Grassucci, R. A., Frank, J., & Sobolevsky, A. I. (2017b). Structural Bases of Desensitization in AMPA Receptor-Auxiliary Subunit Complexes. *Neuron*, 94(3), 569-580.e565. <https://doi.org/10.1016/j.neuron.2017.04.025>
- Vincill, E. D., Clarin, A. E., Molenda, J. N., & Spalding, E. P. (2013). Interacting Glutamate Receptor-Like Proteins in Phloem Regulate Lateral Root Initiation in Arabidopsis. *The Plant Cell*, 25(4), 1304-1313. <https://doi.org/10.1105/tpc.113.110668>



- Volk, L., Chiu, S.-L., Sharma, K., & Huganir, R. L. (2015). Glutamate Synapses in Human Cognitive Disorders. *Annual Review of Neuroscience*, 38(1), 127-149.  
<https://doi.org/10.1146/annurev-neuro-071714-033821>
- Wachsman, G., & Benfey, P. N. (2020). Lateral Root Initiation: The Emergence of New Primordia Following Cell Death. *Current Biology*, 30(3), R121-R122.  
<https://doi.org/10.1016/j.cub.2019.12.032>
- Weiland, M., Mancuso, S., Baluska, F., Weiland, M., Mancuso, S., & Baluska, F. (2015). Signalling via glutamate and GLRs in *Arabidopsis thaliana*. *Functional Plant Biology*, 43(1), 1-25. <https://doi.org/10.1071/FP15109>
- WHO, F. I. U. W. (2022). *The state of Food Security and Nutrition in the World 2022*. *The State of Food Security and Nutrition in the World 2022. Repurposing food and agricultural policies to make healthy diets more affordable.* (978-92-5-136499-4).  
<https://www.fao.org/3/cc0639en/online/cc0639en.html>  
[files/802/cc0639en.html](https://www.fao.org/3/cc0639en/html/802/cc0639en.html)
- Wo, Z. G., & Oswald, R. E. (1994). Transmembrane topology of two kainate receptor subunits revealed by N-glycosylation. *Proceedings of the National Academy of Sciences of the United States of America*, 91(15), 7154-7158.  
<https://www.ncbi.nlm.nih.gov/pmc/articles/PMC44357/>
- Wollmuth, L. P., & Sobolevsky, A. I. (2004). Structure and gating of the glutamate receptor ion channel. *Trends in Neurosciences*, 27(6), 321-328.  
<https://doi.org/10.1016/j.tins.2004.04.005>

- Wu, S.-H., Ho, C.-T., Nah, S.-L., & Chau, C.-F. (2014). Global Hunger: A Challenge to Agricultural, Food, and Nutritional Sciences. *Critical Reviews in Food Science and Nutrition*, 54(2), 151-162. <https://doi.org/10.1080/10408398.2011.578764>
- Wudick, M. M., Michard, E., Oliveira Nunes, C., & Feijó, J. A. (2018). Comparing plant and animal glutamate receptors: common traits but different fates? *Journal of Experimental Botany*, 69(17), 4151-4163. <https://doi.org/10.1093/jxb/ery153>
- Wudick, M. M., Portes, M. T., Michard, E., Rosas-Santiago, P., Lizzio, M. A., Nunes, C. O., Campos, C., Santa Cruz Damineli, D., Carvalho, J. C., Lima, P. T., Pantoja, O., & Feijó, J. A. (2018). CORNICHON sorting and regulation of GLR channels underlie pollen tube Ca<sup>2+</sup> homeostasis. *Science*, 360(6388), 533-536. <https://doi.org/10.1126/science.aar6464>
- Yang, J., Sun, C., Fu, D., & Yu, T. (2017). Test for l-glutamate inhibition of growth of *Alternaria alternata* by inducing resistance in tomato fruit. *Food Chemistry*, 230, 145-153. <https://doi.org/10.1016/j.foodchem.2017.03.033>
- Yelshanskaya, M. V., Patel, D. S., Kottke, C. M., Kurnikova, M. G., & Sobolevsky, A. I. (2022). Opening of glutamate receptor channel to subconductance levels. *Nature*, 605(7908), 172-178. <https://doi.org/10.1038/s41586-022-04637-w>
- Yelshanskaya, M. V., Singh, A. K., Sampson, J. M., Narangoda, C., Kurnikova, M., & Sobolevsky, A. I. (2016). Structural Bases of Noncompetitive Inhibition of AMPA-Subtype Ionotropic Glutamate Receptors by Antiepileptic Drugs. *Neuron*, 91(6), 1305-1315. <https://doi.org/10.1016/j.neuron.2016.08.012>
- Yelshanskaya, M. V., & Sobolevsky, A. I. (2022). Structural Insights into Function of Ionotropic Glutamate Receptors. *Biochemistry (Moscow), Supplement Series A: Membrane and Cell Biology*, 16(3), 190-206. <https://doi.org/10.1134/S1990747822040043>

- Yu, B., Wu, Q., Li, X., Zeng, R., Min, Q., & Huang, J. (2022). GLUTAMATE RECEPTOR-like gene OsGLR3.4 is required for plant growth and systemic wound signaling in rice (*Oryza sativa*). *New Phytologist*, 233(3), 1238-1256. <https://doi.org/10.1111/nph.17859>
- Zhou, Y., & Danbolt, N. C. (2014). Glutamate as a neurotransmitter in the healthy brain. *Journal of Neural Transmission*, 121(8), 799-817. <https://doi.org/10.1007/s00702-014-1180-8>
- Zhu, J.-K. (2002). Salt and Drought Stress Signal Transduction in Plants. *Annual review of plant biology*, 53, 247-273. <https://doi.org/10.1146/annurev.arplant.53.091401.143329>
- Zhu, J.-K. (2016). Abiotic Stress Signaling and Responses in Plants. *Cell*, 167(2), 313-324. <https://doi.org/10.1016/j.cell.2016.08.029>
- Acosta, I. F., & Farmer, E. E. (2010). Jasmonates. *The Arabidopsis Book / American Society of Plant Biologists*, 8, e0129. <https://doi.org/10.1199/tab.0129>
- Adhikari, P. B., Liu, X., & Kasahara, R. D. (2020). Mechanics of Pollen Tube Elongation: A Perspective. *Frontiers in Plant Science*, 11. <https://www.frontiersin.org/articles/10.3389/fpls.2020.589712>
- Armstrong, N., & Gouaux, E. (2000). Mechanisms for Activation and Antagonism of an AMPA-Sensitive Glutamate Receptor: Crystal Structures of the GluR2 Ligand Binding Core. *Neuron*, 28(1), 165-181. [https://doi.org/10.1016/S0896-6273\(00\)00094-5](https://doi.org/10.1016/S0896-6273(00)00094-5)
- Armstrong, N., Sun, Y., Chen, G.-Q., & Gouaux, E. (1998). Structure of a glutamate-receptor ligand-binding core in complex with kainate. *Nature*, 395(6705), 913-917. <https://doi.org/10.1038/27692>
- Arvola, M., & Keinänen, K. (1996). Characterization of the Ligand-binding Domains of Glutamate Receptor (GluR)-B and GluR-D Subunits Expressed in *Escherichia coli* as

Periplasmic Proteins\*. *Journal of Biological Chemistry*, 271(26), 15527-15532.

<https://doi.org/10.1074/jbc.271.26.15527>

Auerbach, A., & Zhou, Y. (2005). Gating Reaction Mechanisms for NMDA Receptor Channels.

*Journal of Neuroscience*, 25(35), 7914-7923. <https://doi.org/10.1523/JNEUROSCI.1471-05.2005>

Baum, D. (2008). Reading a Phylogenetic Tree: The Meaning of Monophyletic Groups.

*1(1):190*. <http://www.nature.com/scitable/topicpage/reading-a-phylogenetic-tree-the-meaning-of-41956>

files/932/reading-a-phylogenetic-tree-the-meaning-of-41956.html

Bethke, G., Unthan, T., Uhrig, J. F., Pöschl, Y., Gust, A. A., Scheel, D., & Lee, J. (2009). Flg22

regulates the release of an ethylene response factor substrate from MAP kinase 6 in

*Arabidopsis thaliana* via ethylene signaling. *Proceedings of the National Academy of*

*Sciences*, 106(19), 8067-8072. <https://doi.org/10.1073/pnas.0810206106>

Bowie, D. (2010). Ion-dependent gating of kainate receptors. *The Journal of Physiology*, 588(Pt

1), 67-81. <https://doi.org/10.1113/jphysiol.2009.178863>

Brenner, E. D., Stahlberg, R., Mancuso, S., Vivanco, J., Baluška, F., & Van Volkenburgh, E.

(2006). Plant neurobiology: an integrated view of plant signaling. *Trends in Plant*

*Science*, 11(8), 413-419. <https://doi.org/10.1016/j.tplants.2006.06.009>

Brodth, S., Six, J., Feenstra, G., Ingels, C. & Campbell, D. . (2011). Sustainable Agriculture

*Nature Education Knowledge* 3(10):1.

<https://www.nature.com/scitable/knowledge/library/sustainable-agriculture-23562787/>

files/837/sustainable-agriculture-23562787.html

- Brogi, S., Campiani, G., Brindisi, M., & Butini, S. (2019). Allosteric Modulation of Ionotropic Glutamate Receptors: An Outlook on New Therapeutic Approaches To Treat Central Nervous System Disorders. *ACS Medicinal Chemistry Letters*, 10(3), 228-236.  
<https://doi.org/10.1021/acsmmedchemlett.8b00450>
- Burada, A. P., Vinnakota, R., & Kumar, J. (2020a). The architecture of GluD2 ionotropic delta glutamate receptor elucidated by cryo-EM. *Journal of Structural Biology*, 211(2), 107546. <https://doi.org/10.1016/j.jsb.2020.107546>
- Burada, A. P., Vinnakota, R., & Kumar, J. (2020b). Cryo-EM structures of the ionotropic glutamate receptor GluD1 reveal a non-swapped architecture. *Nature Structural & Molecular Biology*, 27(1), 84-91. <https://doi.org/10.1038/s41594-019-0359-y>
- Carrillo, E., Gonzalez, C. U., Berka, V., & Jayaraman, V. (2021). Delta glutamate receptors are functional glycine- and D-serine-gated cation channels in situ. *Science Advances*, 7(52), eabk2200. <https://doi.org/10.1126/sciadv.abk2200>
- Chang, H.-R., & Kuo, C.-C. (2008). The Activation Gate and Gating Mechanism of the NMDA Receptor. *Journal of Neuroscience*, 28(7), 1546-1556.  
<https://doi.org/10.1523/JNEUROSCI.3485-07.2008>
- Chen, J.-T., & Heidari, P. (2020). Cell Signaling in Model Plants. *International Journal of Molecular Sciences*, 21(17), 6062. <https://doi.org/10.3390/ijms21176062>
- Chen, J., & Ham, B.-K. (2022). Systemic Signaling: A Role in Propelling Crop Yield. *Plants*, 11(11), 1400. <https://doi.org/10.3390/plants11111400>
- Chen, J., Jing, Y., Zhang, X., Li, L., Wang, P., Zhang, S., Zhou, H., & Wu, J. (2016). Evolutionary and Expression Analysis Provides Evidence for the Plant Glutamate-like

- Receptors Family is Involved in Woody Growth-related Function. *Scientific Reports*, 6(1), 32013. <https://doi.org/10.1038/srep32013>
- Chen, N., Li, B., Murphy, T. H., & Raymond, L. A. (2004). Site within N-Methyl-d-aspartate Receptor Pore Modulates Channel Gating. *Molecular Pharmacology*, 65(1), 157-164. <https://doi.org/10.1124/mol.65.1.157>
- Chen, S., Zhao, Y., Wang, Y., Shekhar, M., Tajkhorshid, E., & Gouaux, E. (2017). Activation and Desensitization Mechanism of AMPA Receptor-TARP Complex by Cryo-EM. *Cell*, 170(6), 1234-1246.e1214. <https://doi.org/10.1016/j.cell.2017.07.045>
- Cheng, Y., Zhang, X., Sun, T., Tian, Q., & Zhang, W.-H. (2018). Glutamate Receptor Homolog3.4 is Involved in Regulation of Seed Germination Under Salt Stress in Arabidopsis. *Plant and Cell Physiology*, 59(5), 978-988. <https://doi.org/10.1093/pcp/pcy034>
- Chiu, J., DeSalle, R., Lam, H. M., Meisel, L., & Coruzzi, G. (1999). Molecular evolution of glutamate receptors: a primitive signaling mechanism that existed before plants and animals diverged. *Molecular Biology and Evolution*, 16(6), 826-838. <https://doi.org/10.1093/oxfordjournals.molbev.a026167>
- Cull-Candy, S. G., & Usowicz, M. M. (1987). Multiple-conductance channels activated by excitatory amino acids in cerebellar neurons. *Nature*, 325(6104), 525-528. <https://doi.org/10.1038/325525a0>
- De Bortoli, S., Teardo, E., Szabò, I., Morosinotto, T., & Alboresi, A. (2016). Evolutionary insight into the ionotropic glutamate receptor superfamily of photosynthetic organisms. *Biophysical Chemistry*, 218, 14-26. <https://doi.org/10.1016/j.bpc.2016.07.004>

- Deinlein, U., Stephan, A. B., Horie, T., Luo, W., Xu, G., & Schroeder, J. I. (2014). Plant salt-tolerance mechanisms. *Trends in Plant Science*, 19(6), 371-379.  
<https://doi.org/10.1016/j.tplants.2014.02.001>
- Dolphin, A. C., Insel, P. A., Blaschke, T. F., & Meyer, U. A. (2020). Introduction to the Theme “Ion Channels and Neuropharmacology: From the Past to the Future”. *Annual Review of Pharmacology and Toxicology*, 60(1), 1-6. <https://doi.org/10.1146/annurev-pharmtox-082719-110050>
- Dürr, K. L., Chen, L., Stein, R. A., De Zorzi, R., Folea, I. M., Walz, T., McHaourab, H. S., & Gouaux, E. (2014). Structure and Dynamics of AMPA Receptor GluA2 in Resting, Pre-Open, and Desensitized States. *Cell*, 158(4), 778-792.  
<https://doi.org/10.1016/j.cell.2014.07.023>
- Fernández-Marcos, M., Desvoyes, B., Manzano, C., Liberman, L. M., Benfey, P. N., del Pozo, J. C., & Gutierrez, C. (2017). Control of Arabidopsis lateral root primordium boundaries by MYB36. *New Phytologist*, 213(1), 105-112. <https://doi.org/10.1111/nph.14304>
- Forde, B. G., & Roberts, M. R. (2014). Glutamate receptor-like channels in plants: a role as amino acid sensors in plant defence? *F1000Prime Reports*, 6, 37.  
<https://doi.org/10.12703/P6-37>
- Goto, Y., Maki, N., Ichihashi, Y., Kitazawa, D., Igarashi, D., Kadota, Y., & Shirasu, K. (2020). Exogenous Treatment with Glutamate Induces Immune Responses in Arabidopsis. *Molecular Plant-Microbe Interactions®*, 33(3), 474-487. <https://doi.org/10.1094/MPMI-09-19-0262-R>
- Green, M. N., Gangwar, S. P., Michard, E., Simon, A. A., Portes, M. T., Barbosa-Caro, J., Wudick, M. M., Lizzio, M. A., Klykov, O., Yelshanskaya, M. V., Feijó, J. A., &



- Sobolevsky, A. I. (2021). Structure of the *Arabidopsis thaliana* glutamate receptor-like channel GLR3.4. *Molecular Cell*, 81(15), 3216-3226.e3218.  
<https://doi.org/10.1016/j.molcel.2021.05.025>
- Grenzi, M., Bonza, M. C., & Costa, A. (2022). Signaling by plant glutamate receptor-like channels: What else! *Current Opinion in Plant Biology*, 68, 102253.  
<https://doi.org/10.1016/j.pbi.2022.102253>
- Hansen, K. B., Wollmuth, L. P., Bowie, D., Furukawa, H., Menniti, F. S., Sobolevsky, A. I., Swanson, G. T., Swanger, S. A., Greger, I. H., Nakagawa, T., McBain, C. J., Jayaraman, V., Low, C.-M., Dell'Acqua, M. L., Diamond, J. S., Camp, C. R., Perszyk, R. E., Yuan, H., & Traynelis, S. F. (2021). Structure, Function, and Pharmacology of Glutamate Receptor Ion Channels. *Pharmacological Reviews*, 73(4), 1469-1658.  
<https://doi.org/10.1124/pharmrev.120.000131>
- Herguedas, B., Krieger, J., & Greger, I. H. (2013). Receptor Heteromeric Assembly—How It Works and Why It Matters. In *Progress in Molecular Biology and Translational Science* (Vol. 117, pp. 361-386). Elsevier.  
<https://linkinghub.elsevier.com/retrieve/pii/B9780123869319000131>
- Hollmann, M., Maron, C., & Heinemann, S. (1994). N-glycosylation site tagging suggests a three transmembrane domain topology for the glutamate receptor GluR1. *Neuron*, 13(6), 1331-1343. [https://doi.org/10.1016/0896-6273\(94\)90419-7](https://doi.org/10.1016/0896-6273(94)90419-7)
- Huettnner, J. E. (2015). Glutamate receptor pores. *The Journal of Physiology*, 593(1), 49-59.  
<https://doi.org/10.1113/jphysiol.2014.272724>
- Jahr, C. E., & Stevens, C. F. (1987). Glutamate activates multiple single channel conductances in hippocampal neurons. *Nature*, 325(6104), 522-525. <https://doi.org/10.1038/325522a0>

- Jin, L., Cai, Y., Sun, C., Huang, Y., & Yu, T. (2019). Exogenous l-glutamate treatment could induce resistance against *Penicillium expansum* in pear fruit by activating defense-related proteins and amino acids metabolism. *Postharvest Biology and Technology*, 150, 148-157. <https://doi.org/10.1016/j.postharvbio.2018.11.009>
- Jin, R., Singh, S. K., Gu, S., Furukawa, H., Sobolevsky, A. I., Zhou, J., Jin, Y., & Gouaux, E. (2009). Crystal structure and association behaviour of the GluR2 amino-terminal domain. *The EMBO Journal*, 28(12), 1812-1823. <https://doi.org/10.1038/emboj.2009.140>
- Jones, J. D. G., & Dangl, J. L. (2006). The plant immune system. *Nature*, 444(7117), 323-329. <https://doi.org/10.1038/nature05286>
- Kadotani, N., Akagi, A., Takatsuji, H., Miwa, T., & Igarashi, D. (2016). Exogenous proteinogenic amino acids induce systemic resistance in rice. *BMC Plant Biology*, 16(1), 60. <https://doi.org/10.1186/s12870-016-0748-x>
- Katz, B., & Thesleff, S. (1957). A study of the ‘desensitization’ produced by acetylcholine at the motor end-plate. *The Journal of Physiology*, 138(1), 63-80. <https://doi.org/10.1113/jphysiol.1957.sp005838>
- Kc, K. B., Dias, G. M., Veeramani, A., Swanton, C. J., Fraser, D., Steinke, D., Lee, E., Wittman, H., Farber, J. M., Dunfield, K., McCann, K., Anand, M., Campbell, M., Rooney, N., Raine, N. E., Acker, R. V., Hanner, R., Pascoal, S., Sharif, S., . . . Fraser, E. D. G. (2018). When too much isn’t enough: Does current food production meet global nutritional needs? *PLOS ONE*, 13(10), e0205683. <https://doi.org/10.1371/journal.pone.0205683>
- Khanra, N., Brown, P. M. G. E., Perozzo, A. M., Bowie, D., & Meyerson, J. R. (2021). Architecture and structural dynamics of the heteromeric GluK2/K5 kainate receptor. *eLife*, 10, e66097. <https://doi.org/10.7554/eLife.66097>

- Kim, M.-J., Jeon, B. W., Oh, E., Seo, P. J., & Kim, J. (2021). Peptide Signaling during Plant Reproduction. *Trends in Plant Science*, 26(8), 822-835.  
<https://doi.org/10.1016/j.tplants.2021.02.008>
- Klykov, O., Gangwar, S. P., Yelshanskaya, M. V., Yen, L., & Sobolevsky, A. I. (2021). Structure and desensitization of AMPA receptor complexes with type II TARP  $\gamma 5$  and GSG1L. *Molecular Cell*, 81(23), 4771-4783.e4777.  
<https://doi.org/10.1016/j.molcel.2021.09.030>
- Kunishima, N., Shimada, Y., Tsuji, Y., Sato, T., Yamamoto, M., Kumasaka, T., Nakanishi, S., Jingami, H., & Morikawa, K. (2000). Structural basis of glutamate recognition by a dimeric metabotropic glutamate receptor. *Nature*, 407(6807), 971-977.  
<https://doi.org/10.1038/35039564>
- Kussius, C. L., Popescu, A. M., & Popescu, G. K. (2010). Agonist-specific Gating of NMDA Receptors. *Channels (Austin, Tex.)*, 4(2), 78-82.  
<https://www.ncbi.nlm.nih.gov/pmc/articles/PMC3150751/>
- Kuusinen, A., Arvola, M., & Keinänen, K. (1995). Molecular dissection of the agonist binding site of an AMPA receptor. *The EMBO Journal*, 14(24), 6327-6332.  
<https://www.ncbi.nlm.nih.gov/pmc/articles/PMC394757/>
- Lam, H.-M., Chiu, J., Hsieh, M.-H., Meisel, L., Oliveira, I. C., Shin, M., & Coruzzi, G. (1998). Glutamate-receptor genes in plants. *Nature*, 396(6707), 125-126.  
<https://doi.org/10.1038/24066>
- Li, F., Wang, J., Ma, C., Zhao, Y., Wang, Y., Hasi, A., & Qi, Z. (2013). Glutamate Receptor-Like Channel3.3 Is Involved in Mediating Glutathione-Triggered Cytosolic Calcium

- Transients, Transcriptional Changes, and Innate Immunity Responses in Arabidopsis. *Plant Physiology*, 162(3), 1497-1509. <https://doi.org/10.1104/pp.113.217208>
- Mauseth, J. D. (2021). *Botany: An Introduction to Plant Biology* (Vol. Vol Seventh edition.). Jones & Bartlett Learning.
- <https://web.s.ebscohost.com/ehost/ebookviewer/ebook/bmxlYmtfXzIyNTgzOTZfX0FO0?sid=52a09324-d9b2-464d-8484-96ff9c271b8f@redis&vid=0&format=EK&rid=1files/1447/bmxlYmtfXzIyNTgzOTZfX0FO0.html>
- Meyerhoff, O., Müller, K., Roelfsema, M. R. G., Latz, A., Lacombe, B., Hedrich, R., Dietrich, P., & Becker, D. (2005). AtGLR3.4, a glutamate receptor channel-like gene is sensitive to touch and cold. *Planta*, 222(3), 418-427. <https://www.jstor.org/stable/23389017>
- Michard, E., Lima, P. T., Borges, F., Silva, A. C., Portes, M. T., Carvalho, J. E., Gilliam, M., Liu, L.-H., Obermeyer, G., & Feijó, J. A. (2011). Glutamate Receptor–Like Genes Form Ca<sup>2+</sup> Channels in Pollen Tubes and Are Regulated by Pistil d-Serine. *Science*, 332(6028), 434-437. <https://doi.org/10.1126/science.1201101>
- Michard, E., Simon, A. A., Tavares, B., Wudick, M. M., & Feijó, J. A. (2017). Signaling with Ions: The Keystone for Apical Cell Growth and Morphogenesis in Pollen Tubes1[OPEN]. *Plant Physiology*, 173(1), 91-111. <https://doi.org/10.1104/pp.16.01561>
- Moe-Lange, J., Gappel, N. M., Machado, M., Wudick, M. M., Sies, C. S. A., Schott-Verdugo, S. N., Bonus, M., Mishra, S., Hartwig, T., Bezruczyk, M., Basu, D., Farmer, E. E., Gohlke, H., Malkovskiy, A., Haswell, E. S., Lercher, M. J., Ehrhardt, D. W., Frommer, W. B., & Kleist, T. J. (2021). Interdependence of a mechanosensitive anion channel and glutamate receptors in distal wound signaling. *Science Advances*, 7(37), eabg4298. <https://doi.org/10.1126/sciadv.abg4298>

- Nayeem, N., Mayans, O., & Green, T. (2011). Conformational Flexibility of the Ligand-Binding Domain Dimer in Kainate Receptor Gating and Desensitization. *Journal of Neuroscience*, 31(8), 2916-2924. <https://doi.org/10.1523/JNEUROSCI.4771-10.2011>
- Nguyen, C. T., Kurenda, A., Stolz, S., Chételat, A., & Farmer, E. E. (2018). Identification of cell populations necessary for leaf-to-leaf electrical signaling in a wounded plant. *Proceedings of the National Academy of Sciences*, 115(40), 10178-10183. <https://doi.org/10.1073/pnas.1807049115>
- Pankevich, D. E. (2011). Overview of the Glutamatergic System. In a. B. M. A. Miriam Davis (Ed.), *Institute of Medicine (US) Forum on Neuroscience and Nervous System Disorders. Glutamate-Related Biomarkers in Drug Development for Disorders of the Nervous System: Workshop Summary*. Washington (DC): National Academies Press (US).
- Pechanova, O., & Pechan, T. (2017). Chapter 3 - Proteomics as a Tool to Understand Maize Biology and to Improve Maize Crop. In M. L. Colgrave (Ed.), *Proteomics in Food Science* (pp. 35-56). Academic Press. <https://www.sciencedirect.com/science/article/pii/B9780128040072000035>
- [files/1443/B9780128040072000035.html](https://www.sciencedirect.com/science/article/pii/B9780128040072000035)
- Perrais, D., Veran, J., & Mulle, C. (2010). Gating and permeation of kainate receptors: differences unveiled. *Trends in Pharmacological Sciences*, 31(11), 516-522. <https://doi.org/10.1016/j.tips.2010.08.004>
- Price, M. B., Jelesko, J., & Okumoto, S. (2012). Glutamate Receptor Homologs in Plants: Functions and Evolutionary Origins. *Frontiers in Plant Science*, 3, 235. <https://doi.org/10.3389/fpls.2012.00235>

- Quiococho, F. A., & Ledvina, P. S. (1996). Atomic structure and specificity of bacterial periplasmic receptors for active transport and chemotaxis: variation of common themes. *Molecular Microbiology*, 20(1), 17-25. <https://doi.org/10.1111/j.1365-2958.1996.tb02484.x>
- Relations, F. M. (2021). FAO - News Article: Climate change fans spread of pests and threatens plants and crops, new FAO study. *FAO Food and Agriculture Organization of the United Nations*. <https://www.fao.org/news/story/en/item/1402920/icode/>
- Sather, W., Dieudonné, S., MacDonald, J. F., & Ascher, P. (1992). Activation and desensitization of N-methyl-D-aspartate receptors in nucleated outside-out patches from mouse neurones. *The Journal of Physiology*, 450, 643-672. <https://www.ncbi.nlm.nih.gov/pmc/articles/PMC1176143/>
- Sather, W., Johnson, J. W., Henderson, G., & Ascher, P. (1990). Glycine-insensitive desensitization of NMDA responses in cultured mouse embryonic neurons. *Neuron*, 4(5), 725-731. [https://doi.org/10.1016/0896-6273\(90\)90198-O](https://doi.org/10.1016/0896-6273(90)90198-O)
- Scientific review of the impact of climate change on plant pests*. (2021). FAO on behalf of the IPPC Secretariat. <http://www.fao.org/documents/card/en/c/cb4769en>
- Shipman, E. N., Yu, J., Zhou, J., Albornoz, K., & Beckles, D. M. (2021). Can gene editing reduce postharvest waste and loss of fruit, vegetables, and ornamentals? *Horticulture Research*, 8(1), 1-21. <https://doi.org/10.1038/s41438-020-00428-4>
- Smith, T. C., & Howe, J. R. (2000). Concentration-dependent substate behavior of native AMPA receptors. *Nature Neuroscience*, 3(10), 992-997. <https://doi.org/10.1038/79931>

- Sobolevsky, A. I., Rosconi, M. P., & Gouaux, E. (2009). X-ray structure of AMPA-subtype glutamate receptor: symmetry and mechanism. *Nature*, 462(7274), 745-756.  
<https://doi.org/10.1038/nature08624>
- Stern-Bach, Y., Bettler, B., Hartley, M., Sheppard, P. O., O'Hara, P. J., & Heinemann, S. F. (1994). Agonist selectivity of glutamate receptors is specified by two domains structurally related to bacterial amino acid-binding proteins. *Neuron*, 13(6), 1345-1357.  
[https://doi.org/10.1016/0896-6273\(94\)90420-0](https://doi.org/10.1016/0896-6273(94)90420-0)
- Stroebe, D., & Paoletti, P. (2021). Architecture and function of NMDA receptors: an evolutionary perspective. *The Journal of Physiology*, 599(10), 2615-2638.  
<https://doi.org/10.1113/JP279028>
- Teardo, E., Carraretto, L., De Bortoli, S., Costa, A., Behera, S., Wagner, R., Lo Schiavo, F., Formentin, E., & Szabo, I. (2015). Alternative Splicing-Mediated Targeting of the Arabidopsis GLUTAMATE RECEPTOR3.5 to Mitochondria Affects Organelle Morphology1. *Plant Physiology*, 167(1), 216-227. <https://doi.org/10.1104/pp.114.242602>
- Teardo, E., Formentin, E., Segalla, A., Giacometti, G. M., Marin, O., Zanetti, M., Lo Schiavo, F., Zoratti, M., & Szabò, I. (2011). Dual localization of plant glutamate receptor AtGLR3.4 to plastids and plasmamembrane. *Biochimica et Biophysica Acta (BBA) - Bioenergetics*, 1807(3), 359-367. <https://doi.org/10.1016/j.bbabi.2010.11.008>
- Tian, W., Wang, C., Gao, Q., Li, L., & Luan, S. (2020). Calcium spikes, waves and oscillations in plant development and biotic interactions. *Nature Plants*, 6(7), 750-759.  
<https://doi.org/10.1038/s41477-020-0667-6>
- Tikhonov, D. B., & Zhorov, B. S. (2020). The pore domain in glutamate-gated ion channels: Structure, drug binding and similarity with potassium channels. *Biochimica et Biophysica*

- Acta (BBA) - Biomembranes*, 1862(10), 183401.  
<https://doi.org/10.1016/j.bbamem.2020.183401>
- Torres-Martínez, H. H., Rodríguez-Alonso, G., Shishkova, S., & Dubrovsky, J. G. (2019). Lateral Root Primordium Morphogenesis in Angiosperms. *Frontiers in Plant Science*, 10, 206. <https://doi.org/10.3389/fpls.2019.00206>
- Toyota, M., Spencer, D., Sawai-Toyota, S., Jiaqi, W., Zhang, T., Koo, A. J., Howe, G. A., & Gilroy, S. (2018). Glutamate triggers long-distance, calcium-based plant defense signaling. *Science*, 361(6407), 1112-1115. <https://doi.org/10.1126/science.aat7744>
- Traynelis, S. F., Wollmuth, L. P., McBain, C. J., Menniti, F. S., Vance, K. M., Ogden, K. K., Hansen, K. B., Yuan, H., Myers, S. J., & Dingledine, R. (2010). Glutamate Receptor Ion Channels: Structure, Regulation, and Function. *Pharmacological Reviews*, 62(3), 405-496. <https://doi.org/10.1124/pr.109.002451>
- Twomey, E. C., & Sobolevsky, A. I. (2018). Structural Mechanisms of Gating in Ionotropic Glutamate Receptors. *Biochemistry*, 57(3), 267-276.  
<https://doi.org/10.1021/acs.biochem.7b00891>
- Twomey, E. C., Yelshanskaya, M. V., Grassucci, R. A., Frank, J., & Sobolevsky, A. I. (2017a). Channel opening and gating mechanism in AMPA-subtype glutamate receptors. *Nature*, 549(7670), 60-65. <https://doi.org/10.1038/nature23479>
- Twomey, E. C., Yelshanskaya, M. V., Grassucci, R. A., Frank, J., & Sobolevsky, A. I. (2017b). Structural Bases of Desensitization in AMPA Receptor-Auxiliary Subunit Complexes. *Neuron*, 94(3), 569-580.e565. <https://doi.org/10.1016/j.neuron.2017.04.025>



- Vincill, E. D., Clarin, A. E., Molenda, J. N., & Spalding, E. P. (2013). Interacting Glutamate Receptor-Like Proteins in Phloem Regulate Lateral Root Initiation in Arabidopsis. *The Plant Cell*, 25(4), 1304-1313. <https://doi.org/10.1105/tpc.113.110668>
- Volk, L., Chiu, S.-L., Sharma, K., & Huganir, R. L. (2015). Glutamate Synapses in Human Cognitive Disorders. *Annual Review of Neuroscience*, 38(1), 127-149. <https://doi.org/10.1146/annurev-neuro-071714-033821>
- Wachsman, G., & Benfey, P. N. (2020). Lateral Root Initiation: The Emergence of New Primordia Following Cell Death. *Current Biology*, 30(3), R121-R122. <https://doi.org/10.1016/j.cub.2019.12.032>
- Weiland, M., Mancuso, S., Baluska, F., Weiland, M., Mancuso, S., & Baluska, F. (2015). Signalling via glutamate and GLRs in Arabidopsis thaliana. *Functional Plant Biology*, 43(1), 1-25. <https://doi.org/10.1071/FP15109>
- WHO, F. I. U. W. (2022). *The state of Food Security and Nutrition in the World 2022*
- The State of Food Security and Nutrition in the World 2022. Repurposing food and agricultural policies to make healthy diets more affordable.* (978-92-5-136499-4). <https://www.fao.org/3/cc0639en/online/cc0639en.html>
- files/802/cc0639en.html
- Wo, Z. G., & Oswald, R. E. (1994). Transmembrane topology of two kainate receptor subunits revealed by N-glycosylation. *Proceedings of the National Academy of Sciences of the United States of America*, 91(15), 7154-7158. <https://www.ncbi.nlm.nih.gov/pmc/articles/PMC44357/>

- Wollmuth, L. P., & Sobolevsky, A. I. (2004). Structure and gating of the glutamate receptor ion channel. *Trends in Neurosciences*, 27(6), 321-328.  
<https://doi.org/10.1016/j.tins.2004.04.005>
- Wu, S.-H., Ho, C.-T., Nah, S.-L., & Chau, C.-F. (2014). Global Hunger: A Challenge to Agricultural, Food, and Nutritional Sciences. *Critical Reviews in Food Science and Nutrition*, 54(2), 151-162. <https://doi.org/10.1080/10408398.2011.578764>
- Wudick, M. M., Michard, E., Oliveira Nunes, C., & Feijó, J. A. (2018). Comparing plant and animal glutamate receptors: common traits but different fates? *Journal of Experimental Botany*, 69(17), 4151-4163. <https://doi.org/10.1093/jxb/ery153>
- Wudick, M. M., Portes, M. T., Michard, E., Rosas-Santiago, P., Lizzio, M. A., Nunes, C. O., Campos, C., Santa Cruz Damineli, D., Carvalho, J. C., Lima, P. T., Pantoja, O., & Feijó, J. A. (2018). CORNICHON sorting and regulation of GLR channels underlie pollen tube Ca<sup>2+</sup> homeostasis. *Science*, 360(6388), 533-536. <https://doi.org/10.1126/science.aar6464>
- Yang, J., Sun, C., Fu, D., & Yu, T. (2017). Test for l-glutamate inhibition of growth of *Alternaria alternata* by inducing resistance in tomato fruit. *Food Chemistry*, 230, 145-153.  
<https://doi.org/10.1016/j.foodchem.2017.03.033>
- Yelshanskaya, M. V., Patel, D. S., Kottke, C. M., Kurnikova, M. G., & Sobolevsky, A. I. (2022). Opening of glutamate receptor channel to subconductance levels. *Nature*, 605(7908), 172-178. <https://doi.org/10.1038/s41586-022-04637-w>
- Yelshanskaya, M. V., Singh, A. K., Sampson, J. M., Narangoda, C., Kurnikova, M., & Sobolevsky, A. I. (2016). Structural Bases of Noncompetitive Inhibition of AMPA-Subtype Ionotropic Glutamate Receptors by Antiepileptic Drugs. *Neuron*, 91(6), 1305-1315. <https://doi.org/10.1016/j.neuron.2016.08.012>

- Yelshanskaya, M. V., & Sobolevsky, A. I. (2022). Structural Insights into Function of Ionotropic Glutamate Receptors. *Biochemistry (Moscow), Supplement Series A: Membrane and Cell Biology*, 16(3), 190-206. <https://doi.org/10.1134/S1990747822040043>
- Yu, B., Wu, Q., Li, X., Zeng, R., Min, Q., & Huang, J. (2022). GLUTAMATE RECEPTOR-like gene OsGLR3.4 is required for plant growth and systemic wound signaling in rice (*Oryza sativa*). *New Phytologist*, 233(3), 1238-1256. <https://doi.org/10.1111/nph.17859>
- Zhou, Y., & Danbolt, N. C. (2014). Glutamate as a neurotransmitter in the healthy brain. *Journal of Neural Transmission*, 121(8), 799-817. <https://doi.org/10.1007/s00702-014-1180-8>
- Zhu, J.-K. (2002). Salt and Drought Stress Signal Transduction in Plants. *Annual review of plant biology*, 53, 247-273. <https://doi.org/10.1146/annurev.arplant.53.091401.143329>
- Zhu, J.-K. (2016). Abiotic Stress Signaling and Responses in Plants. *Cell*, 167(2), 313-324. <https://doi.org/10.1016/j.cell.2016.08.029>
- Acosta, I. F., & Farmer, E. E. (2010). Jasmonates. *The Arabidopsis Book / American Society of Plant Biologists*, 8, e0129. <https://doi.org/10.1199/tab.0129>
- Adhikari, P. B., Liu, X., & Kasahara, R. D. (2020). Mechanics of Pollen Tube Elongation: A Perspective. *Frontiers in Plant Science*, 11. <https://www.frontiersin.org/articles/10.3389/fpls.2020.589712>
- Alfieri, A., Doccia, F. G., Pederzoli, R., Grenzi, M., Bonza, M. C., Luoni, L., Candeo, A., Romano Armada, N., Barbiroli, A., Valentini, G., Schneider, T. R., Bassi, A., Bolognesi, M., Nardini, M., & Costa, A. (2020). The structural bases for agonist diversity in an *Arabidopsis thaliana* glutamate receptor-like channel. *Proceedings of the National Academy of Sciences of the United States of America*, 117(1), 752-760. <https://doi.org/10.1073/pnas.1905142117>

- Altschul, S. F., Madden, T. L., Schäffer, A. A., Zhang, J., Zhang, Z., Miller, W., & Lipman, D. J. (1997). Gapped BLAST and PSI-BLAST: a new generation of protein database search programs. *Nucleic Acids Research*, 25(17), 3389-3402.  
<https://doi.org/10.1093/nar/25.17.3389>
- Altschul, S. F., Wootton, J. C., Gertz, E. M., Agarwala, R., Morgulis, A., Schäffer, A. A., & Yu, Y.-K. (2005). Protein database searches using compositionally adjusted substitution matrices. *The FEBS journal*, 272(20), 5101-5109. <https://doi.org/10.1111/j.1742-4658.2005.04945.x>
- Armstrong, N., & Gouaux, E. (2000). Mechanisms for Activation and Antagonism of an AMPA-Sensitive Glutamate Receptor: Crystal Structures of the GluR2 Ligand Binding Core. *Neuron*, 28(1), 165-181. [https://doi.org/10.1016/S0896-6273\(00\)00094-5](https://doi.org/10.1016/S0896-6273(00)00094-5)
- Armstrong, N., Jasti, J., Beich-Frandsen, M., & Gouaux, E. (2006). Measurement of Conformational Changes accompanying Desensitization in an Ionotropic Glutamate Receptor. *Cell*, 127(1), 85-97. <https://doi.org/10.1016/j.cell.2006.08.037>
- Armstrong, N., Sun, Y., Chen, G.-Q., & Gouaux, E. (1998). Structure of a glutamate-receptor ligand-binding core in complex with kainate. *Nature*, 395(6705), 913-917.  
<https://doi.org/10.1038/27692>
- Arvola, M., & Keinänen, K. (1996). Characterization of the Ligand-binding Domains of Glutamate Receptor (GluR)-B and GluR-D Subunits Expressed in Escherichia coli as Periplasmic Proteins\*. *Journal of Biological Chemistry*, 271(26), 15527-15532.  
<https://doi.org/10.1074/jbc.271.26.15527>

Auerbach, A., & Zhou, Y. (2005). Gating Reaction Mechanisms for NMDA Receptor Channels. *Journal of Neuroscience*, 25(35), 7914-7923. <https://doi.org/10.1523/JNEUROSCI.1471-05.2005>

Ayalon, G., & Stern-Bach, Y. (2001). Functional Assembly of AMPA and Kainate Receptors Is Mediated by Several Discrete Protein-Protein Interactions. *Neuron*, 31(1), 103-113. [https://doi.org/10.1016/S0896-6273\(01\)00333-6](https://doi.org/10.1016/S0896-6273(01)00333-6)

Baum, D. (2008). Reading a Phylogenetic Tree: The Meaning of Monophyletic Groups. *1(1):190*. <http://www.nature.com/scitable/topicpage/reading-a-phylogenetic-tree-the-meaning-of-41956>

files/932/reading-a-phylogenetic-tree-the-meaning-of-41956.html

Bethke, G., Unthan, T., Uhrig, J. F., Pöschl, Y., Gust, A. A., Scheel, D., & Lee, J. (2009). Flg22 regulates the release of an ethylene response factor substrate from MAP kinase 6 in *Arabidopsis thaliana* via ethylene signaling. *Proceedings of the National Academy of Sciences*, 106(19), 8067-8072. <https://doi.org/10.1073/pnas.0810206106>

Bowie, D. (2010). Ion-dependent gating of kainate receptors. *The Journal of Physiology*, 588(Pt 1), 67-81. <https://doi.org/10.1113/jphysiol.2009.178863>

Brenner, E. D., Stahlberg, R., Mancuso, S., Vivanco, J., Baluška, F., & Van Volkenburgh, E. (2006). Plant neurobiology: an integrated view of plant signaling. *Trends in Plant Science*, 11(8), 413-419. <https://doi.org/10.1016/j.tplants.2006.06.009>

Brodth, S., Six, J., Feenstra, G., Ingels, C. & Campbell, D. . (2011). Sustainable Agriculture *Nature Education Knowledge 3(10):1*. <https://www.nature.com/scitable/knowledge/library/sustainable-agriculture-23562787/>

files/837/sustainable-agriculture-23562787.html

- Brogi, S., Campiani, G., Brindisi, M., & Butini, S. (2019). Allosteric Modulation of Ionotropic Glutamate Receptors: An Outlook on New Therapeutic Approaches To Treat Central Nervous System Disorders. *ACS Medicinal Chemistry Letters*, 10(3), 228-236.  
<https://doi.org/10.1021/acsmmedchemlett.8b00450>
- Burada, A. P., Vinnakota, R., & Kumar, J. (2020a). The architecture of GluD2 ionotropic delta glutamate receptor elucidated by cryo-EM. *Journal of Structural Biology*, 211(2), 107546. <https://doi.org/10.1016/j.jsb.2020.107546>
- Burada, A. P., Vinnakota, R., & Kumar, J. (2020b). Cryo-EM structures of the ionotropic glutamate receptor GluD1 reveal a non-swapped architecture. *Nature Structural & Molecular Biology*, 27(1), 84-91. <https://doi.org/10.1038/s41594-019-0359-y>
- Carrillo, E., Gonzalez, C. U., Berka, V., & Jayaraman, V. (2021). Delta glutamate receptors are functional glycine- and D-serine-gated cation channels in situ. *Science Advances*, 7(52), eabk2200. <https://doi.org/10.1126/sciadv.abk2200>
- Chang, H.-R., & Kuo, C.-C. (2008). The Activation Gate and Gating Mechanism of the NMDA Receptor. *Journal of Neuroscience*, 28(7), 1546-1556.  
<https://doi.org/10.1523/JNEUROSCI.3485-07.2008>
- Chen, J.-T., & Heidari, P. (2020). Cell Signaling in Model Plants. *International Journal of Molecular Sciences*, 21(17), 6062. <https://doi.org/10.3390/ijms21176062>
- Chen, J., & Ham, B.-K. (2022). Systemic Signaling: A Role in Propelling Crop Yield. *Plants*, 11(11), 1400. <https://doi.org/10.3390/plants11111400>
- Chen, J., Jing, Y., Zhang, X., Li, L., Wang, P., Zhang, S., Zhou, H., & Wu, J. (2016). Evolutionary and Expression Analysis Provides Evidence for the Plant Glutamate-like

- Receptors Family is Involved in Woody Growth-related Function. *Scientific Reports*, 6(1), 32013. <https://doi.org/10.1038/srep32013>
- Chen, N., Li, B., Murphy, T. H., & Raymond, L. A. (2004). Site within N-Methyl-d-aspartate Receptor Pore Modulates Channel Gating. *Molecular Pharmacology*, 65(1), 157-164. <https://doi.org/10.1124/mol.65.1.157>
- Chen, S., Zhao, Y., Wang, Y., Shekhar, M., Tajkhorshid, E., & Gouaux, E. (2017). Activation and Desensitization Mechanism of AMPA Receptor-TARP Complex by Cryo-EM. *Cell*, 170(6), 1234-1246.e1214. <https://doi.org/10.1016/j.cell.2017.07.045>
- Cheng, Y., Zhang, X., Sun, T., Tian, Q., & Zhang, W.-H. (2018). Glutamate Receptor Homolog3.4 is Involved in Regulation of Seed Germination Under Salt Stress in Arabidopsis. *Plant and Cell Physiology*, 59(5), 978-988. <https://doi.org/10.1093/pcp/pcy034>
- Chiu, J., DeSalle, R., Lam, H. M., Meisel, L., & Coruzzi, G. (1999). Molecular evolution of glutamate receptors: a primitive signaling mechanism that existed before plants and animals diverged. *Molecular Biology and Evolution*, 16(6), 826-838. <https://doi.org/10.1093/oxfordjournals.molbev.a026167>
- Cull-Candy, S. G., & Usowicz, M. M. (1987). Multiple-conductance channels activated by excitatory amino acids in cerebellar neurons. *Nature*, 325(6104), 525-528. <https://doi.org/10.1038/325525a0>
- De Bortoli, S., Teardo, E., Szabò, I., Morosinotto, T., & Alboresi, A. (2016). Evolutionary insight into the ionotropic glutamate receptor superfamily of photosynthetic organisms. *Biophysical Chemistry*, 218, 14-26. <https://doi.org/10.1016/j.bpc.2016.07.004>

- Deinlein, U., Stephan, A. B., Horie, T., Luo, W., Xu, G., & Schroeder, J. I. (2014). Plant salt-tolerance mechanisms. *Trends in Plant Science*, 19(6), 371-379.  
<https://doi.org/10.1016/j.tplants.2014.02.001>
- Dolphin, A. C., Insel, P. A., Blaschke, T. F., & Meyer, U. A. (2020). Introduction to the Theme “Ion Channels and Neuropharmacology: From the Past to the Future”. *Annual Review of Pharmacology and Toxicology*, 60(1), 1-6. <https://doi.org/10.1146/annurev-pharmtox-082719-110050>
- Dürr, K. L., Chen, L., Stein, R. A., De Zorzi, R., Folea, I. M., Walz, T., McHaourab, H. S., & Gouaux, E. (2014). Structure and Dynamics of AMPA Receptor GluA2 in Resting, Pre-Open, and Desensitized States. *Cell*, 158(4), 778-792.  
<https://doi.org/10.1016/j.cell.2014.07.023>
- Fernández-Marcos, M., Desvoyes, B., Manzano, C., Liberman, L. M., Benfey, P. N., del Pozo, J. C., & Gutierrez, C. (2017). Control of Arabidopsis lateral root primordium boundaries by MYB36. *New Phytologist*, 213(1), 105-112. <https://doi.org/10.1111/nph.14304>
- Forde, B. G., & Roberts, M. R. (2014). Glutamate receptor-like channels in plants: a role as amino acid sensors in plant defence? *F1000Prime Reports*, 6, 37.  
<https://doi.org/10.12703/P6-37>
- Gangwar, S. P., Green, M. N., Michard, E., Simon, A. A., Feijó, J. A., & Sobolevsky, A. I. (2021). Structure of the Arabidopsis Glutamate Receptor-like Channel GLR3.2 Ligand-Binding Domain. *Structure*, 29(2), 161-169.e164.  
<https://doi.org/10.1016/j.str.2020.09.006>
- Goto, Y., Maki, N., Ichihashi, Y., Kitazawa, D., Igarashi, D., Kadota, Y., & Shirasu, K. (2020). Exogenous Treatment with Glutamate Induces Immune Responses in Arabidopsis.



- Molecular Plant-Microbe Interactions*®, 33(3), 474-487. <https://doi.org/10.1094/MPMI-09-19-0262-R>
- Green, M. N., Gangwar, S. P., Michard, E., Simon, A. A., Portes, M. T., Barbosa-Caro, J., Wudick, M. M., Lizzio, M. A., Klykov, O., Yelshanskaya, M. V., Feijó, J. A., & Sobolevsky, A. I. (2021). Structure of the *Arabidopsis thaliana* glutamate receptor-like channel GLR3.4. *Molecular Cell*, 81(15), 3216-3226.e3218. <https://doi.org/10.1016/j.molcel.2021.05.025>
- Grenzi, M., Bonza, M. C., & Costa, A. (2022). Signaling by plant glutamate receptor-like channels: What else! *Current Opinion in Plant Biology*, 68, 102253. <https://doi.org/10.1016/j.pbi.2022.102253>
- Hansen, K. B., Wollmuth, L. P., Bowie, D., Furukawa, H., Menniti, F. S., Sobolevsky, A. I., Swanson, G. T., Swanger, S. A., Greger, I. H., Nakagawa, T., McBain, C. J., Jayaraman, V., Low, C.-M., Dell'Acqua, M. L., Diamond, J. S., Camp, C. R., Perszyk, R. E., Yuan, H., & Traynelis, S. F. (2021). Structure, Function, and Pharmacology of Glutamate Receptor Ion Channels. *Pharmacological Reviews*, 73(4), 1469-1658. <https://doi.org/10.1124/pharmrev.120.000131>
- Herguedas, B., Krieger, J., & Greger, I. H. (2013). Receptor Heteromeric Assembly—How It Works and Why It Matters. In *Progress in Molecular Biology and Translational Science* (Vol. 117, pp. 361-386). Elsevier. <https://linkinghub.elsevier.com/retrieve/pii/B9780123869319000131>
- Hernández-Coronado, M., Dias Araujo, P. C., Ip, P.-L., Nunes, C. O., Rahni, R., Wudick, M. M., Lizzio, M. A., Feijó, J. A., & Birnbaum, K. D. (2022). Plant glutamate receptors mediate

- a bet-hedging strategy between regeneration and defense. *Developmental Cell*, 57(4), 451-465.e456. <https://doi.org/10.1016/j.devcel.2022.01.013>
- Hogner, A., Kastrup, J. S., Jin, R., Liljefors, T., Mayer, M. L., Egebjerg, J., Larsen, I. K., & Gouaux, E. (2002). Structural Basis for AMPA Receptor Activation and Ligand Selectivity: Crystal Structures of Five Agonist Complexes with the GluR2 Ligand-binding Core. *Journal of Molecular Biology*, 322(1), 93-109. [https://doi.org/10.1016/S0022-2836\(02\)00650-2](https://doi.org/10.1016/S0022-2836(02)00650-2)
- Hollmann, M., Maron, C., & Heinemann, S. (1994). N-glycosylation site tagging suggests a three transmembrane domain topology for the glutamate receptor GluR1. *Neuron*, 13(6), 1331-1343. [https://doi.org/10.1016/0896-6273\(94\)90419-7](https://doi.org/10.1016/0896-6273(94)90419-7)
- Huettner, J. E. (2015). Glutamate receptor pores. *The Journal of Physiology*, 593(1), 49-59. <https://doi.org/10.1113/jphysiol.2014.272724>
- Jahr, C. E., & Stevens, C. F. (1987). Glutamate activates multiple single channel conductances in hippocampal neurons. *Nature*, 325(6104), 522-525. <https://doi.org/10.1038/325522a0>
- Jin, L., Cai, Y., Sun, C., Huang, Y., & Yu, T. (2019). Exogenous l-glutamate treatment could induce resistance against *Penicillium expansum* in pear fruit by activating defense-related proteins and amino acids metabolism. *Postharvest Biology and Technology*, 150, 148-157. <https://doi.org/10.1016/j.postharvbio.2018.11.009>
- Jin, R., Singh, S. K., Gu, S., Furukawa, H., Sobolevsky, A. I., Zhou, J., Jin, Y., & Gouaux, E. (2009). Crystal structure and association behaviour of the GluR2 amino-terminal domain. *The EMBO Journal*, 28(12), 1812-1823. <https://doi.org/10.1038/emboj.2009.140>
- Jones, J. D. G., & Dangl, J. L. (2006). The plant immune system. *Nature*, 444(7117), 323-329. <https://doi.org/10.1038/nature05286>

- Kadotani, N., Akagi, A., Takatsuji, H., Miwa, T., & Igarashi, D. (2016). Exogenous proteinogenic amino acids induce systemic resistance in rice. *BMC Plant Biology*, 16(1), 60. <https://doi.org/10.1186/s12870-016-0748-x>
- Katz, B., & Thesleff, S. (1957). A study of the ‘desensitization’ produced by acetylcholine at the motor end-plate. *The Journal of Physiology*, 138(1), 63-80. <https://doi.org/10.1113/jphysiol.1957.sp005838>
- Kc, K. B., Dias, G. M., Veeramani, A., Swanton, C. J., Fraser, D., Steinke, D., Lee, E., Wittman, H., Farber, J. M., Dunfield, K., McCann, K., Anand, M., Campbell, M., Rooney, N., Raine, N. E., Acker, R. V., Hanner, R., Pascoal, S., Sharif, S., . . . Fraser, E. D. G. (2018). When too much isn’t enough: Does current food production meet global nutritional needs? *PLOS ONE*, 13(10), e0205683. <https://doi.org/10.1371/journal.pone.0205683>
- Khanra, N., Brown, P. M. G. E., Perozzo, A. M., Bowie, D., & Meyerson, J. R. (2021). Architecture and structural dynamics of the heteromeric GluK2/K5 kainate receptor. *eLife*, 10, e66097. <https://doi.org/10.7554/eLife.66097>
- Kim, M.-J., Jeon, B. W., Oh, E., Seo, P. J., & Kim, J. (2021). Peptide Signaling during Plant Reproduction. *Trends in Plant Science*, 26(8), 822-835. <https://doi.org/10.1016/j.tplants.2021.02.008>
- Klykov, O., Gangwar, S. P., Yelshanskaya, M. V., Yen, L., & Sobolevsky, A. I. (2021). Structure and desensitization of AMPA receptor complexes with type II TARP  $\gamma 5$  and GSG1L. *Molecular Cell*, 81(23), 4771-4783.e4777. <https://doi.org/10.1016/j.molcel.2021.09.030>
- Kunishima, N., Shimada, Y., Tsuji, Y., Sato, T., Yamamoto, M., Kumasaka, T., Nakanishi, S., Jingami, H., & Morikawa, K. (2000). Structural basis of glutamate recognition by a

- dimeric metabotropic glutamate receptor. *Nature*, 407(6807), 971-977.  
<https://doi.org/10.1038/35039564>
- Kussius, C. L., Popescu, A. M., & Popescu, G. K. (2010). Agonist-specific Gating of NMDA Receptors. *Channels (Austin, Tex.)*, 4(2), 78-82.  
<https://www.ncbi.nlm.nih.gov/pmc/articles/PMC3150751/>
- Kuusinen, A., Arvola, M., & Keinänen, K. (1995). Molecular dissection of the agonist binding site of an AMPA receptor. *The EMBO Journal*, 14(24), 6327-6332.  
<https://www.ncbi.nlm.nih.gov/pmc/articles/PMC394757/>
- Lam, H.-M., Chiu, J., Hsieh, M.-H., Meisel, L., Oliveira, I. C., Shin, M., & Coruzzi, G. (1998). Glutamate-receptor genes in plants. *Nature*, 396(6707), 125-126.  
<https://doi.org/10.1038/24066>
- Li, C., Xu, M., Cai, X., Han, Z., Si, J., & Chen, D. (2022). Jasmonate Signaling Pathway Modulates Plant Defense, Growth, and Their Trade-Offs. *International Journal of Molecular Sciences*, 23(7), 3945. <https://doi.org/10.3390/ijms23073945>
- Li, F., Wang, J., Ma, C., Zhao, Y., Wang, Y., Hasi, A., & Qi, Z. (2013). Glutamate Receptor-Like Channel3.3 Is Involved in Mediating Glutathione-Triggered Cytosolic Calcium Transients, Transcriptional Changes, and Innate Immunity Responses in Arabidopsis. *Plant Physiology*, 162(3), 1497-1509. <https://doi.org/10.1104/pp.113.217208>
- Li, M., Wang, F., Li, S., Yu, G., Wang, L., Li, Q., Zhu, X., Li, Z., Yuan, L., & Liu, P. (2020). Importers Drive Leaf-to-Leaf Jasmonic Acid Transmission in Wound-Induced Systemic Immunity. *Molecular Plant*, 13(10), 1485-1498.  
<https://doi.org/10.1016/j.molp.2020.08.017> (Special Issue on Plant-Microbe Interactions)

Mauseth, J. D. (2021). *Botany: An Introduction to Plant Biology* (Vol. Vol Seventh edition.).

Jones & Bartlett Learning.

<https://web.s.ebscohost.com/ehost/ebookviewer/ebook/bmxlYmtfXzIyNTgzOTZfX0FO0?sid=52a09324-d9b2-464d-8484-96ff9c271b8f@redis&vid=0&format=EK&rid=1>

files/1447/bmxlYmtfXzIyNTgzOTZfX0FO0.html

Meyerhoff, O., Müller, K., Roelfsema, M. R. G., Latz, A., Lacombe, B., Hedrich, R., Dietrich, P., & Becker, D. (2005). AtGLR3.4, a glutamate receptor channel-like gene is sensitive to touch and cold. *Planta*, 222(3), 418-427. <https://www.jstor.org/stable/23389017>

Michard, E., Lima, P. T., Borges, F., Silva, A. C., Portes, M. T., Carvalho, J. E., Gilliam, M., Liu, L.-H., Obermeyer, G., & Feijó, J. A. (2011). Glutamate Receptor–Like Genes Form Ca<sup>2+</sup> Channels in Pollen Tubes and Are Regulated by Pistil d-Serine. *Science*, 332(6028), 434-437. <https://doi.org/10.1126/science.1201101>

Michard, E., Simon, A. A., Tavares, B., Wudick, M. M., & Feijó, J. A. (2017). Signaling with Ions: The Keystone for Apical Cell Growth and Morphogenesis in Pollen Tubes1[OPEN]. *Plant Physiology*, 173(1), 91-111. <https://doi.org/10.1104/pp.16.01561>

Moe-Lange, J., Gappel, N. M., Machado, M., Wudick, M. M., Sies, C. S. A., Schott-Verdugo, S. N., Bonus, M., Mishra, S., Hartwig, T., Bezruczyk, M., Basu, D., Farmer, E. E., Gohlke, H., Malkovskiy, A., Haswell, E. S., Lercher, M. J., Ehrhardt, D. W., Frommer, W. B., & Kleist, T. J. (2021). Interdependence of a mechanosensitive anion channel and glutamate receptors in distal wound signaling. *Science Advances*, 7(37), eabg4298. <https://doi.org/10.1126/sciadv.abg4298>

- Nayeem, N., Mayans, O., & Green, T. (2011). Conformational Flexibility of the Ligand-Binding Domain Dimer in Kainate Receptor Gating and Desensitization. *Journal of Neuroscience*, 31(8), 2916-2924. <https://doi.org/10.1523/JNEUROSCI.4771-10.2011>
- Nguyen, C. T., Kurenda, A., Stolz, S., Chételat, A., & Farmer, E. E. (2018). Identification of cell populations necessary for leaf-to-leaf electrical signaling in a wounded plant. *Proceedings of the National Academy of Sciences*, 115(40), 10178-10183. <https://doi.org/10.1073/pnas.1807049115>
- Pankevich, D. E. (2011). Overview of the Glutamatergic System. In a. B. M. A. Miriam Davis (Ed.), *Institute of Medicine (US) Forum on Neuroscience and Nervous System Disorders. Glutamate-Related Biomarkers in Drug Development for Disorders of the Nervous System: Workshop Summary*. Washington (DC): National Academies Press (US).
- Pechanova, O., & Pechan, T. (2017). Chapter 3 - Proteomics as a Tool to Understand Maize Biology and to Improve Maize Crop. In M. L. Colgrave (Ed.), *Proteomics in Food Science* (pp. 35-56). Academic Press. <https://www.sciencedirect.com/science/article/pii/B9780128040072000035>
- [files/1443/B9780128040072000035.html](https://www.sciencedirect.com/science/article/pii/B9780128040072000035)
- Perrais, D., Veran, J., & Mulle, C. (2010). Gating and permeation of kainate receptors: differences unveiled. *Trends in Pharmacological Sciences*, 31(11), 516-522. <https://doi.org/10.1016/j.tips.2010.08.004>
- Price, M. B., Jelesko, J., & Okumoto, S. (2012). Glutamate Receptor Homologs in Plants: Functions and Evolutionary Origins. *Frontiers in Plant Science*, 3, 235. <https://doi.org/10.3389/fpls.2012.00235>

- Quiococho, F. A., & Ledvina, P. S. (1996). Atomic structure and specificity of bacterial periplasmic receptors for active transport and chemotaxis: variation of common themes. *Molecular Microbiology*, 20(1), 17-25. <https://doi.org/10.1111/j.1365-2958.1996.tb02484.x>
- Relations, F. M. (2021). FAO - News Article: Climate change fans spread of pests and threatens plants and crops, new FAO study. *FAO Food and Agriculture Organization of the United Nations*. <https://www.fao.org/news/story/en/item/1402920/icode/>
- Sather, W., Dieudonné, S., MacDonald, J. F., & Ascher, P. (1992). Activation and desensitization of N-methyl-D-aspartate receptors in nucleated outside-out patches from mouse neurones. *The Journal of Physiology*, 450, 643-672. <https://www.ncbi.nlm.nih.gov/pmc/articles/PMC1176143/>
- Sather, W., Johnson, J. W., Henderson, G., & Ascher, P. (1990). Glycine-insensitive desensitization of NMDA responses in cultured mouse embryonic neurons. *Neuron*, 4(5), 725-731. [https://doi.org/10.1016/0896-6273\(90\)90198-O](https://doi.org/10.1016/0896-6273(90)90198-O)
- Scientific review of the impact of climate change on plant pests*. (2021). FAO on behalf of the IPPC Secretariat. <http://www.fao.org/documents/card/en/c/cb4769en>
- Shanmukhan, A. P., Mathew, M. M., Radhakrishnan, D., Aiyaz, M., & Prasad, K. (2020). Regrowing the damaged or lost body parts. *Current Opinion in Plant Biology*, 53, 117-127. <https://doi.org/10.1016/j.pbi.2019.12.007> (Growth and development)
- Shipman, E. N., Yu, J., Zhou, J., Albornoz, K., & Beckles, D. M. (2021). Can gene editing reduce postharvest waste and loss of fruit, vegetables, and ornamentals? *Horticulture Research*, 8(1), 1-21. <https://doi.org/10.1038/s41438-020-00428-4>

- Smith, T. C., & Howe, J. R. (2000). Concentration-dependent substate behavior of native AMPA receptors. *Nature Neuroscience*, 3(10), 992-997. <https://doi.org/10.1038/79931>
- Sobolevsky, A. I., Rosconi, M. P., & Gouaux, E. (2009). X-ray structure of AMPA-subtype glutamate receptor: symmetry and mechanism. *Nature*, 462(7274), 745-756. <https://doi.org/10.1038/nature08624>
- Stern-Bach, Y., Bettler, B., Hartley, M., Sheppard, P. O., O'Hara, P. J., & Heinemann, S. F. (1994). Agonist selectivity of glutamate receptors is specified by two domains structurally related to bacterial amino acid-binding proteins. *Neuron*, 13(6), 1345-1357. [https://doi.org/10.1016/0896-6273\(94\)90420-0](https://doi.org/10.1016/0896-6273(94)90420-0)
- Stroebe, D., & Paoletti, P. (2021). Architecture and function of NMDA receptors: an evolutionary perspective. *The Journal of Physiology*, 599(10), 2615-2638. <https://doi.org/10.1113/JP279028>
- Teardo, E., Carraretto, L., De Bortoli, S., Costa, A., Behera, S., Wagner, R., Lo Schiavo, F., Formentin, E., & Szabo, I. (2015). Alternative Splicing-Mediated Targeting of the Arabidopsis GLUTAMATE RECEPTOR3.5 to Mitochondria Affects Organelle Morphology1. *Plant Physiology*, 167(1), 216-227. <https://doi.org/10.1104/pp.114.242602>
- Teardo, E., Formentin, E., Segalla, A., Giacometti, G. M., Marin, O., Zanetti, M., Lo Schiavo, F., Zoratti, M., & Szabò, I. (2011). Dual localization of plant glutamate receptor AtGLR3.4 to plastids and plasmamembrane. *Biochimica et Biophysica Acta (BBA) - Bioenergetics*, 1807(3), 359-367. <https://doi.org/10.1016/j.bbabi.2010.11.008>
- Tian, W., Wang, C., Gao, Q., Li, L., & Luan, S. (2020). Calcium spikes, waves and oscillations in plant development and biotic interactions. *Nature Plants*, 6(7), 750-759. <https://doi.org/10.1038/s41477-020-0667-6>



- Tikhonov, D. B., & Zhorov, B. S. (2020). The pore domain in glutamate-gated ion channels: Structure, drug binding and similarity with potassium channels. *Biochimica et Biophysica Acta (BBA) - Biomembranes*, 1862(10), 183401. <https://doi.org/10.1016/j.bbamem.2020.183401>
- Torres-Martínez, H. H., Rodríguez-Alonso, G., Shishkova, S., & Dubrovsky, J. G. (2019). Lateral Root Primordium Morphogenesis in Angiosperms. *Frontiers in Plant Science*, 10, 206. <https://doi.org/10.3389/fpls.2019.00206>
- Toyota, M., Spencer, D., Sawai-Toyota, S., Jiaqi, W., Zhang, T., Koo, A. J., Howe, G. A., & Gilroy, S. (2018). Glutamate triggers long-distance, calcium-based plant defense signaling. *Science*, 361(6407), 1112-1115. <https://doi.org/10.1126/science.aat7744>
- Traynelis, S. F., Wollmuth, L. P., McBain, C. J., Menniti, F. S., Vance, K. M., Ogden, K. K., Hansen, K. B., Yuan, H., Myers, S. J., & Dingledine, R. (2010). Glutamate Receptor Ion Channels: Structure, Regulation, and Function. *Pharmacological Reviews*, 62(3), 405-496. <https://doi.org/10.1124/pr.109.002451>
- Twomey, E. C., & Sobolevsky, A. I. (2018). Structural Mechanisms of Gating in Ionotropic Glutamate Receptors. *Biochemistry*, 57(3), 267-276. <https://doi.org/10.1021/acs.biochem.7b00891>
- Twomey, E. C., Yelshanskaya, M. V., Grassucci, R. A., Frank, J., & Sobolevsky, A. I. (2017a). Channel opening and gating mechanism in AMPA-subtype glutamate receptors. *Nature*, 549(7670), 60-65. <https://doi.org/10.1038/nature23479>
- Twomey, E. C., Yelshanskaya, M. V., Grassucci, R. A., Frank, J., & Sobolevsky, A. I. (2017b). Structural Bases of Desensitization in AMPA Receptor-Auxiliary Subunit Complexes. *Neuron*, 94(3), 569-580.e565. <https://doi.org/10.1016/j.neuron.2017.04.025>

- Vincill, E. D., Clarin, A. E., Molenda, J. N., & Spalding, E. P. (2013). Interacting Glutamate Receptor-Like Proteins in Phloem Regulate Lateral Root Initiation in Arabidopsis. *The Plant Cell*, 25(4), 1304-1313. <https://doi.org/10.1105/tpc.113.110668>
- Volk, L., Chiu, S.-L., Sharma, K., & Huganir, R. L. (2015). Glutamate Synapses in Human Cognitive Disorders. *Annual Review of Neuroscience*, 38(1), 127-149. <https://doi.org/10.1146/annurev-neuro-071714-033821>
- Wachsman, G., & Benfey, P. N. (2020). Lateral Root Initiation: The Emergence of New Primordia Following Cell Death. *Current Biology*, 30(3), R121-R122. <https://doi.org/10.1016/j.cub.2019.12.032>
- Weiland, M., Mancuso, S., Baluska, F., Weiland, M., Mancuso, S., & Baluska, F. (2015). Signalling via glutamate and GLRs in Arabidopsis thaliana. *Functional Plant Biology*, 43(1), 1-25. <https://doi.org/10.1071/FP15109>
- WHO, F. I. U. W. (2022). *The state of Food Security and Nutrition in the World 2022*
- The State of Food Security and Nutrition in the World 2022. Repurposing food and agricultural policies to make healthy diets more affordable.* (978-92-5-136499-4). <https://www.fao.org/3/cc0639en/online/cc0639en.html>
- files/802/cc0639en.html
- Wo, Z. G., & Oswald, R. E. (1994). Transmembrane topology of two kainate receptor subunits revealed by N-glycosylation. *Proceedings of the National Academy of Sciences of the United States of America*, 91(15), 7154-7158. <https://www.ncbi.nlm.nih.gov/pmc/articles/PMC44357/>

- Wollmuth, L. P., & Sobolevsky, A. I. (2004). Structure and gating of the glutamate receptor ion channel. *Trends in Neurosciences*, 27(6), 321-328.  
<https://doi.org/10.1016/j.tins.2004.04.005>
- Wu, S.-H., Ho, C.-T., Nah, S.-L., & Chau, C.-F. (2014). Global Hunger: A Challenge to Agricultural, Food, and Nutritional Sciences. *Critical Reviews in Food Science and Nutrition*, 54(2), 151-162. <https://doi.org/10.1080/10408398.2011.578764>
- Wudick, M. M., Michard, E., Oliveira Nunes, C., & Feijó, J. A. (2018). Comparing plant and animal glutamate receptors: common traits but different fates? *Journal of Experimental Botany*, 69(17), 4151-4163. <https://doi.org/10.1093/jxb/ery153>
- Wudick, M. M., Portes, M. T., Michard, E., Rosas-Santiago, P., Lizzio, M. A., Nunes, C. O., Campos, C., Santa Cruz Damineli, D., Carvalho, J. C., Lima, P. T., Pantoja, O., & Feijó, J. A. (2018). CORNICHON sorting and regulation of GLR channels underlie pollen tube Ca<sup>2+</sup> homeostasis. *Science*, 360(6388), 533-536. <https://doi.org/10.1126/science.aar6464>
- Yang, J., Sun, C., Fu, D., & Yu, T. (2017). Test for l-glutamate inhibition of growth of *Alternaria alternata* by inducing resistance in tomato fruit. *Food Chemistry*, 230, 145-153.  
<https://doi.org/10.1016/j.foodchem.2017.03.033>
- Yelshanskaya, M. V., Patel, D. S., Kottke, C. M., Kurnikova, M. G., & Sobolevsky, A. I. (2022). Opening of glutamate receptor channel to subconductance levels. *Nature*, 605(7908), 172-178. <https://doi.org/10.1038/s41586-022-04637-w>
- Yelshanskaya, M. V., Singh, A. K., Sampson, J. M., Narangoda, C., Kurnikova, M., & Sobolevsky, A. I. (2016). Structural Bases of Noncompetitive Inhibition of AMPA-Subtype Ionotropic Glutamate Receptors by Antiepileptic Drugs. *Neuron*, 91(6), 1305-1315. <https://doi.org/10.1016/j.neuron.2016.08.012>

- Yelshanskaya, M. V., & Sobolevsky, A. I. (2022). Structural Insights into Function of Ionotropic Glutamate Receptors. *Biochemistry (Moscow), Supplement Series A: Membrane and Cell Biology*, 16(3), 190-206. <https://doi.org/10.1134/S1990747822040043>
- Yu, B., Wu, Q., Li, X., Zeng, R., Min, Q., & Huang, J. (2022). GLUTAMATE RECEPTOR-like gene OsGLR3.4 is required for plant growth and systemic wound signaling in rice (*Oryza sativa*). *New Phytologist*, 233(3), 1238-1256. <https://doi.org/10.1111/nph.17859>
- Zhou, Y., & Danbolt, N. C. (2014). Glutamate as a neurotransmitter in the healthy brain. *Journal of Neural Transmission*, 121(8), 799-817. <https://doi.org/10.1007/s00702-014-1180-8>
- Zhu, J.-K. (2002). Salt and Drought Stress Signal Transduction in Plants. *Annual review of plant biology*, 53, 247-273. <https://doi.org/10.1146/annurev.arplant.53.091401.143329>
- Zhu, J.-K. (2016). Abiotic Stress Signaling and Responses in Plants. *Cell*, 167(2), 313-324. <https://doi.org/10.1016/j.cell.2016.08.029>